UNIVERSITÀ DI PARMA

UNIVERSITÀ DEGLI STUDI DI PARMA

DOTTORATO DI RICERCA IN

NEUROSCIENZE

XXXI ciclo

Generation of fluorescent reporter lines for hiPSCs derived midbrain dopaminergic neurons: using a CRISPR/Cas9 based knock-in approach to mark TH and GIRK2 expression *in vitro*

Coordinatore:
Chiar.mo Prof. Vittorio Gallese

Tutor:
Chiar.mo Prof. Michele Zoli

Dottoranda:
Dr.ssa Christa Überbacher

Anni 2015/2018

Contents

1 Introduction

1.1 Parkinson's Disease

Parkinson's Disease (PD) and its main clinical features were properly described for the first time in 1817 when James Parkinson published "An Essay on Shaking Palsy" (Parkinson 1817). However, its current nomenclature was later proposed by neurologist Jean Martin Charcot, who used the term "Maladie de Parkinson" in his continuative study of the disease between 1868 and 1881 (Kempster, Hurwitz, and Lees 2007).

PD is the second most common neurodegenerative disorder after Alzheimer's disease, and the most common neurodegenerative movement disorder(Nussbaum and Ellis 2003). It is characterised by resting tremor, rigidity, bradykinesia and postural instability. The disease also presents with non-motor symptoms like autonomic, psychiatric, sensory and sleep disturbances, cognitive impairment and dementia (Stern, Lang, and Poewe 2012).

The motor symptoms of PD are associated with a profound loss of dopaminergic (DA) neurons in the substantia nigra pars compacta (SNpc) resulting in depletion of dopamine (DA) in the striatum and other projection areas. Surviving neurons present intracellular inclusions called Lewy bodies, containing mainly filamentous alpha-synuclein (aSyn). An analysis of Lewy body accumulation in PD patients showed that aSyn pathology spreads from the lower brainstem to the higher cortical areas (Braak et al. 2003).

The term parkinsonism is used to describe the (motor) clinical phenotype of a movement disorder, consisting of one or more symptoms like tremor, bradykinesia and rigidity. But parkinsonism does not implicate a progression of the symptoms or neurodegeneration, whereas in PD the symptoms typically worsen with the duration of the disease (Lin and Farrer 2014).

1.2 Etiology

The major risk factor for the development of PD is represented by ageing. The median age at onset is 60 years and about 2-3% of people over the age of 65 are affected (Lees, Hardy, and Revesz 2009; Cantuti-Castelvetri et al. 2007). PD was long thought to be caused by environmental factors, supported also by the identification of N-methyl-4-phenyl-1,2,3,6 -tetrahydropyridine (MPTP) in the early 1980's. MPTP is a

neurotoxin that inhibits mitochondrial complex 1 leading to nigral cell death and a parkinsonian syndrome in rodents, primates and humans (Langston et al. 1983). Other environmental toxins like cyanide, pesticides, carbon disulphide and toluene can lead to clinical symptoms, similar to PD (Lees, Hardy, and Revesz 2009). After the first description of a pathogenic missense mutation in the gene coding for aSyn (SNCA), the heredity of PD was confirmed (Polymeropoulos et al. 1997). The identification of SNCA allowed the discovery of candidate genes using linkage analysis, genome sequencing and genetic association, through which several loci (PARK loci) were found (Trinh and Farrer 2013). Indeed, additional genetic evidence was recently provided by genome-wide association studies (GWAS) (Kalinderi, Bostantjopoulou, and Fidani 2016; Chang et al. 2017; Nalls et al. 2018).

1.3 Selective vulnerability of dopaminergic neurons

The causes of the selective vulnerability to neurodegeneration in PD of the DA neurons are still unclear, despite several hypotheses have been proposed throughout the years (Bolam and Pissadaki 2012). More than 40 years ago, the main morphological and biochemical alterations of PD patient brains was clear (Bernheimer et al. 1973), but even though in 1997 aSyn mutations and their connection to PD etiology were discovered, the selective vulnerability of SN neurons and the etiological factor(s) responsible for it are unanswered questions.

Dopaminergic cell groups are classified as proposed by (Dahlstroem and Fuxe 1964) into A8-A16 groups. The A9 group is localized in the ventral tier of the SNpc (Chung et al. 2005), and represents the subtype of neurons most susceptible to early degeneration in PD, while the A10 group is mainly found in the ventral tegmental area (VTA). The A9 SNpc DA neurons and A10 VTA DA neurons share the molecular marker protein tyrosine hydroxylase (TH). The A9 in the SNpc are tightly clustered. Contrary to A10 VTA neurons, they do not express Calbindin, while being positive for the potassium channel GIRK2 (G-protein activated inward rectifying potassium channel 2) and the dopamine transporter (DAT) (Bjorklund and Dunnett 2007).

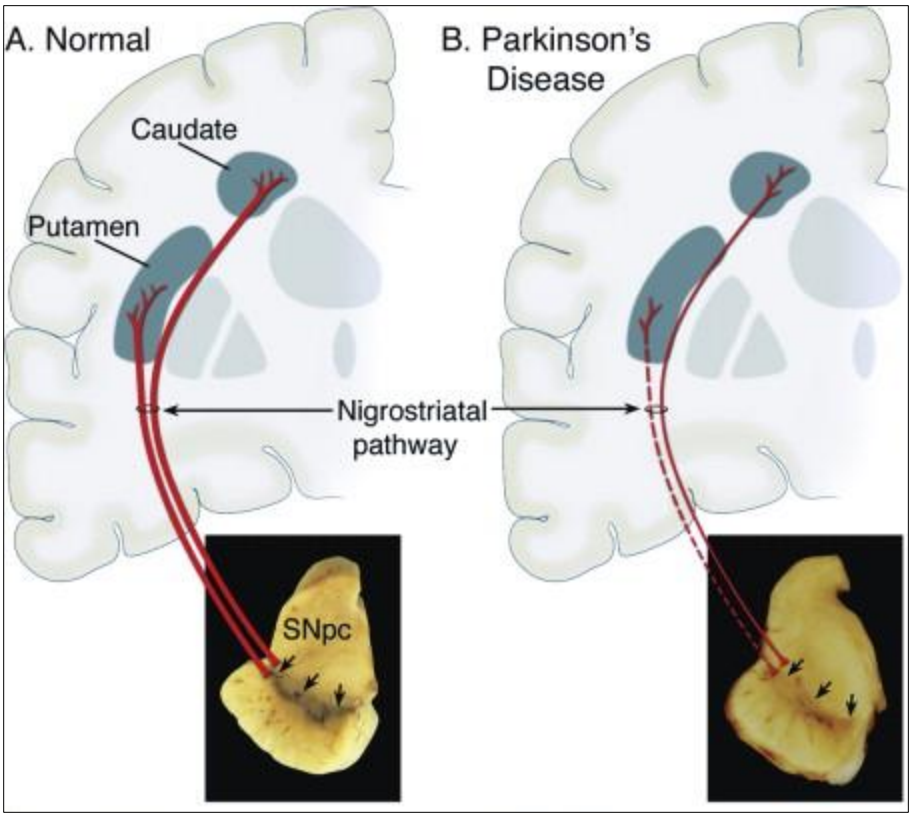

Fig. 1 A. Representation of the nigrostriatal pathway of a healthy person. Originating in the SNpc, the neurons project to the dorsal striatum (putamen and caudate nucleus; red line). Neuromelanin-containing cells are indicated by black arrows. B. Representation the nigrostriatal pathway in PD. There is a loss of DA neurons that project to the putamen (striped line) and a less extensive loss of cells that project to the caudate (thinned line). There is a visible reduction of neuromelanin-containing cells in the SNpc. (picture modified after(Dauer and Przedborski 2003b))

The SNpc neurons project to the dorsal striatum (see Fig. 1) where they synapse with the GABAergic spiny projection neurons (SPNs) and release DA. This connection constitutes the nigrostriatal pathway, which directly influences the direct and indirect pathways of motor control.

In PD, the loss of DA neurons is observed in the SNpc while neurons of the neighbouring region VTA are mostly spared (Dauer and Przedborski 2003a). Especially the ventrolateral tier of SNpc undergoes devastating neurodegeneration (Kordower et al. 2013).

To the present day, little is known about differential expression patterns of TH-positive SNpc and VTA neurons. There are several markers that can be used to distinguish the subgroups of DA neurons (GIRK2, Calbindin), but none has given clear indications on how they contribute to susceptibility differences especially not between ventral and dorsal tier of SNpc.

There are differences in expression of DA receptors and the DAT in SNpc and VTA (Reyes et al. 2013). In addition, MPTP, which is selectively taken up by DA neurons and damaging them, is entering the cells

through the DAT which shows a higher expression in the ventral SNpc neurons compared to VTA (Lammel et al. 2008). However, the mechanisms underlying the contribution of DAT to selective vulnerability is yet to be elucidated.

It is known that in rat brains, a single SNpc DA neuron can form more than 100,000 synapses in the brain areas it projects to, mainly the striatum, and its arborisation can measure up to 78cm in length (Matsuda et al. 2009), whereas VTA neurons are much shorter and with less complex axonal arborisation. Also, "pacemaking" activity, which is unique to midbrain DA (mDA) neurons, is shown to underlie different mechanisms in SNpc neurons in comparison do VTA neurons (Khaliq and Bean 2010). Lastly, SNpc axonal arbours are unmyelinated. Taken all these things into consideration, (Bolam and Pissadaki 2012) provide a proposal of excessive energy demand being the biggest risk factor for DA neurons. This implicates that the nature of their constitution is the reason for their susceptibility to damage and not an unknown extrinsic factor. Combined with the "multiple hit hypotheses" (Sulzer 2007) this may be the most plausible explanation for pathogenesis we have today, at least for idiopathic PD.

1.4 Familial PD and possible therapeutic targets

1.4.1 aSyn (alpha-Synuclein)

aSyn is a cardinal point in PD because of its abundant presence in Lewy bodies and its linkage to many genes implicated in the disease. Missense mutations in aSyn increase the propensity of the protein to self-aggregate (Li, Uversky, and Fink 2001; Kruger et al. 1998; Polymeropoulos et al. 1997) and gene multiplications, resulting in an overabundance of aSyn, lead to early onset cases of PD (Olgiati et al. 2015; Oliveira et al. 2015; Ferese et al. 2015). Also, more recent findings have suggested that aSyn may have infectious potential in a prion-like fashion (Olanow and Prusiner 2009; Li et al. 2008), stemming from the observation of Braak et al. (2003) who suggested that aSyn pathology spreads through the brain.

In this context, inflammation appears to be an aggravating factor in PD and contributes to the pathogenesis. Toll-like receptor (TLR) signalling, which is a major pathway mediating inflammation, is implicated in PD patients and TLR2 is found to be increased in post-mortem brains of PD patients (Dzamko et al. 2017). Further, microglia are known to be able to detect oligomeric aSyn through TLRs (Kim et al. 2013). These observations make aSyn an interesting target for immunization as a disease modifying strategy. In fact, there are several current clinical trials aiming for passive immunization by direct administration of antibodies against aSyn (Bae et al. 2012) or active immunization by subcutaneous

injection of short immunogenic peptides mimicking aSyn (Kalia, Kalia, and Lang 2015). However, all these studies are carried out in patients with already advanced stages of the pathology and therefore aiming only to slow or reduce the spreading of the synucleinopathy rather than having a regenerative effect.

1.4.2 LRRK2 (Leucine-rich repeat Kinase 2)

LRRK2 is a complex multi-domain protein consisting of a catalytic core with a GTPase and a kinase domain surrounded by a series of potential protein–protein interaction domains (Cookson 2010).

The LRRK2 gene was found to be located at the PARK8 locus and was shown to cause familial autosomal-dominant late-onset PD. Patients with LRRK2 mutations show a clinical phenotype almost indistinguishable from patients with idiopathic PD. The majority of patients carrying a LRRK2 mutation exhibit Lewy body pathology (Zimprich et al. 2004; Lin and Farrer 2014). All mutations occur in the enzymatic core of LRRK2. The G2019S, the most common one, is found in the kinase domain leading to a gain-of-function (West et al. 2005) that was shown to mediate neuronal toxicity of mutant LRRK2 (Greggio et al. 2006; Smith et al. 2006). There are eleven key LRRK2 kinase inhibitors (Taymans and Greggio 2016) which have shown promising results in preclinical models and indicate neuroprotective effects (Mendivil-Perez, Velez-Pardo, and Jimenez-Del-Rio 2016; Lobbestael et al. 2016; Daher et al. 2015; Saez-Atienzar et al. 2014; Ramsden et al. 2011). It is, however, questionable how translatable these findings are to the clinic and safety concerns remain to be addressed, as recent study on non-human primates revealed pulmonary changes similar to LRRK2 knockout phenotypes in mice (Fuji et al. 2015).

1.4.3 Parkin

Parkin is encoded by the PARK2 gene. Mutations in Parkin, leading to loss-of-function, are the second most common cause of parkinsonism and result in an autosomal-recessive form of early-onset PD, although mostly lacking Lewy body pathology. On the other hand, Parkin is found in Lewy bodies of sporadic and familial PD patients. Parkin acts as a redox sensor for oxidative stress in cells, working in the degradation of damaged mitochondria. It acts as an E3 ubiquitin ligase responsible for poly- and monoubiquitination for the targeting of proteins to proteasomal degradation (Abou-Sleiman, Muqit, and Wood 2006).

Increased oxidative stress, impaired mitochondrial function, and increased aSyn levels were observed in PARK2 iPSC-derived neurons (Imaizumi et al. 2012). Parkin has been shown to have a neuroprotective

effect for synucleinopathies making it a promising protein for viral mediated gene therapy (Lo Bianco et al. 2004; Choong and Mochizuki 2017).

1.4.4 PINK1 (PTEN-induced kinase 1)

Mutations in PINK1 are linked to ~1-2% of early-onset PD cases (Hatano et al. 2004). PINK1 is a protein kinase, with a highly conserved kinase domain and is associated to mitochondria (Narendra, Walker, and Youle 2012). The wild type protein appears to protect from stress-induced mitochondrial dysfunction and apoptosis (Deng et al. 2005). An involvement of mutated PINK1 in the pathogenesis of PD was shown in several studies. PINK1, together with parkin, plays an important role in mitophagy. Without PINK1, it is not possible to recruit parkin to the mitochondria. PINK1 phosphorylates ubiquitin, which is required for the activation of parkin (Koyano et al. 2014).

PINK1 has been shown to interact with aSyn and provides protective effect against aSyn-induced neurodegeneration, thus presenting a possible therapeutic target (Liu et al. 2017). PINK1 itself can be targeted pharmacologically: the substance Kinetin has been found to restore catalytic activity of mutated PINK1 (Hertz et al. 2013) and just recently it was found that niclosamide can indirectly activate endogenous PINK1 in cells (Barini et al. 2018).

1.4.5 GBA1 (glucocerebrosidase)

The GBA1 gene encodes for the lysosomal hydrolase glucocerebrosidase (GCase) which catalyses the cleavage of glucocerebroside within the lysosome. Homozygous mutations in GBA1 cause Gaucher's disease, an autosomal recessive lysosomal storage disorder (Stirnemann et al. 2017). Heterozygous mutations in GBA1 gene are also associated with strongly increased risk for PD (Sidransky et al. 2009). Experimental therapeutic interventions include increasing GCase activity by AAV-mediated expression in the CNS (Sardi et al. 2013) and inhibiting glycosylcerebroside synthesis. For the latter, a clinical trial by Sanofi has started 1.5 years ago (ClinicalTrials.gov identifier NCT02906020). The major limiting factor to developing therapeutic targets for GBA1 in PD is the lack of understanding of the precise mechanism by which GBA1 contributes to disease acceleration and synucleinopathy formation (Sardi et al. 2013).

1.5 Current Therapies

1.5.1 L-DOPA

Nowadays the most effective therapeutic strategy for the management of parkinsonism is the replacement of DA with L-DOPA but the treatment does not alter disease progression, inadequately controls non-motor symptoms and also leads to severe side-effects because of the required increase in dosage with disease progression (Volta, Milnerwood, and Farrer 2015). L-DOPA is able to cross the blood-brain barrier and is then decarboxylated to DA within the nigrostriatal neurons (Pallone 2007). Overall, it is effective in the first phase of therapy (honeymoon period), but with the progression of PD complications like the shortening of effect duration, dyskinesia (abnormal, involuntary movement) and motor fluctuations appear in most of the patients. A different strategy is to utilize direct DA receptor agonists, which can be used early in disease or in combination with L-DOPA in later phases (Rao, Hofmann, and Shakil 2006). The major unmet medical need in PD is the availability of therapies slowing down the progression of the disease.

1.5.2 Deep Brain Stimulation (DBS)

Besides pharmacological therapy, deep brain stimulation (DBS) is an alternative approach for advanced PD therapy (Okun et al. 2007) which involves the surgical implantation of stimulating electrodes into specific areas of the brain, the subthalamic nucleus (STN) being the most common target. The treatment helps to improve motor symptoms, particularly when long term medication ceases to provide rescue of motor and non-motor symptoms (Deuschl, Paschen, and Witt 2013). There are also indications that with long-term treatment by DBS symptom worsening is slowed down (Tagliati, Martin, and Alterman 2010). However, it has to be noted that mechanisms underlying the effects of this treatment are still unclear. It is speculated that the therapy might not act only as a stimulation but has a modulating effect on neurons, neuronal plasticity, and long-term neuronal reorganization (Ashkan et al. 2017).

1.5.3 Gene Therapy

A lot of effort has been invested into gene therapy approaches. There have been different clinical trials based on either the delivery of a neurotransmitter-producing enzyme (Emborg et al. 2007; Luo et al. 2002; Kaplitt et al. 2007; LeWitt et al. 2011) or a neurotrophic factor (Kirik et al. 2017; Kells et al. 2010; Eberling

et al. 2009). Delivery is generally based on AAV2 vectors, which are characterized by little to no safety issues or side effects, but outcomes remained mostly disappointing mainly due to hardly controllable transgene expression (Bartus, Weinberg, and Samulski 2014; Warren Olanow et al. 2015).

1.5.4 Cell Replacement Therapy

In the last two decades, stem cells revealed as a new approach in PD understanding and potential therapy development. Human induced pluripotent stem cells (hiPSCs) are easily accessible and can be differentiated into genetically identical DA neurons (Swistowski et al. 2010; Kirkeby et al. 2012; Kriks et al. 2011; Hartfield et al. 2014). Results in drug screening assays therefore can be translated to humans more easily. More importantly, a lot of expectation is now placed on the so-called regenerative medicine, using patient-derived cells for replacement of lesions. Patient-derived cells, either being from healthy or PD donors, can have different origins, the most relevant being neuronal stem cells (NSCs), bone marrow mesenchymal stem cells (BM-MSCs) and human embryonic stem cells (hESCs) or hiPSCs-derived neurons. NSCs and BM-MSCs have already entered clinical phase trials, whereas hiPSCs-derived neurons are still in preclinical phases. Except hESCs, all donor cells are fit for autologous and allogenic transplantation.

Until now, preclinical studies using hESCs or hiPSCS are mainly conducted on lesion models in rodents (Grealish et al. 2010) and numerous preclinical studies have presented satisfying engraftment in those models (Grealish et al. 2014; Kriks et al. 2011; Kirkeby et al. 2017). Successful engraftment of hiPSC derived DA neurons has also been observed in non-human primate models (Kikuchi et al., 2017). However, considerations remain that hinder the step to translational application, like robust quality and quantity of obtained neurons and unclear mode of action of the engrafted tissue (Steinbeck and Studer 2015). A more detailed report on application of stem cells as models and clinical trials is given in chapter 1.7.2(Human stem cells, Disease modelling and cell therapy*).*

1.6 Experimental models for PD

1.6.1 Animal models

The aim of animal models is to replicate features of PD in a systemic environment as closely to disease as possible. For this purpose, an ideal model would need to replicate the hallmarks of the disease, namely:

- Progressive loss of SNpc DA neurons
- Loss of striatal DA
- Lewy body pathology formation
- Presentation of the first three phenomena with age

Animal models in PD can be categorized into toxin and genetic models. None of the models however can reproduce all the above-mentioned characteristics.

The most used toxin models are 1-methyl-4-phenyl-1,2,3,6-tetrahydropyridine (MPTP) and 6-hydroxydopamine (6-OHDA). MPTP is a prodrug to the neurotoxin 1-methyl-4-phenylpyridinium (MPP+). MPTP is able to cross the blood brain barrier and is then captured in lysosomes of astrocytes, which convert MPTP to MPP+. MPP+ is released from the astrocytes and taken via DAT into DA neurons where it disrupts the mitochondrial respiration chain. From the histological point of view, MPTP-induced neurodegeneration is very similar to what happens in PD (Seniuk, Tatton, and Greenwood 1990) but does not lead to Lewy body formation (Halliday et al. 2009).

In contrast to MPTP, 6-OHDA cannot cross the blood-brain barrier and has to be actively administered by stereotaxic injection, normally unilaterally, into the striatum or medial forebrain bundle (MFB). This procedure causes neurodegeneration of DA neurons without induction of Lewy pathology, similar to MPTP. Both models display impairment of motor functions, evaluated via behavioural assessments, due to disruption of the nigrostriatal pathway and striatal DA depletion. However, DA neuron loss is rapid and neither age-dependent nor progressive, thus differing substantially from the disease presentation in humans.

The advent of PD genetics led to the generation of genetic models, whether animal or cellular, that recreate the genetic lesions observed in familial PD. Through creation of animal or cell models carrying mutations in the genes *LRRK2* or *SNCA,* one can model autosomal dominant PD; mutations in PINK1, Parkin or DJ-1 recreate the genotype of autosomal recessive cases. Genetic modelling of PD in animals is not a straightforward approach. Rodents, for instance, do not develop PD naturally, probably because of their shorter lifespan and thus lacking (relative) advanced age as a major risk factor. Invertebrate models

such as *Drosophila melanogaster* and *Caenorhabditis elegans* do not express key genes correlated to the disease and rely on transgenic methods. There are several models for autosomal dominant PD, carrying gene mutations in LRRK2 or SNCA, that have shed light on the consequences of those mutations. The same holds true for autosomal recessive models. For both, autosomal dominant and recessive models, an age dependent disease progression was observed in *Drosophila melanogaster*, whereas it could not be seen in mouse models (Dawson, Ko, and Dawson 2010).

Toxin animal models have limitations in terms of failing to reproduce the disease in full. Also genetic animal models can fail to reproduce disease phenotype, like for example Parkin knock-out mice that do not show any phenotypical symptom suggestive of PD (Perez and Palmiter 2005). Yet, genetic models, even if they do not reproduce the entire phenotypical spectrum of the disease, recapitulate dysfunctions of the nigrostriatal system, neuropathologies and motor or cognitive alterations and are useful for modelling early and asymptomatic stages of the disease.

1.6.2 Cellular models

Cellular models in an *in vitro* system clearly have the drawback that they take the disease out of a systemic context. In comparison to animal models, pathology can be reproduced much quicker and work can be up-scaled easier, which is the reason why cellular models often are the go-to approach for drug screenings. Important non-patient specific cellular models are neuroblastoma cell lines SH-SY5Y, SK-N-MC, SK-N-BE, embryonic carcinoma cell line NTera-2/NT2 line, hNT (or LBS), pheochromocytoma cell line PC12, immortalized human embryonic mesencephalic cells (LUHMES, ReNcell VM NSCs) and mesencephalic neuroblastoma cells (MES) (Schüle 2009; Falkenburger, Saridaki, and Dinter 2016). In the same context, one should mention the significance of primary mouse or rat neuron cultures.

The above mentioned cell models are helpful for disease investigation as many of them provide the most important molecular characteristics of DA neurons (Pahlman et al. 1990; Presgraves et al. 2004) and respond to PD associated toxins (Storch et al. 2000; Kutty et al. 1991) and therefore offer an important platform for pathway investigation connected to the disease. Neuroblastoma cells can be differentiated into neuron-like cells using Retinoic Acid and in this way become more similar to the cell type they are intended to mimic (Lopes et al. 2010). However, being of tumorigenic origin, they do not only present a bias due to the gene expression of tumour suppressor genes, but they also are of clonal origin and present

chromosomal aberrations (Gilbert et al. 1984), and for these reasons clearly fail in reproducing a natural neuronal phenotype.

1.7 Human stem cells

1.7.1 Derivation of embryonic and induced stem cells

Embryonic stem cells (ESCs) are pluripotent cells derived from the inner cell mass of the mammalian blastocyst. They are capable of unlimited, undifferentiated proliferation *in vitro*, which has been proven almost 40 years ago by isolating mouse embryonic stem cells (Martin 1981; Evans and Kaufman 1981). The first human ESCs (hESCs) were isolated in 1998 (Thomson et al. 1998). The ability of providing human embryonic stem cells together with their potential to develop into theoretically any other cell type of the human body was a major breakthrough. However, the use of hESCs raises important ethical concerns, as the only possibility to obtain this cell type is by ending the developmental process of a potentially viable and healthy human being. For these critical reason, access to this highly valuable cell model has been limited and underlies strict ethical and legal regulations.

In 2006, the group of Shinya Yamanaka presented a method to derive hESCs-like cells from human fibroblasts by introduction of four factors: Oct3/4, Sox2, c-Myc, and Klf4 (the so called “Yamanaka factors”, (Takahashi and Yamanaka 2006). They called these cells human induced pluripotent stem cells (hiPSCs). This Nobel Prize-awarded work opened the era of stem cell derived cell modelling systems.

1.7.2 Disease modelling and cell therapy

To differentiate neurons from hiPSCs or hESCs (together further on referred to as human pluripotent stem cells, hPSCs), neuroectoderm formation is necessary (Begum et al. 2015), a concept which was already established by (Spemann and Mangold 1924). The pathways underlying these mechanisms have been established over many years in model systems like frog, chicken, mouse and zebrafish embryos (Munoz-Sanjuan and Brivanlou 2002) and the interplay of BMP-, Wnt- and FGF-signalling that leads to neuroectoderm and neural tube formation had been known already in the early 2000s (Wilson et al. 2001). Sonic hedgehog (Shh) is a crucial morphogen, whose signalling is gradient dependent along the dorso-ventral axis of the neural tube and leads to induction of different neuronal and glial cell types (Patten and

Placzek 2000). Most importantly, a sensitive balance between Wnt- and Shh-signalling leads to the floor plate formation of the neural tube (Joksimovic et al. 2009) which is the developmental origin of mDA neurons (Ono et al. 2007).

Nowadays, one can roughly distinguish two approaches to derive neural cells from stem cells: embryoid body directed, and monolayer directed. More relevant for this project is the monolayer approach, where hPSCs are driven to commit directly to a floor plate cell identity. The ground for this methods was laid by (Chambers et al. 2009), who identified small molecules that allow a highly efficient neuronal induction by inhibition of SMAD-signalling. The protocol was complemented subsequently (Fasano et al. 2010) and completed to one of the most cited protocols for derivation of DA neurons from hPSCs (Kriks et al. 2011).

Modelling PD with stem cell derived neurons holds the potential to solve the problem that has hampered PD modelling efforts until now: the lack of access to cells relevant to the disease from PD patients. Not only, can one have an *in vitro* culture of human DA neurons that can help to understand this cell type generally, but also cells can be derived from both familial and idiopathic PD patients, in addition to at-risk individuals carrying PD-linked genetic alterations. In fact, implications in oxidative stress management have been observed in mDA neurons derived from patients with SNCA triplication and LRRK2 G2019S mutation (Byers et al. 2011; Nguyen et al. 2011). The ability to generate isogenic controls from the same patients carrying mutations (Soldner, Laganiere, et al. 2011) further increases the relevance and accuracy of this model.

Efficiency of hPSCs derivation is variable from patient to patient, as is also the efficiency to generate mDA neurons from patient-derived cells. It is highly dependent on protocol type and there is no consistency in literature on percentages of TH positive cells obtained. This major consideration has to be taken into account when using this cell model, as depending on the readout method, it is not possible to exclude non-DA cells from analyses or to distinguish them morphologically from other neuronal types. In addition, the functionality and maturation of mDA neurons derived from hPSCs is a hot debate in the field. In recent years, research efforts have grown in order to prove functionality of patient-derived mDA neurons (Hartfield et al. 2014; Fedele et al. 2017) but there is still no robust timeline for maturity. Transcriptomic analyses indicate that hPSCs derived mDA neurons are more similar to prenatal neurons (Sandor et al. 2017), hinting the possibility that one may miss different information with this model system, when investigating a disease whose major risk factor is age.

A second important branch of application of patient derived DA neurons, with a huge potential for development, is cell replacement therapy. Preclinical trials with 6-OHDA lesioned rodents have shown that transplanted hPSCs derived mDA neurons do successfully engraft (Kriks et al. 2011; Kirkeby et al.

2012), re-establish projections and eventually ameliorate motor phenotypes (Grealish et al. 2014; Grealish et al. 2010).

Clinical studies using hESCs derived neural precursor cells for treatment of PD have recently started (clinicaltrials.gov identifier NCT03119636;) and a new initiative was formed by different groups around the world that share an interest for using hPSC derived DA neurons for PD (httP://gforce-pd.com"). Teams from this initiative plan to start clinical trials in the upcoming years and efforts are made to harmonize these trials to gain maximal comparability and decrease risks as much as possible (Barker et al. 2017).

In the past decade, genome engineering using targeted nucleases like TALENs (Tal-effector-like-nucleases) or Cas9 has gained major significance in the stem cell field, providing the possibility to correct genetic mutations that lead to disease. In this way, one can create isogenic controls for *in vitro* models and, as a future perspective, correct patient derived cells for subsequent autologous transplantation.

1.8 CRISPR/Cas9

The CRISPR/Cas9 system as a programmable DNA cleaving machinery has been described simultaneously by Jennifer A. Doudna together with Emmanuelle Charpentier (Jinek et al. 2012) and Feng Zhang's group (Ran et al. 2013b).

Necessary for the establishment of this method was the preceding discovery of repetitive sequences with common structural motifs in more than 40 prokaryotes genomes made by many research groups, and the eventual classification as CRISPRs: Clustered Regularly Interspaced Short Palindromic Repeats (Jansen et al. 2002). Jansen et al. also discovered four CRISPR-associated genes (Cas genes) although at the time their function was not clear. Only later on it was discovered that the CRISPR repeats derive from foreign pre-existing sequences (Bolotin et al. 2005; Mojica et al. 2005) and are part of an adaptive self-defence system that protects bacteria from invading phages (Barrangou et al. 2007). Three types of CRISPR systems are known (I-III). Here I will focus on the discussion of Type II, as it is the system usually employed for targeted genomic engineering and therefore most relevant to this work.

The CRISPR Type II system consists of a cluster of Cas genes, non-coding RNAs and the CRISPRs. Upon invasion, foreign DNA is selected by sequences called protospacer adjacent motifs (PAMs) and part of the foreign DNA is incorporated as a protospacer into the CRISPR locus by Cas1 and Cas2 (see Fig. 2, Phase I Immunization). The recognition of the PAM works in an unknown fashion (Makarova et al. 2011). In this manner, the CRISPR locus is build. The CRISPR locus containing the integrated spacers is expressed as a

long transcript (pre-crRNA) which is processed as small crRNA molecules. The crRNA consists of a 20-nt sequence stemming from a foreign sequence and a partial direct repeat (Ran et al. 2013b) which pairs with the trans-encoded small RNA (tracrRNA). This tracrRNA-crRNA structure is necessary for the Cas9 enzyme to recognize a target sequence, where it is led to by the homologue sequence in the crRNA (see Fig. 2 Phase II Immunity).

The *Streptococcus pyogenes* (*S.pyogenes*) Cas9 is the most studied of the Cas9 enzymes. Its PAM sequence is NGG and it can be programmed with a chimeric tracrRNA:crRNA molecule duplex, called single guide RNA (sgRNA) (Jinek et al. 2012). Once the Cas9 is guided with the sgRNA to its target, it induces a double strand break (DSB) in the DNA. Under these conditions, the only limitation for specifically targeting any genomic sequence is the location of the PAM sequence that has to be immediately downstream of the 20nt guide RNA sequence.

Upon cleavage, it is the cell´s own repair system that introduces mutations at the cutting site. Without a repair template provided, the DNA damage is repaired by Non-homologous-End-Joining (NHEJ), a conserved mechanism that ensures cell survival but is very error prone and based on random base insertion (Chen et al. 2001; Gong et al. 2005). However, when a repair template is given as a partially homologue DNA template, a faithful repair of the DSB is possible through the process of homologous recombination (HR). In this process, an exchange of identical or semi-identical sequences between the DNA strand carrying the DSB and the intact repair template takes place (San Filippo, Sung, and Klein 2008; Pardo, Gómez-González, and Aguilera 2009).

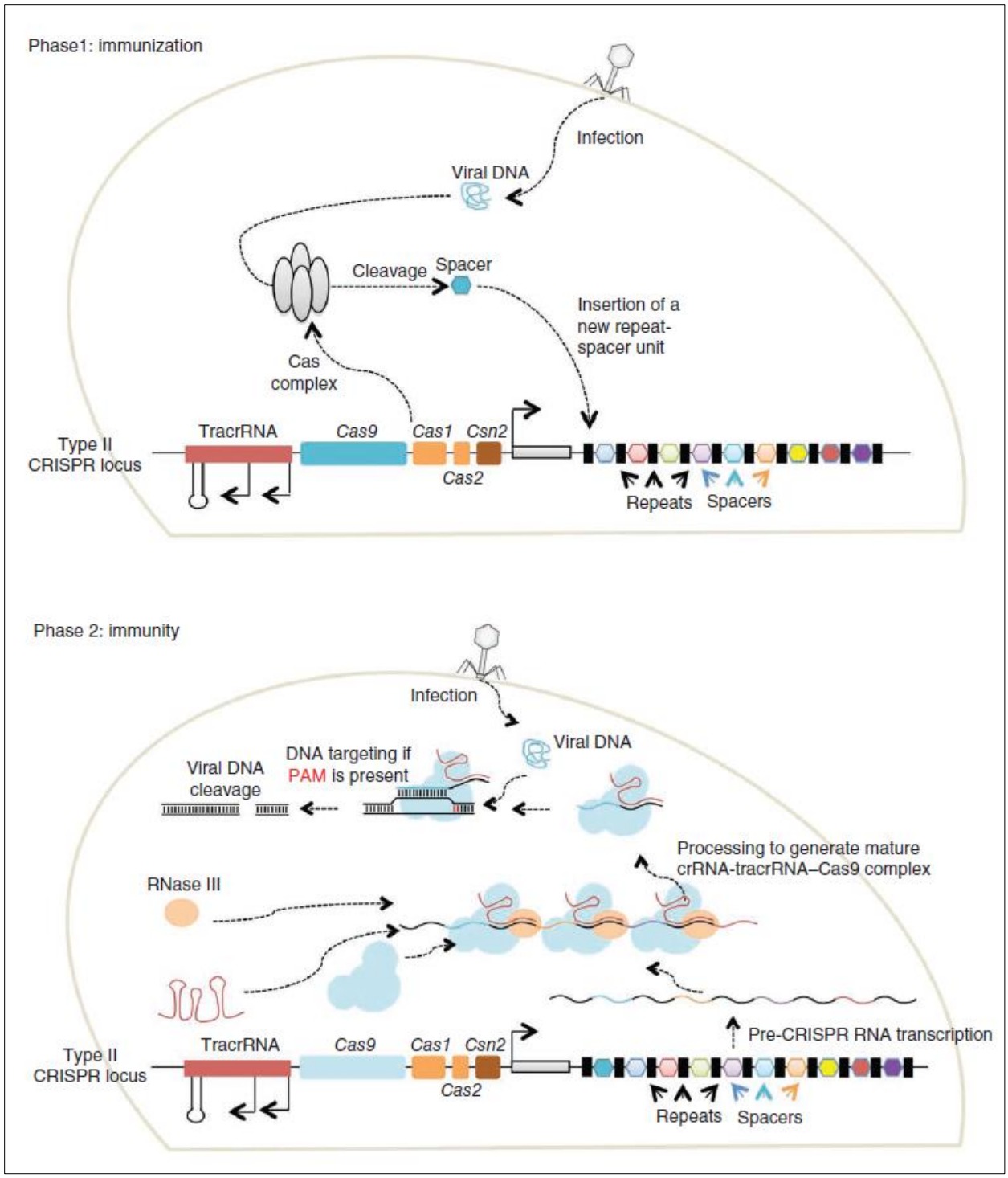

Fig. 2 Schematic representation of functioning of Type II Cas9 system in bacteria ((Mali, Esvelt, and Church 2013)

2 Aim of the thesis

The aim of this thesis was to create knock-in hiPSCs that carry fluorescent reporter genes at two distinct loci, whose gene expression is supposed to be characteristic of dedication to mDA cell fate, which are *TH* gene for tyrosine hydroxylase (TH) and *KCNJ6* gene for G protein activated inward rectifier potassium channel 2 (GIRK2). The combined presence of these two proteins is marking the A9 subtype of DA neurons, most susceptible in PD.

For CRISPR/Cas9 editing, specific sgRNAs were designed for targeting the two different loci. For both loci, a donor template was designed in order to be delivered to the target site and enable HR at the stop codon of two loci. A knock-in strategy was designed which implied replacing the stop codon of both loci with an approximately 1500bp fragment containing the sequence for a T2A peptide, a fluorescent protein and an antibiotic resistance cassette with a promoter flanked by loxP sites. The T2A peptide's function is to allow "cleavage" of the fluorescent protein from the target protein, to ensure evading fusion protein formation. In this manner, during *in vitro* differentiation of hiPSCs to DA neurons, once TH and GIRK2 are expressed through an endogenous promoter, also the fluorescent proteins will be expressed and mark neurons that are of A9 identity.

The overall objective of this work is to present a genetic engineering method to enable identification of DA neurons, and specifically A9 DA neurons, that are derived *in vitro* from induces pluripotent stem cells.

3 Material and Methods

All reagents used in this work, together with catalogue number and manufacturer, as well as primers mentioned in the text with full DNA sequence can be looked up in Appendix, 7.2 and 7.4List of reagents.

3.1 CRISPR/Cas9 constructs

3.1.1 Design of single guide RNAs

In order to enable Cas9 targeting of genomic loci, single guide RNAs had to be designed around the stop codon of both *TH* and *KCNJ6* genes in order to induce double strand breaks (DSBs) in this region. The Cas9 usually cuts 3bp upstream of the PAM sequence so we were looking for PAM sites as near as possible to the stop codon.

Custom sgRNAs for each target were designed *in silico* via the CRISPR Design Tool ("http://crispr.mit.edu/") developed by the Zhang Lab at MIT in 2015. A region of 50bp up and downstream of the target site was inserted as query sequence. Target genome was set to human. The guide RNAs nearest to the target site, the stop codon, were chosen. A total of four guide RNAs for the *TH* locus and five for the *KCNJ6* locus were selected, as it is advisable to test out at least four guide RNAs for efficiency to induce double strand breaks.

The sequences of the guide RNAs are listed in Tab 1.

Locus	Guide RNA Sequence 5' → 3'	PAM Sequence	Inverse likelihood for off target
TH sgRNA 1	GCCCATGCGCTGAGTGCCAT	TGG	66
TH sgRNA 2	TGCGCTGAGTGCCATTGGCT	AGG	76
TH sgRNA 3	AGTGCCATTGGCTAGGTGCA	CGG	71
TH sgRNA 4	GACGCCGTGCACCTAGCCAA	TGG	90
GIRK sgRNA 1	CCAAAGTTTAGTGCCCTAGC	TGG	88
GIRK sgRNA 2	CCAGCTAGGGCACTAAACTT	TGG	83
GIRK sgRNA 3	CAAAGTTTAGTGCCCTAGCT	GGG	83
GIRK sgRNA 4	GAGAAGGGTTTGCCCAGCTA	GGG	69
GIRK sgRNA 5	AGAGAAGGGTTTGCCCAGCT	AGG	59

Tab 1 Sequences of sgRNAs designed *in silico* with respective PAM sequence and inverse likelihood for making off target cuts.

3.1.2 Cloning of single guide RNAs

To clone in the sgRNA sequence into the selected expression vector (pX459V2.0-eSpCas9(1.1); Addgene plasmid # 108292), two partially complementary oligos with 4nt overhangs compatible for cloning into the vector were synthesized. We ordered oligos (CU23-CU40) according to sgRNA sequence established with *in silico* analysis (Tab 1) and added 5' overhang CACCG on the forward strand and 5' overhang AAAC on the reverse complement strand. These overhangs allow the sgRNA to be integrated into the BbsI restriction site of the vector.

3.1.2.1 Annealing of sgRNAs

To generate the double stranded sgRNAs to be cloned into the expression vector, the complementary single stranded oligonucleotides were annealed as follows:

Annealing reaction:
1 µl oligo 1 (100 µM)
1 µl oligo 2 (100 µM)
Nuclease free H_2O to final volume of 10 µl

The annealing reaction was carried out in a thermocycler (Eppendorf Mastercycler® pro S) at 95°C 5 min followed by a step at 20°C for 30 min. The annealed oligo were then diluted 1:250.

3.1.2.2 Cloning of sgRNAs into PX459

The expression vector was linearized with BbsI enzyme to allow the integration of the sgRNA with compatible cohesive ends. The restriction reaction was as follows:

Digest reaction of PX459:

1µg PX459	3.2 µl
10X NEBuffer 2.1	3 µl
BbsI	1 µl
H_2O	23.8 µl

The digestion reaction was incubated at 37°C for 1h in a water bath. After 1h, an additional 1 µl of BbsI was added and the reaction continued for 1h to ensure complete digest of the plasmid.
The linearized plasmid was purified from buffer and enzyme using the QIAquick® PCR Purification Kit. BbsI enzyme excised a 23-bp fragment from PX459 plasmid that cannot be retained by the Qiaquick Spin Column, which has a cut-off of 50bp. Purification was carried out according to manufacturer's instructions. BbsI is a Type IIS restriction enzyme. It cleaves at asymmetric sites, distant from its recognition sites. In this manner, it does not create sticky ends, which make dephosphorylation of the plasmid and phosphorylation of the oligos unnecessary and one can immediately proceed to the ligation.

Ligation reaction:

BbsI digested PX459 column purified	4 µl
annealed oligo duplex from step 3.1.2.1, 1:250	2 µl
T4 DNA Ligase	1 µl
T4 DNA Ligase Reaction Buffer	1 µl
H_2O	2 µl

The ligation reaction was incubated on 16°C in a thermoblock overnight.

The plasmid was transformed into One Shot™ Stbl3™ Chemically Competent *E. coli* according to the protocol provided by manufacturer. In short, bacteria were thawed on ice and incubated with 5µl of the ligation reaction for 30 min. A heat shock was performed on 42°C for 45 sec. After that, the bacteria were immediately placed on ice for 2 min. Then 450µl S.O.C. medium were added and the bacterial suspension incubated on 37°C shaking for 1 hour. After incubation in shaking incubator, the bacteria were plated onto an Agar plate containing 50µg/ml ampicillin and incubated on 37°C overnight.
In the morning, 5 colonies from each plate, one plate for each transformed sgRNA plasmid, were picked with a 20µl pipet tip and suspended in 10 µl H_2O.

To verify the correct insertion of the sgRNA into the plasmid, a colony PCR was performed. For this purpose, the reverse oligo of the corresponding sgRNA (CU24, 26, 28, 30, 32, 34, 36, 38, and 40) was used in combination with a forward primer annealing to the U6 promoter sequence in the plasmid (RF34).

Colony PCR reaction:

AmpliTaq Gold	0.3 µl
Buffer II	3 µl
dNTPs 10 mM	0.6 µl
Forward Primer 10 µM	0.45 µl
Reverse Primer 10 µM	0.45 µl
$MgCl_2$ 50 mM	4.2 µl
Betaine 5 M	9 µl
Bacteria suspension	1 µl
H_2O	11 µl

The PCR was run with the following cycling protocol:

95°C	10 min	
95°C	30 sec	} 40 cycles
X °C *	30 sec	
72°C	1 min	
72°C	7 min	
4°C	∞	

* annealing temperature was adapted according to different reverse primers

10µl of each PCR reaction were loaded on a 1% agarose gel (w/v) to verify correct band size.

For each sgRNA a positive colony was selected. 2ml of LB liquid culture medium containing 50 µg/ml ampicillin were inoculated with 5µl of colony suspension and grown at 37°C overnight.

The day after, the LB culture was pelleted leaving a small quantity for re-growing the culture. The plasmid DNA was extracted using the NucleoSpin® Plasmid Kit. The manufacturer's protocol was followed except for elution, which was carried out in H_2O.
A restriction digest was carried out to check that the purified plasmid DNA was not recombined. The enzymes used for the enzymatic restriction were NotI HF® and EcoRI HF®.

Restriction Digest Mix:

NotI HF®	1 µl
EcoRI HF®	1 µl
CutSmart® Buffer	2 µl
200 ng of plasmid	Variable
H_2O	Up to 20µl

Successful integration was confirmed by loading the digest on a 1% Agarose gel. The sgRNA plasmids were then sequenced to confirm the correct sequence of the sgRNA (Eurofins Genomics, Germany).

Once the sequence was confirmed, the plasmid was further amplified for a Midiprep. To allow this, the selected bacterial clone was grown in 100 ml of LB with 50ug/ml ampicillin ON at 37°C. The plasmids were isolated using the PureLink™ HiPure Plasmid Midiprep Kit according to manufacturer's instructions. Midireps were stored until use at -20°C.

3.1.3 Screening of sgRNAs in HEK293T-Cas9-TetON cells

3.1.3.1 Transfection of HEK293T-Cas9-TetON cells

24h before the transfection, cells were detached using Trypsin and plated in a 6-well culture plate (for each transfection 300.000 cells/well). HEK 293T Cas9 cells were cultured in DMEM high Glucose GlutaMAX™ with 10% Fetal bovine serum (FBS) and 1% Penicillin/Streptomycin, containing 2µg/ml Puromycine for antibiotic resistance selection. Cas9 expression was induced with addition of Tetracycline at a final concentration of 10µg/ml.
The following day, before transfection, cell medium was replaced with fresh medium.

Transfection reaction mix:

1µg of sgRNA plasmid	variable
OPTIMEM	200 µl
Lipofectamine LTX Reagent	12.5 µl
PLUS Reagent	2.5 µl

First, Lipofectamine LTX Reagent was mixed with OPTIMEM medium. Then the DNA was added and lastly the PLUS reagent. Lipid complex formation was allowed for 25 min at RT. Then the whole reaction mix was dispensed into the media of cells.

Cells were kept in the same media for at least 72h. Then cells were lysed for gDNA extraction with QIAamp® DNA Blood Mini Kit. Lysis and extraction was carried out following manufacturer's instructions.

The region around the cutting site of Cas9 was amplified with Q5® High-Fidelity polymerase. Primers were designed 400bp upstream and 1000bp downstream of the cutting site. The reason for this was, after T7 Endonuclease cleavage, to have eventually asymmetrically sized fragments that are easily distinguishable on an Agarose Gel.

Surveyor PCR Mix:

2x Q5 MasterMix	25µl
10µM Fw Primer	2.5µl
10µM Rv Primer	2.5µl
$MgCl_2$ 25mM	4.2µl
Betaine 5M	6µl
gDNA template 100ng	variable
H_2O	up to 50µl

Primer pair for *TH* locus: CU 59 + CU 60

Primer pair for *KCNJ6* locus: CU 61 + CU 62

98°C	30 min	
98°C	10 sec	} 40 cycles
X °C *	10 sec	
72°C	2 min	
72°C	7 min	
4°C	∞	

* annealing temperature was adapted according to different reverse primers

5µl of PCR was loaded onto a 1% Agarose Gel to check for correct amplification length. Once confirmed, PCR product was purified with QIAquick ® PCR Purification Kit according to manufacturer's instructions. After elution, concentration of purified PCR product was quantified by Nanodrop.
This PCR was used for downstream T7 Endonuclease Assay and a small quantity was sent for sequencing to the Eurofins sequencing facility (Germany) for "Tide" analysis (see chapter 4.2.2).

3.1.3.2 T7 Endonuclease Assay

Mix for Heteroduplex formation:

DNA		200ng
10X NEBuffer 2		2µl
H_2O		Up to 19µl

Heteroduplex formation in the thermocycler using the following conditions:

Initial Denaturation	95°C		5 minutes
Annealing	95-85°C	-2°C/second	
	85-25°C	-0.1°C/second	
Hold	4°C		∞

To the annealed product, 1µl of T7 Endonuclease was added and the mixture was incubated for 15min at 37°C.
Reaction was stopped by adding 1.5µl of 0.25M EDTA.

To analyse the fragmented PCR, the whole reaction was loaded onto a 2% Agarose gel with a loading buffer without bromophenol blue. For DNA visualization, GelStar™ Nucleic Acid Gel Stain was used.
The gel image was acquired using on ChemiDoc™ Imaging Systems and analyzed using ImageLab to measure the integrated intensity of not cleaved and cleaved bands.
For each lane, the fraction of the cleaved PCR product (f_{cut}) was calculated using the following formulas (Ran et al. 2013a):

$$f_{cut} = (\mathrm{b} + \mathrm{c})/(\mathrm{a} + \mathrm{b} + \mathrm{c})$$

Where “a” is the integrated intensity of the undigested PCR product, and “b” and “c” are the integrated intensities of each cleavage product.

The percentage of Indel formation was calculated with this formula:

$$\text{Indel } \% = 100 \text{ x } (1 - \sqrt{(1 - fcut\ )})$$

3.1.4 Design of Donor plasmids

For homologous recombination with CRISPR, for both genes, *TH* and *KCNJ6*, a donor sequence had to be designed, serving as a template for homologous recombination. The donor template had to consist of the sequence desired to be inserted into the genome, which is flanked by two homology arms left and right of this sequence.

Completed, the donor sequence had to consist in both cases of:

- The sequence for the fluorescent reporter gene
- Upstream of the fluorescent reporter the sequence for a T2A peptide allowing post-translational “cleavage” and thereby liberation of the tag from the protein of interest

And antibiotic resistance cassette with a viral core promoter, together flanked by two loxP sites 800bp homologue to the genomic region were the recombination was targeted. The length of these homology arms was based on findings, that large inserts require homology arm of this size (Ran et al. 2013a).

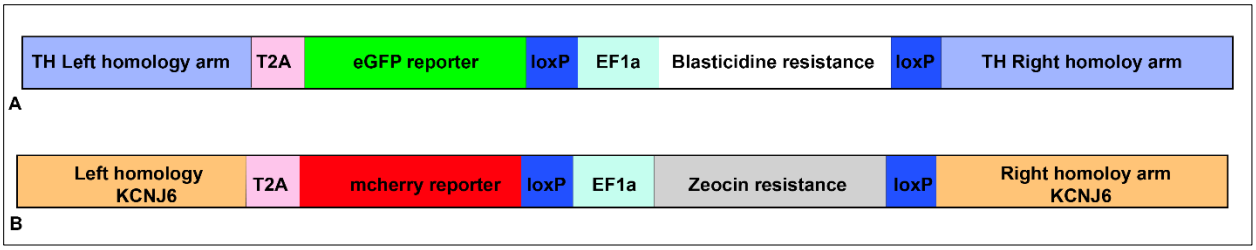

Fig. 3 Schematic representation of the design HR constructs for the TH locus (A) and the KCNJ6 locus (B).

3.1.5 Cloning of Donor plasmids for *TH* and *KCNJ6*

The design of the homologous sequences oligonucleotides was carried out with a specific strategy, identical for both genes. Homology sequences for both genes were amplified from human genomic DNA obtained from the MICROS study (Pattaro et al. 2007). The forward primer for the left homology arm and the reverse primer of the right homology arm were homologue to the genomic sequence and of 20 bp length. The reverse primer of the left homology arm was of 70bp length, spanning the sequence around

the stop codon of *TH* or *KCNJ6* respectively, but carrying the sequence of two restriction enzyme recognition sites (XbaI and XhoI) in the middle. In this way, the stop codon was split in the middle and a restriction site for subsequent cloning of the insert sequence was formed. The same was true for the right homology arm forward primer. A schematic representation of this primer can be seen in Fig. 4 at the example of the *TH* gene.

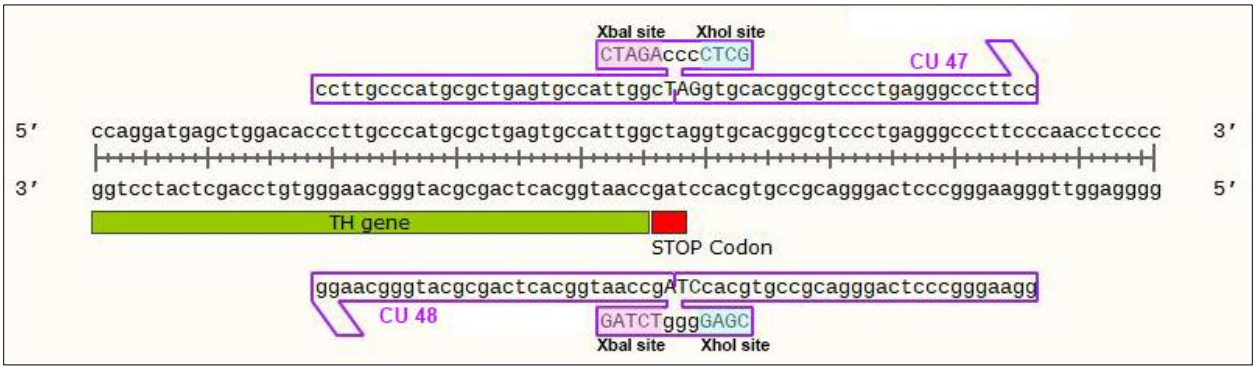

Fig. 4 Schematic representation of the design strategy for the homology arm left Rv primer (CU 48) and homology arm right Fw primer (CU 47), which creates the restriction sites for XbaI and XhoI at the stop codon of the *TH* gene.

These primers were then used to initially amplify the sequence for each homology arm separately. As can be seen on Fig. 4, the two separate homology arms share an overlapping part. This allows the two pieces to anneal to each other in the subsequent overlap extension PCR. After the overlap extension PCR, the 1600 bp fragment is cloned into a TOPO cloning vector. This vector is then digested with XbaI and XhoI to allow cloning of the insert sequence in between the homology arms. The insert sequence containing T2A peptide, fluorescent protein sequence, antibiotic resistance cassette with promoter and loxP sites, had been previously cloned into a TA cloning vector and kindly provided by Serena Gianelli (Stem cells and neurogenesis Unit, IRCSS Ospedale San Raffaele, Milano). The TA cloning vector containing the insert sequence had to be digested with XbaI and XhoI too.

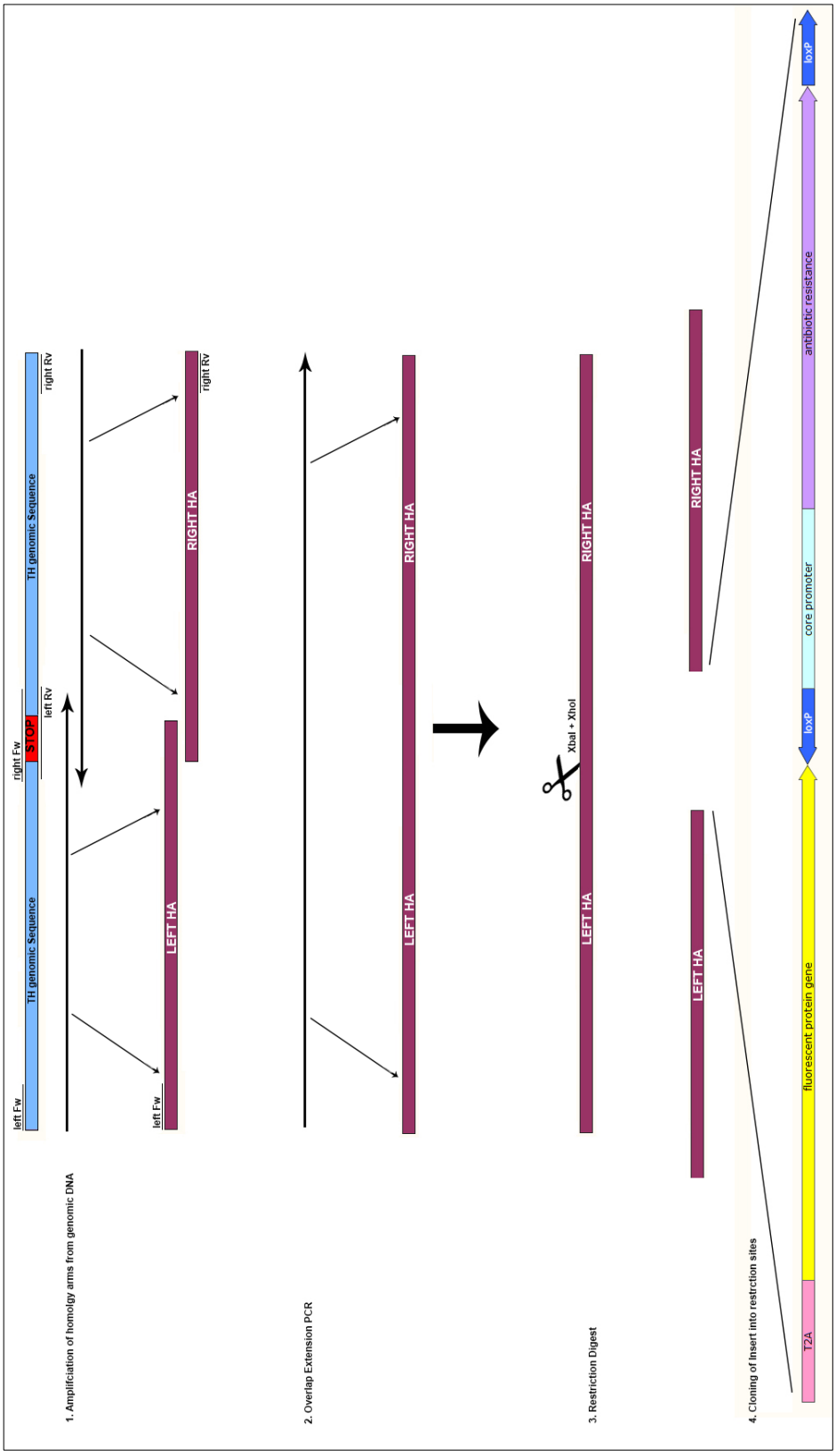

Fig. 5 Cloning strategy for homology arm following steps (1) Amplification from genomic DNA, (2) Overlap Extension PCR, (3) Restriction digest and (4) Cloning of insert into restriction site

Primer pairs used for this amplification process were:

TH Homology arms	Left HA	CU 41
		CU 48
	Right HA	CU 47
		CU 42
	Overlap extension	CU 41
		CU 42
GIRK Homology arms	Left HA	CU 43
		CU 46
	Right HA	CU 45
		CU 44
	Overlap extension	CU 43
		CU 44

PCR Reaction Mix:

2x Q5 Master Mix	25µl
10µM Fw Primer	2.5µl
10µM Rv Primer	2.5µl
$MgCl_2$ 25mM	4.2µl
Betaine 5M	6µl
gDNA template 100ng	variable
H_2O	up to 50µl

98°C	30 min	
98°C	10 sec	} 40 cycles
X °C *	10 sec	
72°C	2 min	
72°C	7 min	
4°C	∞	

* annealing temperature was adapted according to different reverse primers

5µl of PCR was loaded onto a 1% agarose gel to control for correct amplification length. Once confirmed, PCR products were purified with QIAquick ® PCR Purification Kit according to manufacturer's instructions. After elution, concentration of purified PCR product was quantified on Nanodrop.

Overlap Extension PCR:

Before the actual PCR, the two homology arms had to be annealed to each other in the annealing mix:

2x Q5 Master Mix	15µl
Left Homology arm ≈ 500ng	Variable
Right Homology arm ≈ 500ng	Variable
$MgCl_2$ 25mM	2.52 µl
Betaine 5M	3.6 µl
H_2O	up to 30µl

Annealing was carried out in a thermocylcer according to the following cycling protocol:

98°C	20 sec	} 20 cycles
49-69°C*	30 sec	
72°C	2 min	
4°C	∞	

* rise temperature by 2°C every second cycle.

After the annealing, the PCR reaction mix was completed by adding primers and adjusting all the reagents concentration to a 50µl reaction for the extension PCR:

Annealing Mix	30 µl
2x Q5 Master Mix	10µl
$MgCl_2$ 25mM	1.68 µl
Betaine 5M	2.4 µl
Left HA Fw Primer 10µM	2.5 µl
Right HA Rv Primer 10µM	2.5 µl
H_2O	to 50 µl

98°C	30 min	
98°C	10 sec	} 40 cycles
68 °C	10 sec	
72°C	2 min	
72°C	7 min	
4°C	∞	

Ligation into cloning vector:

The amplified 1600 bp long homology arms were cloned into the Zero Blunt® TOPO® from Invitrogen™.

PCR Product	4µl
Salt Solution	1µl
pCR™-Blunt II-TOPO®	1µl

Ligation mix was incubated for 5 minutes at room temperature and then placed on ice.

The plasmid was transformed into One Shot™ TOP10 Chemically Competent E. coli according to the protocol provided by manufacturer.

To verify the correct insertion into the plasmid a colony PCR was performed as described before, using the same oligo used for the overlap extension PCR.

For each Donor plasmid, three positive colonies were selected and grown in 2ml of LB liquid culture medium containing 50 µg/ml ampicillin at 37°C ON.
The day after, the LB culture was pelleted leaving a small quantity for re-growing the culture. The plasmid DNA was extracted using the NucleoSpin® Plasmid Kit (Macherey-Nagel). The manufacturer's protocol was followed except for elution, which was carried out in H_2O.

Before sending the plasmid for sequencing, a restriction digest with EcoRI was performed to check for possible bacterial recombination and that the plasmid was correctly amplified.
Successful integration and amplification was confirmed by loading the digest on a 1% Agarose gel. The donor plasmids were sent to sequencing to MWG sequencing facility to confirm the correctness of the homology arm and insert sequence (Eurofins Genomics, Germany).
Once the sequence was confirmed, the plasmids were further amplified for a Midiprep using the PureLink™ HiPure Plasmid Midiprep Kit (Invitrogen™) according to manufacturer's instructions. Midipreps were stored until use at -20°C.

3.2 hiPSC culture work

3.2.1 hiPS cell lines

The genetic engineering was carried out on three hiPSC lines in parallel, obtained from healthy donors were used. Namely:

- 802#7
- SFC 856-03-04 (STBCi063-A)
- SFC 840-03-05 (STBCi026-C)

Both SFC 856-03-04 and SFC 840-03-04 are cell lines from StemBANCC consortium, derived from skin fibroblast of healthy donors. The reprogramming method was non-integrating with Sendai virus. Cell lines were genotyped by SNP array and karyotyped with no abnormalities by the consortium.

Cell line 802#7 was derived from skin fibroblasts collected at the University of Lübeck and kindly provided by Dr. Alessandra Zanon (Institute for Biomedicine, Eurac Research). Reprogramming method was non-integrating using episomal vectors. Cell lines were karyotype without abnormalities (see chapter 4.1.4).

Cell line	Sex	Sample type	Clinical status
802#7	F	Fibroblast	healthy
SFC 856-03-04 (STBCi063-A)	F	Fibroblast	healthy
SFC 840-03-05 (STBCi026-C)	F	Fibroblast	healthy

3.2.2 hiPSC maintenance

hiPSCs cell lines were maintained in StemMACS™ iPS-Brew XF with supplement completed with 1% Penicillin/Streptomycin cultured on Matrigel coated plates. Cell culture medium was replaced every day. For weekend feeding, the daily volume necessary was added on Friday afternoon.

StemMACS™ iPS-Brew XF with supplement is not thermostable and was always kept at 4°C. Only the daily amount of necessary medium was taken from the medium bottle and warmed at RT to prevent degradation of basic-FGF (b-FGF) in the medium. b-FGF is a critical growth factor that enables the expansion of stem cells in their pluripotent state.

3.2.2.1 Matrigel coating

Matrigel Growth Factor Reduced (GFR) Basement Membrane Matrix was thawed ON on ice at 4°C. The protein concentration was taken from the synthesis report and the Matrigel diluted to a concentration of 1mg/ml proteins with cold Knock-out DMEM. The diluted Matrigel was then aliquoted with precooled tips to 1ml into precooled falcons (15ml) placed on ice. Keeping Matrigel always cool is essential to prevent premature gelling of the matrix. Aliquots were frozen until use at -20°C.

When coating, 1ml of Matrigel 1mg/ml was filled up with 11ml of cold Knock-out DMEM and then used for coating a cell culture dish, e.g. in a multiwell of 6, each well was coated with 1ml of Matrigel/DMEM solution. Matrix formation was allowed either at 37°C for 1h in the incubator or ON at 4°C.

3.2.2.2 Passaging of hiPSCs

hiPSCs were passaged 2-3 times a week based on their growth rate. Cells were passaged when confluence was superior to 80%. On the day of passaging, cells were washed once with PBS w/o Calcium and Magnesium at RT. Then, warm (37°C) TrypLE™ Express reagent was added, e.g. 0.5ml in a 6-well, and cells were moved to the incubator (37°C). After 5min, or when cells started detaching, using a P1000 tip cells were manually detached from the well bottom with careful movements and moved to a 15-ml Falcon tube. The well was then washed once with warm StemMACS medium (e.g. 1ml for a 6 well). Lastly, the TrypLE with the cells was diluted at least 10X with RT PBS w/o Calcium and Magnesium in order to stop the dissociation reaction. Cells were centrifuged at 200g for 5min and supernatant was aspirated with vacuum pump. To mobilize the cell pellet the falcon tip was flicked gently with the finger until pellet was dissolved, then the accurate amount of StemMACS medium was added containing 10µM StemMACS Y27632, ROCK-Inhibitor. This is a cell-permeable inhibitor of Rho-associated kinase (ROCK) and is commonly used to increase the survival and cloning efficiency of human pluripotent stem cells after dissociation into single cells. For amplification, split ratio usually was in a range of 1:3 to 1:5. Medium was changed daily.

3.2.2.3 Freezing and thawing of hiPSCS

When freezing hiPSCs, procedure for splitting was followed until after centrifugation as described above. After mobilizing the pellet, the cells were suspended in hiPSC-freezing medium consisting of KnockOut™ Serum Replacement (KOSR) containing DMSO at a final concentration of 10%. Generally, one 6-well was

detached and suspended in 1ml of freezing medium and transferred into a cryo-vial. The vial was frozen in freezing container (Mr. Frosty) ON at -80°C and then transferred into the liquid nitrogen tank for long-term storage.

When thawing hiPSCs, the vial was retrieved from the liquid nitrogen tank and immediately transferred into the 37°C warm waterbath. Once only small ice crystals were left in the freezing medium, 1ml of warm StemMACS medium was added to the suspension and cells were transferred into a falcon, which was filled up to 5ml with warm medium. Cells were centrifuged at 200g for 5mins. After centrifugation, the pellet was mobilized by flicking and warm medium with 10 µM ROCK-inhibitor was added to the cells. Generally, a vial frozen from a 6-well was replated into two 6-wells. Medium was changed daily.

3.2.3 hiPSC characterization

3.2.3.1 Immunocytochemistry for pluripotency genes

Cells were stained for well-established stem cell markers Oct4, Sox2, SSEA4, TRA-1-60. For immunofluorescence staining of characteristic pluripotency markers, the PSC 4-Marker Immunocytochemistry Kit was used. Fixative and Buffers for immunocytochemistry were provided by the kit and the protocol was followed according to manufacturer's instructions.

Cells were double stained for a nuclear and surface marker in two combinations, which are reported in Tab 2. Antibodies were all supplied in the PSC 4-Marker Immunocytochemistry Kit.

Target	Host species	Secondary antibody	Position	Combination
Oct4	Rabbit	Alexa Fluor®555 donkey anti-rabbit	Nuclear	1
SSEA4	Mouse	Alexa Fluor®488 goat anti-mouse IgG3	Surface	
Sox2	Rat	Alexa Fluor®488 donkey anti-rat	Nuclear	2
TRA-1-60	Rabbit	Alexa Fluor®555 goat anti-mouse IgM	surface	

Tab 2 Antibody combination used for immunostaining of hiPSC cells

Images of immunostained hiPSC cells were acquired with Leica TCS SP8 laser scanning confocal microscope.

3.2.3.2 qRT-PCR Analysis for pluripotency gene expression and transgene exclusion

Gene Expression analysis was performed for four different establishes pluripotency genes: Sox2, Oct3/4 and Nanog. For this purpose, total RNA from hiPSC line 802#7 and parental fibroblast line Fib802 as a negative control was extracted using the RNeasy® Mini Kit according to manufacturer's instructions. To obtain cDNA, 1µg of RNA was reverse transcribed using using SuperScript™ VILO™ cDNA Synthesis Kit:

Retrotranscription Reaction:

VILO-Reaction Mix	4µl
10X SuperScript Enyme Mix	2µl
RNA (1µg)	Variable
H_2O	Up to 20µl

Reaction was incubated at 25°C for 10 min, then at 42°C for 60 min in the thermocycler. Reaction was terminated with a final step at 85°C for 5min.

cDNA was diluted to 5ng/µl with nuclease free H_2O and amplified using All-in-One SYBR® Green qPCRMix using primers for Sox2, Oct3/4 and Nanog

2x qPCR mix	10µl
FW primer 5µM	1µl
Rv primer 5µM	1µl
cDNA5ng/µl	1µl
ddH20	7µl

qRT reaction was run according to the following cycling protocol:

95°C	10 min	
95°C	10 sec	} 40 cycles
60°C	20 sec	
72°C	15 sec	
72°C -95°C	6 sec (0.5°C/step)	
30°C	30 sec	

Amplification and SYBR® Green fluorescent detection was performed on CFX96 Real-Time PCR Detection System.

Expression was normalized using β-actin reference gene *ACTB*. Results were calculated using the $2^{-\Delta\Delta Ct}$ method. Briefly, average cycle times (Cts) of each target and the reference gene were calculated and ΔCt was determined ($Ct_{target} - Ct_{reference}$). $\Delta\Delta Ct$ was determined subsequently ($\Delta Ct_{hiPS} - \Delta ct_{Fibroblast}$). Fold increase was calculated using $2^{-\Delta\Delta Ct}$ equation.

For transgene exclusion, gDNA was extracted from hiPSC line 802#7 at P10 and parental fibroblast line Fib802 24h after transfection with reprogramming plasmids as a positive control. gDNA was extracted using QIAamp ® DNA Blood Mini Kit according to manufacturer's instructions. Amplification of specific episomal plasmid gene EBNA-1 and detection was performed as for pluripotency gene expression analysis normalizing expression to FBXO15 reference gene. As described above, results were calculated using the $2^{-\Delta\Delta Ct}$ method.

3.2.3.3 Alkaline Phosphatase staining

Along with expression of pluripotency markers, high alkaline phosphatase (AP) expression is an indicator of undifferentiated cells with the ability of self-renewal.

For AP staining, hiPSC were washed once with PBS and then fixed in 4% PFA for 15 min. at RT. For staining the commercially available kit Alkaline Phosphatase Staining Kit II was used and procedures followed according to manufacturer's instructions. Images of violet stained cells were taken with ZEISS Axio Vert.A1– Inverted Microscope in phase contrast mode.

3.2.3.4 Karyotyping

To prepare metaphases for karyotyping, cells were incubated in KaryoMAX™ Colecmid Solution™ for 4h in the incubator. Colcemid (N-desacetyl-N-methylocolchicine), 100 ng/mL final concentration, was added to prevent spindle formation during mitosis and helped arresting cells in metaphase, which allows separation of chromosomes for cytogenetic analysis. After 4h, cells were enzymatically detached using TrypLE and centrifuged in 15ml Falcon tube at 200g for 5 min. Then, supernatant was aspirated using the vacuum pump and the cell pellet was reconstituted in 6ml of a hypotonic 0.047M KCl solution. Cells were then incubated at 37°C for 18 min.

After hypotonic treatment, the suspension was inoculated with 0.5 ml fixative solution made of methanol and acetic acid 3:1 (v/v) and centrifuged at 200g for 5 min. Then, cells were suspended in 5ml fixative and incubated -20°C for 30 min.

The pellet was then centrifuged and washed with fixative 3 times and eventually suspended in 1ml of fixative.

Fixed metaphases were sent to the Institute of human genetics at Ludwig Maximilian's University Munich for karyotyping, where 50 metaphases were analysed and 18 metaphases were karyotyped by PD Dr. rer.nat. Stefan Müller.

3.2.4 Electroporation and Clonal Selection

3.2.4.1 Electroporation of hiPSCs

For engineering TH and KCNJ6 locus, hiPSCs were transfected with both sgRNA carrying plasmid and HR-Donor carrying plasmids, respectively. The most efficient way to transfect hiPSCs is with electroporation. For this purpose the Neon® Transfection System was used, which includes using a pipette tip as an electroporation chamber to transfect cell and thereby deliver nucleic acids.

a) Preparations for electroporation

On the day of the electroporation, a Matrigel coated 24-well plate was prepared as described in chapter 3.2.2.1 with four wells for each transfection.

For electroporation, Neon® Transfection System was used. Cells to be electroporated were pre-treated for 1h with 10µM ROCK-Inhibitor. For each transfection, $3x10^6$ cells were necessary, which corresponded to 2-3 confluent 6-wells, depending on cell line. Resuspension Buffer R and Electrolytic Buffer E2 (both part of the Neon® System) were left out of the fridge to come to RT. Neon® device was placed next to culture hood and the Neon® Pipette Station into the culture hood (decontaminated first with ethanol). A Neon® tube containing 3ml of buffer E2 was put into the Pipette Station. Transfection program was pre-set to 1250V, 20ms, 1pulse using the display interface on the Neon® device.

15µg of total DNA for each transfection were prepared (see detailed description below for copy number calculations) and 7.5 µg of a control plasmid expressing Red Fluorescent protein (RFP). For the RFP control, only half the amount of DNA was used as usually control plasmids are much easier to transfect and lead to an overestimation of efficiency. By taking only half the DNA amount, estimation of efficiency would likely be more accurate.

b) Copy number calculation

The total DNA amount to transfect was 15µg for each transfection. To get efficient HR, the ratio between Donor and sgRNA had to be 4:1. Actual 4:1 mixture of both plasmids was calculated based on the copy number of each plasmid. Copy numbers for each plasmids were calculated based on their molecular weight and the ratio adjusted accordingly (see Tab 3).

	TH Donor eGFP	TH sgRNA4	GIRK Donor mcherry	GIRK sg RNA4
bp	7122	9175	7104	9175
MW (g/mole)	4.63×10^6	5.9×10^6	4.62×10^6	5.96×10^6
concentration Midiprep (µg/µl)	1.38	5.3216	1.4	2.6457
copies/ng	1.30×10^8	1.01×10^8	1.30×10^8	1.011×10^8
copies/µl	1.30×10^{11}	1.01×10^{11}	1.30×10^{11}	1.01×10^{11}

Tab 3 Copy numbers calculated for each plasmid. Based on the MW the copy number per µg was calculated and then the copy number per µl based on the yield of the Midipreps.

	4:1 ratio	µg to transfect
µg TH Donor	3.11	11.35
µg TH sgRNA 4	1	3.65
TH total	4.11	15.00
µg GIRK Donor	3.11	11.35
µg GIRK sgRNA 4	1	3.65
GIRK total	4.11	15.00

Tab 4 Calculated actual ratios for Donors and sgRNAs for both constructs pairs and the resulting µg amount for each construct.

c) Electroporation

It was important to work methodically quickly and be well prepared to avoid long waiting periods when cells were detached or in the buffer as this would affect viability of the cells and success of the electroporation.

Electroporation was performed with three different cell lines, which all were transfected with TH constructs and GIRK constructs separately. In addition, each cell line was transfected with a control plasmid expressing RFP to monitor electroporation efficiency.

The following experiments were carried out:

Cell line	TH constructs	GIRK constructs	RFP
802#7	✓		
802#7		✓	
802#7			✓
SFC 856-03-04	✓		
SFC 856-03-04		✓	
SFC 856-03-04			✓
SFC 840-03-05	✓		
SFC 840-03-05		✓	
SFC 840-03-05			✓

For each transfection, 2 or 3 wells of a 6-well plate ($3x10^6$ cells) were detached as described above. After centrifugation, cells were suspended in PBS to a concentration of $3x10^6$ cells/ml. 1ml of the suspension was transferred to a sterile 1.5ml Eppendorf tube and spun at 400g for 3min in a benchtop centrifuge (Eppendorf Centrifuge 5418/R).

In the meantime, Matrigel was aspirated from plates and replaced with StemMACS containing 10µM ROCK-Inhibitor. Once cells were pelleted, PBS was aspirated and cells suspended in 150µl Buffer R. Finally, the DNA mix (Donor + sgRNA or RFP) was added to the cell/buffer mixture and everything was mixed by gently pipetting up and down.

A 100µl Neon® Tip was attached to the Neon® Pipette. This tip was used to draw up 100µl of cell/buffer/DNA mix. At this point, it was crucial to avoid the creating of air bubbles when aspirating as air bubbles would have caused arcing during electroporation leading to failed transfection.

The Neon® Pipet with the sample in the tip was immerged into the E2 Buffer and fixed in the Pipette Station. Electroporation was started by pressing “Start” on the display interface and successfully completed when “Complete” appeared on the display. Then, the pipet with the cells was removed and

the whole content transferred to the culture plate containing 2ml of warm StemMACS medium with 10µM ROCK-Inhibitor and distributed evenly among the four 24 wells.
The same procedure was followed for electroporating the positive RFP control. When changing DNA construct, the pipet tip had to be changed. When changing cell line, both pipet tip and Neon® Tube containing buffer E2 had to be changed.

3.2.4.2 Selection after electroporation

24h after the electroporation, a complete medium change with StemMACS was performed. At this point the positive RFP control was checked. Usually, at least 30% of cells could be observed to be successfully transfected with RFP and cells were 70-100% confluent in the well.
48h after electroporation the selection with Puromycin was started. Puromycin was used because it is the antibiotic resistance encoded on the pSpCas9-plasmid, which carries the Cas9 and the sgRNA. Cells that were not successfully transfected with at least the Cas9 plasmid should be selected out of the pool. In order to ensure maximum yield of resistant cells, four different concentrations of Puromycin were applied (hence the four 24-wells).

- 0.5µg/ml
- 0.25µg/ml
- 0.1µg/ml

The selection ability on different hiPSC lines is very density dependent and there is no generally appropriate concentration of antibiotic. In this manner, one will in any case end up with resistant cells, even if for example 0.5µg/ml is a too high concentration. The 0µg/ml condition was to monitor cell death in non-transfected cells to have an indication of selection success rate.

72h after electroporation medium was changed again completely containing the same Puromycin concentrations as the day before.
96h after electroporation medium was changed completely without Puromycin to allow cells to recover.

3.2.4.3 Low Density Plating

96h after electroporation, for each electroporation experiment a 6-well plate with mouse embryonic fibroblasts (MEF) was prepared. For this purpose, the 6-well plate was coated with 0.1% gelatine in sterile water for 30 min at 37°C.

A cryovial containing $2x10^6$ MEF cells was retrieved from the nitrogen tank and immediately warmed in the waterbath at 37°C. The cell suspension was transferred to a falcon with 5ml warm MEF-medium and centrifuged at 200g for 5min. After centrifugation, the supernatant was aspired with the vacuum pump and the falcon was flicked to mobilize the pellet. Cells were suspended in 12ml of MEF medium and transferred to the gelatine coated plate (2ml per well). MEFs were cultured in DMEM high Glucose GlutaMAX™ with 10% FBS, 1% Penicillin/Streptomycin, 1% MEM-NEAAs (non-essential amino acids). Cell attachment at 37°C in the incubator was allowed ON.

Five days after electroporation, Puromycin-selected cells were plated in low-density manner on MEFs. Upon antibiotic selection, if many cells survived the 0.5µg/ml Puromycin treatment, only this well was used for low-density plating. On the contrary, if only few cells were left in this condition, also the 0.25 and 0.1µg/ml treated wells were replated.

Medium was aspirated from cells with the vacuum pump and cells were washed once with RT PBS. Then 250µl TrypLE was added and immediately after 200µl were aspirated again, leaving only a thin film of TrypLE on the cells. Cells were incubated 5 min at 37°C. Then, the plate was tapped on the side with the hand to help cells detaching. If necessary, plate was moved to make TrypLe run over the centre of the well in order to wash cells off the bottom. In order to dissociate the cells into single cells, 1ml of RT PBS was added to the well and with a P1000 tip last remaining attached cells were detached and 10µl of suspension was taken for cell counting. The cell suspension was transferred to a sterile 1.5ml Eppendorf tube and spun at 200g for 5min.

After centrifugation cells were suspended in warm iPSC-medium composed of KO-DMEM, 20% KOSR, 1% MEM-NEAAs, 1% Penicillin/Streptomycin, 1% GlutaMAX™, 0.1 mM β-mercaptoethanol and 10 ng/ml basic FGF (bFGF). For cell survival, 10µM ROCK-Inhibitor was added. Different numbers of cells were plated: 25,000 cells/well, 10,000 cells/well and 5.000 cells/well. Each condition was plated in double (six wells in total). In case of a high survival rate, the 5,000 cells/well conditions would allow isolation of single colonies. In case of a low survival rate the 25,000 cells/well would present a high enough number of colonies to pick up and still have them as single colonies.

Remaining Puromycin selected cells were pelleted at 200g for 5min and used for genomic DNA extraction using QIAamp ® DNA Blood Mini Kit according to manufacturer's instructions. The DNA was used for early HR screen (see chapter 3.3.1).

Cells were cultured on MEF for approximately one week until appearing colonies were big enough to be picked up and transferred to a 96well. iPSC-Medium was changed daily with freshly added 10ng/ml bFGF.

3.2.4.4 Transferring single cell clones to 96well plate and clonal expansion

After one week, colonies grown from a single cell were big enough to be transferred by hand to a 96well plate coated with Matrigel for single clone expansion. For every transfected cell line, two 96 well plates were prepared and coated for at least 1h at 37°C. The Matrigel was aspirated and 50µl of warm StemMACS with 10µM ROCK-Inhibitor was added to each well. hiPSC colony quality and size was analysed at a stereomicroscope. Only small and uniformly shaped colonies not showing any differentiation were picked up (Fig. 6)

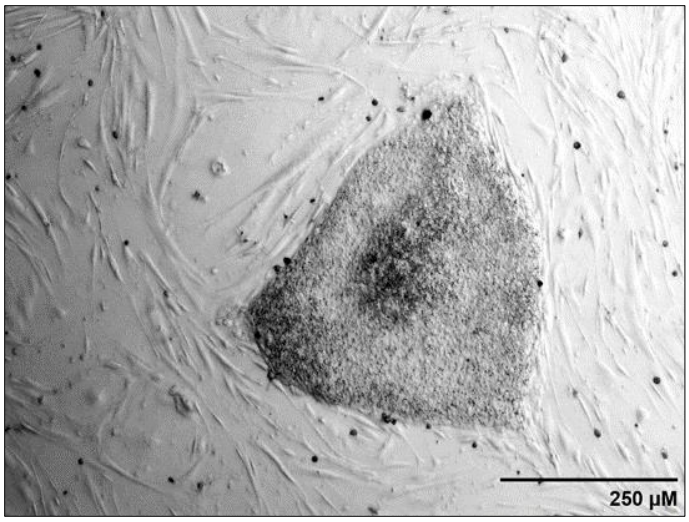

Fig. 6. Ideal morphology of iPSC colonies after one week.

In the well where colonies were picked out from, hiPSC-Medium was replaced with StemMACS containing 10µM ROCK-Inhibitor. Then with a P200 tip set to 50µl colonies were picked up singularly and transferred to the 96well plate. Plates were switched every 20minutes to allow warming up of medium. For each line, 192 colonies were picked.

The day after, medium was changed completely w/o ROCK-Inhibitor.
After approximately one week, most of the wells were confluent and plates ready to be split.

For splitting, a fresh 96 well plate coated with Matrigel was prepared. Medium from 96 well plates with cells was aspirated using the vacuum pump with an 8-channel adaptor. Wells were washed once with PBS. Then, wells were incubated in 50µl of PBS containing 0.5mM EDTA for 5 min at 37°C. After 5 min, EDTA solution was aspirated completely and plate was moved back to incubator for another 5 min. EDTA does not detach the cells so there was no risk to aspirate them. After the second round of incubation to each well 100µl of warm StemMACS with 10µM ROCK-Inhibitor was added. With a multichannel pipet, medium was pipetted up and down for five times in order to detach cells from the well's bottom. 50µl were of the cell suspension were transferred to the freshly plated 96 well. The remaining 50µl were left in the original plate.
Cells were moved back to incubator and medium was again changed daily. After 2 days splitting procedure was repeated in order to have three identical replica plates (see Fig. 7). After another 2-3 days of expansion, two of the three wells were frozen down as back up plates. The original plate of cells was used for genomic DNA extraction (see chapter 3.3.2).

3.2.4.5 Freezing of 96well plates

For freezing the 96 well plates, the procedures for splitting were followed until after EDTA incubation. At this point, cells were suspended in 50µl of Freezing medium consisting of 60% Medium, 30% ES-qualified FCS and 10% DMSO. Cells were again pipetted up and down 5 times and then the plate was sealed with an adhesive aluminium foil. To allow freezing with a controlled temperature gradient, the plates were transferred to a polystyrene box filled with paper towels, which was put into a -80°C freezer ON. The next day, the plate was transferred to the nitrogen tank for long-term storage.

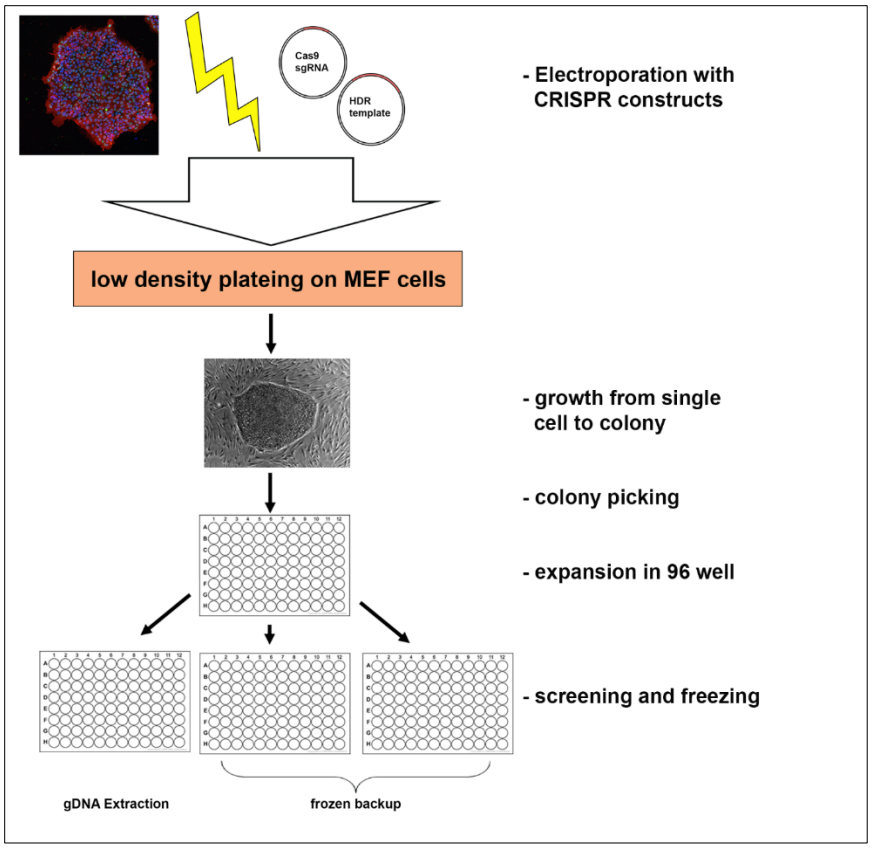

Fig. 7 Schematic representation of single cell clonal expansion of engineered iPSCs from electroporation to freezing down individual clones in 96 well plate.

3.2.4.6 Thawing of 96well plates

Once positive clones were confirmed with ddPCR (see chapter 3.3), they were thawed from the 96well plates. The day before, for each clone one well of a 24 well plate was prepared with MEF cells on gelatine (83.000 MEF cells/well). On the day of thawing, for each clone one well of a 24 well plate coated with Matrigel was prepared.

The 96 well plate with the clones to be thawed was retrieved from the nitrogen tank and placed in the incubator on 37°C. Complete thawing usually took 10 min. In the meantime, the Matrigel was aspirated and replaced with 300µl warm StemMACS with 10µM ROCK-Inhibitor. The MEF medium was replaced with hiPSC-medium containing 10µM ROCK-Inhibitor.

Once the 96 well plate was thawed completely, to the wells containing the clones of interest, 150µl warm StemMACS with 10µM ROCK-inhibitor was added and carefully the cells were pipetted up and down three times. Then, half of the cells were transferred to the Matrigel coated plate, the other half to the MEF

coated plate. MEF feeder cultures of the clones were considered as a backup if cells should not recover from thawing on Matrigel.

3.2.4.7 Expansion of hiPSC clones

Recovery of cells on Matrigel was monitored carefully. If cells recovered well and did not develop any signs of gross differentiation, cells were expanded as usual on Matrigel until enough cells were cultivated to do back up freezing (see chapter 3.2.2.3).

In case of bad recovery or gross differentiation, MEF feeder cultures were used as a backup and cells passage with EDTA onto Matrigel. Then, if recovery was good they were expanded and frozen as usual.

3.3 Genomic screening of engineered cells

For high-resolution detection of rare events digital droplet PCR (ddPCR) was implemented. The technique allows the absolute quantitation of nucleic acid molecules (RNA, DNA). In ddPCR, samples are separated into a large number of partitions and the reaction is carried out in each partition individually. In this way, background is removed from mutant detection and mutant-to-WT ratio is increased, allowing detection of very rare events.

3.3.1 ddPCR HR screening

For HR screening, samples 96h after nucleofection were analyzed. gDNA was extracted with QIAamp ® DNA Blood Mini Kit according to manufacturer's instruction and DNA concentration was measured using Nanodrop. For each reaction 130ng of gDNA were used which correspond to ca. 40,000 DNA copies (one human genome= 3.3 pg).

The hydrolysis probe assays used for HR screen were TH long 1+2 for *TH* locus, GIRK long 1+2 for *KCNJ6* locus and RPP30 for both loci as reference gene.

ddPCR Reaction Mix:

RPP30	1.1 µl
TH/GIRK long 1	1.1 µl
TH/GIRK long 2	1.1 µl
gDNA (130n)	Variable
ddPCR™ Supermix for Probes (No dUTP)	11 µl
H_2O	Up to 22 µl

A positive control was included in the beginning to assess assays quality. Positive control were non-transfected samples spiked with custom gBlocks® (double stranded synthetic DNA fragments) from IDT® consisting of sequences identical to the sequence to be amplified from genomic DNA. gBlocks were used at a 10.000 fold dilution from stock and gDNA from non-transfected samples at the same concentrations as transfected samples.

For droplet generation, a DG8 Cartridge was clipped into a cartridge holder (Fig. 8B). On the gasket holder, labels "sample", "oil" and "droplet" indicate where to load the respective reagents (Fig. 8A). 20µl of

reaction mix were filled with a multichannel pipet into wells marked as “sample”, paying attention not to create air bubbles when loading. Each well marked “oil” was filled with 70µl of droplet generation oil for probes. Every cartridge was closed with a DG8 Gasket and clipped into the cartridge holder (Fig. 8C). The cartridge holder was put into the QX200™ Droplet Generator and the droplet generation was started. After the machine had finished, droplets containing the reaction mix (ca. 50µl) were carefully pulled up from the “droplet” wells using a multichannel pipet and transferred to a 96 well plate suitable for ddPCR (Eppendorf). The plate was sealed with pierceable heat seal foils using the PX1 Plate Sealer.

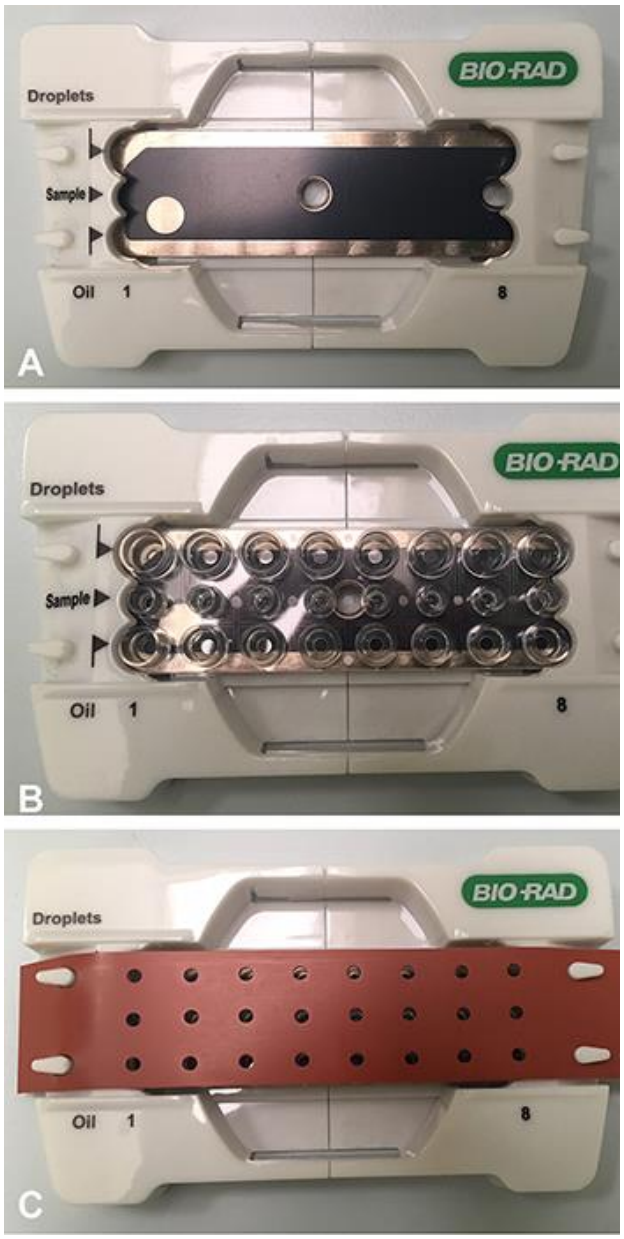

Fig. 8. (A) Cartridge holder with labels “sample”, “oil” and “droplets” indicating where to fill respective reagents; (B) Cartridge clipped into the gasket holder; (C) Cartridge closed with gasket.

Reaction was run under following conditions:

96°C	10 min	
96°C	30 sec	} 5 cycles
58°C	1min	
72°C	3 min	
94°C	30 sec	} 35 cycles
58°C	1 min	
72°C	3 min	
98°C	10 min	
4°C	∞	

After PCR amplification, the plate was analyzed in the QX200 Droplet Reader. Experiment Type was "ABS" (absolute quantitation) and fluorescence was read in FAM/HEX channels. Data was analysed using QuantaSoft™ software from BioRad. Amplitude threshold in Channel 1 and 2 was set individually for each channel and each probe combination. Amplitude threshold variation was possible between separately run plates.

3.3.2 Genomic DNA Extraction from 96well plate

3.3.2.1 Extraction

To screen for positive clones risen from the single cell cloning procedure (see chapter 3.2.4.3), one of the three triplicate 96-well plates was used for genomic DNA extraction. For this, two buffers were prepared.

Lysis Buffer:

10mM Tris pH 7.5

10mM EDTA

10mM NaCl

0.25% Triton X100

1mg/ml Proteinase K (added fresh before lysis)

Precipitation Solution:

75mM NaCl in 100% EtOH, store on -80°C

All the steps were carried out using a multichannel pipet. The 96-well plates had already been washed with PBS before freezing (see chapter 3.2.4.5). To each well, 50µl of lysis buffer containing 1mg/ml Proteinase K was added and the plate was sealed in a plastic bag containing wet tissue papers. The plate was incubated in the bag ON at 55°C in an incubator.

The next day 100µl ice cold (-80°C) precipitation solution was added to the lysis buffer without mixing. Precipitation of DNA was allowed for 2h at RT. After this time, precipitated DNA was visible on the bottom of the well as a white thread. The plate was inverted carefully to discard the buffers, while the gDNA stuck to the plate's bottom. The plate was washed three times with 70% ethanol, always carefully inverting between washes. Remaining ethanol was aspirated with a P10 and residual ethanol evaporated while an incubation at RT with open lid for 10-15 min. gDNA was reconstituted in 50µl H_2O and incubated 1h at 55°C or ON at 4°C for dissolving DNA completely in H_2O. Plate was centrifuged at 800g for 1min.

3.3.2.2 Quantification using PicoGreen®

For a higher throughput gDNA quantification, a fluorescent dye approach compatible with a plate reader was chosen.

Buffers and dye reagent were prepared according to manufacturer's instructions. Shortly, 1x TE was prepared from 20x TE solution contained in Picogreen Kit. 1x TE was used to prepare Picogreen working solution by dissolving Picogreen Stock (200x) in the 1x TE Solution.

A standard curve was prepared each time. For this, the λ-DNA Stock (100µg/ml) contained in the kit was dilute 50-fold in 1x TE to a final concentration of 2µg/ml. A five-pointed high range standard curve was made diluting the 2µg/ml working solution to a final volume of 100µl.

Volume of TE	Volume of 2µg/ml λ DNA solution
0 µl	1000 µl
900 µl	100 µl
990 µl	10 µl
999 µl	1 µl
1000 µl	0 µl

A blank sample was prepared containing 100µl 1x TE. On a separate plate, for each well of a 96-well plate 100µl 1x TE were pipetted into a microplate reader suitable plate with black walls and flat, clear bottom.

Then 1µl of gDNA from each well of 96-well were transferred into the corresponding well on the quantification plate. Also to blank and standard curve, 100µl of Picogreen working solution were added and the mixture pipetted up and down once.

Absorbance was measured using a microplate reader, exciting at 480nm and measuring emission at 520nm. Fluorescence was read from the top of the well.

Linear regression of the standard curve was calculated and concentration of gDNA from 96-well was derived using the regression curve formula.

3.3.3 ddPCR for clone identification

For the identification of single clones on 96-well plates that were correctly engineered, again, ddPCR was used for the detection of the same signal as in the HR screen, looking for a signal enrichment.

The wells of each column of a plate were pooled (see Fig. 9). If in one of these pooled reactions, a positive signal was detected, all wells of this column were analyzed in a separate ddPCR reaction to identify the single positive wells. The strategy is schematically represented in Fig. 9.

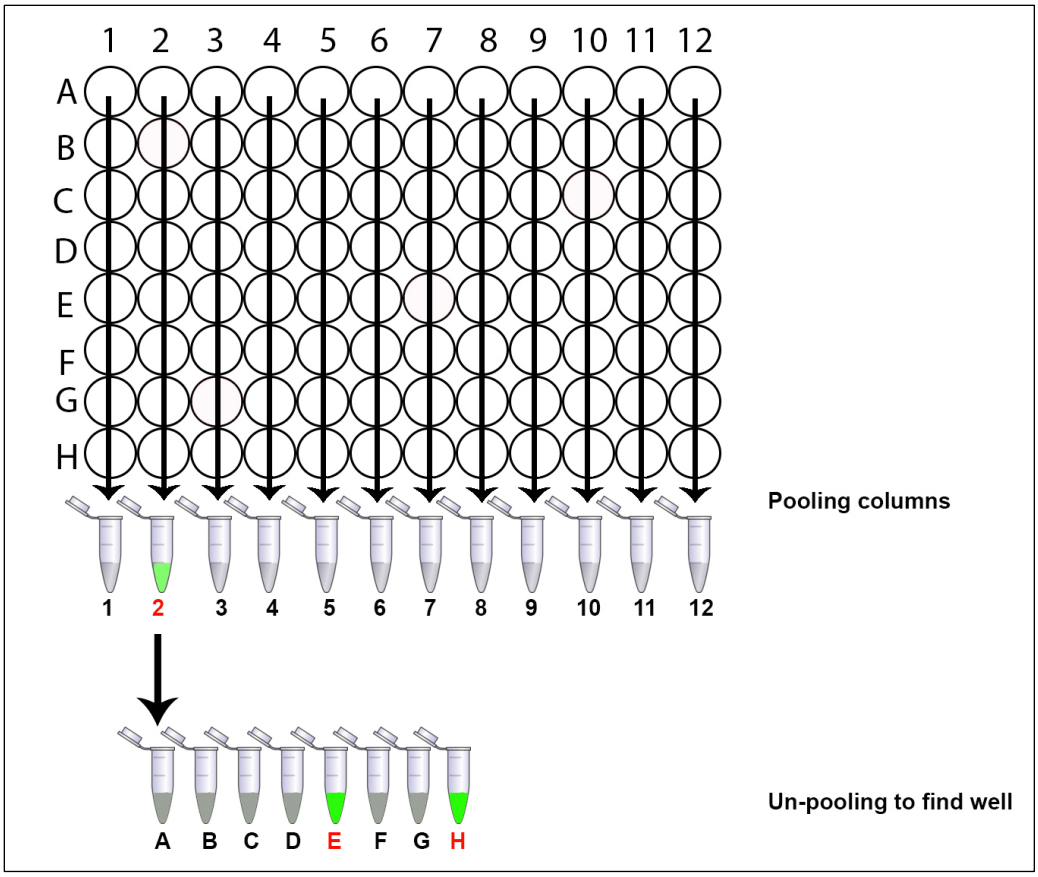

Fig. 9 Schematic representation of pooling and single well identification strategy.

For pooling, 1µl of each well of a column was taken and mixed with 1µl of the other wells of a column. For ddPCR, 1µl of this mixture was used.

Reaction mix

RPP30	1.1 µl
TH/GIRK long 1	1.1 µl
TH/GIRK long 2	1.1 µl
gDNA (from pool)	1 µl
ddPCR™ Supermix for Probes (No dUTP)	11 µl
H_2O	6.7 µl

Droplet formation was performed as described before. ddPCR reaction was run under following conditions:

96°C	10 min	
96°C	30 sec	} 5 cycles
58°C	1min	
72°C	3 min	
94°C	30 sec	} 35 cycles
58°C	1 min	
72°C	3 min	
98°C	10 min	
4°C	∞	

Reactions were analysed on Droplet reader as before. Data analysis was performed with the same quality checks as for HR.

Once a column-pool was tested positive in this run, all the wells from this specific columns were analysed separately again as described above by taking 1µl of gDNA from each well and running the reaction under the same conditions.

3.3.4 Sequencing of insert region

After having confirmed correct engineering, we wanted to check the complete inserted sequence to be correct without single base pair errors. In addition, it was very important to check whether the wild type allele was intact. Even though the insertion was very probable to happen only on one allele, it was likely that the other allele still was targeted by the Cas9-sgRNA complex and had undergone NHEJ, which would lead to a heterozygous knockout of the gene.

For sequencing, an amplicon of the wild type and modified allele was made with PCR. The region was amplified using the same primers used for the surveyor assay (see chapter 3.1.3.2): CU59 and CU60 for TH locus, CU61 and CU62 for KCNJ6 locus.

Reaction Mix:

2x Q5 MasterMix	25µl
10µM Fw Primer	2.5µl
10µM Rv Primer	2.5µl
$MgCl_2$ 25mM	4.2µl
Betaine 5M	6µl
gDNA template 100ng	variable
H_2O	up to 50µl

PCR reaction was run according to the following cycling protocol:

98°C	30 min	
98°C	10 sec	} 40 cycles
X °C *	10 sec	
72°C	2 min	
72°C	7 min	
4°C	∞	

* annealing temperature was adapted according to different reverse primers

Samples were shipped to sequencing at Eurofins Genomics, Germany. Primers for sequencing are listed in Tab 5.

TH wild type allele	CU59
	CU60
TH knock in allele	CU58
	CU83
	CU17
KCNJ6 wild type allele	CU61
	CU62
KCNJ6 knock in allele	CU71
	CU77
	CU79

Tab 5 Primers used for sequencing

3.3.5 Fluorescent *in situ* hybridization

Confirming the correct insertion with the ddPCR assays was the most straightforward approach. However, the exclusion of random integration of the donor plasmid as well as a visualization of the insertion on the correct position in the genome was only possible with a fluorescent *in situ* hybridization (FISH). For this purpose, we had to make our own custom FISH-probe for the insert.

3.3.5.1 Cloning of the FISH probe

The probe sequence for both loci consisted of the donor sequence and an additional 2,000 bp sequence homologue to the genomic sequence upstream of the left homology arm. The reason for adding this 2,000 bp sequence to the probing sequence was that a FISH probe has to have a minimum length of 5,000 bp to be detectable. With a shorter length, the probe cannot be marked with enough fluorescent molecules to be detected. The 2,000 bp genomic sequence had to be cloned into the donor vector.

The sequence was amplified from genomic DNA. Primers used for this amplification are listed in Tab 6. Forward primers carried a 5’ overhang sequence carrying the restriction site for SpeI enzyme. Reverse

primers carried two different 3' overhangs: AatII for TH sequence, EcoRV for KCNJ6 sequence. All restriction sites were necessary for downstream cloning into Donor plasmid.
Genomic DNA was the same used for cloning of homology arms (see chapter 3.1.5).

CU 85	TH genomic for FISH probe
CU 86	
CU 87	KCNJ6 genomic for FISH probe
CU 88	

Tab 6 Primers used for genomic DNA amplification for FISH probe cloning

PCR reaction Mix:

2x Q5 Master Mix	25µl
10µM Fw Primer	2.5µl
10µM Rv Primer	2.5µl
$MgCl_2$ 25mM	4.2µl
Betaine 5M	6µl
gDNA template 100ng	variable
H_2O	up to 50µl

PCR reaction was run according to the following cycling protocol:

98°C	30 min	
98°C	10 sec	} 40 cycles
X °C *	10 sec	
72°C	3 min	
72°C	7 min	
4°C	∞	

* annealing temperature was adapted according to different reverse primers

After the PCR run, the reaction mix was completely loaded onto a 1% Agarose Gel for Gel extraction. The band of 2,000 bp was excised from gel and DNA was extracted using the QIAquick ® Gel Extraction Kit according to manufacturer's instructions.
For cloning, the PCR and the Donor plasmid were digested with SpeI and AatII or SpeI and EcoRV.

Digestion set up:

EcoRV HF®/ AatII	1 µl
SpeI	1 µl
CutSmart® Buffer	2 µl
200 ng of plasmid or PCR product	Variable
H_2O	Up to 20µl

Plasmid and PCR product were digested at 37°C for 1h in a water bath. After 1h, 1µl of enzyme was added to ensure complete digestion.
Digested products were directly used for ligation.

Ligation reaction:

digested donor plasmid	4 µl
Digested PCR product	2 µl
T4 DNA Ligase	1 µl
T4 DNA Ligase Reaction Buffer	1 µl
H_2O	2 µl

The ligation reaction was incubated on 16°C in a thermoblock overnight.

The day after, the plasmids were transformed into One Shot™ Stbl3™ Chemically Competent *E. coli* according to the protocol provided by manufacturer (see chapter 3.1.2.2). The bacteria were plated onto an Agar plate containing 50µg/ml ampicillin and incubate on 37°C overnight.
In the morning, five colonies for transformed plasmid were picked with a 20µl pipet tip and suspended in 10 µl H_2O.

To verify the correct insertion of the PCR products into the respective Donor plasmids, a colony PCR was performed as described in chapter 3.1.2.2 using primers used for PCR amplification of insert from genomic DNA.

For each FISH probe, a positive colony was selected. 2ml of LB liquid culture medium containing 50 µg/ml ampicillin were inoculated with 5µl of colony suspension and grown at 37°C overnight.

The day after the LB culture was pelleted leaving a small quantity for re-growing the culture. The plasmid DNA was extracted using the NucleoSpin® Plasmid Kit. The manufacturer's protocol was followed except for elution, which was carried out in H_2O.

A restriction digest was carried out to check that the purified plasmid DNA was not recombined.

3.3.5.2 Marking of the FISH probe

For marking of the FISH probe, Cy3®-labelled dUTPS were used. The probe was marked using the Nick-Translation assay, where one creates nicks in the DNA using DNase I enzyme. The nicks were then repaired with *E.coli* Polymerase I, which has a 5'-3' exonuclease activity. Repairing the nicks, it adds the marked dUTPs to the DNA.

Plasmid probe (2µg)	Variable
10x Polymerase I Buffer	5 µl
DNase I	1 µl
DNA Polymerase I	1 µl
dNTP mix without dTTP (0.2 mM each of dATP, dCTP, dGTP)	5 µl
100µM Cy3® dUTP Mix	2 µl
H_2O	To 50 µl

The reaction was carried out for 100min at 15°C and was then inactivated for 7 min at 65°C.

DNA was precipitated using salmon sperm DNA and human Cot-1 DNA. For this, 70µl of marked probe was mixed with 3µl salmon sperm DNA and 182.5 µl 100% Ethanol. The mix was incubated for 30min at -20°C and then centrifuged at 30,000 g for 15 min. Precipitated DNA was suspended in 1,5µl H20 and 3,5µl LSI hybridization buffer (50% formamide, 1X saline sodium citrate buffer (SSC), 10% dextran sulphate).

3.3.5.3 Probe hybridization and imaging

For probe hybridization, metaphase fixation protocol was followed as previously described (see 3.2.3.4). After drying of microscope slide, the preparation was dehydrated in increasing alcohol concentrations (80%, 90% and 100%) for 3 min. each. Spreads were aged ON on a heating plate at 50°C.

Prior to hybridization, cover slips were removed and slides were incubated in 70% formamide at 72°C for 1.45 min. Formamide was heated in a coplin jar in the water bath and microscope slides immerged into the coplin jar. FISH probes were denatured at 75°C for 7 min and then pipetted onto the microscopic slide containing the metaphase spreads, covered with a glass cover slip and sealed using rubber cement. Slide denaturation and hybridization was carried out in a programmable temperature controlled slide processing system (HYBrite, Abbott Molecular) at 75°C for 2 min and at 37°C ON, respectively. TH knock-in lines were hybridized with TH FISH probe, GIRK knock-in lines with GIRK FISH probes.

The next day, cover slips were removed and slides were immerged into 75°C 0.4X SSC Tween®20 0.3% (pH 7) for 2min. Immediately after, they were immerged into 4X SSC Tween®20 0.1% (pH 7). Slides were air-dried and mounted in Vectashield mounting medium with DAPI under a cover slide of glass.

Pictures were acquired with an epifluorescence microscope from Zeiss© Axioplan2 and analysed with Isis FISH Imaging System.

3.4 In vitro differentiation of hiPSCs to DA neurons

For differentiation of hiPSCs into DA neurons two different approaches were tested. One is an adaption of the protocol published by (Zhang, Xia, and Reijo Pera 2014; Kriks et al. 2011), the other a commercially available kit by Gibco™. Both are based on inducing floor plate progenitor cells from hiPSCs, which are then further differentiated into DA precursor cells and lastly plated for terminal DA differentiation.

3.4.1 Floor plate induction protocol using a protocol in adaption to Zhang et al.

For the published protocol, cells were plated on day -2 on Matrigel coated dishes. Unlike Matrigel coating for stem cells (see chapter 3.2.2.1), here we used hESC qualified Matrigel diluted according to dilution factor indicated on the quality report. Matrigel was thawed on ice and suspended in cold Knock-out DMEM. The Matrigel solution was pipetted onto culture wells (e.g. 1ml for one well of a 6-well plate) and coating was allowed for 1h at 37°C in the incubator. In some cases, we exchanged Matrigel with Geltrex, which is the same coating mixture supplied by Life Technologies instead of Corning.

hiPSCs were detached with TrypLE as described earlier and plated as a single cell suspension at a density of 35.000 cells/cm^2 (e.g. 350.000 cells in a well of a 6-well plate) in StemMACS medium with 10µM Rock-inhibitor. 24h after plating confluence was assessed at the microscope. Differentiation was started at a confluence of about 50%, which was noted as Day 0 (see Fig. 10). With some cell lines we increased the plating density to 500.000 cells/cm^2 if recovery was after plating was low.

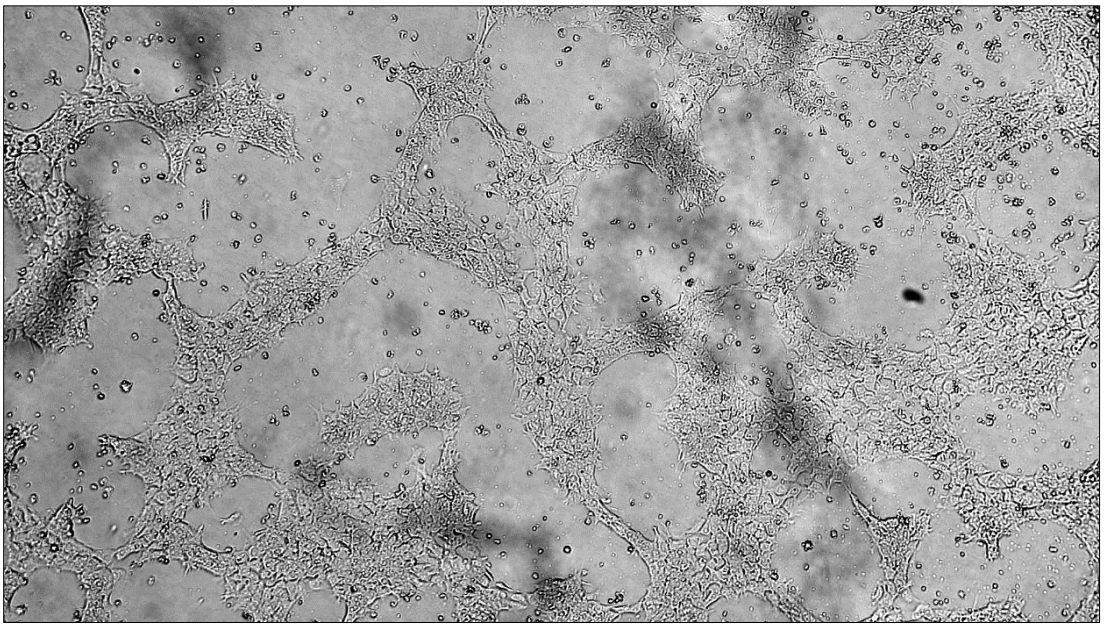

Fig. 10 Ideal confluence of cells at Day 0, which represents the starting day of differentiation.

For the differentiation protocol, three media were needed. The media composition is listed in Tab 7.

Medium N1 100ml		Medium N2 100ml		Medium NB-B27 100ml	
DMEM, high glucose, GlutaMAX™	83ml	DMEM, high glucose, GlutaMAX™	98ml	Neurobasal	96ml
KOSR	15ml	N-2 Supplement (100X)	1ml	B-27™ Supplement (50X)	2ml
NEAA	1ml	Pen/Strep	1ml	GlutaMax	1ml
Pen/Strep	1ml			Pen/Strep	1ml
50mM β-mercaptoethanol	20µl				

Tab 7 Media composition for DA differentiation

Medium was changed daily from Day 0 to Day 20.

On day 0, cells were fed with medium N1 supplemented with 10 µM SB431542 (SB) and 100 nM LDN-193189 (LDN).

On day 1 and 2, cells were fed with medium N1 supplemented with 10 µM SB, 100 nM LDN, 0.25 µM SAG, 2 µM purmorphamine (Pu), and 50 ng/ml FGF8b.

On day 3 and 4, cells were fed with medium N1 supplemented with 10 µM SB, 100 nM LDN, 0.25 µM SAG, 2 µM Pu, 50 ng/ml FGF8b, and 3 µM CHIR99021 (CH).

On day 5 and 6, cells were fed with medium of 75% N1 and 25% N2 supplemented with 100 nM LDN, 0.25 µM SAG, 2 µM Pu, 50 ng/ml FGF8b, and 3 µM CH.

On day 7 and 8, cells were fed with medium of 50% N1 and 50% N2 supplemented with 100 nM LDN and 3 µM CH.

On day 9, were fed with medium of 25% N1 and 75% N2 supplemented with 100 nM LDN and 3 µM CH.

On day 10, cells were washed once with PBS w/o Calcium and Magnesium and then detached with Accutase (e.g. 1ml per well of a 6-well plate). Accutase was added at room temperature and cells were incubated for 5min at 37°C in the incubator. After the incubation, the plate was tapped until cells started detaching. Cells were diluted 10x with PBS and transferred to a centrifuge tube and spun for 3min at 300g. After that, cells were suspended in day 10 medium (identical to day 9 medium) supplemented with 10µM Rock-inhibitor and replated onto a freshly coated Matrigel dishes in ratio 1:1.

On day 11 and 12 cells are fed with medium NB-B27 supplemented with 3 µM CH, 10 ng/ml BDNF, 10 ng/ml GDNF, 1 ng/ml TGF3, 0.2 mM ascorbic acid (AA) and 0.1 mM cAMP.
From day 13 to day 20 cells are fed daily with medium NB-B27 supplemented with 10 ng/ml BDNF, 10 ng/ml GDNF, 1 ng/ml TGF3, 0.2 mM AA and 0.1 mM cAMP.

At day 20, cells were detached and centrifuged as described for day 10. After that, cells were supended in day 20 medium supplemented with 10µM Rock-inhibitor and replated onto a freshly coated Matrigel dishes at a density of 250.000 cells/cm^2. Cells were kept in this wells for terminal maturation and fed with day 20 medium every other day. Once a week, medium was supplemented with 10µg/ml Laminin.

3.4.2 Floor plate induction using a commercially available kit

We used the "PSC Dopaminergic Neuron Differentiation Kit" from Gibco™ with minor modifications to the manufacturer's instructions. Media supplements were contained in the kit and media were prepared according to guidelines in the kit protocols. Shortly, the kit consists of three different media that were prepared as described in Tab 8.

Complete Floor Plate Specification Medium		Complete Floor Plate Cell Expansion Medium		Complete Dopaminergic Neuron Maturation Medium	
Floor Plate Specification Supplement (20X)	5ml	Floor Plate Cell Expansion Supplement (50X)	10ml	Dopaminergic Neuron Maturation Supplement (50X)	10ml
Neurobasal Medium	94ml	Floor Plate Cell Expansion Base Medium	485ml	DMEM/F-12	485ml
Pen/Strep	1ml	Pen/Strep	5ml	Pen/Strep	5ml

Tab 8 Media for DA differentiation, contained in Kit

Cells were culture in StemMACS medium until the day of plating for differentiation. On the day of plating, which is Day -1, cells were plated on Matrigel coated dishes at a density of 50.000 cells/cm^2. Matrigel was prepared as described in chapter 3.4.1. Cells were plated in StemMACS medium containing 10µM Rock-inhibitor.

The day after, differentiation was started by medium exchange into Floor Plate Induction Medium. Cells were fed with this medium on day 3, 5, 7 and 9. Medium change was always complete.

On Day 10, cells were a highly confluent layer and had to be passaged. Laminin coated dishes were prepared by adding Laminin 10µg/ml to the dish (e.g. 1ml per well of a 6-well plate) and incubating the plate for 1h at 37°C in the incubator.

For passaging, cells were detached with Accutase as described above and spun for 3min at 300g. Cells were then suspended in Floor Plate Cell Expansion Medium containing 10µM Rock-inhibitor and replated at a split ratio of 1:2. This passage is referred to as FPp0 (Floor plate passage 0).

On day 11, a complete medium change with Floor Plate Cell Expansion Medium was performed.

On day 12, FPp0 was again 100% confluent and was passaged to FPp1 as described for FPp0. Cells were suspended in Floor Plate Cell Expansion Medium with 10µM Rock-inhibitor and plated onto freshly coated Laminin dishes at a density of 200.000 cells/cm^2.

On the days 13 and 15, Floor Plate Cell Expansion Medium was changed completely without Rock-inhibitor.

On day 16, cells were harvested for liquid nitrogen banking. Cell detachment was carried out as on day 12. $2x10^6$ cells were centrifuged for further expansion, the rest was centrifuged for banking. For freezing, cells were suspended in freezing medium (Floor Plate Cell Expansion Medium with 10% DMSO) at a density of 2-$5x10^6$ cells/ml. They were frozen at constantly decreasing temperature ON to -80°C and transferred to the nitrogen tank the day after for long-term storage.

The rest of the cells was used for sphere formation. For this, after centrifugation they were suspended in Floor Plate Cell Expansion Medium with 10µM Rock-inhibitor at a density of $1x10^6$ cells/ml and plated onto low-attachment plates. Spheres formed autonomously in suspension. Floor Plate Cell Expansion Medium was changed completely on day 17 and 19 without Rock-inhibitor.

On day 20, spheres were dissociated and cells were plated for terminal maturation onto Matrigel coated dishes. For this, the spheres were transferred to a 15ml falcon tube and centrifuged at 300g for 1min. Medium was aspirated and cells washed once with PBS w/o Calcium and Magnesium. Cells were centrifuged again at 300g for 1min and suspended in 1ml of Accutase. The falcon with cells in Accutase was transferred to the incubator and dissociation was allowed for 30min. Every 10min the falcon was

flicked with the finger to mix the suspension. After 30 min cell clumps were dissociated to a single cell suspension with a P1000 pipette and diluted 10-fold in PBS. Cells were centrifuged at 300g for 3min and supended in Dopaminergic Neuron Maturation Medium with 10µM Rock-inhibitor. Cells were plated at a density of 250.000 cells /cm^2 and fed with Maturation medium every other day. Once a week, the medium was supplemented with 10µg/ml Laminin.

3.5 Neuronal characterization

3.5.1 Immunocytochemistry and confocal imaging

Immunocytochemistry was performed on cells at different points of differentiation. On day 10, cells were fixed for staining of floor plate markers FOXA2 and LMX1A.

On day 25 and day 35 *in vitro*, cells were fixed for co-staining of TH and eGFP whereas for GIRK2 and mCherry co-staining, cells were fixed at day 40 of *in vitro* neuronal differentiation.

The latest time point for fixing was day 50, where cells were fixed for staining of neuronal markers.

Cells dedicated to the purpose of immunostaining were plated on glass coverslips coated with Matrigel. On the day of fixing, coverslips were removed from the culture dish with sterile forceps and transferred to a clean culture dish.

For fixing at day 10, 25 or 35, cells were washed carefully once with PBS w/o Calcium and Magnesium and then fixed with 4% Paraformaldehyde (PFA) for 15min at RT. After fixing, cells were washed three times with PBS.

3.5.1.1 Blocking, permeabilization and primary antibody incubation

After washing, cells were permeabilized for 5min at RT in PBS with 0.5% Triton on a shaker. Then, cells were blocked in PBS + 5% donkey serum for 1h at RT on a shaker. After blocking, fixed cells were incubated in primary antibody solution (antibodies diluted in PBS + 2% donkey serum + 0.2% Triton). See Tab 9 for detailed antibodies combination used.

Epitope	Host	Dilution
α TH	mouse	1:500
α eGFP	rabbit	1:1000
α MAP2	chicken	1:5000
α GIRK2	rabbit	1:400
α mcherry	mouse	1:500
α MAP2	chicken	1:5000
α FOXA2	goat	1:100
α LMX1A	rabbit	1:200
α Tau	rabbit	1:1000
α TH	mouse	1:500
α MAP2	chicken	1:5000
α TH	mouse	1:500
α PITX3	rabbit	1:1000
α PSD95	mouse	1:150
α Synapsin	rabbit	1:500
α MAP2	chicken	1:5000

Tab 9 Antibody combinations and dilutions used for co-staining

The primary antibody incubation was carried out O/N at 4°C on a shaker.

3.5.1.2 Staining with directly labelled fluorescent secondary antibody

The day after, primary antibody solution was removed and cells washed three times with PBS. Afterwards, cells were incubated in secondary antibody solution (PBS + 2% donkey serum + 0.2% Triton) for 3h at RT on a shaker covered with aluminium foil to avoid bleaching of fluorophores. See Tab 10 for detailed secondary antibody combinations and dilutions.

Epitope	Host	Fluorophore	Dilution
α rabbit	donkey	AF 488	1:1000
α mouse	donkey	AF 555	1:1000
α chicken	donkey	AF 647	1:500
α rabbit	donkey	AF 555	1:1000
α mouse	donkey	AF 488	1:1000

Tab 10 Secondary antibody combinations and dilutions used respective primary antibody

After the secondary antibody incubation, cells were washed again three times with PBS. In the last PBS wash, NucBlue® Fixed Cell ReadyProbes® Reagentw as added to stain cell nuclei. After washing, cover slips were mounted in mounting medium on a microscope slide and sealed with commercially available nail polish.

Images of immunostained hiPSC cells were acquired with Leica TCS SP8 laser scanning confocal microscope. The confocal microscope was equipped with a white light laser. For detection of AF 647 marked antibodies, excitation wavelength was set at 647nm, emission spectrum was set from 663 to 749nm. For detection of AF 555 marked antibodies, excitation wavelength was set at 555nm and emission spectrum between 571 and 643nm. For detection of AF 488 marked antibodies excitation wavelength was at 488nm and emission spectrum set from 492 and 552nm. Laser power was adapted according to needs of specific signal detection.

3.5.2 Gene expression analysis

Lysates for RNA extraction were made for cells at the very same time points in differentiation as when fixing for immunostaining. For this purpose, medium was aspirated and cells directly lysed in RLT Buffer containing 10µl β-Mercaptoethanol per 1ml of RLT. Lysates were stored at -80°C until extraction.

For RNA extraction RNeasy® Mini Kit from Qiagen was used and extraction was performed according to manufacturer's instructions. RNA was eluted in 30µl nuclease free H_2O and quantified using Nanodrop. Retrotranscription was performed as described in chapter 3.2.3.2.

Gene expression analysis for neuronal characterization was carried out as quantitative realtime PCR according to procedures explained in chapter 3.2.3.2.

Gene expression profiling for reporter gene co-expression was performed using ddPCR to allow the exact copy number detection. For this purpose, commercially available gene expression assays for TH, eGFP and GIRK2 were used (see Appendix, List of primers). For mCherry, a custom assay was ordered (see Appendix, List of primers).

Reaction was set up as follows

ddPCR™ Supermix for Probes	11µl
TH assay /GIRK2 assay 20x	1.1µl
eGFP assay/mcherry assay 20x	1.1µl
cDNA 1ng/µl	2µl
H_2O	6.8µl

95°C	10 min	
94°C	30 sec	} 40 cycles
60°C	1 min	
98°C	10 min	
4°C	∞	

After PCR amplification, the plate was analyzed in the QX200 Droplet Reader. Experiment Type was “ABS” (absolute quantitation) and fluorescence was read in FAM/HEX channels. Data was analyzed using QuantaSoft™ software from BioRad. Amplitude threshold in Channel 1 and 2 was set individually for each channel and each probe combination. Also, amplitude threshold variation was possible between separately run plates.

3.5.3 WB analysis

Lysates for western blot were made at the same day as coverslips were fixed and RNA lysates were made. For this purpose, cells were washed once in PBS and then directly lysed in RIPA Buffer containing phosphatase and protease inhibitors.

RIPA Buffer:
25µM Tris HCl pH 7.4
150 nM NaCl
1% NP-40
1% NaDoc
0.1% SDS

Cell pellets were briefly sonicated with 10 seconds pulse while maintained in ice. For each samples, three pulses were performed with 30 seconds interval while kept in ice.

Determination of total protein concentration in cell lysate was measured against a BSA standard curve, which was diluted in H2O. The standard curve was prepared as follows:

	BSA (2 mg/ml) [µl]	H2O [µl]	final concentration [µg/ml]
1	80	0	2000
2	40	40	1000
3	30	50	750
4	20	60	500
5	10	70	250
6	5	75	125
7	1	79	25
8	0	80	0

For quantification a Bicinchoninic acid assay (BCA) was performed using the Pierce™ BCA Protein Assay Kit. For this, 10µl of each concentration of the standard curve were put in duplicate on a 96-well plate. Also 10µl of the protein lysates to analyse and blank (RIPA with phosphatase and protease inhibitors) were pipetted in duplicates on the plate. BCA reagent A and B were mixed in a ratio of 50:1 and 200µl of the mixed solution were given to the standard curve, sample and blank wells. The plate was incubated for 30

minutes at 37°C and afterwards read in Victor X3 multilabel plate reader at 562 nm. Concentration of protein samples was then determined against the values of the standard curve. The average of the duplicates was used for further calculations.

To separate proteins by their molecular weight, they were run on a polyacrylamide gel and then immobilized onto a membrane. 20µg of protein samples were prepared with 4x LDS sample buffer and 10x reducing agent and heated for 5 minutes to 70°C. A maximum volume of 25µl of sample and 3µl of protein molecular weight marker were loaded on gel. The gel was run in MOPS buffer initially for 5 minutes at 100 V and then for about 60 minutes at 150 V. The resolved proteins on the gel were then transferred and immobilized onto a PVDF membrane prior activated in 100% methanol. For blotting, the order from the negative pole to the positive pole was: blotting pad, filter paper, gel, PVDF membrane, filter paper, blotting pad. The transfer was done overnight at 4°C and 100mA in transfer buffer containing 20% methanol.

The day after, successful transfer of proteins was checked using Ponceau stain followed by destaining in deionized water. Then, the membrane was then washed 5 minutes in TBS for complete destain.

For blocking, the membrane was incubated in 5% blocking solution (milk in TBS-T) 1h. The primary antibody was diluted (see Tab 11) in fresh 5% blocking solution O/N.

The next day, the membrane was washed in TBS-T once for 15 min and twice for 5min. The proper secondary antibody was applied in blocking solution at a dilution of 1:10.000 for 2 hours. After the incubation, the membrane was washed like as before and then assayed with Clarity Western ECL Substrate. The chemiluminescent images were captured using the ChemiDoc™ touch image system.

Epitope	Host	Dilution
α TH	mouse	1:100
α eGFP	rabbit	1:2000
α GIRK2	rabbit	1:200
α mcherry	mouse	1:2000
α β-actin	mouse	1:1000

Tab 11 Antibodies used for protein detection in western blot and the applied dilution

3.5.4 Flow cytometry

For flow cytometric analysis on day 25 and day 35, cells were detached using Accutase. First, cells were washed with PBS and then incubated in Acctuase for 5min at 37°C. Cells were triturated lightly with a P1000 pipet to disaggregate them into single cells. They were transferred to a 15ml falcon tube an Accutase was diluted 10-fold with PBS. Centrifugation was carried out for 3min at 300g.

The supernatant was aspirated and cells were washed with PBS and centrifuged again. After centrifugation cells were resuspended in PBS at a density of $1x10^6$ cells/ml. To the PBS-cell suspension the life and dead discrimination dye, LIVE/DEAD™ Fixable Near-IR Dead Cell Stain, was added at a dilution of 1:1000. Cells were incubated in the dye for 30min on ice in the dark.

After the incubation cells were centrifuged as before, washed with PBS and resuspended in FACS Buffer. The FACS Buffer consisted of PBS w/o Mg^{2+} and Ca^{2+}, 2.5% Horse Serum, 0.4% Glucose, 5mM EDTA and DNase I (50µg/ml). Cells were passed through a 40µm cell strainer to ensure single cell suspension and transferred to polypropylene FACS tubes. Until analysis cells were kept on ice.

Cells were analysed using either FACSCanto™ or FACSAria™ II cytometers. A 100µm ceramic nozzle tip and acquisition rate of 800-1.200 events/second was used. To draw gating parameters of FL1 channel (eGFP), cells without eGFP were used as a negative control.

Cells were analysed in FSC-A and SSC-A to morphologically identify cells of interest and exclude detritus. In SSC-W plotted against SSC-A single cells were distinguished from cell aggregates and a gate set, to exclude aggregates from analysis.

Live and dead cells were identified using the life/dead infrared stain. Cells were excited with the 633nm Laser and signal detected in the APC-Cy7-A channel plotted against cell count. Cells marked with the dye were dead cells and a gate was set in order to exclude dead cells from the analysis.

eGFP signal was monitored in the FITC channel. Cells were excited with a 488nm Laser. Signal was plotted as FITC-A signal against cell count and as FITC-A signal against SSC-A.

3.5.5 Patch Clamp recordings

For whole cell voltage clamp and current clamp recordings, cells were plated onto 14mm glass cover slips on day 20. Recordings were made on different time points during *in vitro* maturation. Experiments were performed at 37°C in a recording chamber mounted on a Eclipse-T*i* microscope using a MultiClamp 700B amplifier.

Voltage- and current-command protocols (indicated below) and data acquisition were performed using pClamp 10.0 software and the Digidata 1550 interface (Molecular Devices, LLC). Data were lowpass-filtered at 3 kHz and sampled at 20 kHz.

Cells were immerged and continuously superfused with extracellular solution (see Tab 12). Glass electrodes for patching were made from borosilicate glass capillaries using Sutter P-1000 puller to a final resistance of 4-6 MΩ. Electrodes were filled with internal solution (see Tab 12).

Voltage-clamp recordings (Vh = -60mV) of evoked ionic currents were performed by applying a voltage step protocol (from -60mV to +60mV, 300ms of duration) while the spontaneous synaptic activity was acquired in gap-free mode. Current-clamp recordings of evoked firing activity were carried out by injecting a hyperpolarizing current to maintain the resting potential of the cells near -60 mV. An online bridge-balance compensation was always performed. The evoked firing activity was evaluated by applying long steps at different current intensities (50-pA increments) and polarities. Series resistance was monitored along the experiments and recordings with changes over 20% of its starting value were discarded.

Internal solution		External solution	
120mM	K-Gluconate	128mM	NaCl
25mM	KCl	5mM	KCl
10mM	EGTA	1mM	$MgCl_2$
10mM	HEPES	2mM	$CaCl_2$
1mM	$CaCl_2$	25mM	HEPES
4mM	Mg-ATP	30mM	Glucose
2mM	Na-GTP		
4mM	Na_2-Phosphocreatine		
pH 7.4, adjusted with KOH		pH 7.3, adjusted with NaOH	

Tab 12 Recipes for internal and external solution

3.5.6 Dopamine ELISA

For DA measurement with ELISA method, medium from cells was collected at different time points of *in vitro* maturation. Collection was performed in the dark and medium was transferred to black tubes. 100µl medium was collected and EDTA was added to the collected medium to a final concentration of 1mM and sodium-metabisulfite was added to a final concentration of 4mM. For the Dopamine Research ELISA ™

the kit from ImmuSmol was used an the protocol followed according to manufacturer's instruction, following the instruction for the 100µl assay.

Absorbance was read using the EnVision Multimode Plate Reader set to 450nm. A reference measurement was read at 650nm wavelength as advised in the kit's manual.

The calibration curve was prepared as explained in the manual. Absorbance values read for standard curve were normalized for a blank sample. The normalized values were plotted against standard values on a logarithmic scale. A nonlinear regression curve was generated using GraphPad Prism software and normalized absorbance values for each sample fitted on the curve.

4 Results

4.1 Characterization of hiPSCs

In order to ascertain an authentic stem cell-like state, hiPSC lines have to undergo a thorough characterization process. This includes assessing pluripotency gene expression, immunostaining for pluripotency surface and nuclear markers and karyotyping. We obtained the SFC 856-03-04 and SFC 840-03-05 cell lines from the international consortium StemBANCC, which provided characterization to a standard protocol before sharing with users.

At Eurac Research, the 802#7 hiPSC line was reprogrammed internally and had to be characterized for effective pluripotency before using it for further applications. The cell line was characterised at passage 10 (P10) after reprogramming once cells were adapted into feeder-free conditions.

4.1.1 Immunofluorescence staining for pluripotency markers

Immunocytochemistry (ICC) for detection of pluripotency markers was performed on hiPSCs at P10 adapted to feeder-free conditions. The presence of two nuclear markers and two surface markers was analyzed. All the hiPSCs used in this study showed strong expression of nuclear markers Oct-4 and surface marker SSEA-4 (Fig. 11A). In a second set of experiments, strong expression of nuclear marker Sox2 and surface marker TRA-1-160 was observed (Fig. 11B).

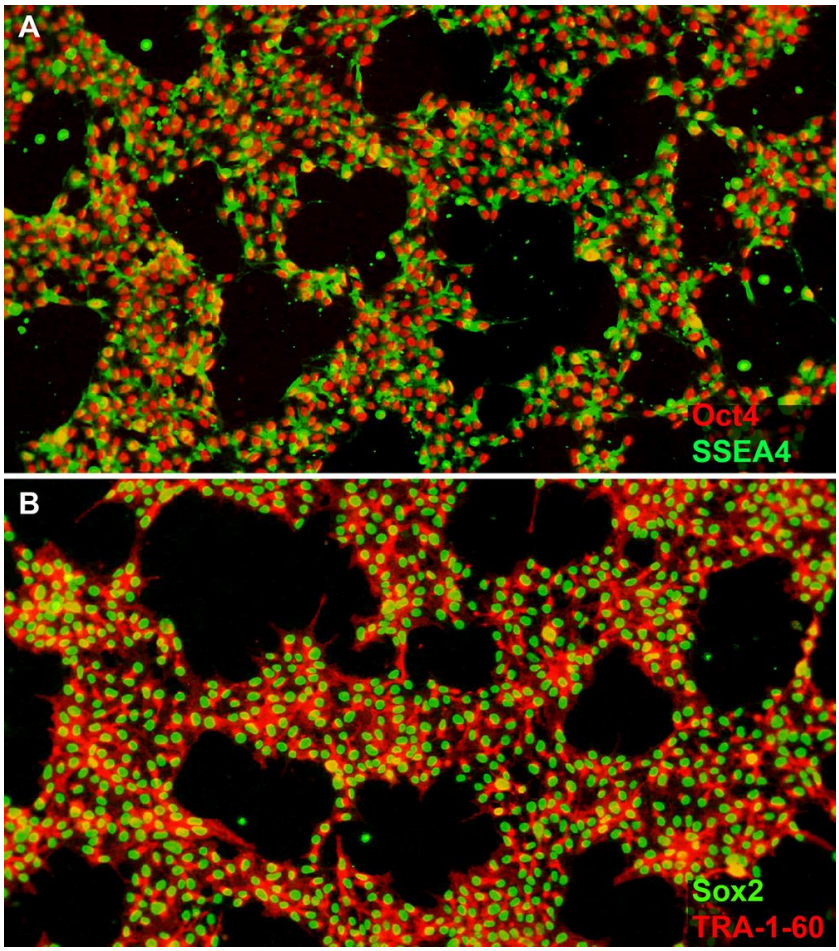

Fig. 11 Double immunostaining of hiPSCs. (A) SSEA-4 in AF®488 (green) and Oct-4 in AF®555 (red) (B) Sox2 in AF®488 (greej) and TRA1-160 in AF®555 (red)

4.1.2 qRT analysis of pluripotency gene expression and transgene exclusion

Gene expression analysis was performed for four different established pluripotency markers: Sox2, Oct3/4, Nanog and GDF3. Expression of these pluripotency genes was studied by qRT. A remarkable increase in the expression of pluripotency genes was detected in hiPSC line 802#7 in comparison to its parent fibroblast line (Fig. 12). The mRNA expression levels increased up to 5000 fold.

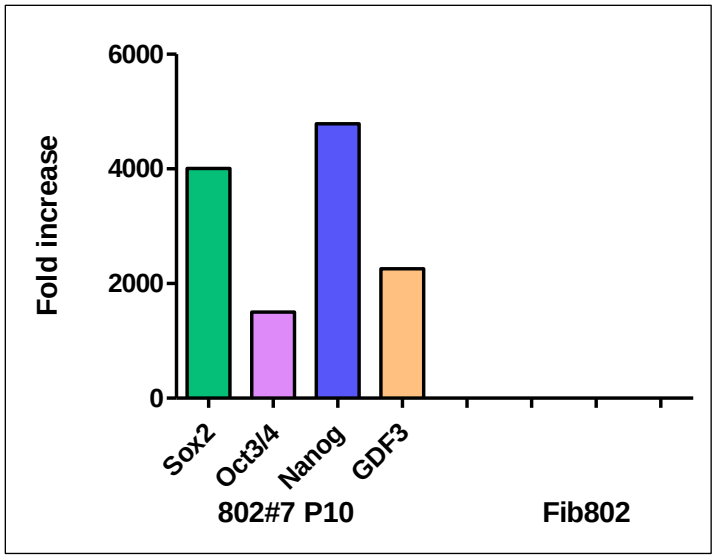

Fig. 12 Graphic representation of fold increase of pluripotency genes calculated for hiPSCs cell line 802 normalized to expression of these genes in parent fibroblast line.

To exclude the presence of any leftover plasmid in the iPSC line, tested for pluripotency gene transcription, qRT with episomal specific primers for EBNA-1 was carried out at the same time. Compared to a positive control, which are hiPSC cells shortly after transfection, the hiPSC line 802#7 at P10 did not show any traces of the transgene thus confirming a successful activation of endogenous pluripotency genes and removal of unwanted, carry over sequences (see Fig. 13).

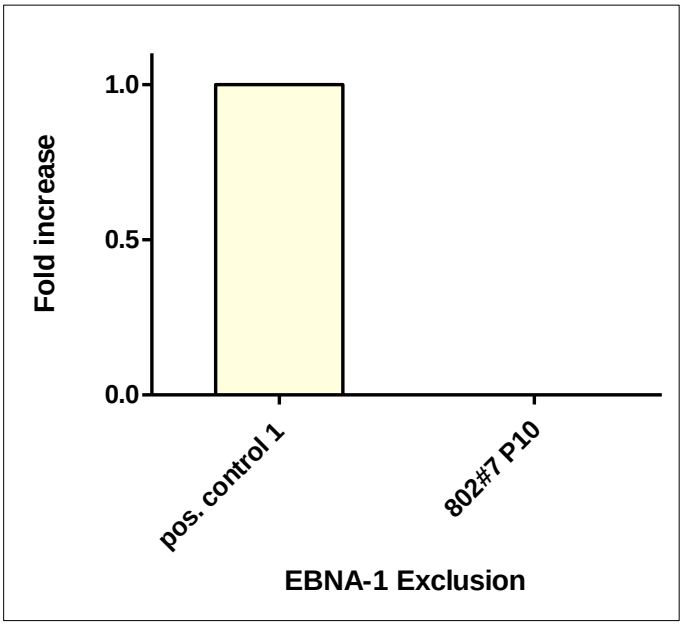

Fig. 13 Graphic representation of fold increase of transgene EBNA-1 present on plasmid carrying pluripotency factors. Comparison between a positive control and hiPSC line 802#7

4.1.3 Alkaline phosphatase staining

Along with other surface markers, alkaline phosphatase (AP) staining is an indicator of undifferentiated embryonic stem cell state. As shown in Fig. 14, hiPSC line 802#7 displays a strong staining for AP, indicated by a purple staining of the cell surface.

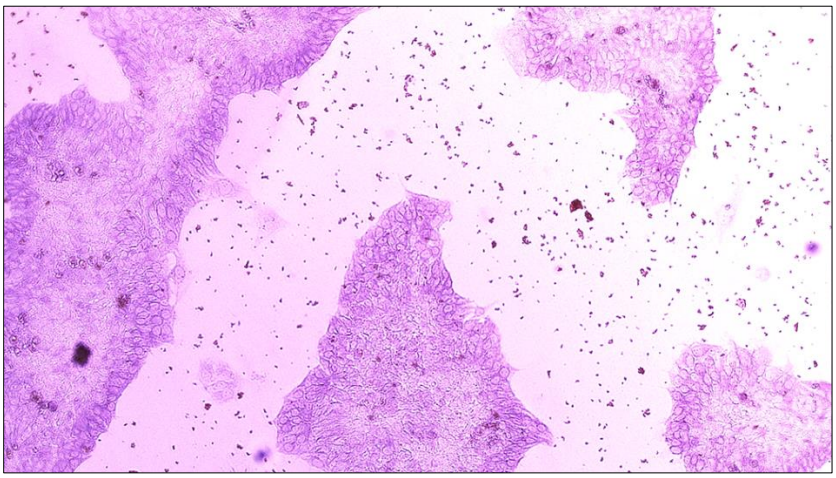

Fig. 14 AP staining of hiPSC line 802#7 at P10

4.1.4 Karyotyping

As stem cells are prone to acquire karyotypical anomalies with passaging (Maitra et al. 2005), karyotyping hiPSC lines is one of the most important quality checks.

Fig. 15 shows a representative karyotype of hiPSC line 802#7 with 46 chromosomes (46, XX), consistent with a normal female karyotype/genomic arrangement. 48/50 metaphases analysed showed 46 chromosomes. 1/50 metaphases analysed showed 45 chromosomes with monosomy 3, which was considered an overspreading related chromosome preparation artefact.

In addition, a single metaphase showed 48 chromosomes with trisomy 6 and trisomy 12. Since this rearrangement was only observed once, it was assumed to be a culture artefact and was not observed in any subsequent analysis of this cell line (data not shown).

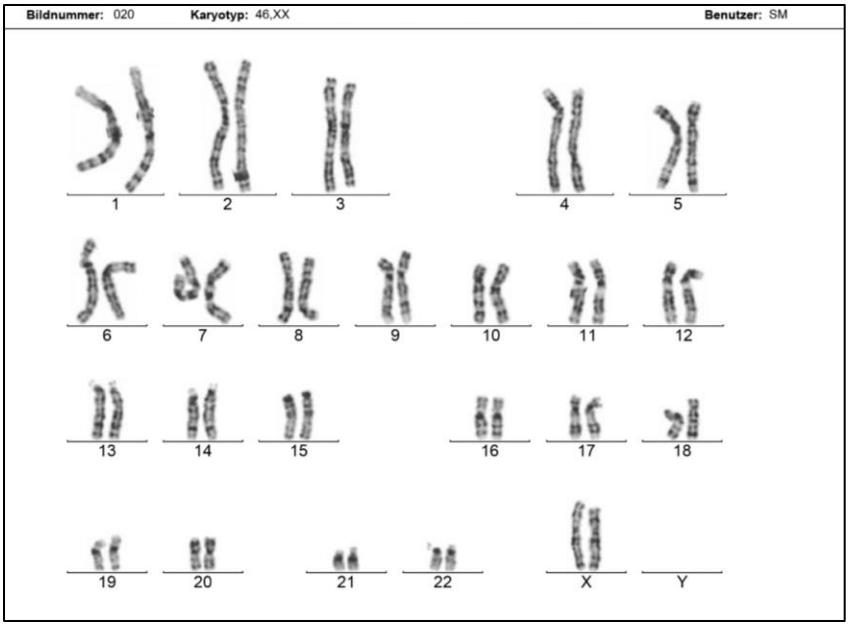

Fig. 15 Karyotype analysis of generated hiPSC line 802#7 at P10

4.2 Screening of sgRNAs in HEK293T-Cas9-TetON cells

The CRISPR/Cas9 system allows targeting of specific DNA sequences and accurate gene editing, such as introduction of single point mutations. Confirmation of cleavage and introduction of mutations with DNA targeting systems is the first step of quality assessment in the experimental procedures and of utmost relevance. For this work, the CRISPR/Cas9 system was exploited to introduce a DSB at two specific loci. The Cas9 is guided to these loci by a chimeric RNA molecule, the sgRNA containing a 20nt sequence homologue to the genomic DNA (see chapter 1.8). As described in chapter 3.1.1, sgRNA design for these experiments was carried out using an online tool. For both loci either four (*TH*) or five (*KCNJ6*) sgRNAs with a similar *in silico* predicted precision were designed. However, the actual capability of each sgRNA to attract the Cas9 protein to the desired cutting site is hard to define exactly a priori and has to be determined experimentally. For this purpose a T7 Endonuclease assay, also called Surveyor Assay (see below), was performed. The Surveyor Assay is a mismatch cleavage assay that exploits the property of the endonuclease to detect and cleave base-pair mismatches. HEK 293T cells with Tetracycline inducible expression of Cas9 were transfected with each sgRNA separately. After 48h, genomic DNA was extracted and the genomic region around the predicted cutting site was amplified via PCR. The PCR fragments were then denatured and reannealed. The reannealing would lead to a hybrid double-strand formation consisting of a WT strand and a strand with insertions or deletions (Indels). The hybrid formation, a sequence asymmetry, would lead to a loop formation, which would be then recognized by the T7 Endonuclease and cleaved. The more cleaved fragments there were in comparison to intact fragments, the better was the efficiency of the sgRNA to attract the Cas9 and induce double-strand breaks (DSBs).

4.2.1 T7 Endonuclease Assay (Surveyor Assay)

Surveyor Assays for *TH* (Fig. 16A) and *KCNJ6* (Fig. 16B) were loaded on gel to get an indication of sgRNA efficiency to induce DSBs. The *TH*-Surveyor Assay shows detectable Indels with three of four sgRNAs. Indel detection was strongest with sgRNA4. sgRNA2 was not detectable on gel. Negative control shows no detectable Indel identifying bands.

Surveyor Assay for *KCNJ6* shows that Indels were detectable for all five sgRNAs. Indel detection was strongest with sgRNA4. sgRNA1 Indel detection was very weak and did not appear at the right height. Negative control shows no detectable Indel identifying bands.

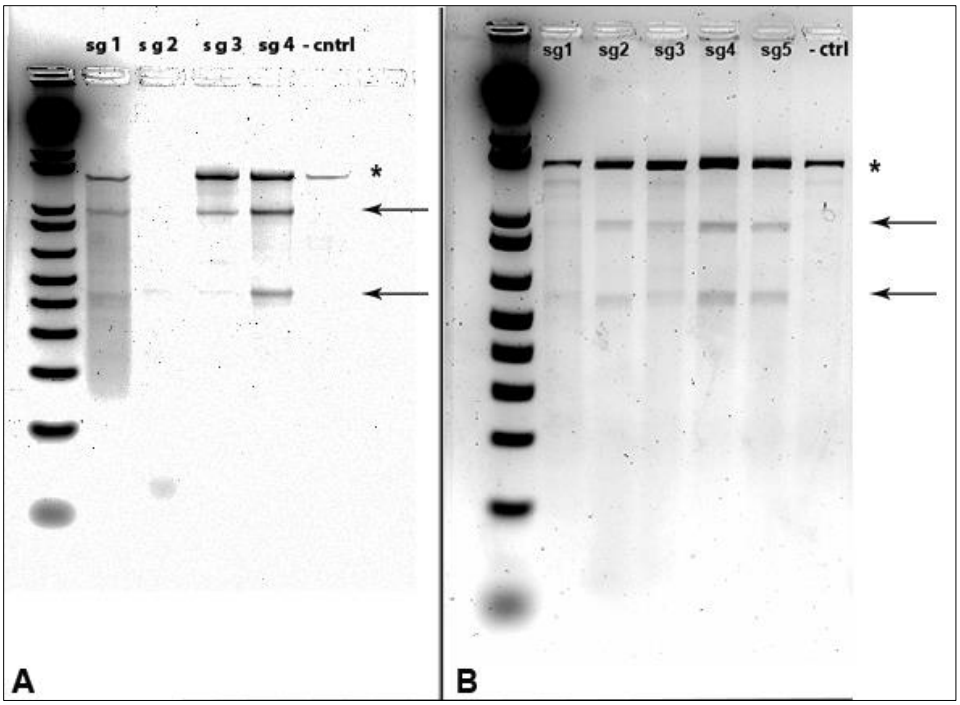

Fig. 16 Surveyor Assay of different sgRNAs. Each asterisk indicates undigested dsDNA, each arrow indicates big (ca 900 bp) and small (ca 500 bp) digested fragment (A) *TH* surveyor gel showing T7 digested dsDNA for TH sgRNA 1-4. (B) *KCNJ6* surveyor gel showing T7 digested dsDNA for GIRK sgRNA 1-5.

For each lane, the fraction of the PCR product cleaved was calculated using a specific formula (Ran et al. 2013a) (see chapter 3.1.3) and the percentage of Indel formation was calculated. Resulting values were the following:

	indel%
GIRK sgRNA1	3.4
GIRK sgRNA2	9.3
GIRK sgRNA3	3.9
GIRK sgRNA4	13.8
GIRK sgRNA5	10.7
TH sgRNA1	4.8
TH sgRNA2	63.3
TH sgRNA3	11.5
TH sgRNA4	23.8

Tab 13 Indel% calculated for each sgRNA

For each gene, the sgRNA4 resulted as the most efficient (see Tab 13). TH sgRNA2 falsely resulted as very efficient due to a non-valid number in the integrated intensity. This result was not considered valid.

4.2.2 *In silico* analysis using "Tide" software

After identifying TH sgRNA4 and GIRK sgRNA4 as the most efficient sgRNAs with the Surveyor Assay, a more accurate estimation of the activity was necessary, as the Surveyor Assay is known to underestimate efficiency. For this purpose, the Surveyor PCR was sequenced in parallel to a PCR of a non-transfected sample. The sequence from HEK293T cells treated with the respective sgRNA4 was analysed against a WT sequence. The relative frequency with which each of four nucleotides was introduced at the break site was calculated by Tide software (Brinkman et al. 2014). Fig. 17 shows that the frequency of unchanged sequence with TH sgRNA4 is 72.1% (A) which leaves a 27.9% frequency for mutagenesis, a value in line with the one calculated with the Surveyor Assay. Fig. 17B shows that the mutagenesis is indeed occurring at the cutting site as expected.

Fig. 18 shows that the frequency of unchanged sequence with GIRK sgRNA4 is 65.9% (A) which leaves a 34.1% frequency for mutagenesis, almost three times higher than that calculated with the Surveyor Assay. Fig. 18B shows that the mutagenesis is indeed occurring at the cutting site as expected.

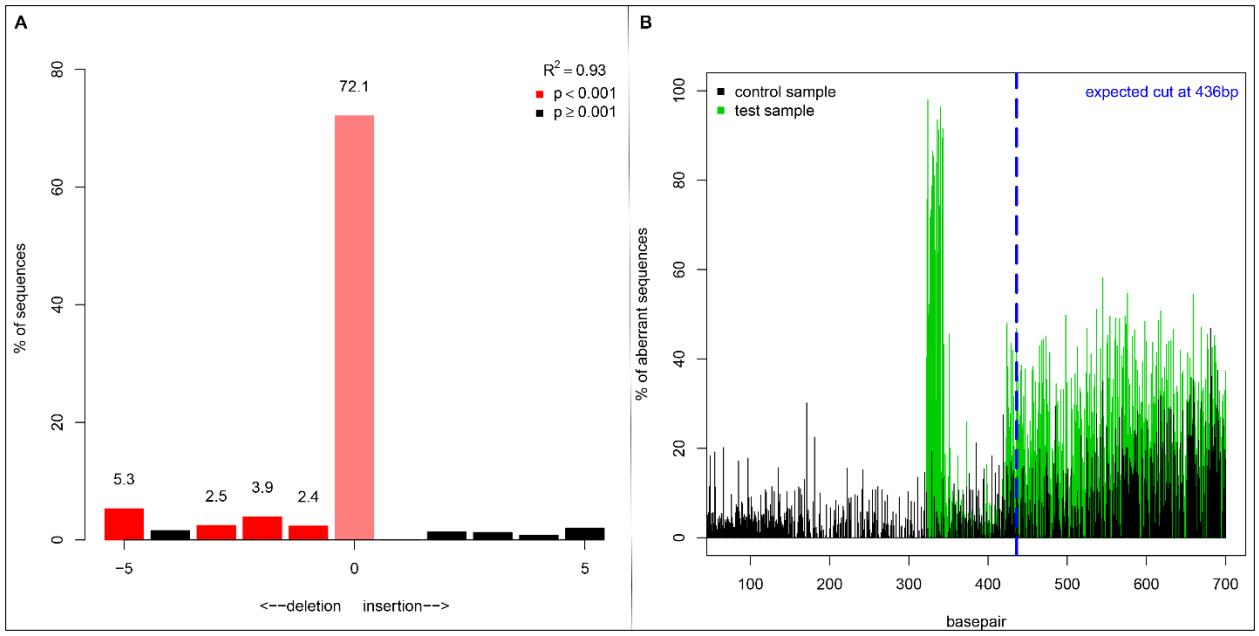

Fig. 17 Application of TIDE to sequenced region of DNA targeted with TH sgRNA4. (A) Indel spectrum for TH sgRNA4 determined by TIDE. (B) Aberrant nucleotide signal of the sample (green) compared to that of the control (black). Blue dotted line indicates the expected cutting site.

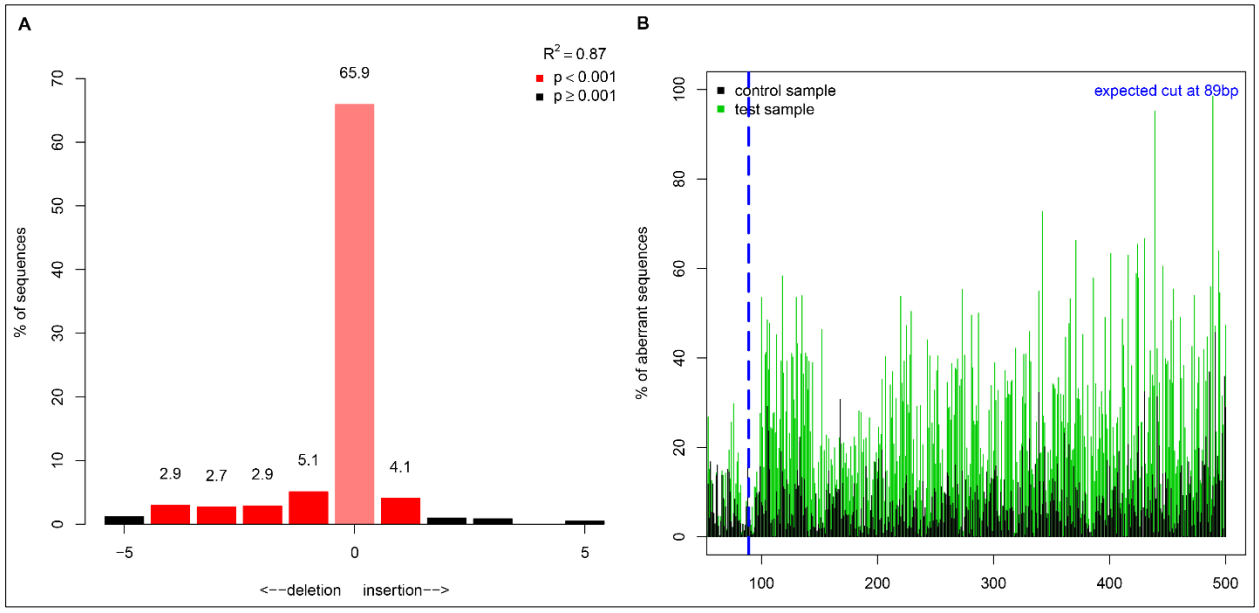

Fig. 18 Application of TIDE to transfected HEK 293T cells. (A) Indel spectrum for GIRK sgRNA 4 determined by TIDE. (B) Aberrant nucleotide signal of the sample (green) compared to that of the control (black). Blue dotted line indicates the expected cutting site.

4.3 Early homologous recombination detection using ddPCR

After electroporation of hiPSC lines, a major issue is how to detect correctly engineered cells. This was not a trivial consideration because HR events are much more unlikely to happen after Cas9 induced DSBs than NHEJ and may occur with frequencies below 1% (Soldner, Laganière, et al. 2011; Miyaoka et al. 2014). Indeed, the downstream work of picking up clones is work and cost intensive, therefore the certainty of actually having generated correct cell clones was of utmost importance. Standard screening techniques like PCR or qRT-PCR did not meet the required resolution at such a small scale of event detection, so we chose digital droplet PCR (ddPCR) instead.

Specifically, for this work ddPCR system from Bio-Rad was used, where partitions are formed with an oil sheath. The PCR reaction is randomly distributed among 20,000 identically sized oil droplets. The PCR reaction is run in a standard thermocycler with standard PCR conditions. Afterwards, fluorescence intensity (coming from a probe or an intercalating dye) of every droplet is analyzed individually with a droplet reader and data is visualized on a dot plot, so much like a FACS analysis. For each droplet, the concentration of the target sequence is calculated by modelling a Poisson distribution. Droplets are assigned negative or positive due to the amount of their fluorescence.

4.3.1 Assays for HR detection

The detection of the correctly engineered clones had to be specific. Accidentally picking up signal from leftover donor plasmid or randomly integrated donor plasmid had by all means to be avoided, as this would have led to an extreme overestimation of engineering efficiency.

The assay for the insert detection was therefore designed to have the forward primer in the genomic sequence of either *TH* or *KCNJ6* gene but upstream of the target 800bp homology sequence present on the donor plasmid. The reverse primer was designed to be in the actual insert sequence region, in the sequence of the T2A peptide (see Fig. 19). An off-shelf assay for a reference gene (RPP30) was included in the analysis to be able to calculate fractional abundance of the insert in comparison to total number of DNA copies.

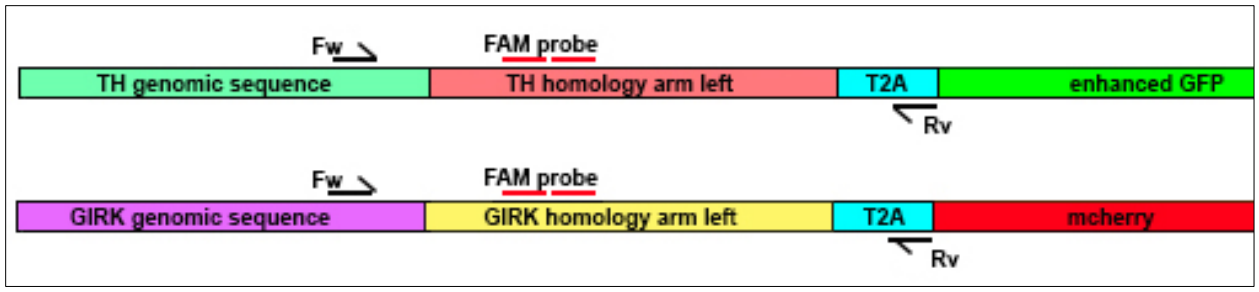

Fig. 19 Schematic representation of primer position for HR screening

4 days after transfection, genomic DNA from pool of cells was extracted for early HR screen with ddPCR. Successful HR was detected with two primer-probe pairs that were designed to detect the starting sequence of the insert (T2A, see Fig. 19). The reverse primer was positioned on the T2A peptide sequence and the forward primer was positioned outside of the homology arm sequence to avoid picking up signal from left over peptide. The probe sequences were positioned on the right homology arm's sequence.

Reactions were run with non-transfected samples of each cell line respectively as negative control in parallel with transfected samples.

4.3.2 ddPCR Quality controls

For each reaction mix, a no-template control (NTC) was run as quality check. A positive control was run for both assays, which were non-transfected samples spiked with custom gBlocks® (double stranded synthetic DNA fragments) from IDT® identical to sequence to be amplified from genomic DNA (see Fig. 20).

Most importantly, NTC had to be completely negative in both channels. Non-transfected samples had to be negative in the Ch1 (insert detection) but positive in Ch2 (reference gene). gBlock samples had to be positive in both Ch1 and Ch2. Event count was checked as a quality control of each single reaction. If droplet count was below 10,000, separation of negative and positive droplets was checked for clear separation. If both of the last quality checks failed, sample was not taken into consideration for analysis.

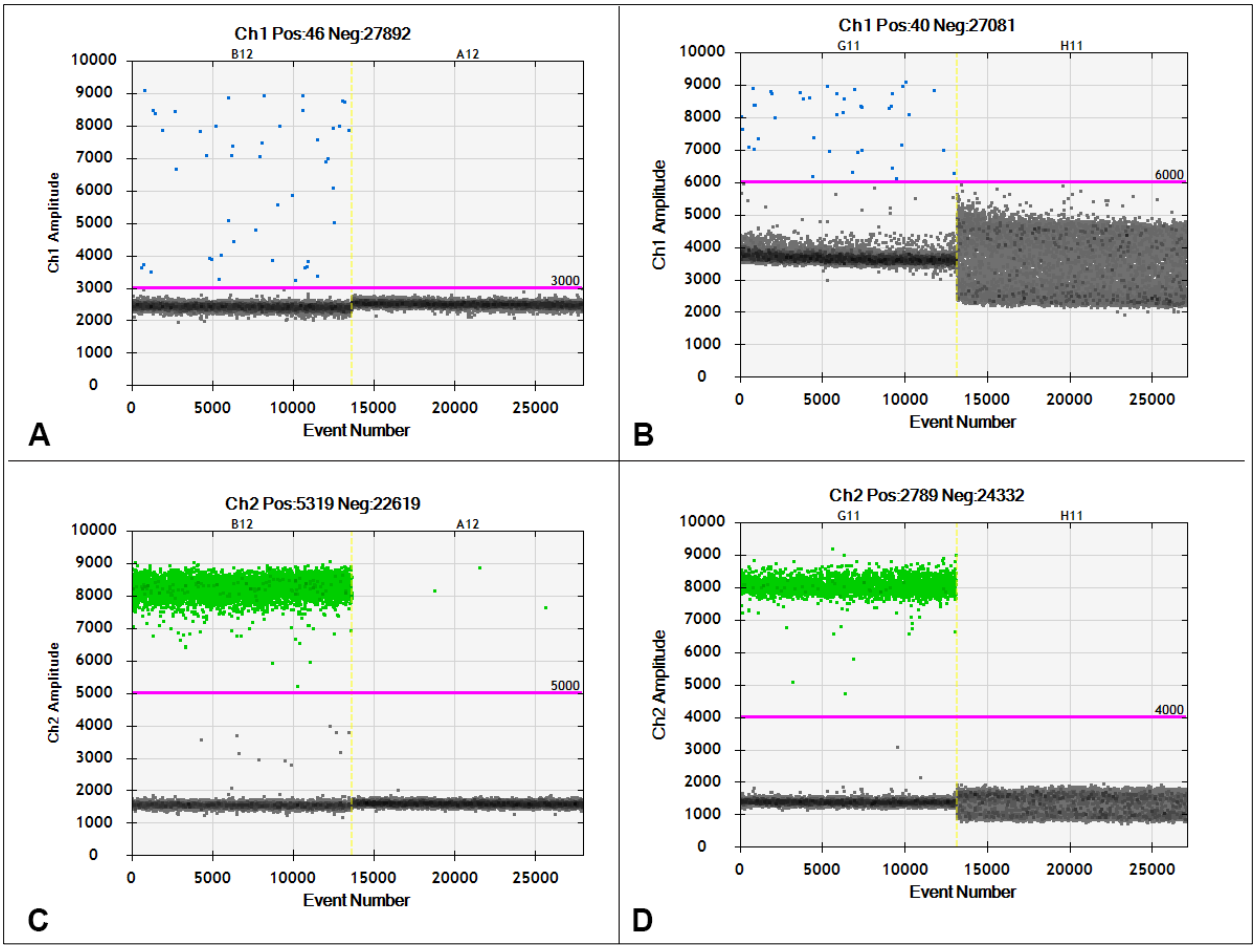

Fig. 20 (A,C) Positive (left) control for TH assay using gDNA of non-transfected cells spiked in with gBlocks containing respective amplicon sequence; and negative control (right) using a no template control. (B,D) Positive (left) control for KCNJ6 assay using gDNA of non-transfected cells spiked in with gBlocks containing respective amplicon sequence; and negative control (right) using a no template control

4.3.3 HR detection for *TH* locus

The three hiPSC lines 802#7, SFC 856-03-04 and SFC 840-03-05 were transfected with the CRISPR constructs for TH engineering. After Puromycin selection, gDNA was extracted from the selected cell pool for HR detection using ddPCR with a two probe based assay mix. The reaction was analyzed in the ddPCR Droplet Reader and results displayed by QuantaSoft® software. First, signals were displayed in 1D amplitude (Fig. 21 and Fig. 22). The 1D amplitude graph shows the signal amplitude of each channel individually plotted against the event number. Ch1 detects the signal for the insert whereas in Ch2 we see the signal for the reference gene RPP30. For all samples, detection was clear in the 1D amplitude. This plot is also used to set thresholds for every individual channel. Threshold setting is individual to every assay and every experimental run.

4.3.3.1 TH HR 1D amplitude

HR signal was measured for each of the three cell lines and always confronted to a respective non-transfected sample. In Fig. 21 we see Ch1 (blue) signal for cell lines 802#7 and SFC 856-03-04 engineered with TH construct (right half of figure) confronted to both lines as non-transfected (NT) samples (left half of figure). In Ch1, the positive events were easily identifiable making reference to the non-transfected control samples. In the non-transfected samples, no positive events were detected at all in Ch1. The threshold was put very low, slightly above the highly abundant population of negative events but high enough to ensure only readout of positive events.

In Ch2 (green), we see the signal for the reference gene RPP30, which was detected for non-transfected samples as well as for engineered samples. The distinction between negative and positive events was clearer and positive events were more abundant. The threshold was put midway between negative and positive event populations to ensure picking up clearly positive events.

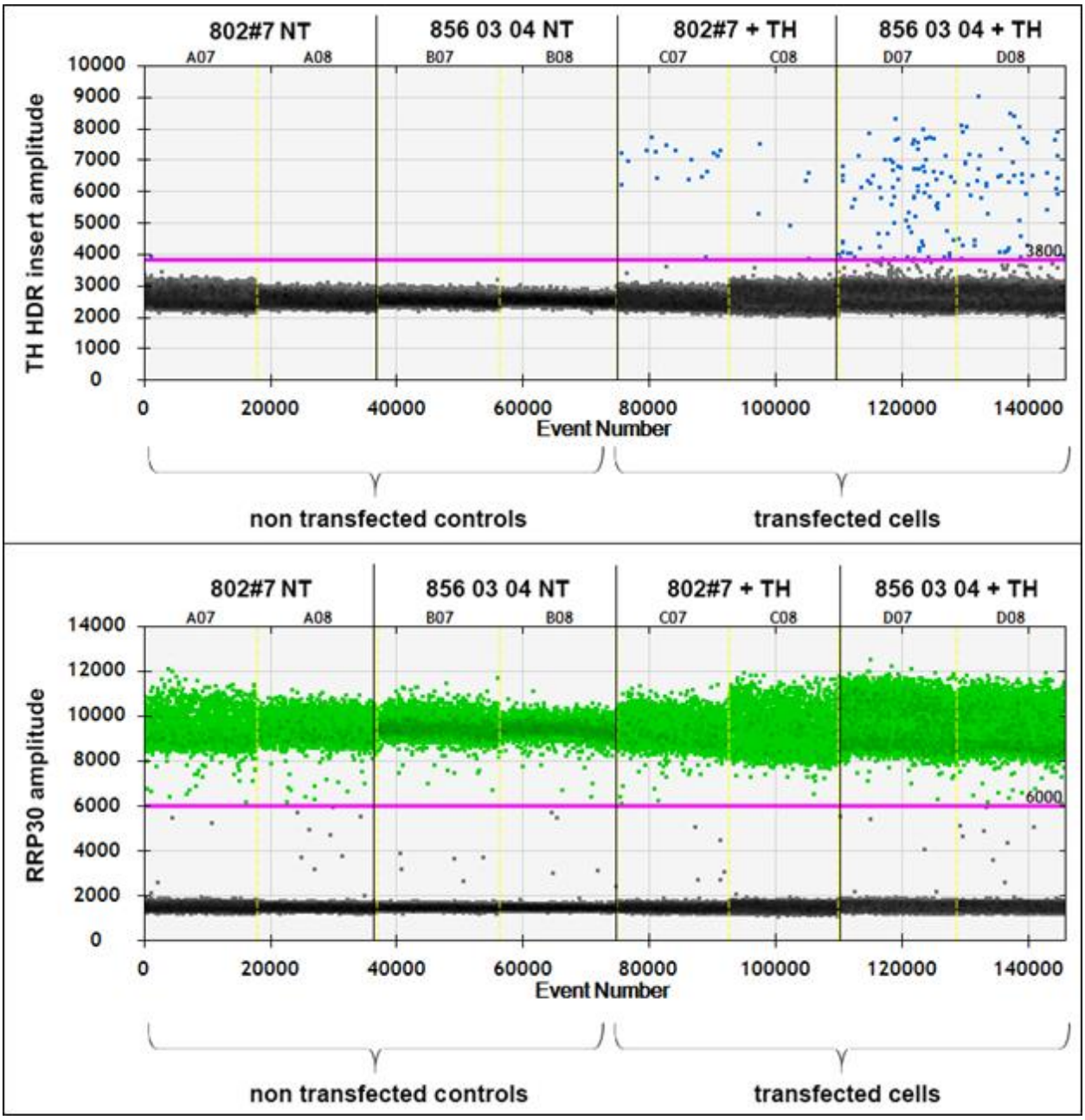

Fig. 21 1D amplitude of signal detection for TH HR screen in hiPSC lines 802#7 and SFC 856-03-04 compared to non-transfected samples of the same cell lines.

In Fig. 22 we see Ch1 signal for cell lines SFC 840-03-05 engineered with TH construct (right half of figure) confronted to both lines as non-transfected (NT) samples (left half of figure). Referring to the non-transfected control sample, Ch1 positive events were easily identifiable. The threshold was put very low to ensure complete readout of positive events.

Ch2 signal for the reference gene was detected for non-transfected samples as well as for engineered samples also for this cell line.

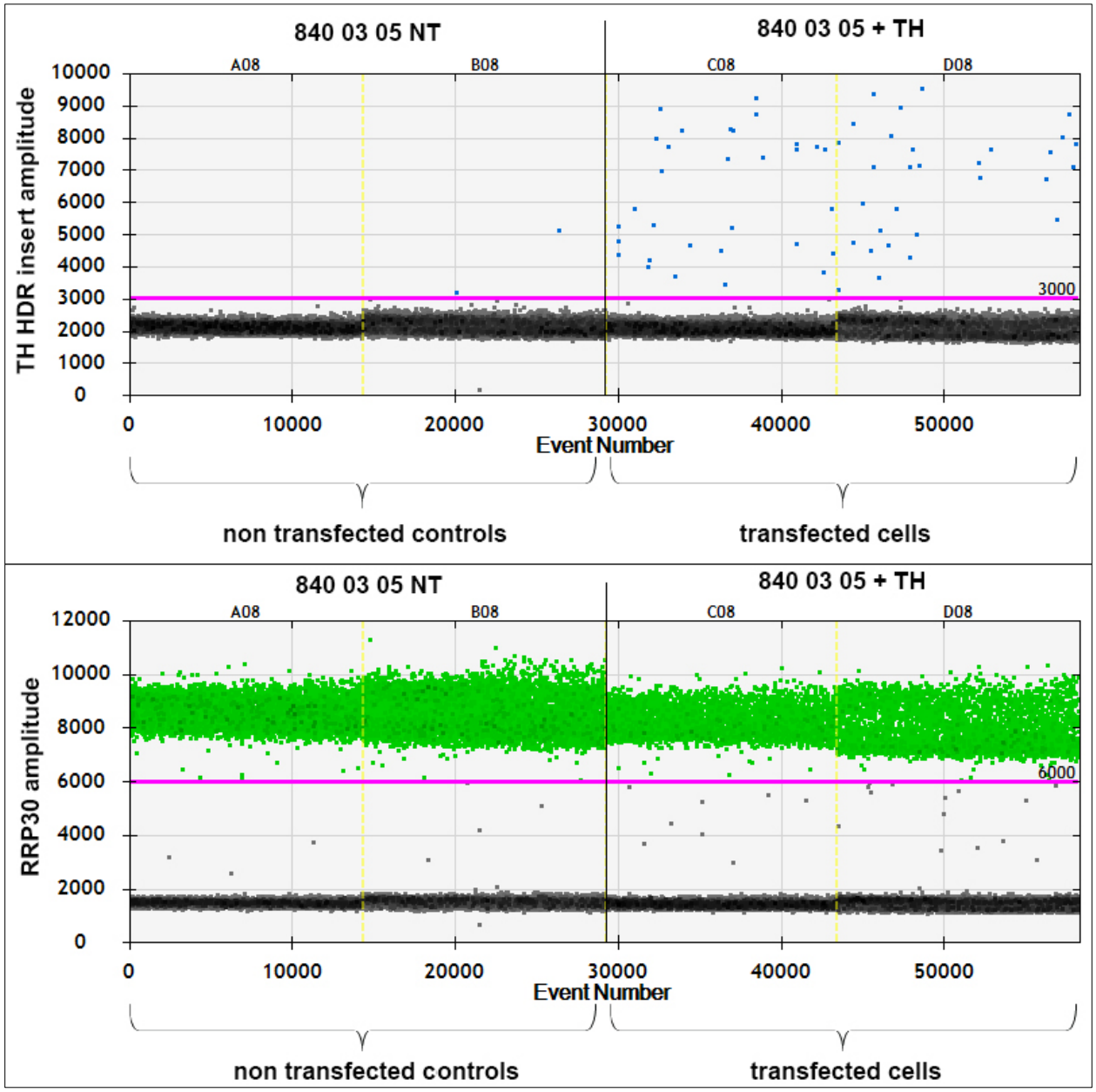

Fig. 22 1D amplitude of signal detection for TH HR screen in hiPSC line SFC 840-04-05 compared to non-transfected sample of the same cell line. reference gene detection is on display in Ch2 (green)

4.3.3.2 TH HR 2D amplitude

In the 2D amplitude, data for both channels is represented together in one plot consisting of X and Y-axis. The Y-axis shows the signal amplitude for the HR detection, the X-axis the signal amplitude for reference gene detection.

There are four possible populations of events, which are expected to cluster in different angles of the plot:

- Double negative: left low
- Single positive Ch1: left high
- Single positive Ch2: right low
- Double positive: right high

In Fig. 23 we see the 2D plot for cell lines 802#7 (Fig. 23A), SFC 856-03-04 (Fig. 23B) and SFC 840-03-05 (Fig. 23C). For all three cell lines, the Ch1 single positive population was clearly clustered at the left high angle of the plot. For cell line 802# 7, the clustering was most clear and highest, whereas in cell lines SFC 856-03-04 and SFC 840-03-05 the population was more disperse and starts as a rising population from the double negative population. For cell line SFC 840-03-05 also a small double positive population was detectable, similar also in SFC 856-03-04 but here the population is shifted to the lower part of the plot and only rises slightly from the Ch2 positive population.

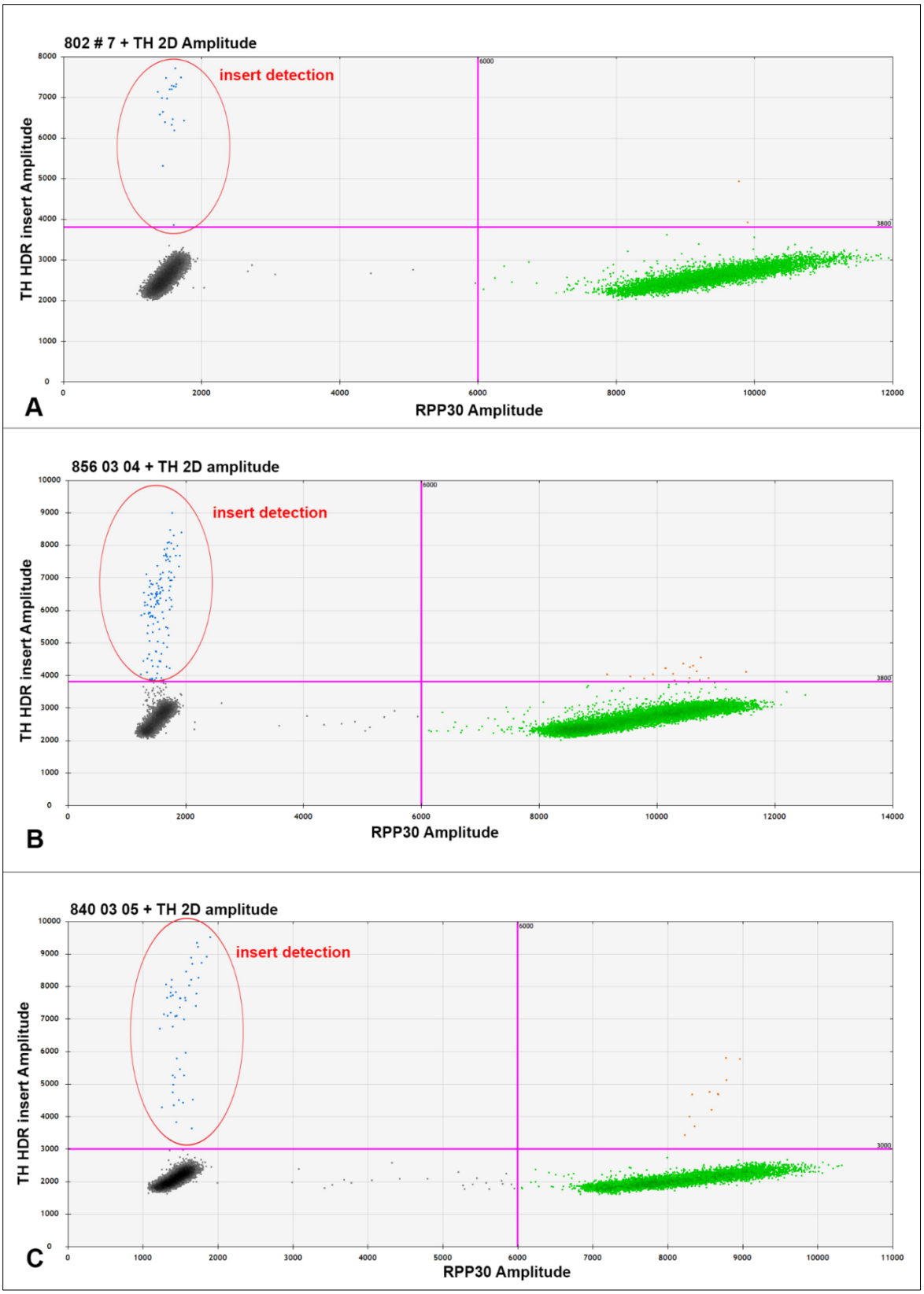

Fig. 23 2D amplitude of TH HR detection of hiPSC lines 802#7 (A), SFC 856-03-04 (B) and SFC 840-04-05 (C). Ch2 is the reference gene.

4.3.3.3 TH HR Fractional abundance

The fractional abundance is calculated automatically by the QuantoSoft™ ddPCR analysis system when comparing target events against a reference gene. The value represents the percentage of events detected with the target sequence, in this case our HR sequence. The abundance was lowest for the 802#7 line, with 0.37%. SFC 856-03-04 had the highest abundance with 0.66% and was almost identical to SFC 840-03-05 with 0.64% (see Fig. 24).

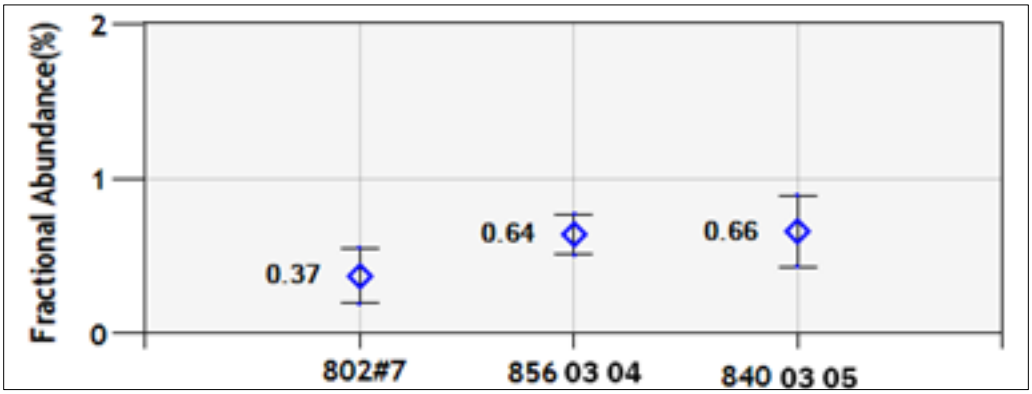

Fig. 24 Fractional abundance (%) for the TH HR sequence calculated for every cell line individually.

4.3.4 HR detection for *KCNJ6*/*GIRK2* locus

4.3.4.1 KCNJ6 HR 1D amplitude

Again, HR signal was measured for each one of the three cell lines and always confronted to a respective non-transfected sample. In Fig. 25 we see Ch1 signal for cell lines 802#7 and SFC 856-03-04 engineered with KCNJ6/GIRK2 construct (right half of figure) confronted to both lines as non-transfected (NT) samples (left half of figure). In the 1D representation of Ch1, positive events detected in the transfected samples can be seen whereas in the non-transfected control samples they are absent. The threshold was put low, slightly above the population of negative events but high enough to ensure complete readout of positive events.

Ch2 was again the display of RPP30 reference gene, which was detected for non-transfected samples as well as for engineered samples. Positive events were abundant. The threshold was put midway between negative and positive event populations to ensure picking up clearly positive events.

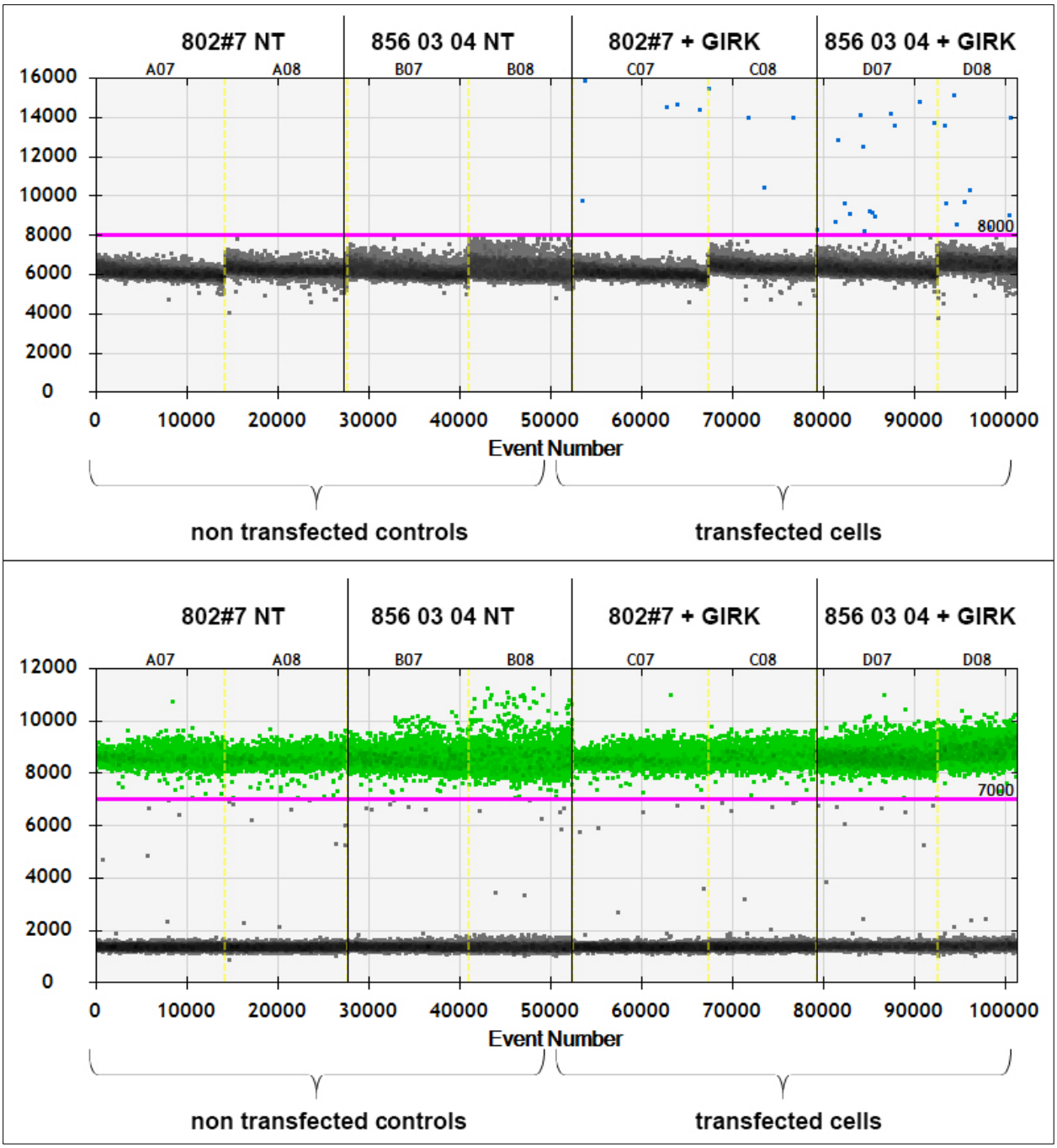

Fig. 25 1D amplitude of signal detection for GIRK2 HR screen in hiPSC lines 802#7 and SFC 856-03-04 and compared to non-transfected samples of the same cell lines. Reference gene RPP30 is displayed as Ch2 in green.

In Fig. 26, we see Ch1 signal for cell line SFC 840-03-05 with KCNJ6/GIRK2 construct (right half of figure) in reference to a non-transfected (NT) sample (left half of figure). Data is consistent with the other two

cell lines, showing positive events in the 1D representation of Ch1, whereas in the non-transfected control sample they are absent. Also for SFC 840-03-05, Ch2 display of RPP30 reference gene was detected for non-transfected samples as well as for engineered samples and positive events were abundant.

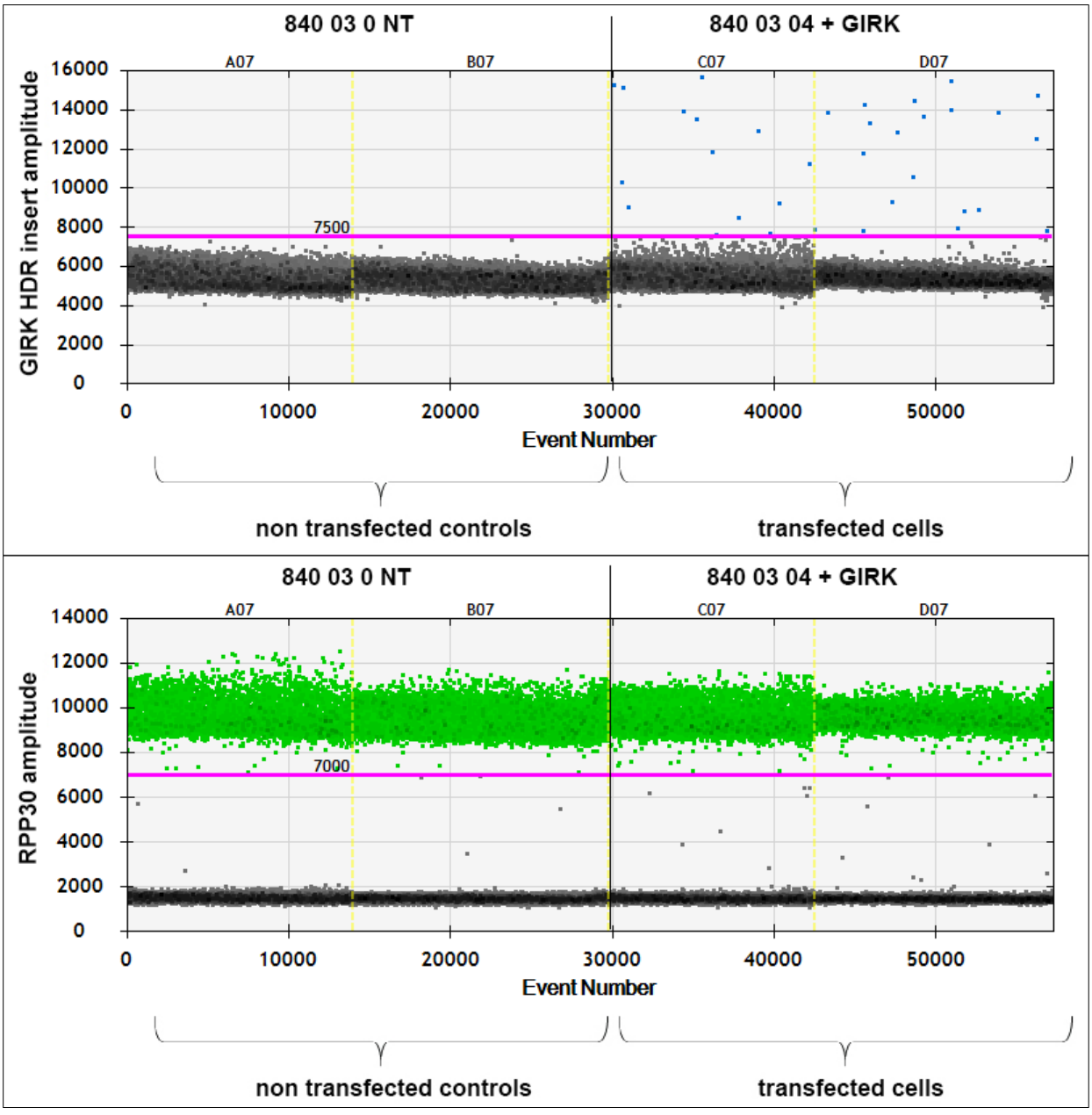

Fig. 26 1D amplitude of signal detection for GIRK2 HR screen in hiPSC line SFC 840-04-05 compared to non-transfected sample of the same cell line. Reference gene RPP30 is displayed as Ch2 in green.

4.3.4.2 KCNJ6 HR 2D amplitude

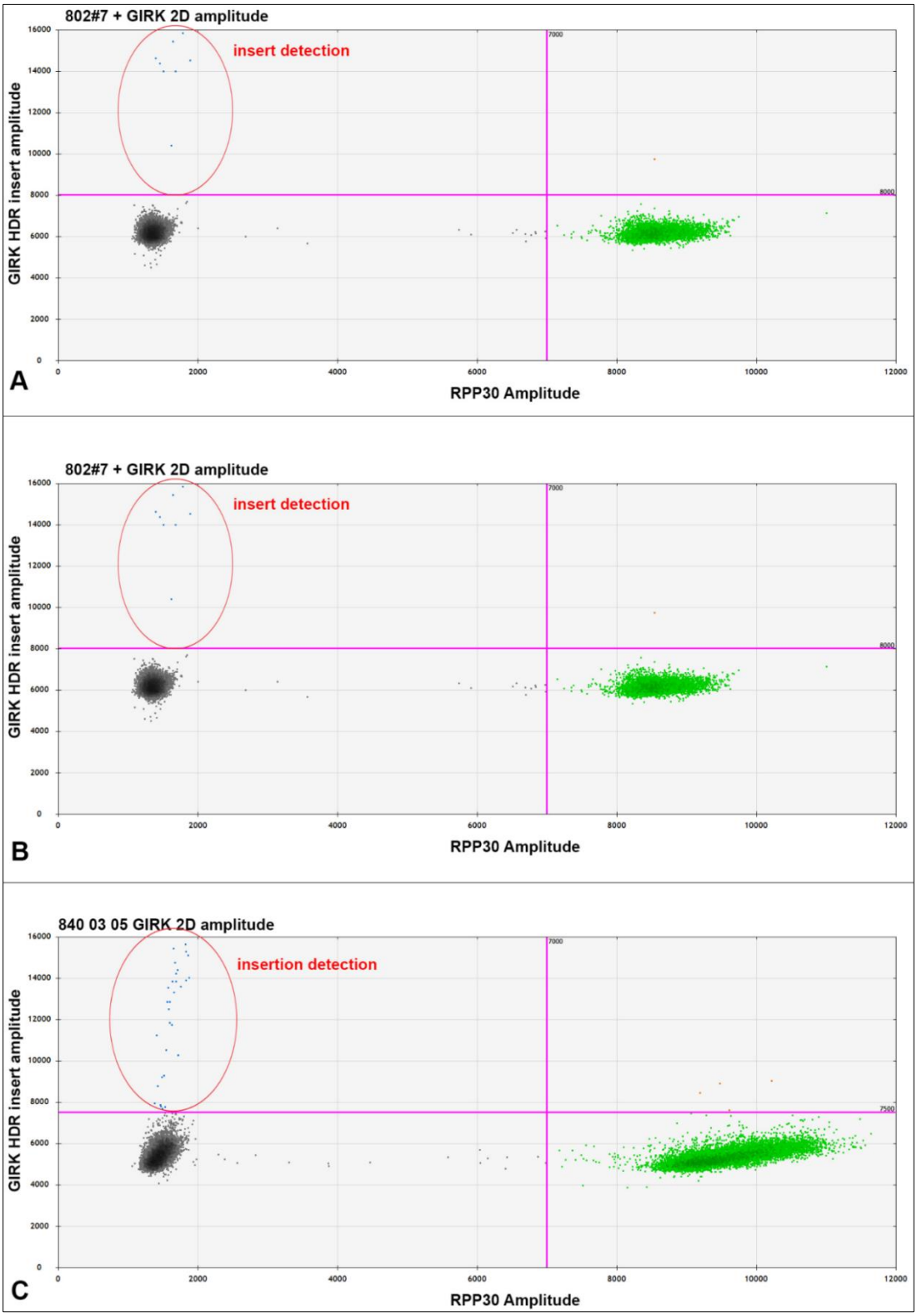

Fig. 27 2D amplitude of GIRK2 HR detection of hiPSC lines 802#7 (A), SFC 856-03-05 (B) and SFC 840-03-04 (C). Reference gene RPP30 is displayed as Ch2 in green.

For KCNJ6/GIRK2 locus, a 2D plot was evaluated showing for all three cell lines a rich cluster on the lower right for RPP30 and a small cluster of GIRK2 HR on the upper left. Very few double positives are detected in the upper right panel of all cell lines (see Fig. 27A-C).

4.3.4.3 KCNJ6 HR Fractional abundance

The fractional abundance calculated for KCNJ6/GIRK2 locus was much lower than that for the TH locus but still detectable. Again, 802#7 was the cell line with the lowest abundance (0.15%) similar to SFC 856-03-04 with 0.17%. SFC 840-04-05 had the highest abundance with 0.24% (see Fig. 28)

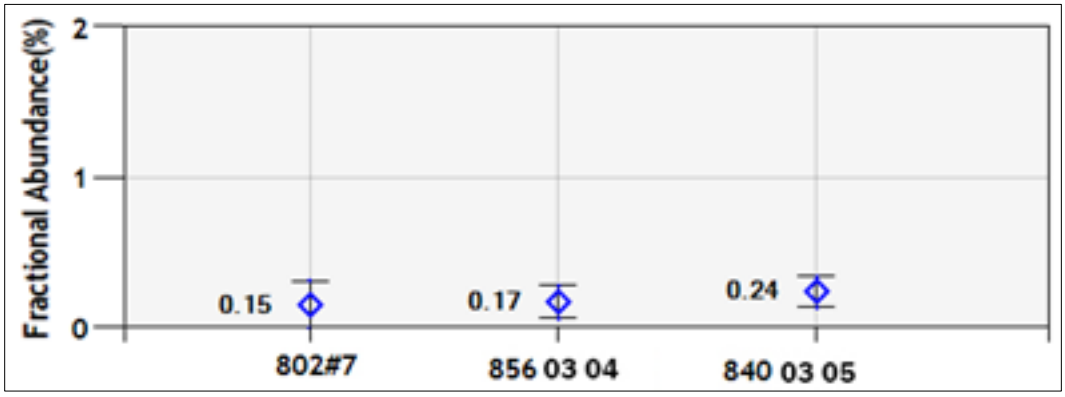

Fig. 28 Fractional abundance calculated for KCNJ6/GIRK2 HR for cell lines 80#7, SFC 856-03-04 and SFC 840-03-05.

4.4 Identification of clonal identity of manually selected hiPSC clones

4.4.1 ddPCR for clonal screening

For the identification of single clones on 96-well plates that were correctly engineered, again, ddPCR was used for the detection of the same signal as in the HR screen (see chapter 4.3.1). After single cell clones were transferred from MEF feeder cells to a feeder free culture in the 96 well plate and frozen (see Material and Methods chapter), their genomic sequence was analysed with ddPCR probes TH long 1+2 and GIRK long 1+2.

A clone-pool strategy was designed where gDNA of different clones was pooled together for analysis to reduce costs and work load: wells of each column of a plate were pooled (see Fig. 9, chapter 3.3.3) together and analysed by ddPCR. Then, when in one of these pooled reactions a positive signal was detected, all wells of this column were analysed in a separate ddPCR reaction to identify the single positive wells.

The 96 well plates that were used for culturing were barcoded and the barcode from the genomic DNA plate was used as acronym for naming the identified clones. For example, all columns from plate 10000**992** were analysed and samples were called 992-1 to 992-12. Once, a positive column was identified, each single well from this column was analysed, calling then the sample and the corresponding clones 992-1A to 992-1H.

In Tab 14, the plate acronyms are listed with the corresponding construct type and cell lines. In this chapter, from the 12 analysed plates only data from plates with positive clones are reported.

10000**992**	802#7	TH eGFP
10000**993**	802#7	GIRK mcherry
10000**999**	802#7	GIRK mcherry
1000**1110**	802#7	TH eGFP
1000**1003**	SFC 840-03-05	TH eGFP
10000**994**	SFC 856-03-04	TH eGFP
10000**997**	SFC 856-03-04	TH eGFP

Tab 14 Plate acronyms with corresponding cell lines and knock-in constructs

4.4.1.1 Clonal screening of TH locus

For the screening of TH locus, custom probes TH long 1+2 were used. Fig. 29 reports the ddPCR reads in 2D amplitude for TH knock-in construct of the pooled sample of each individual plate in numeric order from left to right. The figure shows reads of plates 992, 994, 997, 1003 and 1110. They are reported in 2D amplitude to give the best graphic representation of quantity of signal. Red coloured shadows show the columns that were selected for further single well analyses.

Plate 992 showed only one well with a high number of clearly positive droplets, which is column 9. In plate 994, column 1 and 12 showed positive droplets, with column 12 showing a bigger quantity of positivity.

In Plate 997, columns 3, 4, 7 and 8 showed an elevated number of positive droplets. Columns 3 and 4 showed a higher quantity and where then chosen for further characterization.

In plate 1003, columns 6, 10 and 11 showed positive droplets, where columns 10 and 11 showed a much higher quantity than column 6. Column 11 had the highest density of positive droplets.

In plate 1110, only column 6 showed positive droplets and was then chosen for single well analysis.

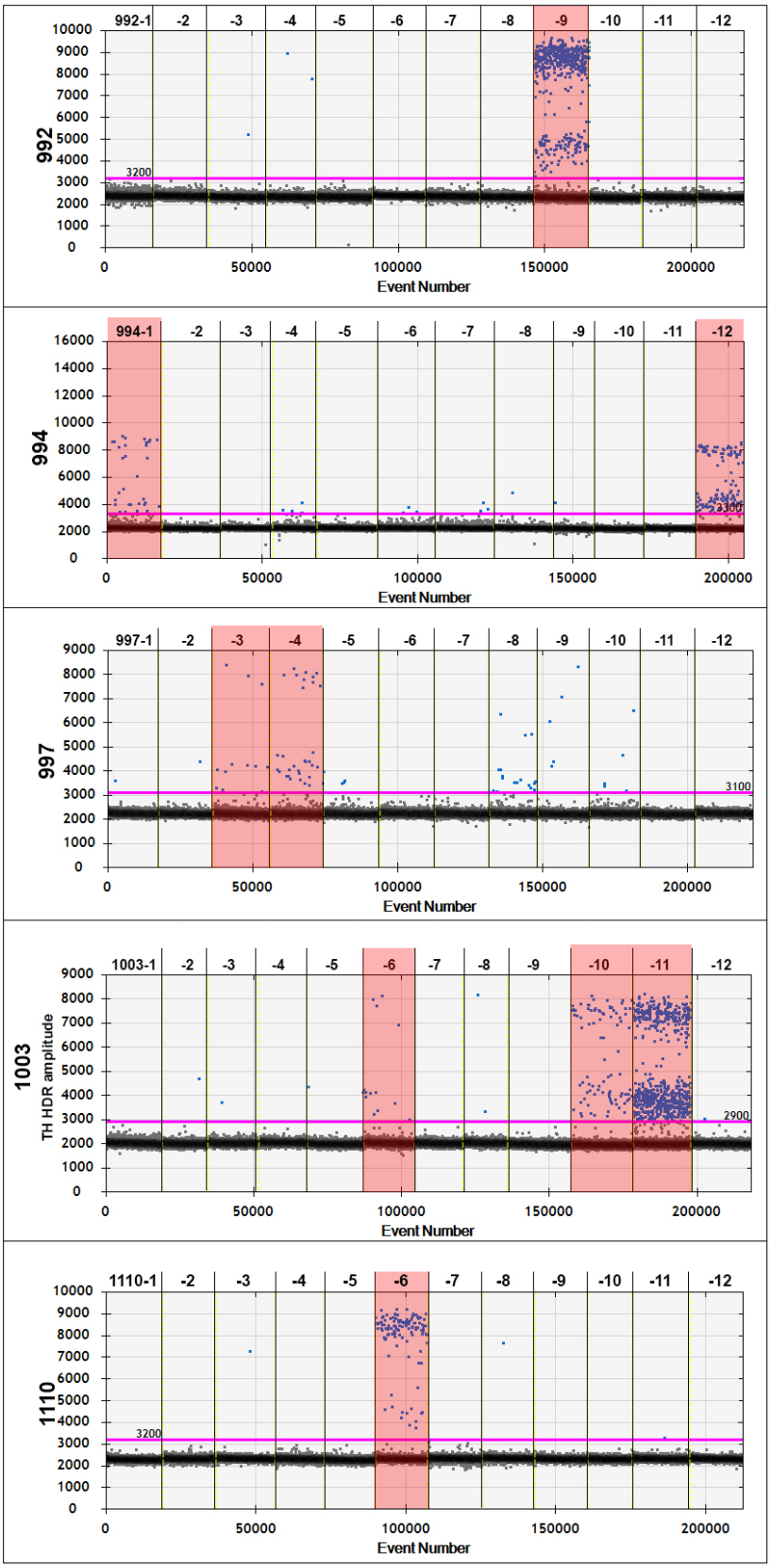

Fig. 29 ddPCR analysis in 2D amplitude of TH knock-in of every single plate. Pooled samples from each column are analyzed and data shown in numeric order from left to right. Red shadow marks indicate the columns chosen for further analyses

Each well was then analysed in a separate run: in Fig. 30 - Fig. 35, data of all individually tested clones is shown. The light red shadows showed the clones that were singled out as positive and subsequently used for sequencing.

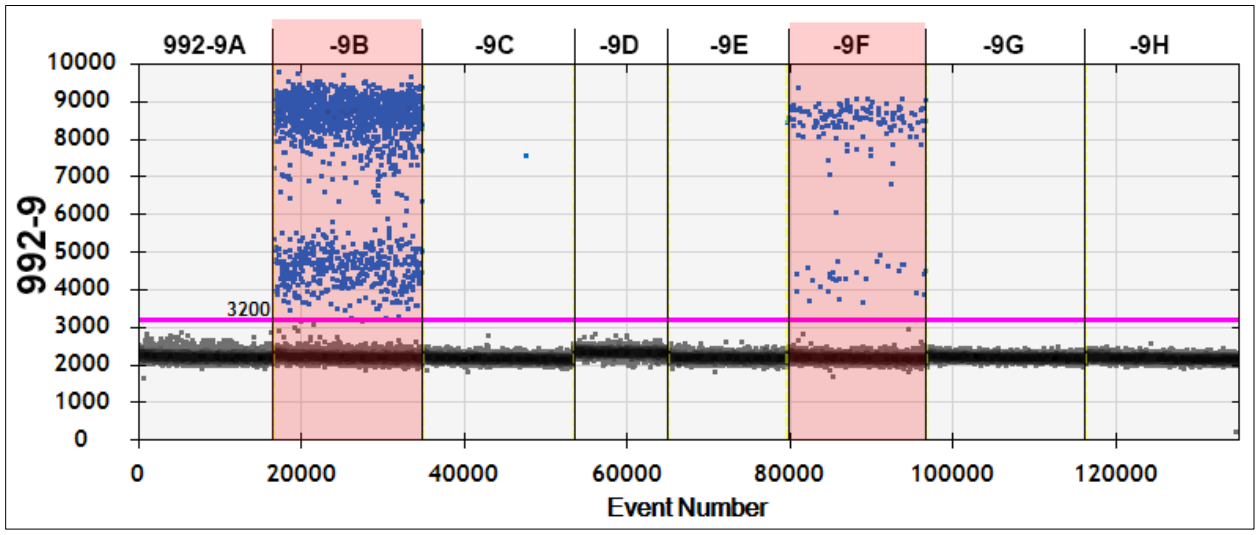

Fig. 30 Single well analyses for column 9 of plate 992 with red shadows showing the single clones identified as positive.

In Fig. 30, analyses of individual clones from plate 992 column 9 are shown. Two clones resulted to be positive in this column, clone 9B and clone 9F, with clone 9B showing a higher quantity of positive droplets. Both clones showed two clusters of positive signal. All the other clones in this column result completely negative for a TH-eGFP knock-in signal.

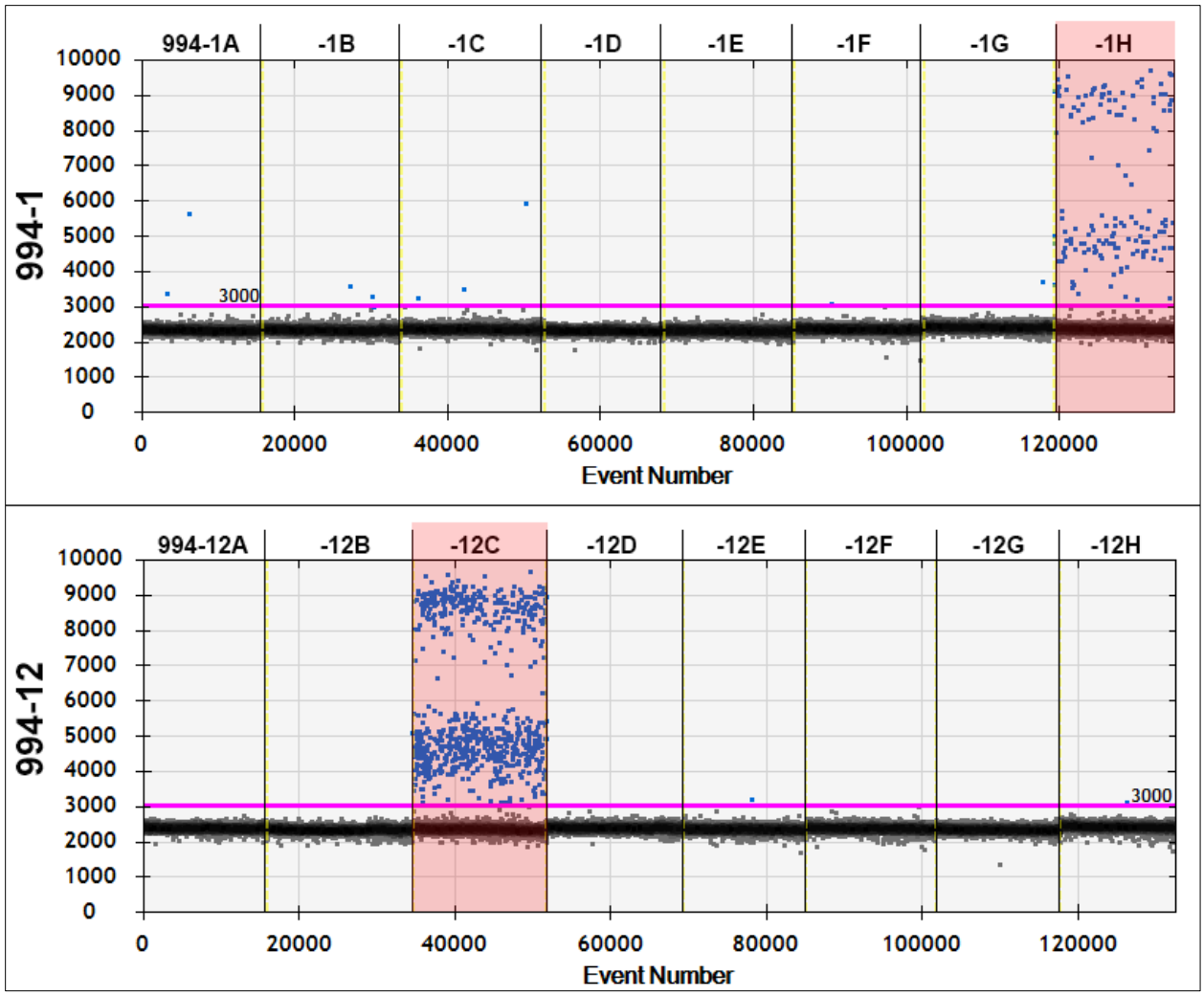

Fig. 31 Single well analyses for columns 1 and 12 of plate 994 with red shadows showing the single clones identified as positive.

In Fig. 31, 2D amplitude data for single clones from plate 994, columns 1 and 12 are shown. In column 1, clone 994-1H that could be confirmed as positive; in column 12, clone 994-12C could be identified as strongly positive as well. Both clones, showed two clusters of positive droplets.

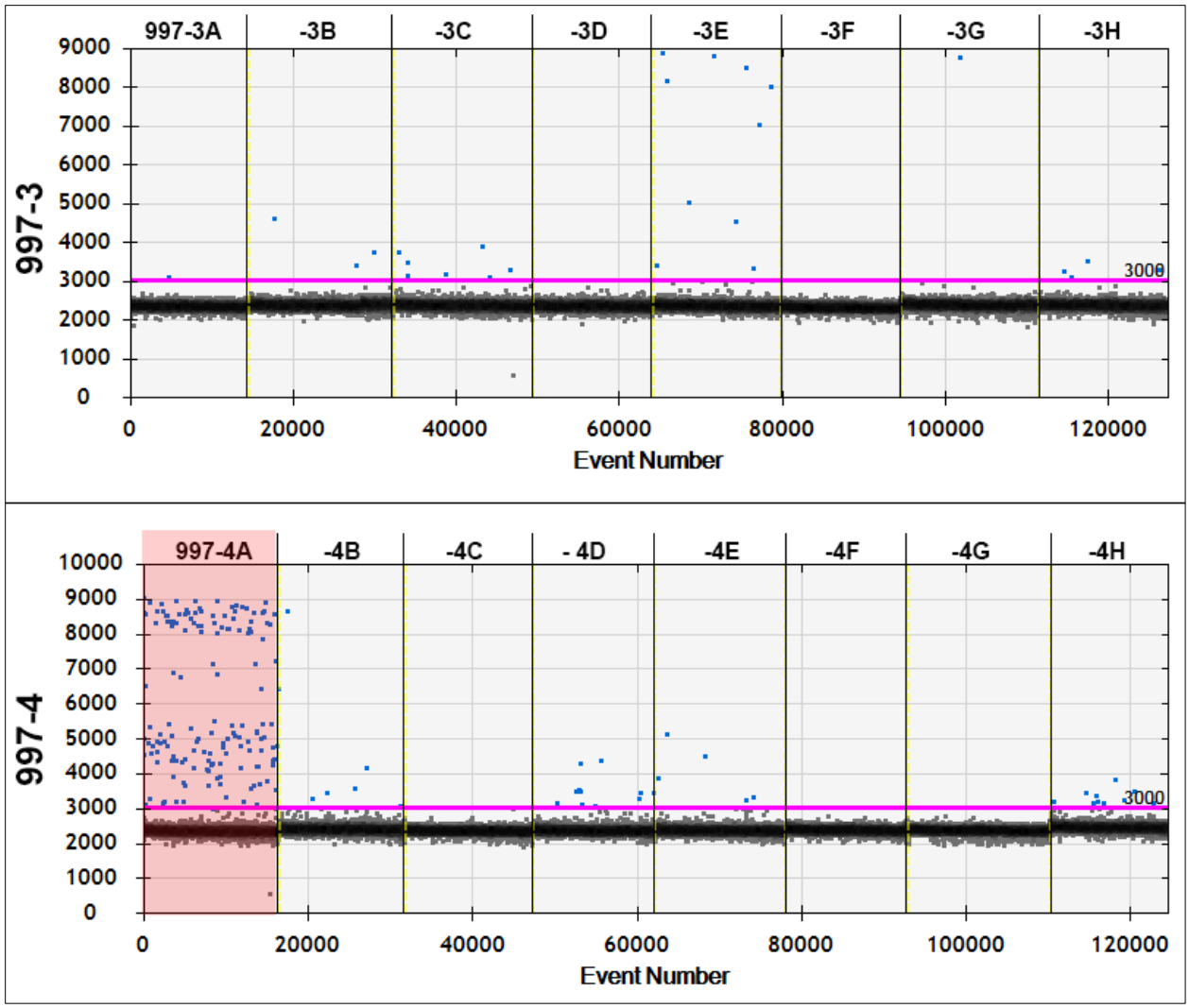

Fig. 32 Single well analyses for columns 3 and 4 of plate 997 with red shadows showing the single clones identified as positive.

In Fig. 32, 2D amplitude of single wells from plate 997 columns 3 and 4 are shown. Clones B, C, E and H from column 3 showed some minimal amount of positive signal but none was selected as clearly positive. In column 4, clones A, B, D and H showed positive droplets, where clone 997-4A showed a high quantity of positive droplets and all the other clones from this column only minimal amounts of positive droplets.

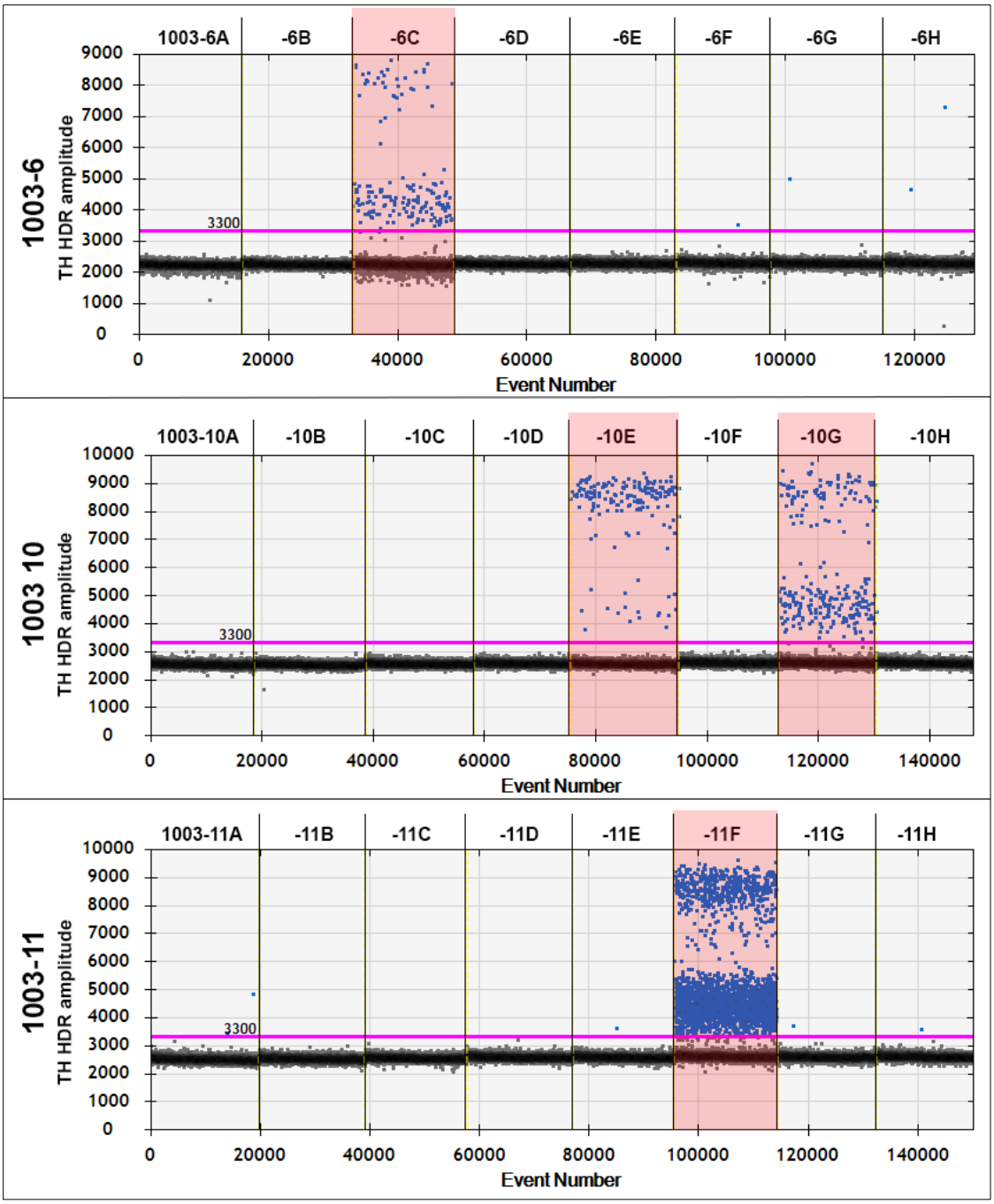

Fig. 33 Single well analyses for columns 6, 10 and 11 of plate 1003 with red shadows showing the single clones identified as positive.

In Fig. 33, data is shown from single clone analyses of plate 1003 and column 6, 10 and 11. In all three columns clearly positive clones could be detected (see red shadows) with clone 1003-11F being the one with the highest quantity of positive droplets.

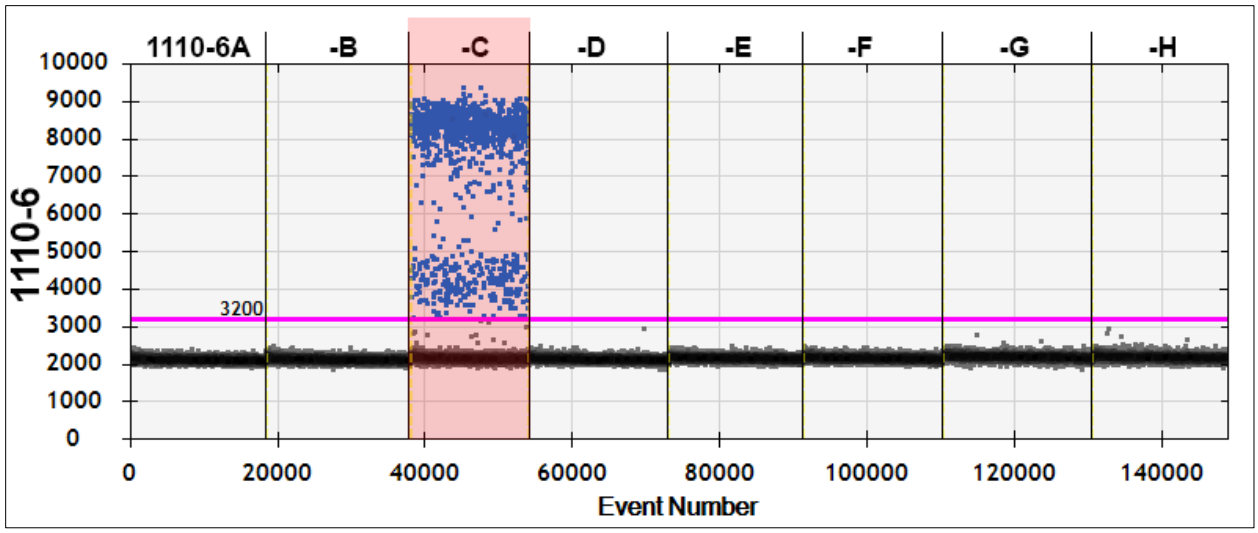

Fig. 34 Single well analyses for column 6 of plate 1110 with red shadows showing the single clones identified as positive.

In Fig. 34, single well analysis of column 6 from plate 1110 is shown. One clone from this plate could be identified as positive, clone 1110-6C and therefore was chosen for further analysis.

4.4.1.2 Clonal screen KCNJ6/GIRK2 locus

For KCNJ6/GIRK2 locus, screening, custom probes GIRK long 1+2 were used. ddPCR reads in 2D amplitude of GIRK2 knock-in construct of the pooled sample of each individual plate in numeric order from left to right are reported in Fig. 35, showing reads from plates 993 and 999.

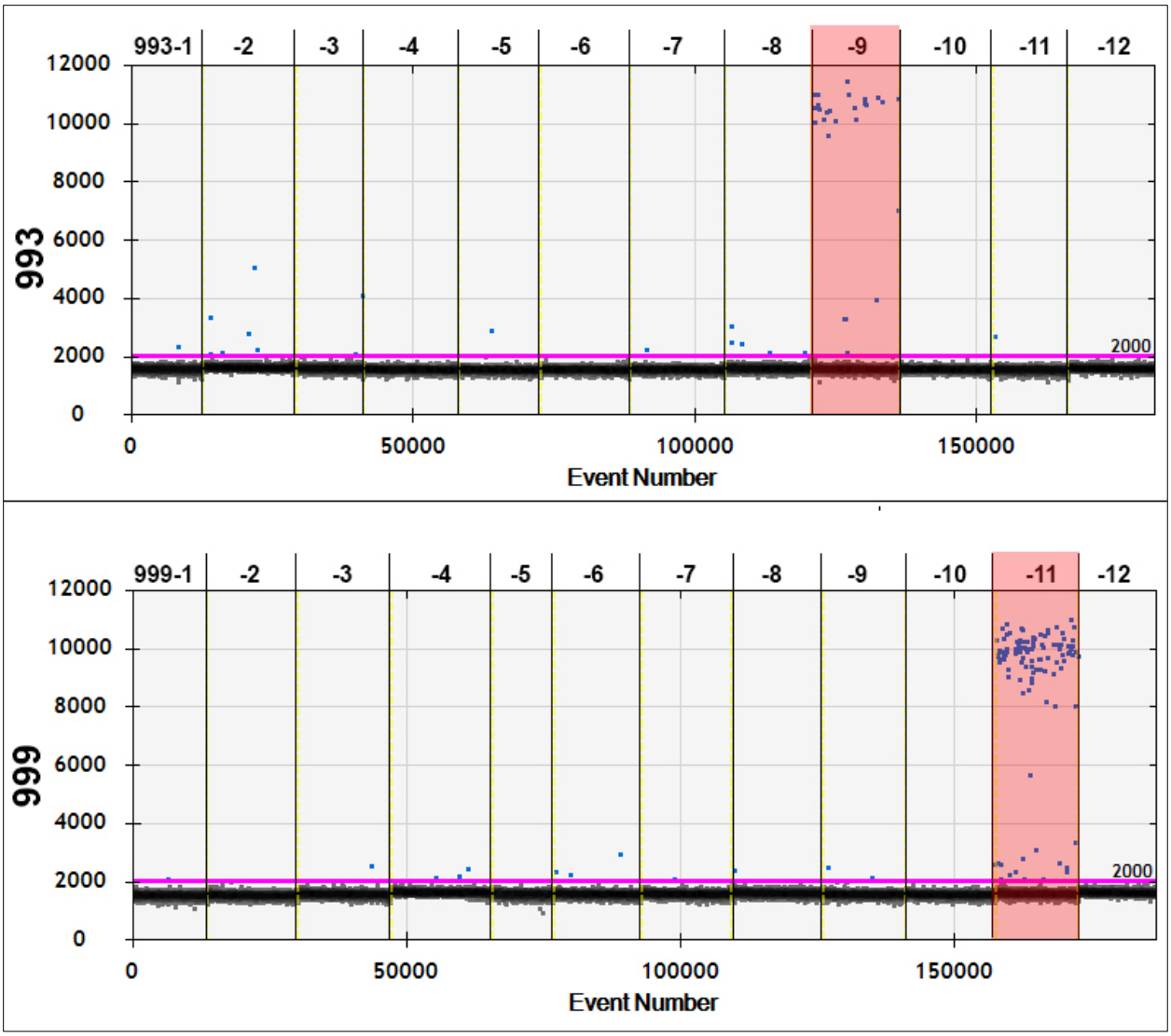

Fig. 35 ddPCR analysis in 2D amplitude for GIRK2 knock-in of both single plate. Pooled samples from each column are analysed and data shown in numeric order from left to right. Red shadow marks indicate the columns chosen for further analyses

Red coloured shadows highlight the columns that were selected for further single well analyses. In plate 993, there is only one positive well that also shows a very low number of clearly positive droplets but it was nevertheless used for analysis of all wells from this column. In plate 999, one well showed positive droplets but also here, the count of positive droplets was not very high. This column was also used nonetheless for further analysis.

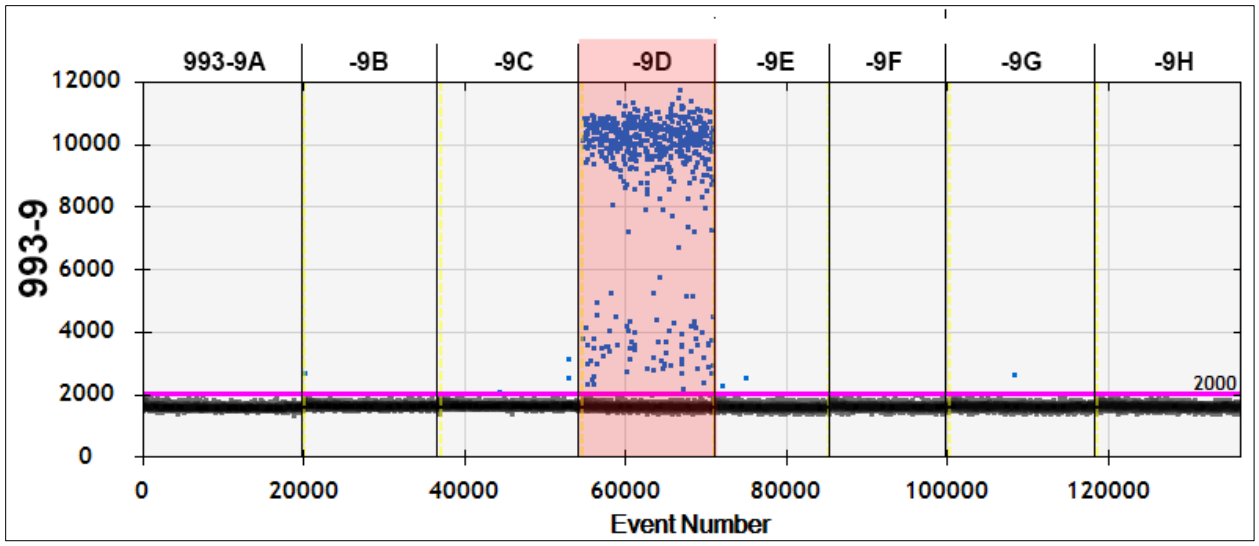

Fig. 36 Single well analyses for column 9 of plate 993 with red shadows showing the single clones identified as positive.

Individual clones from plate 993 column 9 were analysed and data is shown in Fig. 36. One single clone was tested clearly positive, showing two clusters of positive droplets, which is clone 993-9D.

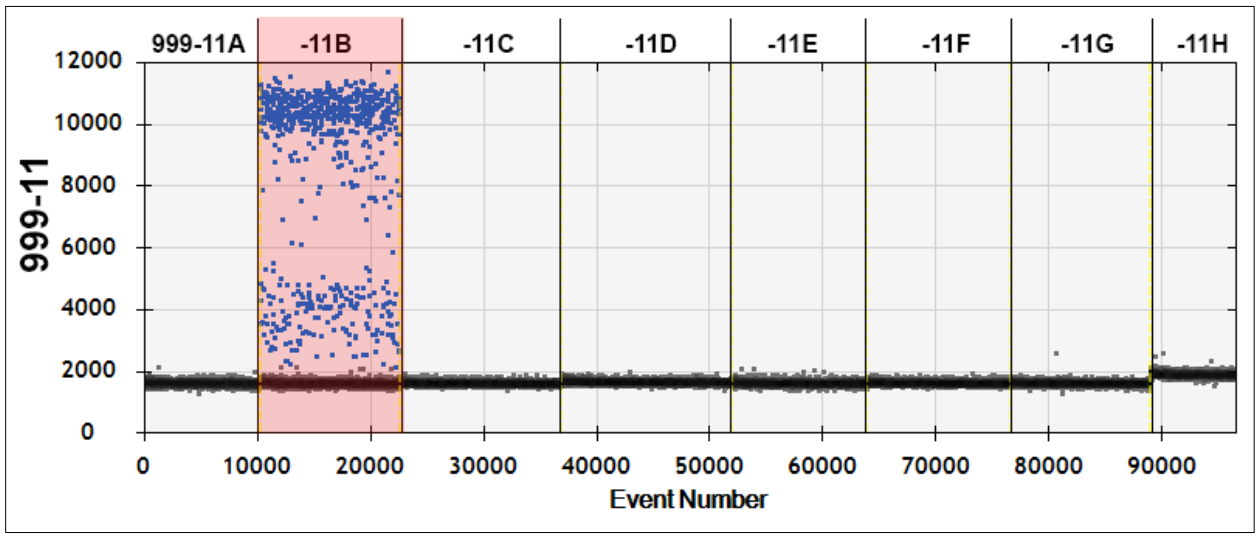

Fig. 37 Single well analyses for column 11 of plate 999 with red shadows showing the single clones identified as positive.

In Fig. 37, 2D amplitude of single clones from column 11 of plate 999 is shown. Here again, a single clone was identified as positive, which is clone 999-11B, showing an elevated number of positive droplets which clusters in two regions.

4.4.2 Sequencing of positive clones

The clones singled out with ddPCR were further analysed by sequencing genomic DNA to confirm that the integration of the knock-in sequence occurred in the correct locus without any frame shift and point mutations. Indeed, sequencing ensured also that the WT allele was still intact and did not undergo NHEJ. To this end, primers spanning the whole homology arm and insert region were selected, validated and the produced amplicons sequenced on both strands. The sequencing data was blasted against a reference sequence.

In Tab 15, a summary of sequencing results is reported for every individual clone, focusing on the cardinal points: insert integrity, WT allele integrity and observed point mutations

There is no sequencing data for clone 994-1H because PCR amplification of the insert allele was not possible; therefore, the clone was no longer used.

Cell clone	Parental cell line	locus	Insert integrity	WT allele integrity	Point mutations
992-9B	802#7	TH	✓	✓	no
992-9F	802#7	TH	✓	✓	no
994-12C	SFC 856-03-04	TH	✓	✓	no
997-4A	SFC 856-03-04	TH	✓	✓	no
1003-6C	SFC 840-03-05	TH	✓	✓	no
1003-10G	SFC 840-03-05	TH	✓	✓	no
1003-10E	SFC 840-03-05	TH	✓	✓	no
1003-11F	SFC 840-03-05	TH	✓	✓	no
1110-6C	802#7	TH	✓	×	no
993-9D	802#7	KCNJ6	✓	✓	no
999-11B	802#7	KCNJ6	✓	✓	no

Tab 15 Summary of sequencing results for TH and GIRK2 clones

For all the analysed clones the insert sequence was flawless and corresponded 100% to the reference sequence (accession number *TH* NG_008128.1 accession number *KCNJ6* NG_029892.2). This holds true for the TH and the KCNJ6 locus. Sequencing analysis confirmed that the sequence was successfully

integrated into open reading frame without any single base pair insertions that could disrupt the open reading frame.

Except for clone 1110-6C, also the WT sequences were intact for all clones. On the WT sequence of clone 1110-6C, a clone with a TH-eGFP knock-in, a large Indel sequence was found around the sequence of the stop codon. Therefore, this clone was no longer used.

4.4.3 Fluorescent *in situ* hybridization

The Fluorescent-*in situ*-hybridization (FISH) was performed to confirm with a different approach, that the insert sequence was located at the right locus. As the probes were made partially of genomic sequence of the gene and the entire insert sequence, it was expected that the FISH signal should appear at the chromosomal localization of either TH- or KCNJ6-gene. Indeed, FISH should exclude any random integration of the donor plasmid in other parts of the genome. The analysis was performed only on cell clones that showed a good recovery after amplification from the 96-well plate.

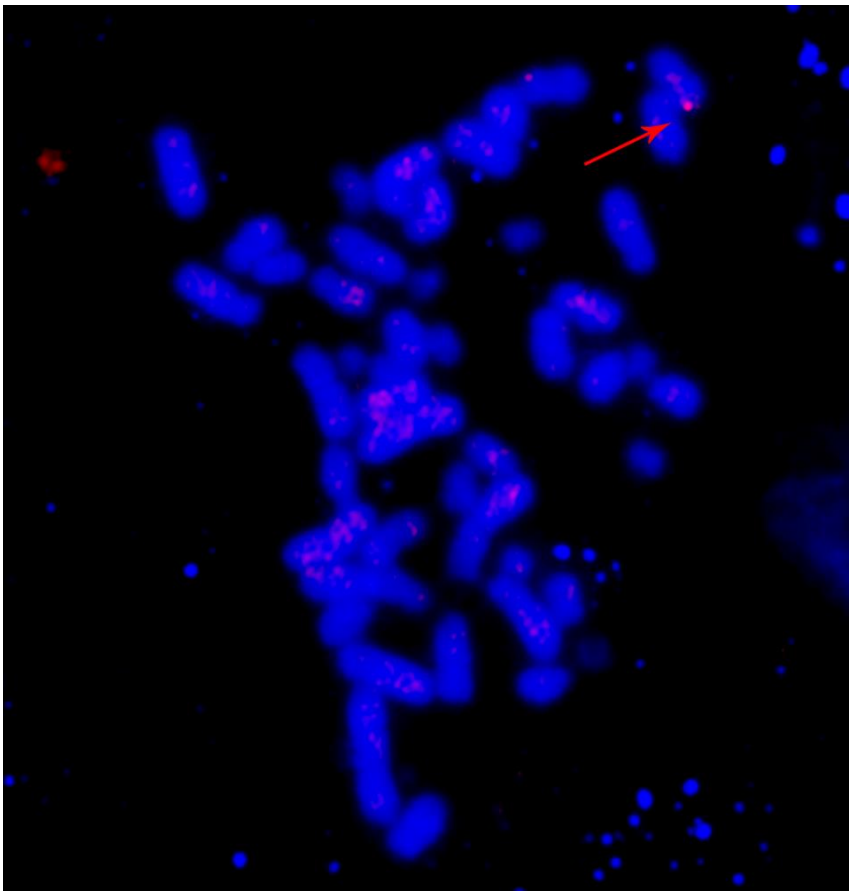

Fig. 38 FISH of clone 992-9F hybridized with TH-FISH probe. Red arrow is indicating the FISH signal on chromosome 11

Fig. 38 shows the FISH signal for clone 992-9F. In red one can see a weak hybridization signal on the terminal end of p-arm of chromosome 11 (11 pter), which is the expected chromosomal position of TH gene. No other signals were detected throughout the rest of the genome thus confirming that for selected clones the HR occurred correctly in the selected locus. Hybridization signal was identified and distinguished from background noise by fluorescence intensity, a signal morphology that is characteristical only in the region indicated by the red arrow. The same result was obtained for cell clone 1003-11F (Fig. 39).

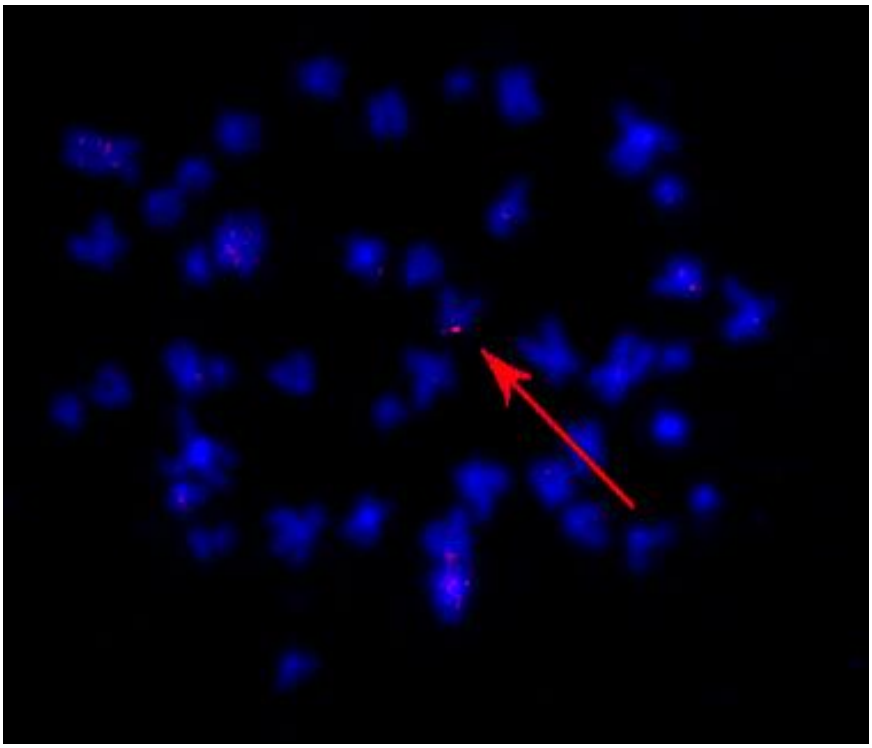

Fig. 39 FISH of clone 1003-11F hybridized with TH-FISH probe. Red arrow is indicating the FISH signal on chromosome 11

For the analysis of clones 994-12C and 992-9B a control hybridization with a WCP (whole chromosome paint) probe was performed. When analysing the metaphases, the hybridization signal was identified and then the result was supported by looking at the green channel and confirming that the signal was positioned on chromosome 11 (see Fig. 40 and Fig. 41).

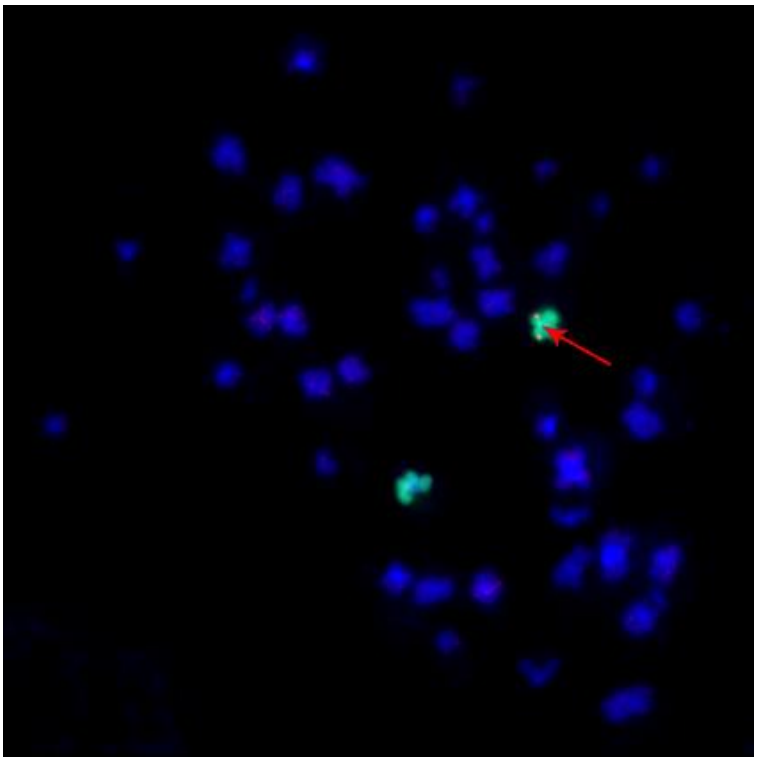

Fig. 40 FISH of clone 994-12C hybridized with TH-FISH probe. Red arrow is indicating the FISH signal on chromosome 11. The green channel shows a control counterstain of a WCP probe for chromosome 11.

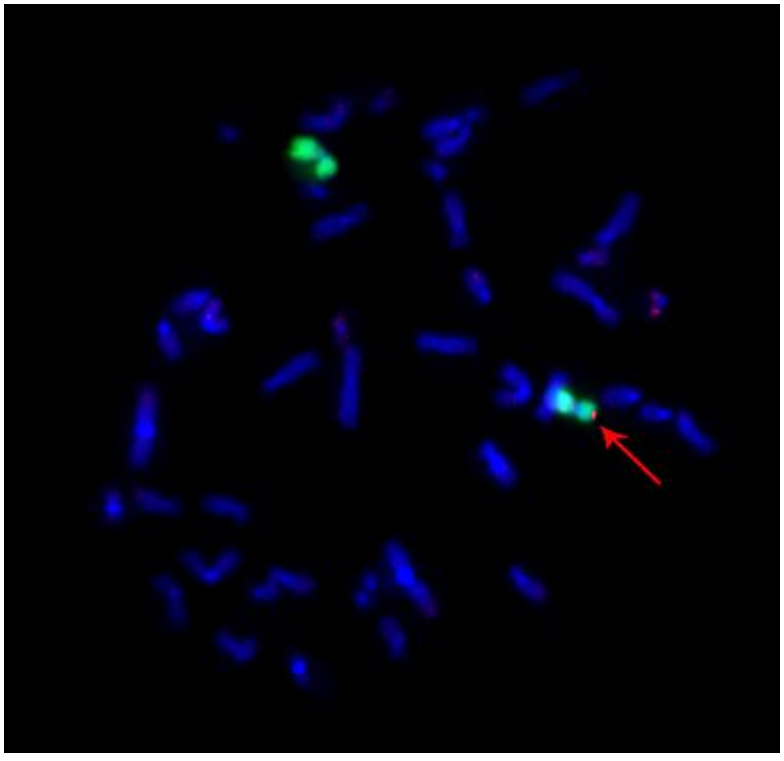

Fig. 41 FISH of clone 992-9B hybridized with TH-FISH probe. Red arrow is indicating the FISH signal on chromosome 11. The green channel shows a control counterstain of a WCP probe for chromosome 11.

For the KCNJ6 locus on clone 993-9D, a clear signal was detected on one chromosome 21 on the terminal part of the q-arm (qter), the known position of KCNJ6 gene (see Fig. 42). For the analysis of clone 999-11B, a control counterstain with a WCP probe for chromosome 21 was added, showing the same hybridization signal on 21 qter on one chromosome (see Fig. 43). For KCNJ6, both clones show hybridization only on one chromosome, confirming a heterozygous insertion of the GIRK2-construct. Random insertion could be excluded by the absence of additional hybridization signals around the genome.

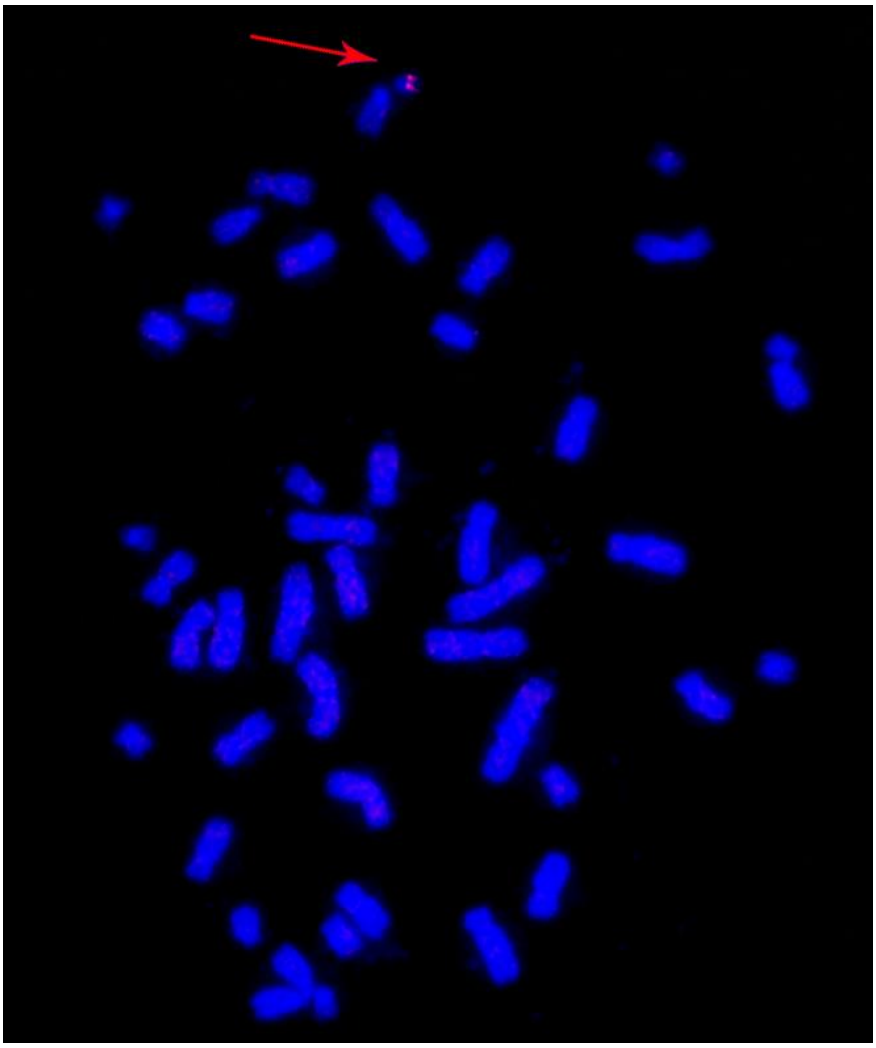

Fig. 42 FISH of clone 993-9D hybridized with GIRK2-FISH probe. Red arrow is indicating the FISH signal on chromosome 21

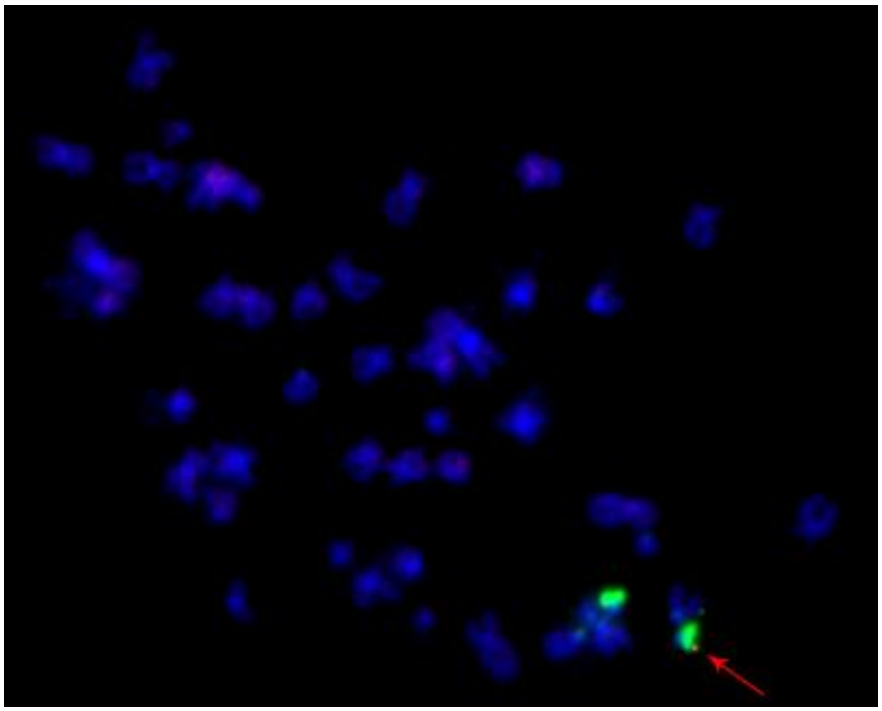

Fig. 43 FISH signal for clone 999-11B. In red, one can see a weak hybridization signal in the interstitial part of q-arm of chromosome 21, the expected localization of KCNJ6 gene. There are no other signals detected throughout the rest of the genome. The green channel shows a control counterstain of a WCP probe for chromosome 21.

4.5 Dopaminergic Differentiation of hiPSCs

4.5.1 Characterization of dopaminergic markers and physiological properties

In this project, we have evaluated alternative DA differentiation protocols to achieve the highest number TH positive neurons in a reproducible manner. One differentiation method was adapted from a protocol published by Zhang et al. 2015. The second differentiation approach was using a commercially available kit by Gibco™/ThermoFisher Scientific (PSC Dopaminergic Neuron Differentiation Kit). Both methods are based on floor plate induction of hiPSCs to obtain mDA neurons.

Neurons from both differentiation methods were characterized for gene expression and line specific marker presence. Physiological characteristics, such as DA release and ability to fire action potentials, were also investigated using ELISA assay and performing patch-clamp recordings. For this characterization, only non-engineered cell lines were used.

4.5.1.1 mRNA expression of dopaminergic markers with qRT-PCR

We investigated the potential of the hiPSCs to create floor plate progenitor cells. mDA neurons are derived from floor plate cells, whose identity is marked by co-expression of forkhead box protein A2 (FOXA2) and LIM homeobox transcription factor 1 (LMX1A) (Ferri et al. 2007). We performed qRT-PCR analysis at day 10 *in vitro*. In Fig. 44, fold increase with SEM for both genes is reported, showing a drastic increase of expression of both markers at day 10. Samples were analyzed from both differentiation protocols resulting in very similar values.

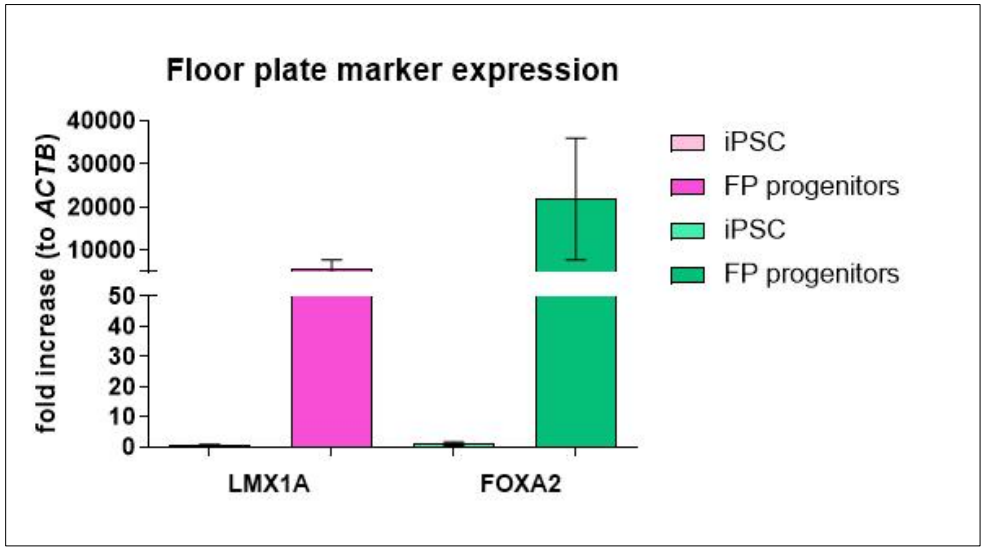

Fig. 44 Bar-plot representing fold increase of gene expression of LMX1A and FOXA2 at day 10 *in vitro* normalized to non-differentiated iPSC cells. Data is shown as mean fold increase with SEM.

After confirmation of floor plate identity marking genes, we performed qRT-PCR analysis for DA marker TH and A9 marker GIRK2. This observation was of importance as to know when fluorescent protein expression under endogenous promoter control would be observable *in vitro*. Fig. 45 shows the time courses for TH (Fig. 45A) and GIRK2 (Fig. 45B) up to a maximum number of days *in vitro* of 75. TH expression levels start to rise at day 20 with a considerable increase at day 35 and a peak at day 45. After day 45, expression levels decrease. GIRK2 expression did not considerably increase from levels at day 20 until day 45 with a steady increase as *in vitro* culture proceeded. We took this data as a reference point for analysis of TH-eGFP expression at day 25 and 35 and GIRK-mCherry expression at day 40 (see chapter 4.5.3.1). The analysis was run on samples collected from three independent differentiations and data is represented as mean fold increase with SEM.

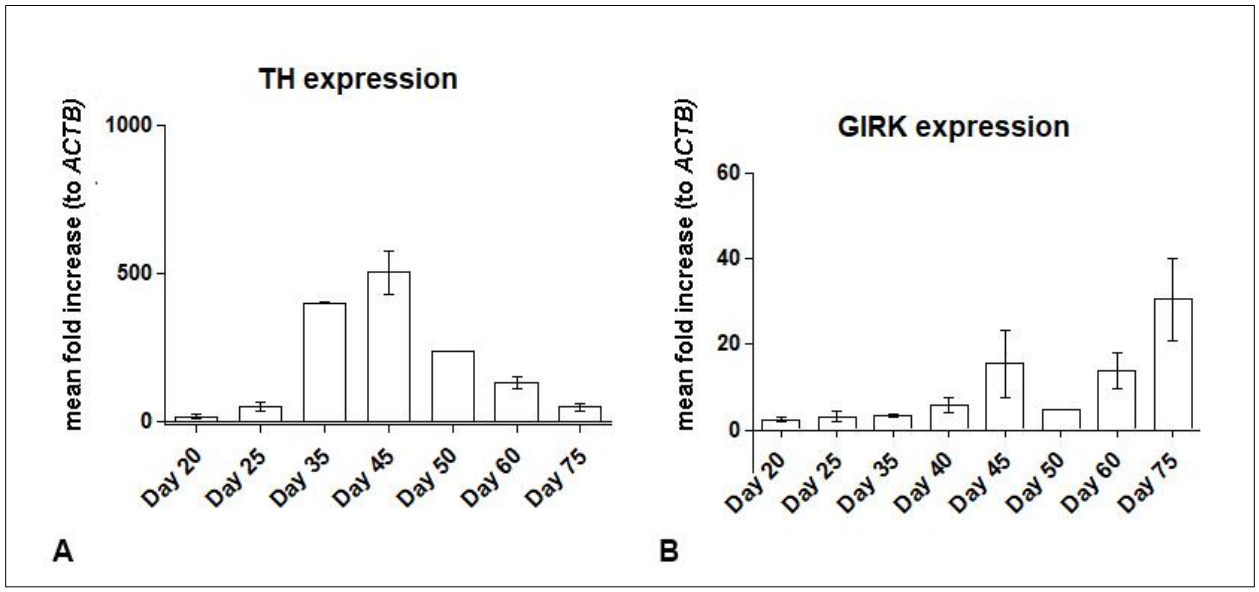

Fig. 45 Mean fold increase of expression. A Fold increase of TH expression of DA neurons from hiPSCs at day *in vitro* 20-75 shown as mean fold increase with SEM; B Fold increase of GIRK2 expression of DA neurons from hiPSCs at day *in vitro* 20-75 shown as mean fold increase with SEM.

4.5.1.2 Immunostaining of cell type specific markers

To support gene expression data measured with qRT-PCR, we performed immunostaining for FOXA2 and LMX1A. Fig. 46 shows the staining observed with the published protocol as well as with the Gibco Kit. It was observed, that with both methods protein levels of LMX1A and FOXA2 were increased compared to iPSC level (data not shown) and the presence of the two proteins could be observed in the same cell nuclei of over 70% of cells (estimation).

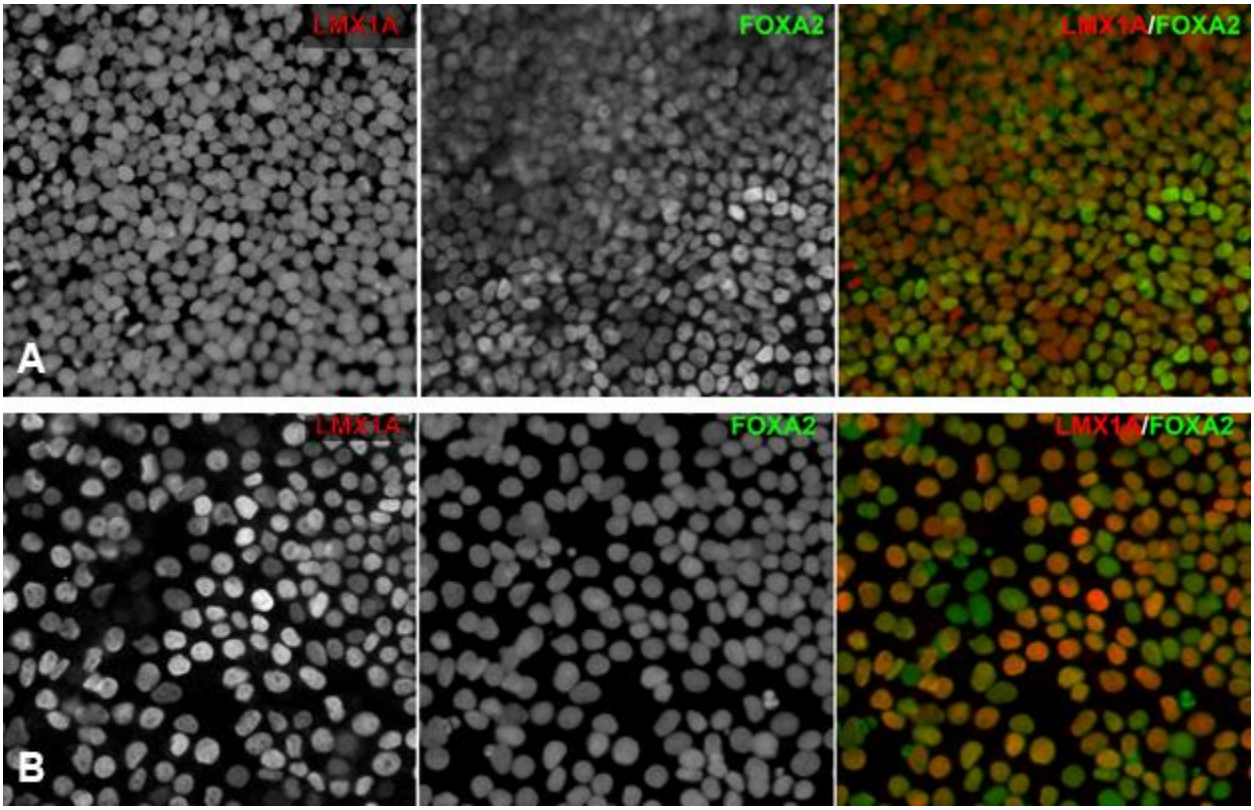

Fig. 46 Co-immunostaining of LMX1A and FOXA2 at day 10 *in vitro* with a published protocol (A) and Gibco differentiation kit (B). LMX1A is secondarily stained with AF555 antibody (red) and FOXA2 with AF488 (green).

At day 35, a time point where TH expression was expected to be considerably increased based on previous observations (chapter 4.5.1.1) an immunostaining for TH was performed. In Fig. 47A we can see that with the publication based protocol at day 35 we have around 15% of TH positive neurons (red) that are already engaged in intense network formation, as can be seen by the elevated number of dendrites and axons stained for TH in comparison with few numbers of cellular bodies stained positively for DAPI. Contrary to the publication based protocol, in the cells differentiated with the Gibco Kit we observed less cellular bodies stained for TH as well as less networking of the present neurons at day 35. These observations were consistent independent of cell lines although we did observe unquantified differences between cell lines using the same protocol.

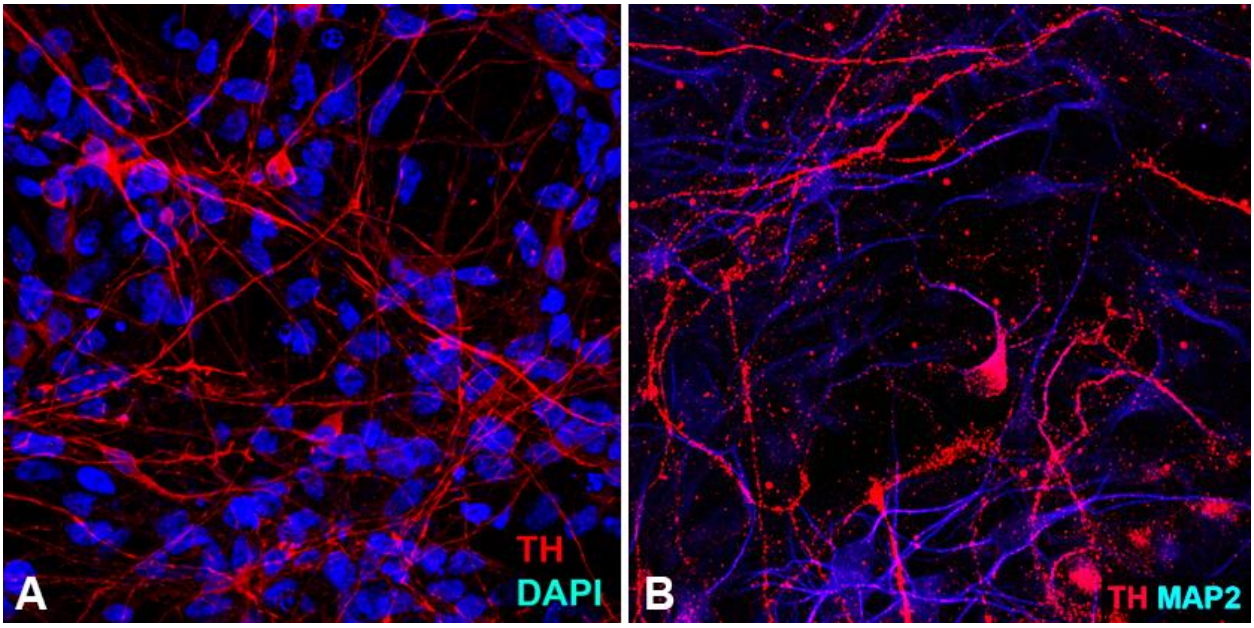

Fig. 47 Day 35 differentiated neurons. A. Staining of TH in Alexa Fluor 555, counterstain for nuclei with DAPI in cells differentiated with published protocol; B. Staining of TH in Alexa Fluor 555 (red) and of MAP2 in Alexa Fluor 647 (blue) in .cells differentiated with Gibco Kit.

With proceeding *in vitro* culture, we characterized differentiated neurons for neuronal markers. At day 50, cells were fixed and stained. In Fig. 48 to Fig. 50, a representative image for one of the two differentiation protocols is shown. Protocols generally showed similar results and staining quality.

Cells were stained for MAP2 (microtubule-associated protein 2), Tau protein to observe axonal and dendritic growth and stabilization of the cells. In Fig. 48 staining of Tau protein with secondary AF555 (red) labelling, TH staining with secondary AF488 (green) labelling and MAP2 staining with secondary AF350 (blue) labelling is shown in cells differentiated with the Gibco Kit.

A staining for TH and PITX3 was performed to prove the stable expression of TH throughout longer periods of *in vitro* culture. In Fig. 49 staining of TH with secondary AF555 (red) labelling, PITX3 (Pituitary homeobox 3) staining with secondary AF488 (green) labelling and DAPI nuclear counterstain (blue) is shown in cells differentiated with the Gibco Kit.

Ultimately, synapse formation was confirmed by staining PSD95 (postsynaptic density protein 95) and Synapsin as shown in Fig. 50. Staining of PSD95, Synapsin and MAP2 was performed with secondary AF555 (red), AF488 (green) and AF350 (blue), respectively in cells differentiated with the published protocol.

All these markers aimed at a qualitative characterization. Quantitative analysis was not performed.

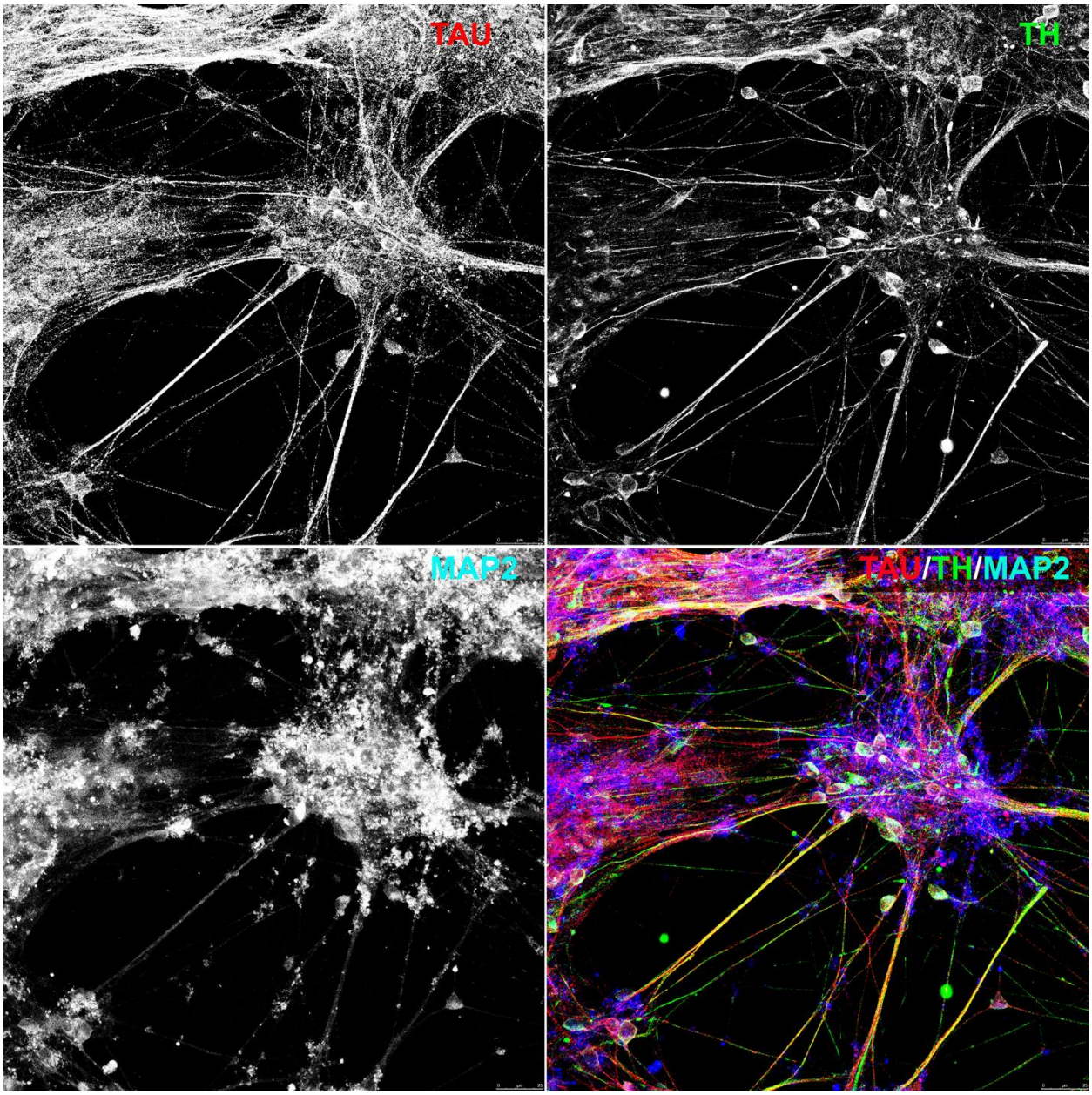

Fig. 48 Gibco Kit differentiated neurons at day 50 stained for Tau-AF555 (upper left), TH-AF488 (upper right) and MAP2-350 (lower left). Merging of channels is represented on the lower right.

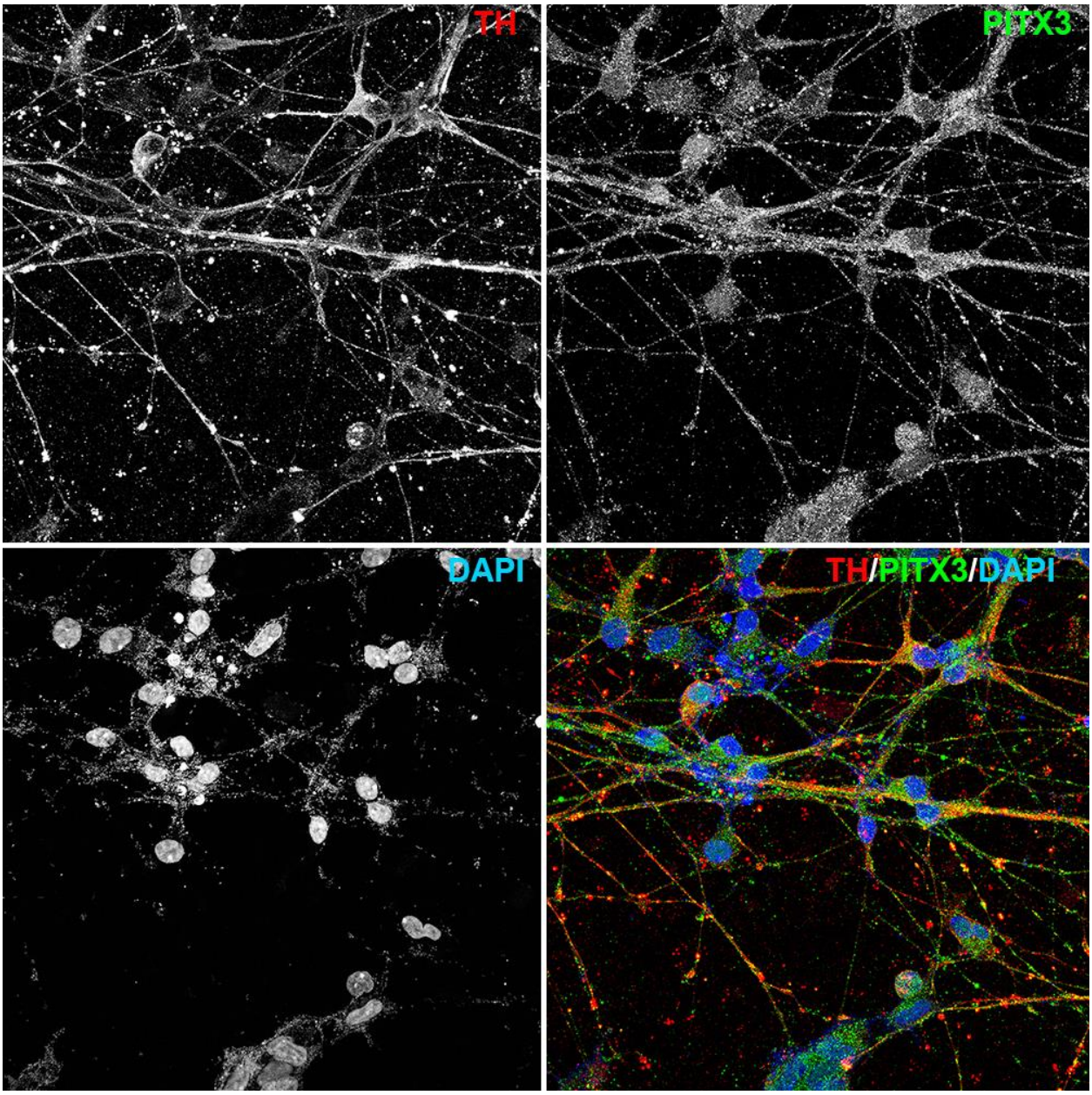

Fig. 49 Gibco Kit differentiated neurons at day 50 stained for TH-AF555 (upper left), PITX3-AF488 (upper right) and DAPI (lower left). Merging of channels is represented on the lower right.

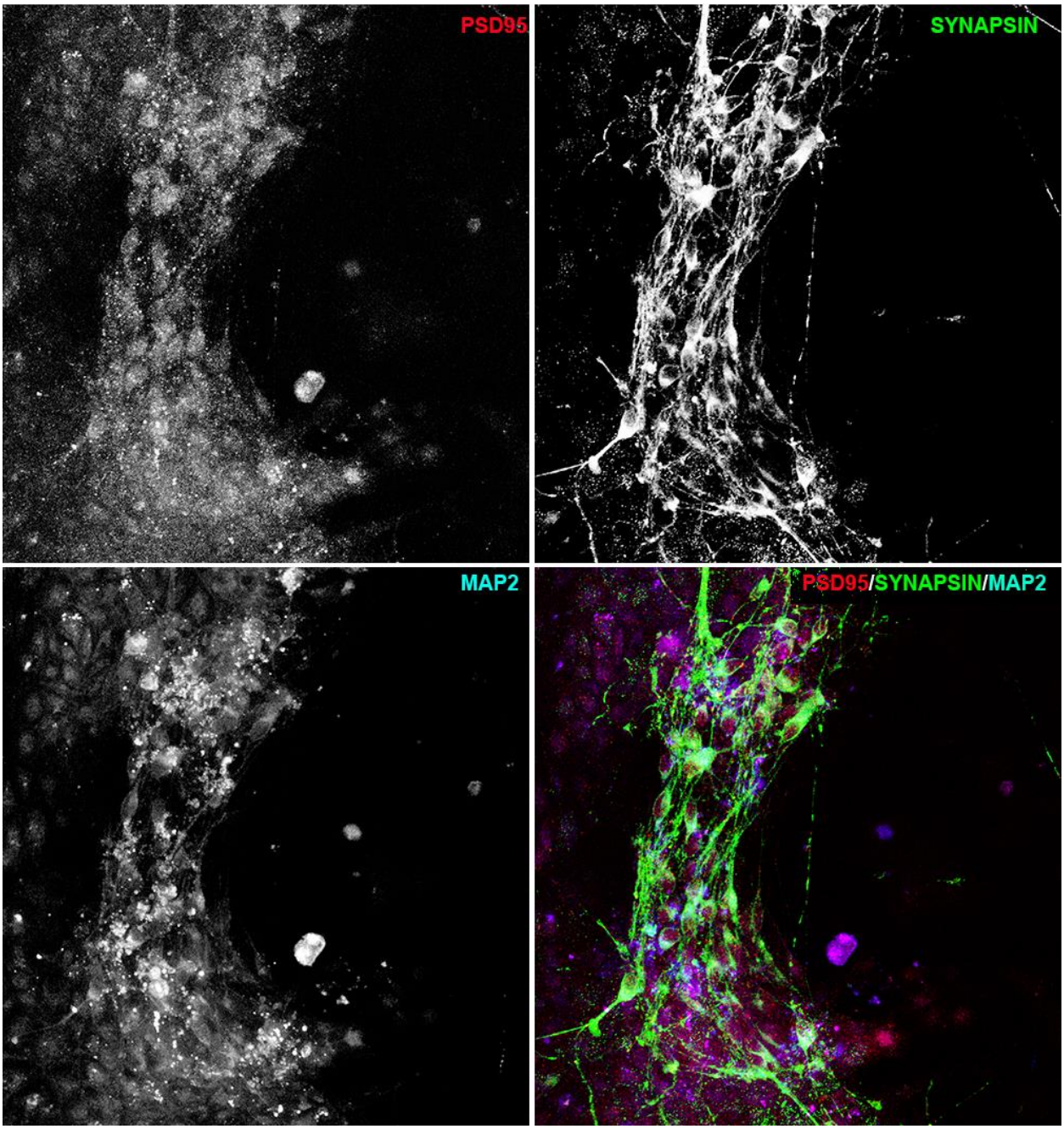

Fig. 50 Differentiated neurons from published protocol at day 50 stained for PSD95-AF555 (upper left), Synapsin-AF488 (upper right) and MAP2-AF350 (lower left). Merging of channels is represented on the lower right.

4.5.2 Functional assessment of dopaminergic neurons

4.5.2.1 Patch Clamp recordings

To assess functional maturation of DA neurons, we performed electrophysiological recordings at time points later than 40 days *in vitro*. The time point was chosen as in previous experiments we could not observe spontaneous activity before day 40. Active electrical properties of individual neurons were recorded in whole-cell voltage-clamp and current-clamp configuration. All recordings are generated from cells differentiated with the published protocol.

Fig. 51A shows a representative trace of voltage activated currents. The holding potential was maintained at 60 mV and when depolarizing voltage steps were applied, we could observe active sodium channel currents with an amplitude up to 2.3nA. Potassium channel currents could be observed in the same recording mode with an amplitude up to 2.2nA. We also observed autonomous action firing currents in voltage-clamp recordings (Fig. 51B) that repeated in a regular fashion.

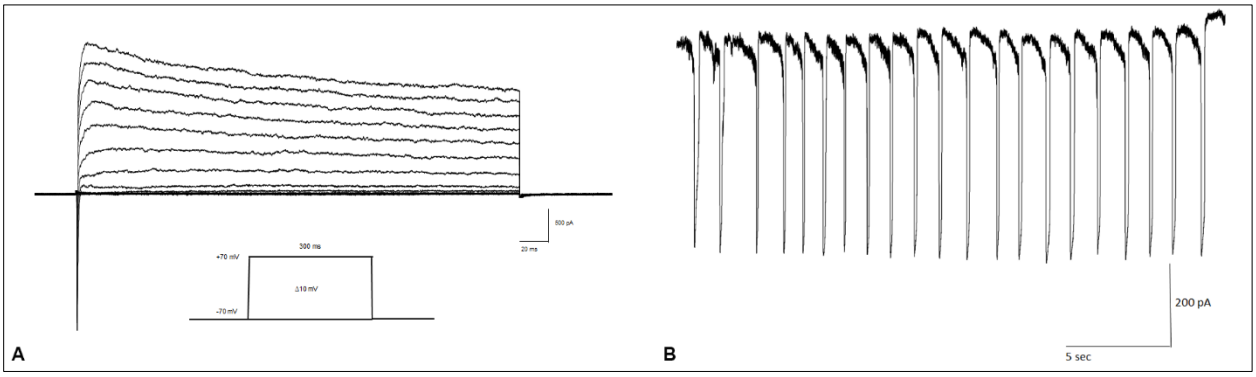

Fig. 51 A. Representative traces of inward and outward voltage-dependent currents recorded at day 45 of in vitro differentiation; B. Action current firing traces obtained from voltage-clamp (whole-cell) recordings at in vitro day 45 after differentiation.

We observed spontaneous excitatory post synaptic currents (sEPSC, Fig. 52A) as well as the ability to produce action potential upon stimulation with injected current steps (see Fig. 52B).

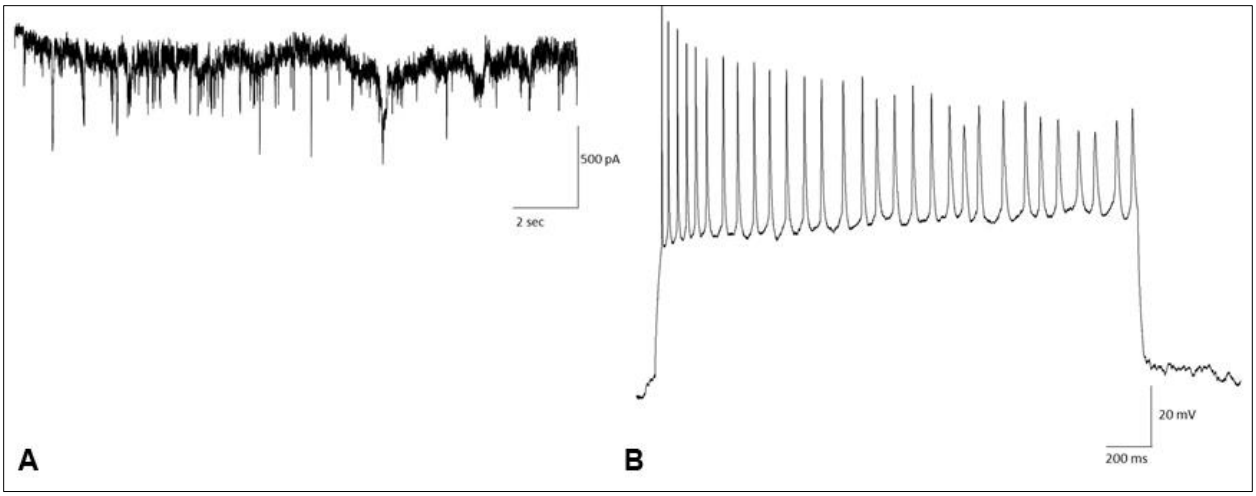

Fig. 52 A. Representative trace of the spontaneous synaptic activity recorded at day 55 of in vitro differentiation; B. Representative trace of evoked action potentials recorded at day 45 of in vitro differentiation. Applied current step of 2 sec duration and 300 pA amplitude.

Interestingly, hyperpolarization-activated cyclic-nucleotide-gated channel (HCN) activity was detected in current clamp (Fig. 53) identified through a hyperpolarizing current injection. We see a current sag due to the activation of the HCN channel by a hyperpolarizing current step. This, being a typical characteristic of pace-making cells (e.g. nodal cardiac cells), matched the molecular phenotype of mature DA neuron described in chapter 4.5.1.2. Of note is the generation of action potentials onto the closure of the hyperpolarizing step.

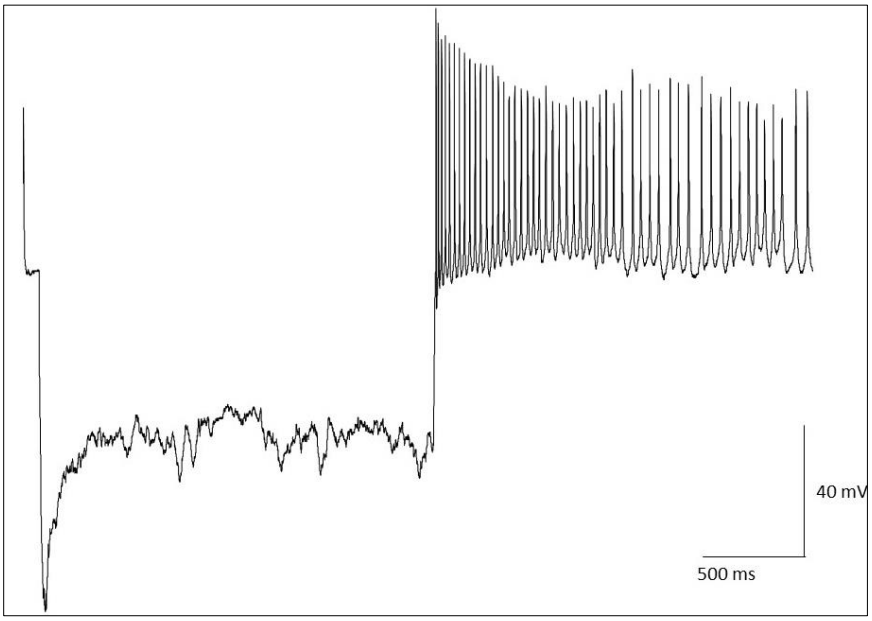

Fig. 53 Current-clamp recording at day 55 of in vitro differentiation: cell showing a voltage sag response to a hyperpolarizing current injection indicative of the presence of HCN-channel.

4.5.2.2 Dopamine ELISA

Dopamine production of the differentiated DA neurons was tested with an ELISA assay to be able to detect even minimal concentration of released DA by DA neuronal cells. Medium was taken from differentiated cells at four different time points: day 35, 45, 55 and 65. Medium was collected in the absence of KCl in order to measure autonomously released DA. Fig. 54 shows the mean concentration of DA at the different time points, normalized to values from undifferentiated cells. We could observe an increase of DA concentration over time until day 55 as reported in Tab 16. After day 55, a decrease in DA concentration was observed.

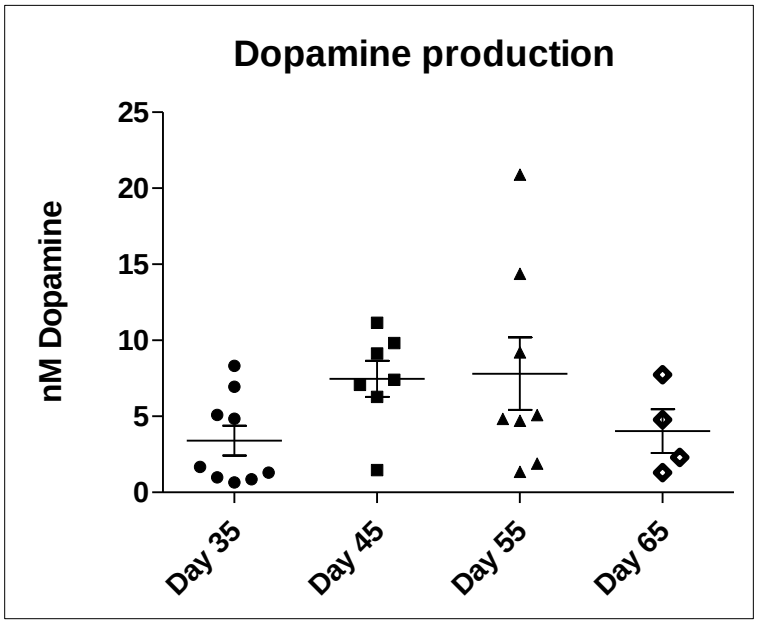

Fig. 54 Non-stimulated Dopamine release quantified with ELISA from medium taken from cells in culture at four different time points. Replicate number is 3. Data are shown as single data points with mean and SEM.

In table 16, the mean DA concentration corresponding to reported data of Fig. 54 is reported. The mean concentrations at day 45 and day 55 are almost identical, however looking at single data points in Fig. 54, DA concentration at day 55 are in some case much higher than at day 45.

Day in vitro	Day 35	Day 45	Day 55	Day 65
Mean dopamine concentration [nM]	3.41	7.48	7.81	4.03

Tab 16 Mean dopamine concentration measured with ELISA corresponding to mean values marked in figure 54.

4.5.3 Reporter expression under endogenous promoter control

In the clonal screening, a total of 9 TH-eGFP clones could be successfully identified for the HR. Of those 9, 1110-6C was immediately discarded, as mutation in the WT allele was discovered.

Of the 8 other clones, 997-4A could not be recovered after thawing and had to be discarded. 1003-10E, 1003-6C and 1003-10G did not show a good morphology when were scaled up from 96-well plate and for these reasons where not chosen to be used for differentiation

4.5.3.1 mRNA co-expression of TH and eGFP

To assess that the reporter system was working in the engineered hiPS cells, a gene expression profiling using ddPCR was carried out. We chose ddPCR over traditional quantitative real time PCR because it was important to reveal the actual amount of copies of both genes, TH and eGFP or GIRK2 and mCherry, respectively. Samples were collected at two different DA differentiation time points to prove that co-expression is stable throughout the differentiation. For TH-eGFP tagging, an earlier time point (day 25) was chosen because it was observed in previous studies to be the time point where TH expression is already active (see Fig. 45). It is also the time point where we expected to be able to see first protein production in ICC and FACS analysis. The later time point, day 35, was chosen as it was known from previous testing (see Fig. 45) that at this stage the TH gene promoter is most active. Similarly, for GIRK2 day 40 was the earlier time point, as we know from previous testing that expression of GIRK2 before day 40 is negligible (see Fig. 45).

For TH and eGFP co-expression analysis, ddPCR analysis was performed on cDNA generated from RNA extracted from cells at day 25 and day 35. We optimized a FAM assay for eGFP and a HEX assay for TH in a multiplexed reaction. Data of four different TH-eGFP clones (992-9F, 992-9B, 994-12C, 1003-11F) compared with two non-tagged WT cell lines (802#7 and SFC 856-03-04) at day 25 and day 35. Samples were taken from up to five different independent differentiation experiments carried out at different times. Fig. 55 shows the calculated ratio between eGFP and TH copy number detected with ddPCR represented in a Box-Whiskers-Plot (ratio = copy number eGFP / copy number TH). The mean ratio (with SD) was approximately 0.5 for both day 25 and day 35, which proved that TH-eGFP selected clones have 50% of eGFP mRNA expression level with respect to TH expression, which was expected due to a heterozygous knock-in. For the mean ratio analysis, mean values for each iPSC clones were calculated with data points from independent differentiations for either day 25 or day 35.

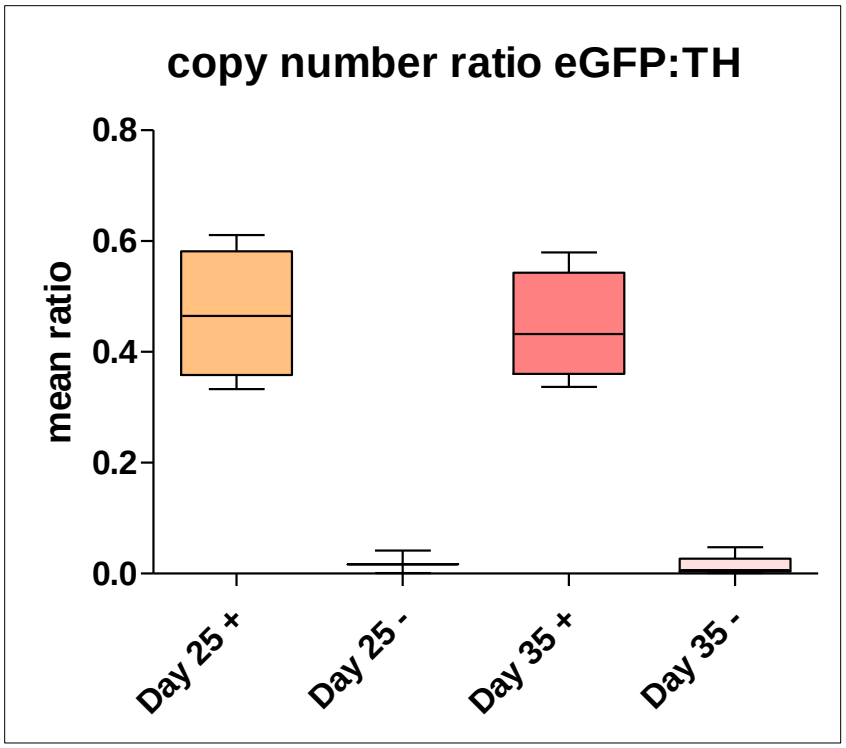

Fig. 55 Box-whiskers plot showing mean ratio of eGFP copy number over TH copy number. Values are measured with ddPCR and ratio calculated by QuantSoft Pro software. Data are from clones co-expressing TH and eGFP and are compared to parental cells at either day 25 or day 35 *in vitro.*

In Fig. 56, a Scatter-Plot shows individual data points for copy numbers per ng at day 25 and day 35. Data points are the same as those used for mean ratio calculation but shown individually not as mean values. This data representation shows that copy number of eGFP cDNA is 50% of copy number of TH cDNA at day 25 as well as at day 35 in TH-eGFP engineered cells. This result clearly shows that the transcript expression of the eGFP gene is under the control of the endogenous TH promoter and that the TH and eGFP reporter strategy delivered a construct that is physiologically “working” during DA neuronal differentiation of TH-eGFP tagged hiPS cells.

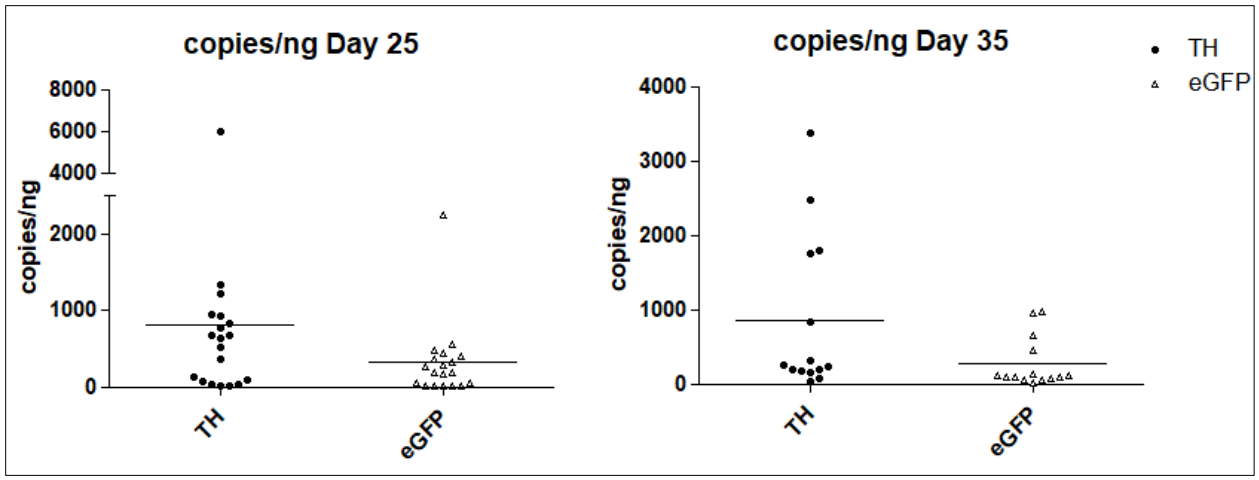

Fig. 56 Scatter plot showing copies/ng of cDNA detected with ddPCR for eGFP and TH at day 25 in vitro and day 35 in vitro. Values are single data points from four different eGFP clones and two WT clones from five independent differentiations. Horizontal bars are marking mean values.

A significant correlation between TH and eGFP copy number was calculated by determining the Spearman correlation coefficient of 0.952 for all differentiated samples ($P<0.0001$; $n=33$).

4.5.3.2 mRNA co-expression of GIRK and mCherry

As for TH, we performed the same analysis with ddPCR also for the GIRK2-mCherry reporter construct. We decided to perform the analysis at day 40 in vitro as we knew from previous testing that expression of GIRK2 before day 40 is negligible (see Fig. 45) and we expected expression of GIRK2 to be strong enough at day 40. The experiment was performed with a standard GIRK2 ddPCR assay in FAM and a custom mCherry assay in HEX. We ran samples of two different GIRK2-mCherry clones from three independent differentiations and compared them to one control non-tagged WT cell line (802#7).

As Fig. 57 shows, in contrast to TH-eGFP lines, we do not see the same ratio of 0.5 with GIRK2 mcherry lines. The ratio of this co-expression is lower, about 0.15 on average. The control line does not show any co-expression, as expected.

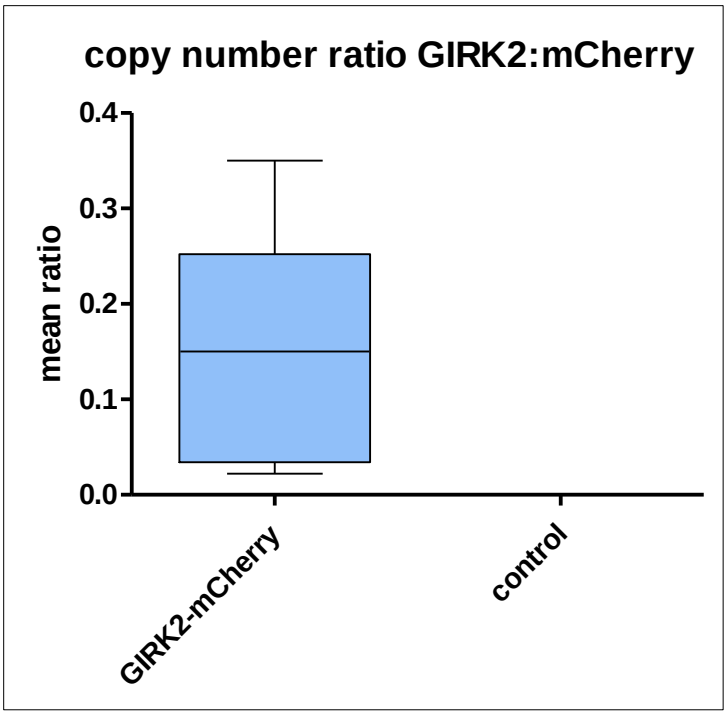

Fig. 57 Box-whiskers plot showing mean ratio of mCherry copy number over GIRK2 copy number. Values are measured with ddPCR and ratio calculated by QuantSoft Pro software. Data are from clones co-expressing GIRK2 and mCherry and are compared to parental cells at day 40 *in vitro.*

Also the copy number comparison does not go to the same direction as with TH-eGFP. Whereas the TH-eGFP construct resulted in half the amount of eGFP compared to TH, the GIRK2-mCherry construct does not show equal coherence of data. We have much less mCherry compared to GIRK2. GIRK2 copy numbers also are very variable, ranging from 270 to 2460 copies/ng. Given that the correlation coefficient is -0.321 we cannot conclude that a reliable co-expression takes place for GIRK2-mCherry as for TH-eGFP.

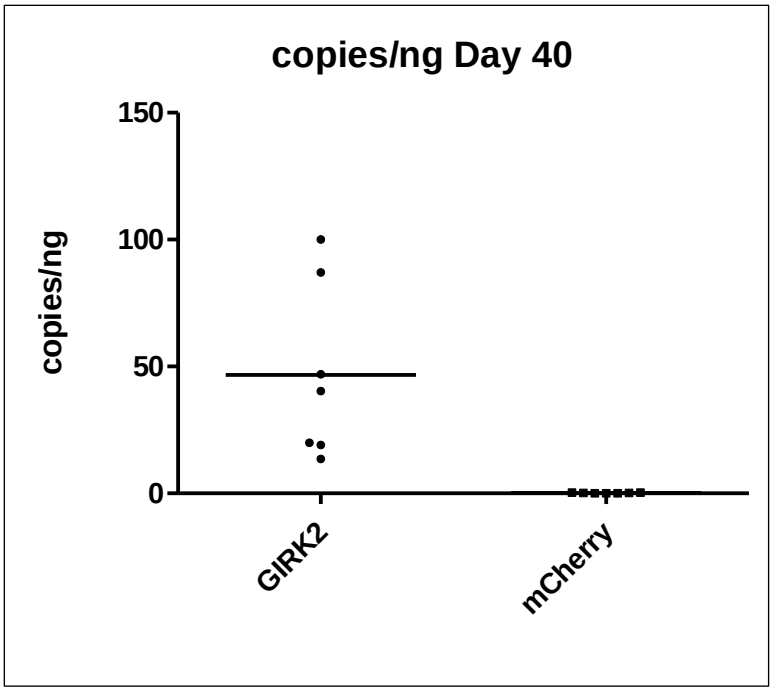

Fig. 58 Scatter plot showing copies/ng of cDNA detected with ddPCR for mCherry and GIRK2 at day 40 *in vitro*. Values are single data points from two different mCherry clones and one WT clone from three independent differentiations. Horizontal bars are marking mean values.

4.5.3.3 Immunocytochemistry and confocal imaging

a) TH and eGFP co-staining Day 25

To confirm that the reporter system for TH is working not only at gene expression level, but also at protein level, a co-immunostaining of TH and eGFP was performed. As eGFP often is at limit of detection, in some cases we had to apply different methods of immuno-labelling to enhance the signal. Beside a classical immunocytochemistry protocol, we also performed secondary labelling with a secondary Biotin conjugated antibody. This antibody was then again marked with a Streptavidin-HRP antibody. Ultimately, the signal was amplified with a TSA-488 reagent. We routinely also used an autofluorescence quenching reagent from Vectashield, to reduce endogenous unspecific fluorescence of cells that allowed us to better distinguish specific from non-specific signal.

In Fig. 59, we can see that we have a complete overlay of TH (red) and eGFP (green) staining. A neuronal counterstain was performed with MAP2 (blue), which is present in the cells stained for TH and eGFP. This image was taken from clone 1003-11F differentiated with the Gibco Kit.

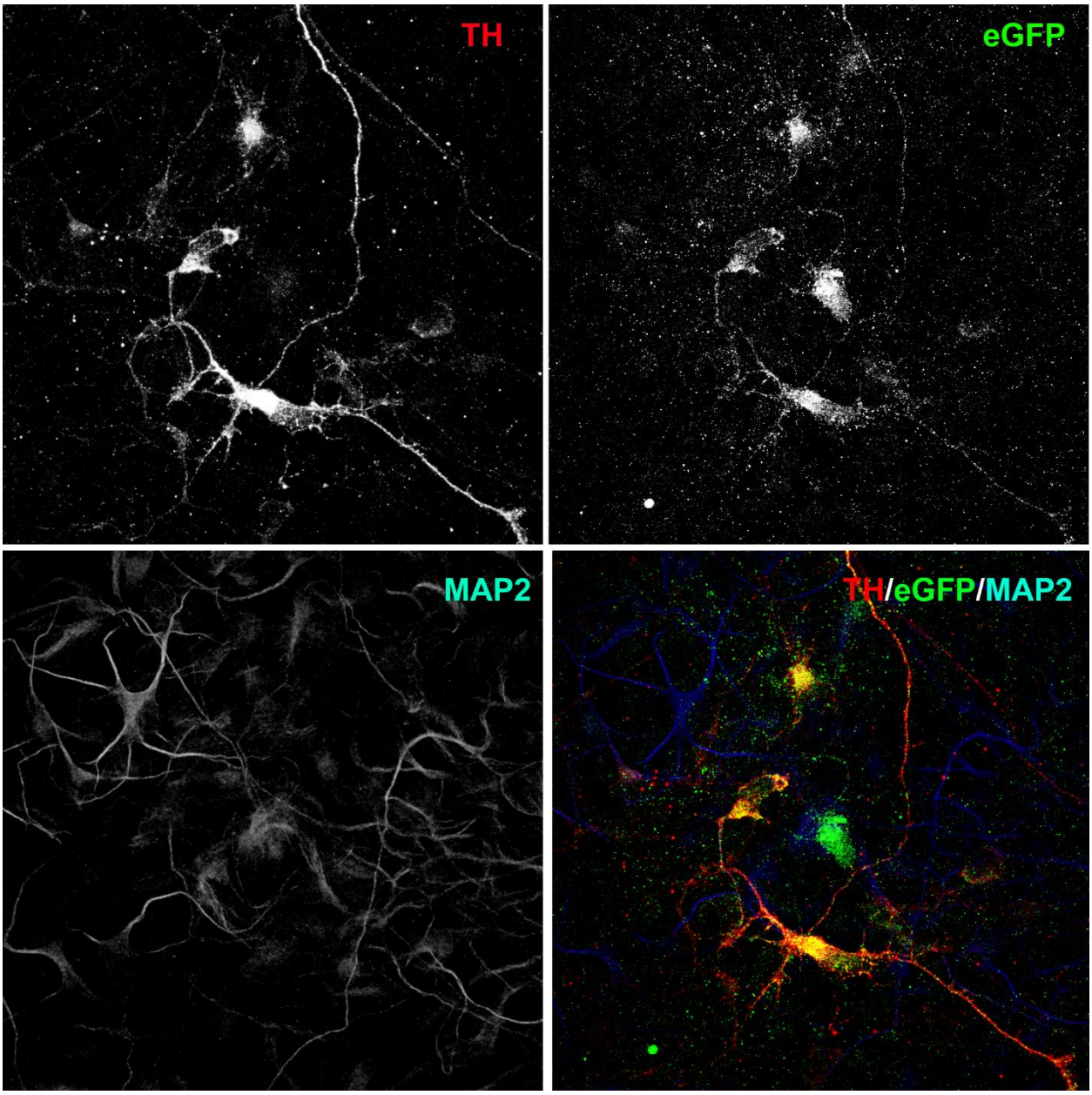

Fig. 59 Co-immunostaining of TH, eGFP and MAP2 in clone 1003 11F at Day 25 with Gibco differentiation (Differentiation 20) protocol. Upper left: red channel for TH staining in AlexaFluor 555; upper right: green channel for eGFP staining in AlexaFluor488; bottom left: infrared channel for MAP2 staining in AlexaFluor647; bottom right: overlay of channels in RGB of TH (red), eGFP (green), MAP2 (blue);

On the same line, repeating a differentiation with 1003-11F using the publication based protocol we could observe a TH-eGFP co-staining as well (Fig. 60).

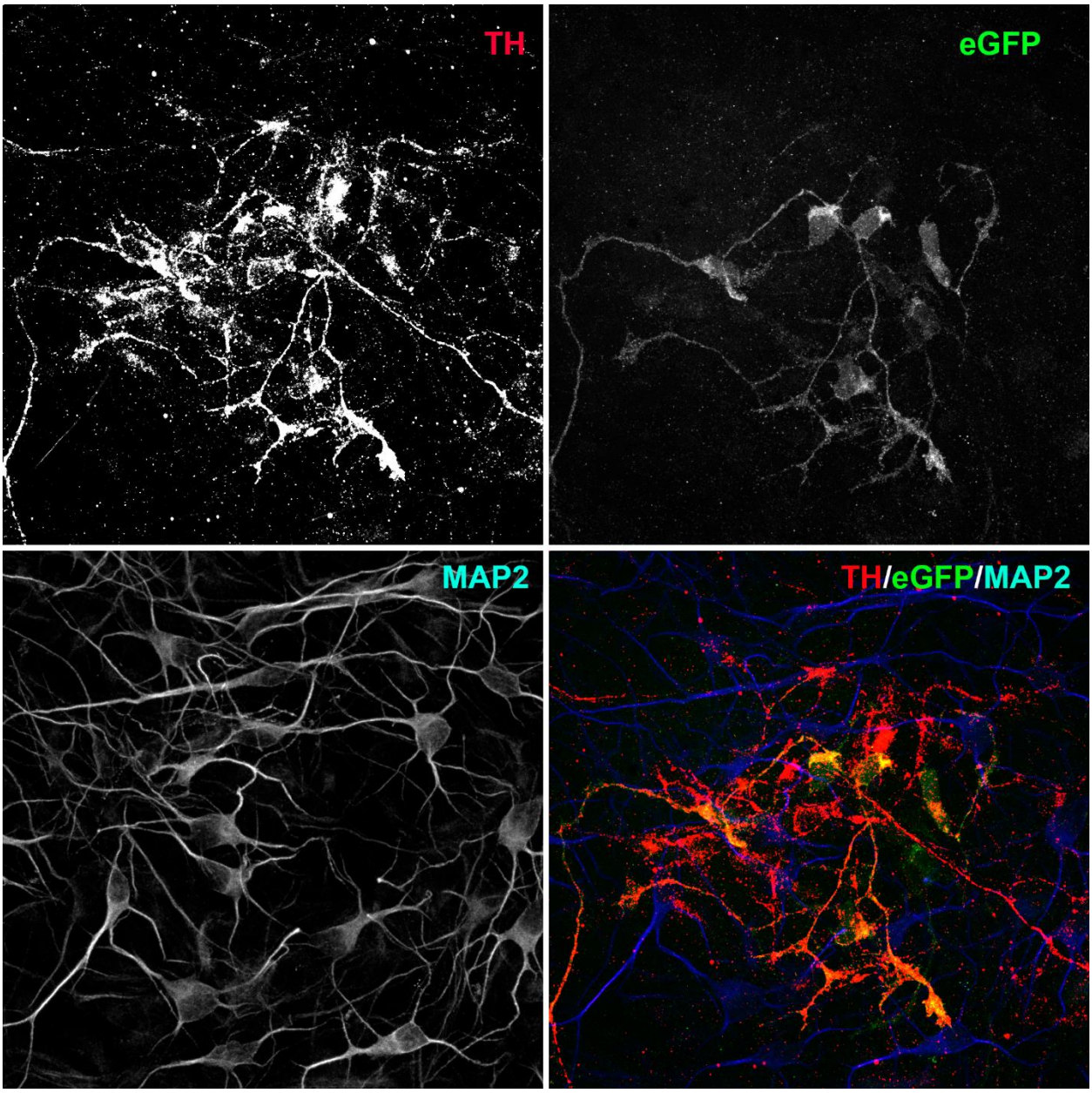

Fig. 60 Co-immunostaining of TH, eGFP and MAP2 in clone 1003 11F at Day 25 with published protocol (Differentiation 25). Upper left: red channel for TH staining in AlexaFluor 555; upper right: green channel for eGFP staining in AlexaFluor488; bottom left: infrared channel for MAP2 staining in AlexaFluor647; bottom right: overlay of channels in RGB of TH (red), eGFP (green), MAP2 (blue);

b) TH and eGFP co-staining Day 35

The co-staining was also performed at a later time point of the differentiation. In Fig. 61, we see a co-immunostaining in clone 1003 11F differentiated with the published protocol. An evident co-staining of TH and eGFP was observed with a clear MAP2 staining in the co-stained cells.

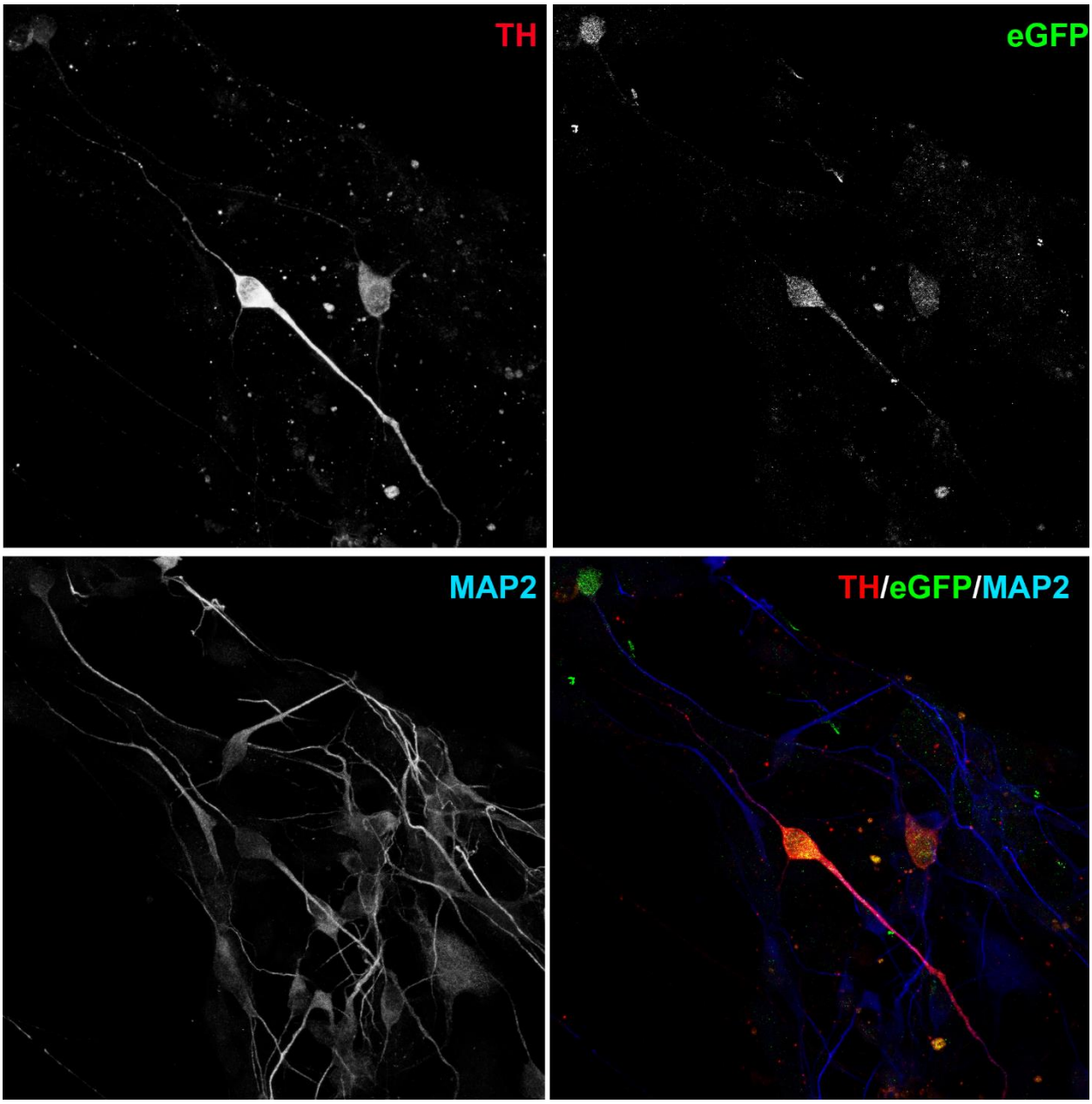

Fig. 61 Co-immunostaining of TH, eGFP and MAP2 in clone 1003 11F at Day 35 with published protocol (Differentiation 12). Upper left: red channel for TH staining in AlexaFluor 555; upper right: green channel for eGFP staining in AlexaFluor488; bottom left: infrared channel for MAP2 staining in AlexaFluor647; bottom right: overlay of channels in RGB of TH (red), eGFP (green), MAP2 (blue);

The same pattern of co-staining could be observed for cell clones 992-9F and 994-12C differentiated with Gibco Kit (Fig. 62 and Fig. 63), respectively).

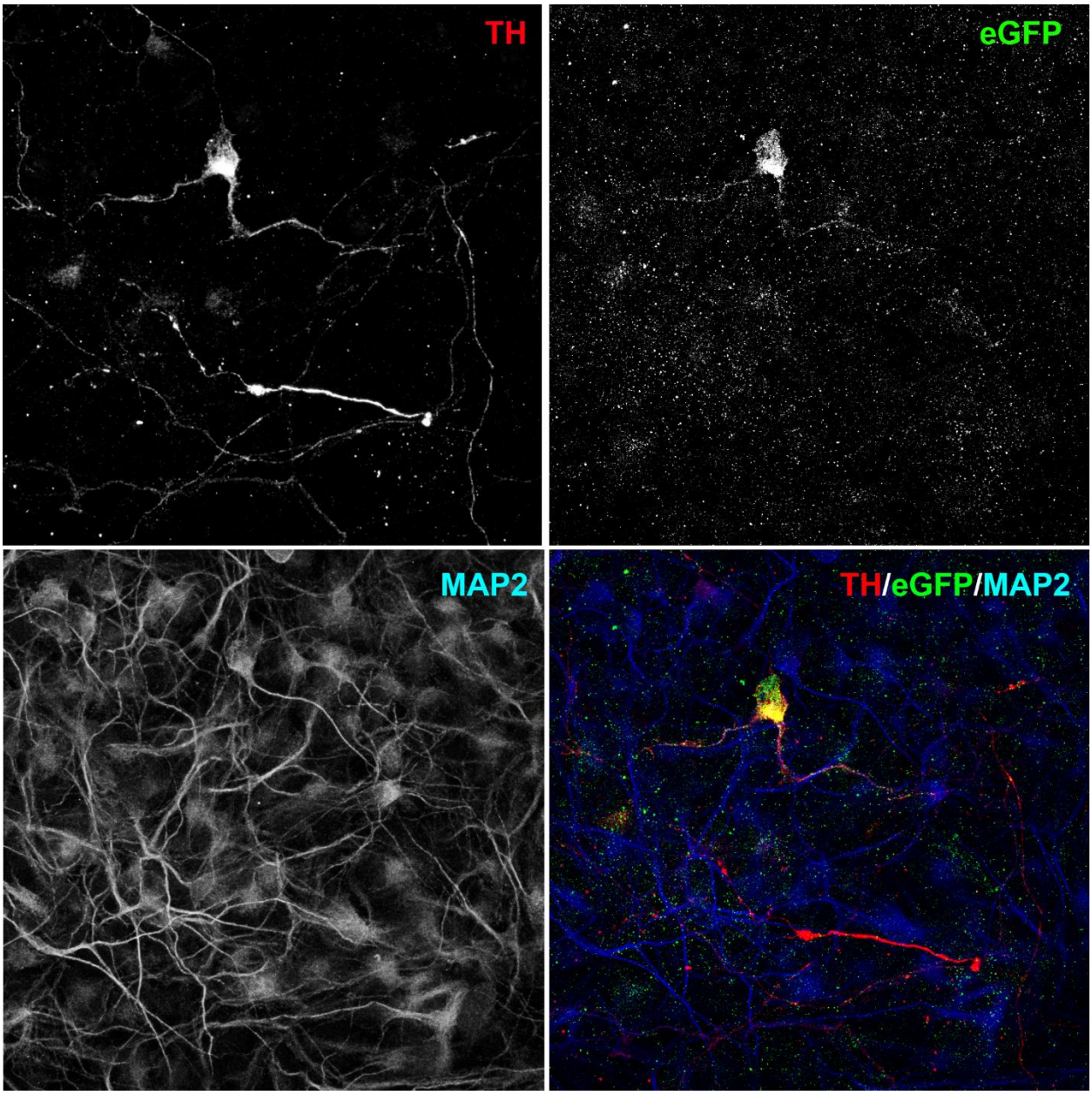

Fig. 62 Co-immunostaining of TH, eGFP and MAP2 in clone 994-12C at Day 35 with Gibco Kit (Differentiation 24). Upper left: red channel for TH staining in AlexaFluor 555; upper right: green channel for eGFP staining in AlexaFluor488; bottom left: infrared channel for MAP2 staining in AlexaFluor647; bottom right: overlay of channels in RGB of TH (red), eGFP (green), MAP2 (blue);

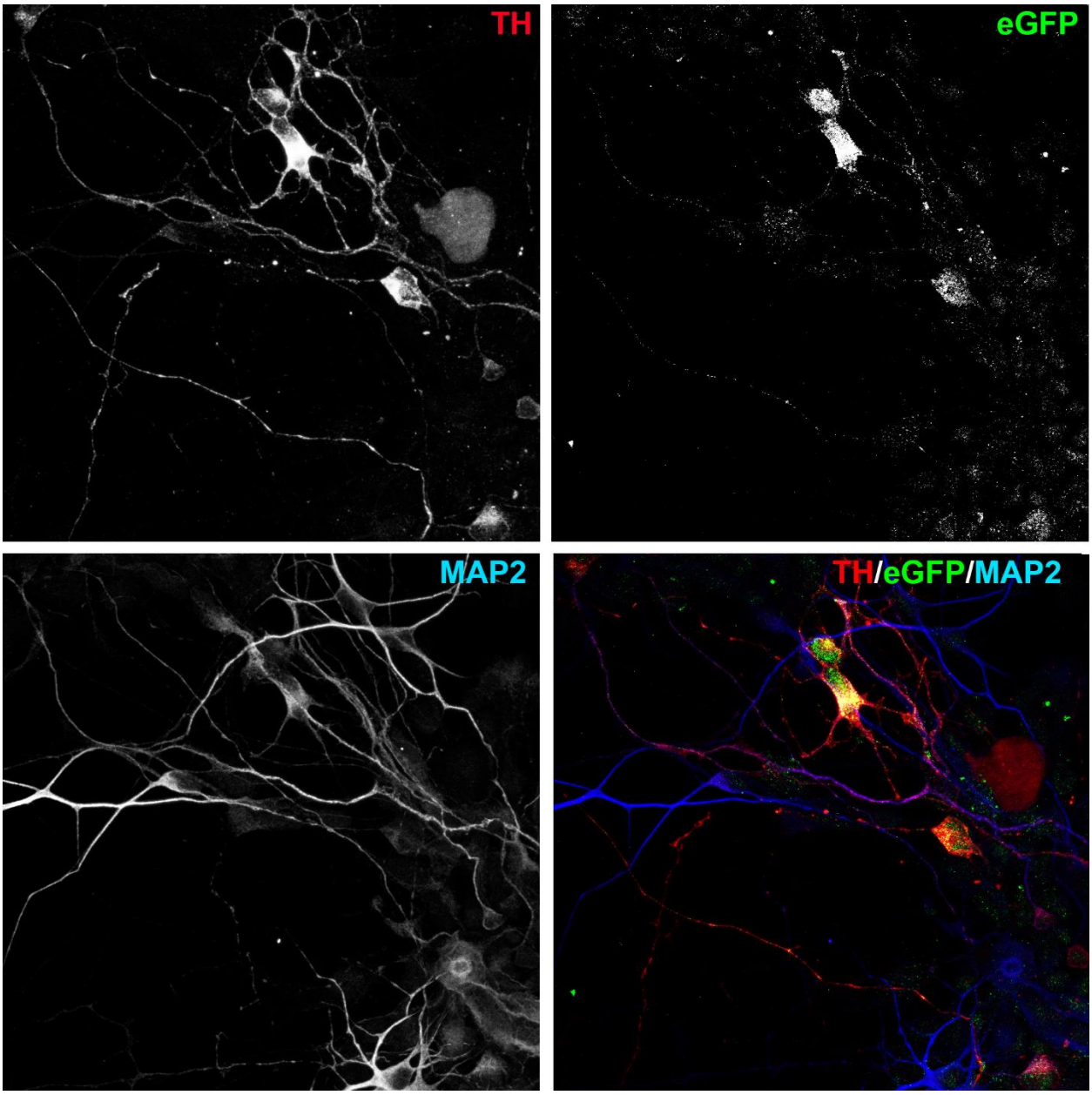

Fig. 63 Co-immunostaining of TH, eGFP and MAP2 in clone 992-9F at Day 35 with Gibco Kit differentiation (Differentiation 20). Upper left: red channel for TH staining in AlexaFluor 555; upper right: green channel for eGFP staining in AlexaFluor488; bottom left: infrared channel for MAP2 staining in AlexaFluor647; bottom right: overlay of channels in RGB of TH (red), eGFP (green), MAP2 (blue);

This data, taken from cells at day 25 and day 35 is independent of cell clone and differentiation of cell protocol, a positive readout on the capability of the knock-in system to deliver a valid reporter system for TH expressing cells. However, we found that differentiation with the Gibco Kit generally was more

reproducible and gave a more stable readout, whereas with the published protocol we encountered a lot of variability from one differentiation to the next.

For all differentiations, we also looked for eGFP endogenous signal that could not be observed in any experiments at the confocal microscope mainly due to a high level of autofluorescence of cells in the green channel that made it impossible to identify specific signal (data not shown).

c) GIRK2 and mCherry co-staining on Day 40

As for TH and eGFP, a co-staining experiment was performed for GIRK2-mCherry knock-in clones. The cells were fixed at later time points than for TH-eGFP, as we know from previous observations (see Fig. 64) that GIRK2 expression is to be observed from day 40 *in vitro* onwards and not earlier. For this reason, the first co-staining experiment was performed at day 40 of differentiation. We performed experiments only with cells from Gibco Kit differentiations, as we found this protocol to be more suitable for robust and reproducible conditions.

We could observe co-staining of mCherry and GIRK2 in clone 999-11B (Fig. 64) and 993-9D (Fig. 65) at day 40. Staining for mCherry and GIRK2 resulted to overlap in these experiments and match with the MAP2 staining. As we could not confirm this data with any other method (immunoblotting, ddPCR), the specificity of the mCherry staining is seen very critical. Although we have seen less staining in wild-type cells (data not shown), the quality of the staining seems similar to the staining we see in GIRK2-mCherry clones and clearly staining conditions for this antibody were not optimal.

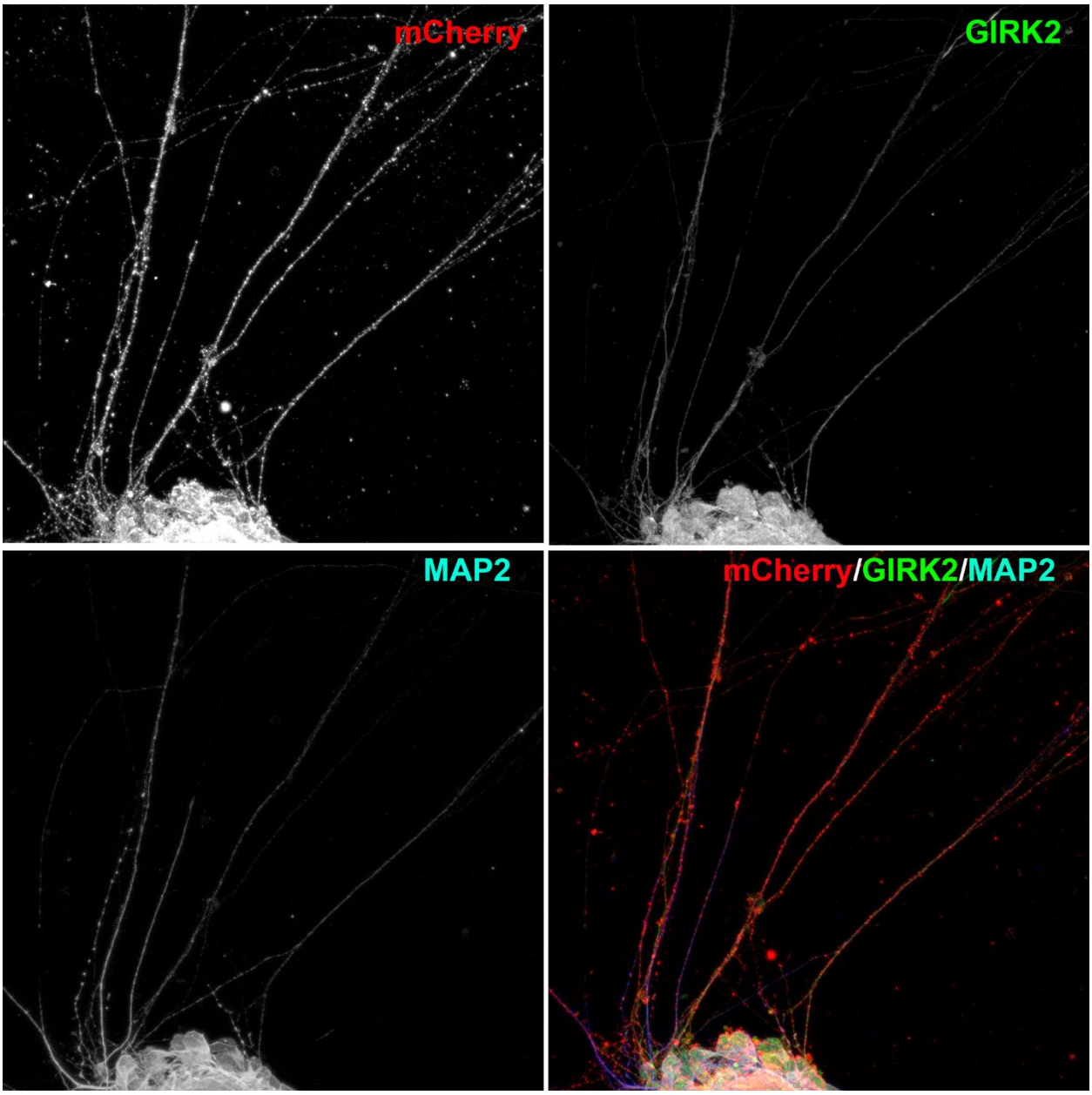

Fig. 64 Co-immunostaining of GIRK, mCherry and MAP2 in clone 999-11B at Day 40 with Gibco protocol (Differentiation 23). Upper left: red channel for mCherry staining in AlexaFluor 555; upper right: green channel for GIRK2 staining in AlexaFluor488; bottom left: infrared channel for MAP2 staining in AlexaFluor647; bottom right: overlay of channels in RGB of mCherry (red), GIRK2 (green), MAP2 (blue);

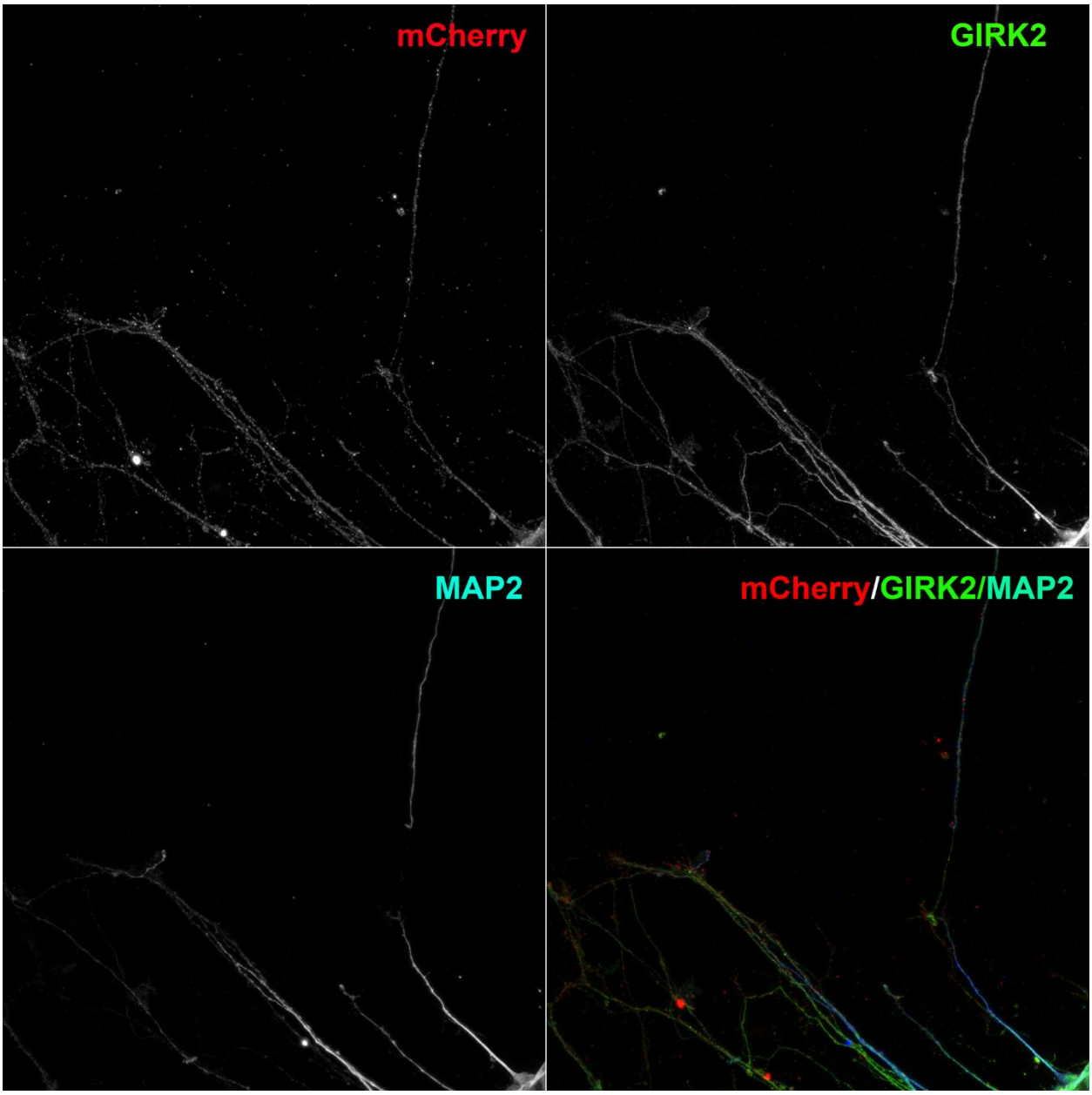

Fig. 65 Co-immunostaining of GIRK, mCherry and MAP2 in clone 993-9D at Day 40 with Gibco protocol (Differentiation 23). Upper left: red channel for mCherry staining in AlexaFluor 555; upper right: green channel for GIRK2 staining in AlexaFluor488; bottom left: infrared channel for MAP2 staining in AlexaFluor647; bottom right: overlay of channels in RGB of mCherry (red), GIRK2 (green), MAP2 (blue);

4.5.3.4 Immunoblotting

We blotted protein samples on a PVDF membrane in order to detect TH and eGFP in protein lysates to support our ICC data. We loaded protein lysates from samples that were positively stained for TH and eGFP in ICC (see Fig. 63). Lysates from the same differentiation were used. For eGFP we used SH-SY-5Y

cells transiently transfected with an eGFP expression plasmid as a positive control. For TH, undifferentiated iPSCs were used as a negative control. In

Fig. 66 A, we see that only differentiated neurons at day 35 express TH, which was expected. The band is slightly above the 50kDA marker band, which is in line with the expected MW for TH at approximately 60kDa. In

Fig. 66 B, we see a clear band for eGFP in SHY-SY5Y cells overexpressing the protein. The expected MW is 32 kDa, and we see a band at approximately this size. We do not see any band for eGFP in differentiated neurons from TH-eGFP lines at day 35. Also with longer exposure, no band could be detected in those samples (data not shown).

Fig. 66 C shows a β-actin staining as a loading control for samples.

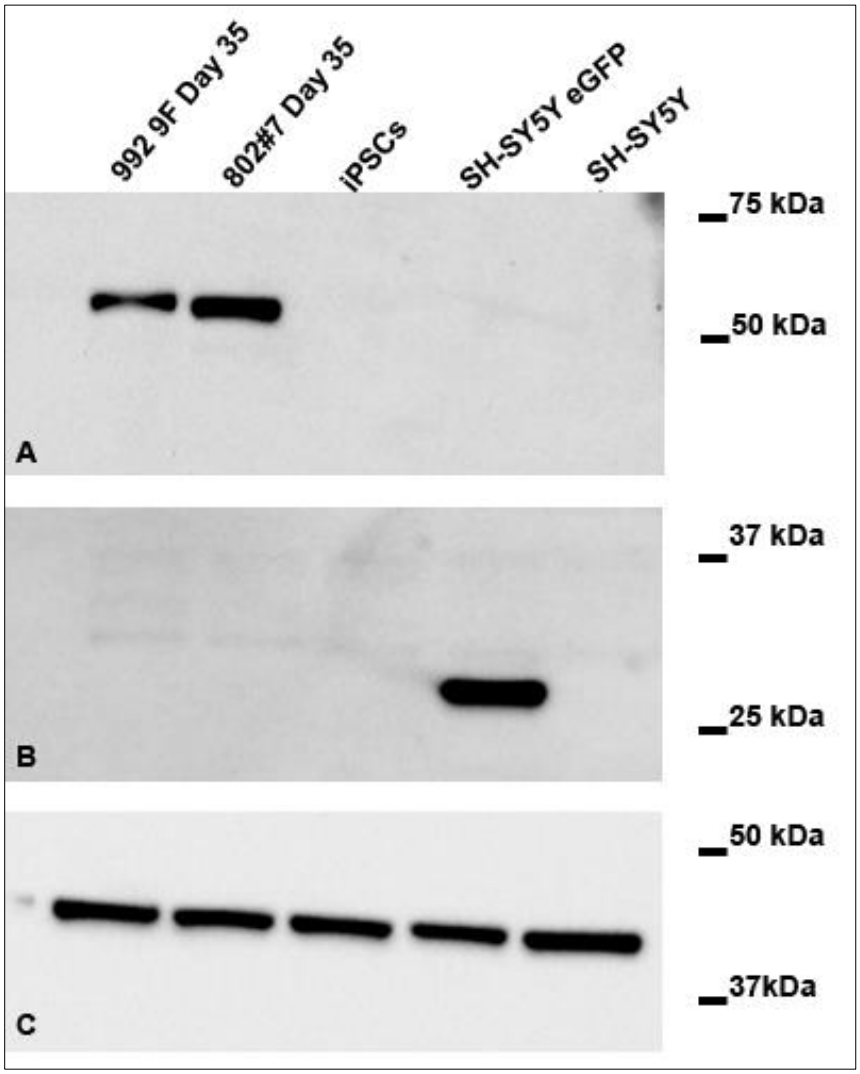

Fig. 66 Western Blot for TH and eGFP. Blot was incubated with (A) anti-TH antibody, (B) anti-eGFP antibody and (C) anti-β-actin antibody as loading control.

GIRK2-mCherry clones were also blotted as protein lysates (Fig. 67). mCherry could be detected only in overexpressing neuroblastoma SH-SY5Y cells but in none of the samples from differentiated neurons (Fig. 67B). GIRK2 detection was indeed problematic. GIRK2 has a molecular weight of 48.5 kDa. We could detect weak bands in samples at this approximate molecular weight only in differentiated neurons whereas this band was absent in iPSCs and neuroblastoma cells. β-actin was used as loading control, with the exception of SH-SY5Y cells transfected with mCherry plasmid that were loaded in lower total protein amount to avoid over saturation of the signal.

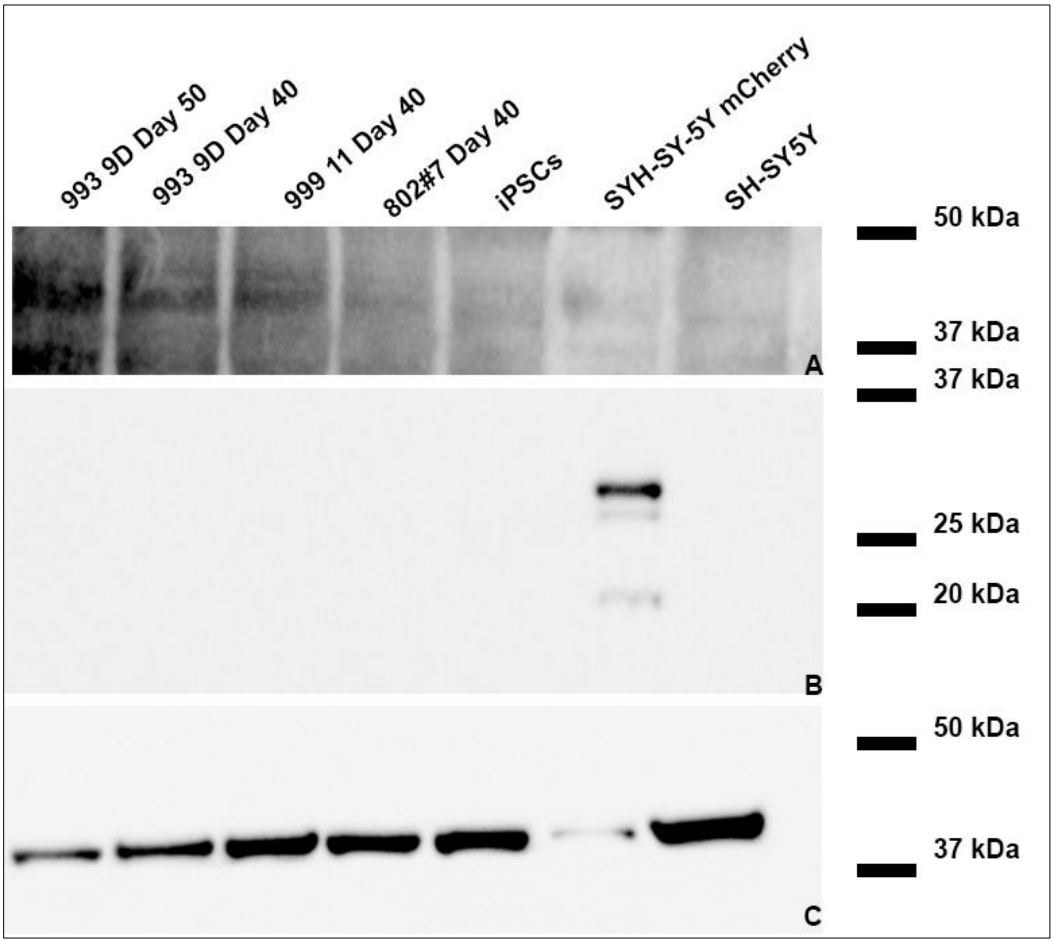

Fig. 67 Western Blot for GIRK2 and mCherry. Blot was incubated with (A) anti-GIRK2 antibody, (B) anti-mCherry antibody and (C) anti-β actin antibody as loading control.

4.5.3.5 Flow cytometry

The signal of TH and eGFP in immunostaining was clear and provided proof for the presence of eGFP. However, we did not observe endogenous fluorescence with confocal microscopy. For this reason, we decided to run cells on a flow cytometer, as we expected fluorescence detection to be much more sensitive at single cell level. The throughput of cells to be analysed on a flow cytometer is much higher and we expected to get a better readout with this technique. In addition, concerning future applications of this reporter system, flow cytometry and synchronized cell sorting was a very interesting approach to pursue in order to obtain a pure DA cell culture.

The concomitant expression of TH and eGFP on day 25 of *in vitro* differentiation observed in immunostaining, indicated this as the earliest day to perform flow cytometry on DA cells. Cell clone 992-9F was analysed and compared to non-transfected control line 802#7. Cells differentiated with the publication-based protocol were analysed on a FACSCanto^{TM} II. 802#7 was used to draw gates in forward scatter (FSC) and sideward scatter (SSC) plot and in the FITC channel for eGFP fluorescence.

As is shown in Fig. 68A, when overlaying the dot plots for 802#7 and 992-9F measured under the same conditions, there was a weak but distinct difference in fluorescence amplitude. The histogram in Fig. 68B shows an even clearer picture of differences in fluorescence intensity between control and 992-9F. As measured by BD FACS software, there were 13.1% of the cells in 992-9F clone that exceeded the fluorescence signal of the control cell line. This indicates that the expression of eGFP could allow separation and identification of DA cells

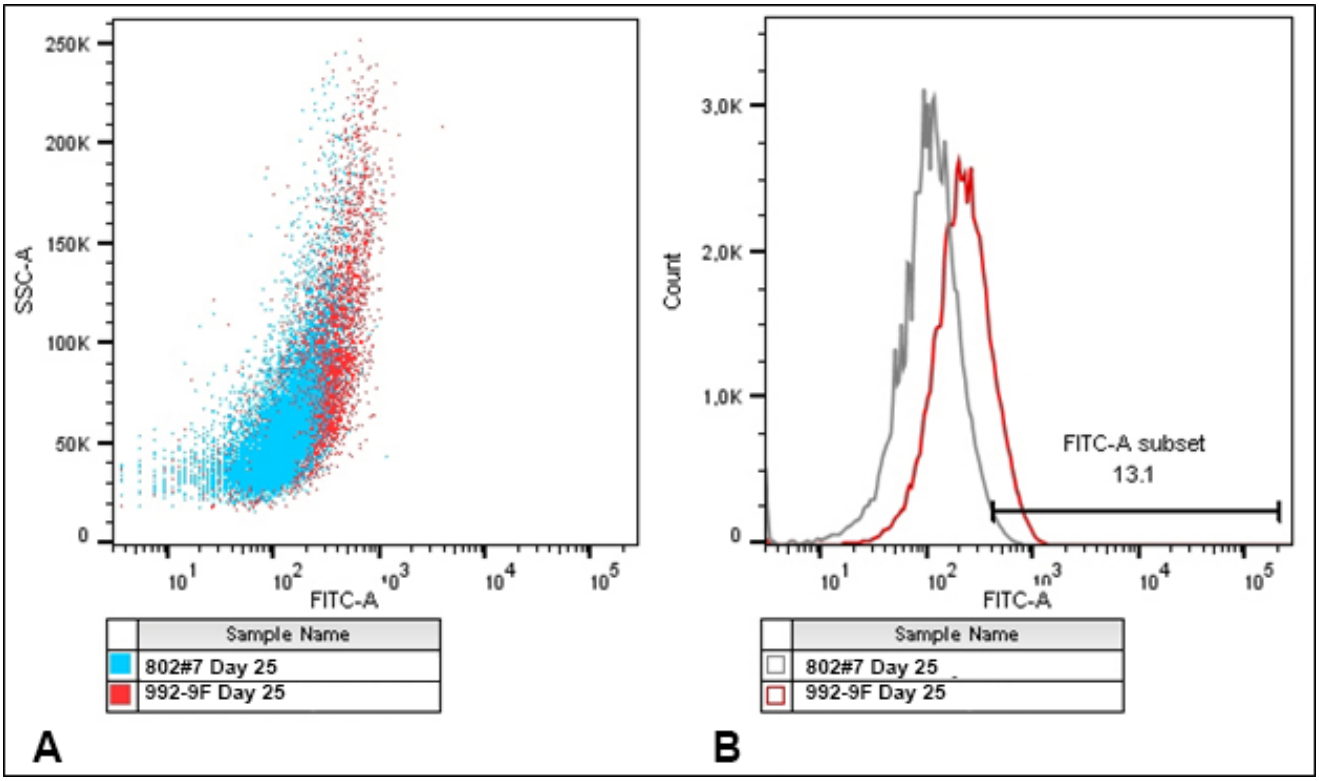

Fig. 68 FACS analysis of cell line 992-9F compared to parental cell line 802#7; (A) Merge of scatter plot showing SSC-A against FITC-A channel for eGFP fluorescence. 992-9F (red dots) is compared to parental cell line 802#7 (blue dots); (B) Histogram of fluorescence intensity in FITC-A channel showing eGFP signal. Histograms for 992-9F (red) and 802#7 (grey) are overlain to show fluorescence intensity increase in cell line 992-9F.

Flow cytometry for GIRK2-mCherry clones was not performed. Considering gene and protein co-expression analysis (described above) for GIRK2 and mCherry, we decided not to perform flow cytometry analysis of GIRK2-mCherry cell lines as we could not guarantee the ability to specifically detect GIRK2 fluorescence.

5 Discussion

The significance of stem cell derived DA neurons is unarguable. The perspective to create a neuronal model in a dish to observe patient specific disease aspects is one of the most promising applications after the discovery of hiPSCs. Amazingly, the investigative progress using this system is remarkable considering the little time that has passed since the discovery of hiPSCs by Yamanaka in 2007. The challenges concerning the use of hiPSCs and neuronal cells derived from hiPSCs have been recognized (Dolmetsch and Geschwind 2011) and a lot of effort has been made to overcome these challenges.

Combining genome-editing techniques with stem cell derived cells harvests an even more interesting potential for disease modelling and stem cell therapy approaches. This has been tremendously facilitated by the establishment of CRISPR/Cas9 technique.

Here we discuss how the work of this thesis can contribute to the use of patient derived cells as a model for PD, not only by pushing technical boundaries intrinsic to stem cell work but also by improving the capabilities of hiPSC-derived neurons to present a valid model for the disease.

5.1 Creating knock-in hiPSCs with CRISPR/Cas9

We showed in this thesis that the CRISPR/Cas9 system could represent the technique of choice for creating knock-in hiPSC lines. Specifically, we successfully integrated two different 1,500 bp long fragments separately into control hiPSC lines by providing a plasmid based donor sequence flanked by 800bp homologous sequences. The resulted was a “scarless” integration without disrupting the genes’ open reading frames, thereby producing hiPSC cells with fluorescent tags under the control of endogenously expressed genes. This aspect is particularly relevant, as it allows the targeting and identification of specific neuronal cell types characterized by a temporal expression pattern during differentiation, as it occurs for TH and GIRK2 proteins.

The donor sequence for both knock-in constructs contained an antibiotic resistance cassette that was intended to be used as selection method for successfully engineered clones. However, we encountered major difficulties applying this selection marker to the engineered hiPSCs. According to the literature, these difficulties cannot be explained by a low activity of the promoter sequence integrated with the selection cassette, as EF1α is reported to be a promoter with high activity also in stem cells (Norrman et al. 2010). We argue that the encountered difficulties are due to the low engineering efficiency. Trying to

apply selection pressure to a hiPSC population with as little as 0.5% of cells expressing the resistance most probably lead to a stress-induced cell death of resistant cells as they will remain as single cells dispersed in the dish which is an effect known to decrease cloning efficiency, viability and quality of human stem cells (Amit et al. 2000; Bajpai et al. 2008)

In our hands, the antibiotic selection was not the method of choice for isolating cell clones. Due to low transfection efficiency in hiPSCs, we expected recombination efficiency to be below 1% (Miyaoka et al. 2014; Zhang et al. 2017). Therefore, the major concern was how to identify such a low number of correctly engineered cells. This issue was overcome by introducing a highly specific screening method by using ddPCR for screening a pool of transfected cells. The ddPCR method, for both the targeted genes, was designed and validated not only to detect the insertion of the fluorescent tag but also to determine the correct locus of recombination. In fact, even though CRISPR/Cas9 technology guarantees a higher level of recombinant accuracy, we could not exclude random plasmid integration and expression of the fluorescent tag. We designed a ddPCR assay spanning the targeted genomic region upstream of the homology sequence cloned and fused with the fluorescent tag. Therefore, only in the presence of correct integration, the PCR product could be amplified allowing identification of positive clones. We optimized this technology in order to be able to identify even very low abundant events of successful homologous recombination. We introduced this screening as early as 4 days after transfection, which allowed us to estimate the number of clones that would have to be selected by hand, or on the other hand discard unsuccessful experiments.

The ddPCR screening method allowed us to determine the absolute value of successfully engineered cells. This clearly indicated that differences in engineering efficiency exist and that they are cell line dependent. Comparing the two targeted loci, it appeared that a very low efficiency occurred at the *KCNJ6* locus. Compared to the *TH* locus recombination, the efficiency was approximately half as high. We therefore re-analysed the engineering strategy in all the plasmid reagents. We found an error in the engineering strategy: the PAM site, necessary for the Cas9 to recognize its destined cutting site, was in fact present also in the donor plasmid. This leads to cutting not only of the desired site at the genomic locus, but also to undesired cutting of the donor vector, leading to a decreased homologous recombination capacity. The specificity of the ddPCR assay, designed and validated for the two targeting approaches, allowed us to discover this discrepancy in engineering efficiencies. This data reinforce the importance of carefully designing and validating the ddPCR-based genomic screening assay. Indeed, this is particularly true when the knock-in involves large DNA fragments (as eGFP and mCherry) and targets large homology arms and not single base-pair mutation.

Most important is that applying this screening method for genome engineering experiments allows us to perform a clone screening *a-priori*, before continuing with the manual selection of the hiPS clones, which is really cost and work intensive and can be avoided if cause is given.

5.2 Differentiation of dopaminergic neurons from hiPSCs

In this work, the expression of the fluorescent probes relies on the relative expression of the targeted gene that in turn depends from the differentiation into DA neurons of hiPSCs. Therefore, the DA differentiation protocols, their validation and efficiency represented key experimental parts of this thesis in order to find the optimal method. Eventually, we were successful in differentiating DA neurons not only using a published protocol, but also using a commercially available kit (Gibco kit, see Material and methods). As reported in various sources in literature (Abeliovich and Hammond 2007; Fasano et al. 2010; Hartfield et al. 2014; Kirkeby et al. 2012; Kriks et al. 2011; Fedele et al. 2017; Woodard et al. 2014), differentiation potential of hiPSCs is variable and can range from 10-50%. We investigated the potential of both differentiation protocols to produce DA neurons and the reproducibility of the two methods.

The first step was to perform a staining for LMX1A and FOXA2 as a first readout after 10 days of *in vitro* differentiation, as well as qRT-PCR analysis for the same markers. This is a commonly used approach to monitor floor plate induction efficiency (Fedele et al. 2017; Zhang, Xia, and Reijo Pera 2014) that should result in an at least 70% of co-staining. Indeed, we saw a very efficient co-staining with both protocols at about 80% (see Fig. 46), which is indicative of proper induction of floor plate fate. At this stage, we could not note any significant differences between protocols as far as marker quantity and quality is concerned. We did though encounter some technical difficulties with the published protocol at this time point of differentiation. Around 8-10 days *in vitro*, we could often observe cells detaching, which was cell line independent and could not be prevented by changing coating or plating parameters (exchanging Matrigel for Geltrex and varying plating density of cells). This phenomenon appears to be quite common as encountered also by colleagues in other independent laboratories (personal communication of Dr. Dayne Beccano-Kelly, University of Oxford) and with no unique solution. We did not have the same problems with the Gibco Kit differentiation, as the kit's protocol includes two splitting steps before day 10. Floor plate induced cells are highly proliferative, which could be observed with the published protocol by a formation of a very thick layer of cells, which are not all viable. To overcome detaching and reduce the cell loss, we introduced a re-plating step also with the published protocol at day 8, similar to the Gibco

protocol, and eventually cell culture quality could be increased in most cases. In our hands, the Gibco Kit differentiation was much more reproducible and stable from this point of view.

The assessment and efficiency of differentiation into DA neurons was done by staining for TH by immunofluorescence. We could show that at day 35 with both protocols neurons were positively stained for TH. With the Gibco differentiation Kit, generally we observed a tendency to lower numbers of TH positive cells compared to the published protocol. However, once again the Gibco Kit differentiation could deliver much more reproducible results, not the least because it allows banking of progenitors and in this way permits to reproduce data more easily among differentiation batches. On the other hand, we encountered big variation in outcome of differentiation with the published method, varying from high numbers of TH positive neurons to no neurons obtained at all. Again, this is an overall known issue that is encountered by many laboratories and has been addressed by the community in the last years especially by developing GMP grade reagents and protocols (Kirkeby et al. 2017). The effort of synchronizing methods and reagents is shown also in the endeavour of the *g-force* teams to align differentiation methods.

Alongside with TH, DA neurons from both differentiation protocols could successfully be stained for specific synaptic markers like PSD95 and Synapsin (Hu et al. 2017; Tada and Sheng 2006). This shows that the neurons we derived *in vitro* do engage in network and synapse formation, an indispensable step to becoming mature DA neurons. The maturity of neurons could further be confirmed by functional assessments. In medium from DA neurons, taken at different time points, we could detect up to 20nM concentration of DA. Important is that DA was released autonomously into the medium by the cells without prior stimulation. This shows that the cells we have differentiated into DA neurons are capable of producing, transporting and releasing the neurotransmitter into the synaptic cleft. We take this as a promising indication of the presence of a functioning DA machinery including besides TH, VMAT2 (vesicular monoamine transporter 2), DDC (DOPA decarboxylase) and DAT (dopamine transporter).
Electrophysiological recordings of sEPSPs support our molecular evaluation and demonstrate the presence of synaptic activity driven by the network. Basal electrophysiological properties as sodium and potassium currents are present. It is important to mention that we did not analyse cells in particular pharmacological conditions, that allow us to identify specifically sodium and/or potassium channels and it is likely, that the maximum amplitude of currents was underestimated. Especially, A type potassium channels, that should be present in DA neurons, were not explicitly identified with these recordings.

We were able to show that these neurons have spontaneous synaptic activity and are able to fire action potentials spontaneously and upon stimulation. The presence of pace-making acitivty observed in these cells is a characteristic feature of DA neurons. *In vivo*, SNpc DA cells show a firing frequency between 1-8 Hz (Kuznetsova et al. 2010). Our representative trace shows a frequency of 1 Hz. We speculate that further maturation is still needed for cells to develop a faster firing pattern. We could show traces indicative of HCN channel presence, which is characteristic for DA neurons with pace making ability. The HCN channel opens upon hyperpolarization and mediates the depolarizing cation current "I_h" that is critical for rhythmic activity.

This supports our thesis that prolonged maturation would be beneficial to develop all the key physiological features of these neurons. For better maturation a differential approach, using mouse or rat astrocyte co-culture could be beneficial.

5.3 Expression of fluorescent reporters

The combination of co-expression of TH-eGFP was a key data to confirm the success of the genetic engineering and we addressed it in different ways. First, we could show that mRNA expression for target gene and reporter is perfectly aligned: by ddPCR we detected half of eGFP mRNA compared to the total TH mRNA content. This proved that, at the genomic level, the tandem of TH-t2A-eGFP is functioning perfectly. Unfortunately, the same effect was not observed for the GIRK2-mCherry tandem. We do see a mCherry expression but it does not reach a 0.5 ratio as TH-eGFP and we could not detect a correlation of the expression between the two genes (see Fig. 57 and Fig. 58).

At protein level, to visualize the fluorescent reporter tag we have encountered difficulties. We are not able to detect an endogenous fluorescence neither for eGFP, nor for mCherry. This had mainly to do with a relatively high autofluorescence especially in the green emission spectrum of cells that overlaps the fluorescent signal produced by the reporter tags. The expression of the reporter tags is under the control of endogenous regulated genes, therefore quite different from standard recombination situations with expression of a gene under the control of a viral promoter (e.g. CMV). Thus, the signal-to-noise ratio between reporter tag driven fluorescence versus autofluorescence is reduced. Indeed, we have observed that DA neurons do often grow in clusters of cells that are sphere-like, where many cells are already dead and produce a high autofluorescence that is not possible to reduce when imaging at the confocal microscope, even with fine-tuning of eGFP excitation and emission spectra and/or using specific autofluorescence quencher as VectaShield.

On the other hand, we were able to detect the fluorescent proteins with indirect labelling in immunocytochemistry experiments. An overlap of TH-eGFP expression could be observed in different cell clones upon differentiation into DA neurons. We have focused initially on characterizing the TH-eGFP reporter system, as we argue it is the more important reporter, as GIRK2 is not a specific DA marker, but only allows identifying A9 DA neurons when co-expressed with TH, making TH the cardinal point of a dual reporter system. We have observed better reproducibility with the Gibco Kit differentiation when characterizing the TH-eGFP system in terms of consistency of a successful DA differentiation and cells positive for TH and therefore also for eGFP. This is the reason why we strongly focused on this differentiation method when we started the GIRK2-mCherry system characterization.

Using this differentiation protocol we could see a co-staining of GIRK2-mCherry at day 40 (seeFig. 64 and Fig. 65) but the data should be seen very critically as we could not see a good correlation of gene expression. As the gene expression data showed us, that both genes are expressed but not in a correlated way that leads to a double quantity of GIRK2 compared to mCherry, we think it most unlikely that the staining for mCherry that we detected is specific. Also Western Blot experiments support these data of a GIRK2 presence, but unfortunately also mCherry absence.

Another variability we could observe was that TH and eGFP co-expression was consistently observed, but sometimes we found regions where a co-staining was not present and only either TH or eGFP were present in the cell (see Fig. 69).

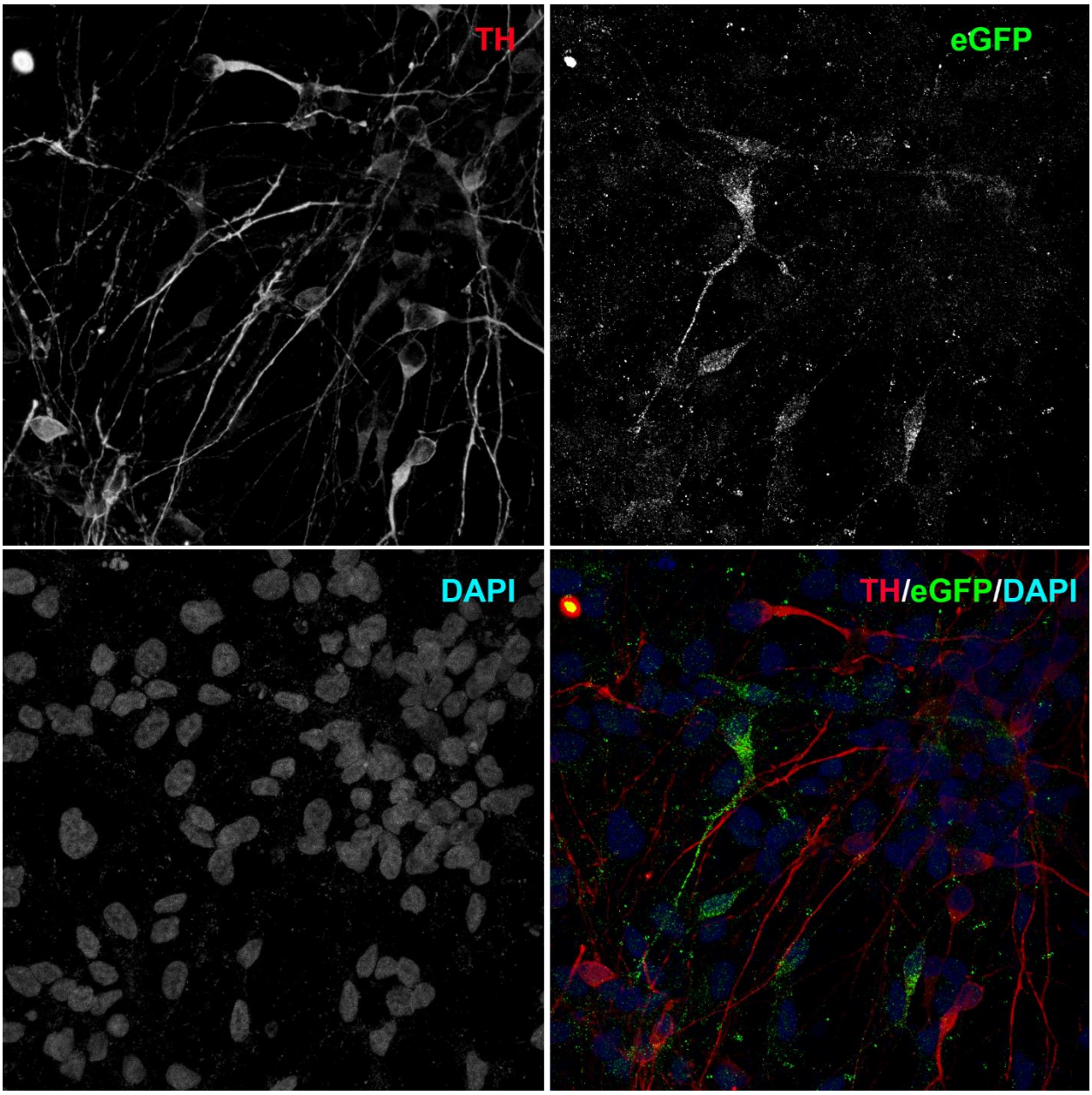

Fig. 69 Co-immunostaining of TH, eGFP and MAP2 in clone 992-9F at Day 35 with published protocol (Differentiation 22). Upper left: red channel for TH staining in AlexaFluor 555; upper right: green channel for eGFP staining in AlexaFluor488; bottom left: infrared channel for MAP2 staining in AlexaFluor647; bottom right: overlay of channels in RGB of TH (red), eGFP (green), MAP2 (blue);

This peculiarity was observed in cell clones that had shown perfect co-staining in previous differentiations; also it was detected in numerous clones. The reason for this lack of co-staining is, in our opinion, the peculiarity of T2A peptide system. In fact, the T2A peptide is a peptide with viral origin, whose function is to cause a ribosome skipping during translation. There are observations that report that this ribosome

skipping however does not necessarily take place, but results either in a ribosome “fall-off” or a continued translation, thus leading to fusion-protein formation (Wang et al. 2015). The same observation also reports that the downstream protein is more likely not to be expressed, but also a decrease in the upstream protein translation is possible. This is supported by Western Blot analysis, where the detection of eGFP protein failed in our TH-eGFP positive clones after differentiation although we selected an eGFP antibody that we proved to recognize eGFP protein upon transient overexpression in human neuroblastoma cells. Both immunocytochemistry and Western Blot show that eGFP expression is probably at detection limit due to a faulty function of the T2A peptide. This is a system that is working well with viral expression methods where the presence of viral promoter results in protein overload even upon faulty T2A function and ribosome fall-off. When creating reporter lines like the ones in discussion, the expression of the reporter protein is under the control of an endogenous promoter, where a decrease in expression can have remarkable impact on detection of the protein in question. In our opinion, this is also supported by the fact that we can see an endogenous eGFP signal in flow cytometry, which is the most sensitive method of all, which helps us to succeed in detection, where other methods failed.

The fact that endogenous eGFP fluorescence is detectable in flow cytometry is pivotal. On the one hand, it shows that the detection of the endogenous fluorescence is a question of sensitivity of detection and background compensation, which is important to be taken into account for any fluorescently tagged protein, also if it was tagged with a different fluorophore. Next, it proves that the created knock-in faithfully reports TH expression *in vitro*. This is remarkable, as previous approaches to a TH-reporter system could not deliver faithful co-presence of both proteins (Kelly et al. 2006). A study was published in 2017 (Xia et al. 2017) with a similar construct for DA neurons, with a red fluorescent protein reporter, reporting the feasibility of this kind of reporter systems. It potentially enables sorting of viable TH expressing cells while maintaining the integrity of the cell membrane. At the same time, it delivers the most important application of this kind of reporter construct. Being intended to distinguish DA neurons from non-DA neurons, we could in this manner not only discriminate a certain population but also separate it to enrich the DA neuronal population in culture. As there is no widely accepted surface marker for DA neurons, an endogenous fluorescent reporter is a major step forward to producing pure TH positive neuronal cultures. Indeed, we see in contrast to Xia’s study from 2017 an increase of detectable signal with our fluorescent reporter and engineering strategy, which is an indication that a green signal may be of advantage at such sensitive rates of detection even considering the before mentioned drawbacks of the green channel. The system has the potential to facilitate a variety of studies investigating DA neurons. The data also shows that day 25 is a feasible time point for analysis and eventually sorting, which

furthermore facilitates the experimental process because cells have to be passaged anyway around this time *in vitro* for terminal maturation. Also, the approach is compatible with transplantation of TH neurons to lesioned rodent models and could improve engraftment (Lehnen et al. 2017). We are very confident about this data as we saw the same effect of fluorescent separation on two different machines, a FACS Canto II and a S3 Sorter (Biorad, data not shown). FACS sorting of neurons will be a major challenge for future studies and is something that we are already working on. Following sorting, the application of an enriched population will be manifold. Most simply, genetic analysis can be performed on DA neurons, and if also the GIRK2 mCherry reporter results to be identifiable with flow cytometry, we will be able to sort out A9 DA neurons from other DA neurons and look for gene expression differences.

In the same manner, functional testing can be performed on distinct populations as well as pharmacological treatments with degenerative agents like Rotenone or 6-OHDA and draw conclusions on differential susceptibility of DA neurons and DA neuron subtypes. It is important to mention at this point, that an enriched or even purified DA culture cannot develop a naturally functional network, as up to 70% of afferent projections to DA neurons are from GABAergic neurons (Bolam and Smith 1990). Still, having an enriched population can certainly give an advantage respect to a mixed population where the mixture is of unknown composition. A possibility to allow network formation could be a co-culture with GABAergic neurons in order to create a complex *in vitro* environment.

5.4 Future perspectives and possible applications

This work's intent was to produce a reporter line to identify A9 DA neurons. We have shown that CRISPR/Cas9 is a valid method to integrate large fragments into the genome of hiPSCs without creating further genomic alterations. Most importantly, we developed a novel strategy for bona fide screening of engineered cells that can be easily applied to any other genome editing approach. The reporter system is working which has been shown by different methods, though we have revealed some weak points of this tagging strategy. First, the endogenous signal results to be weak and detectable only by flow cytometry. Secondly, a reduction in fluorescent protein expression can be observed due to a malfunction of the T2A system. For this reason, we propose for *de novo* projects a strategical change for the genomic construct, by choosing a more valid system that allows the production of a reporter without creating fusion proteins. A possible solution is replacing the T2A by in IRES (internal ribosome entry site). One can also argue whether a green fluorescent protein is the best tag of choice for this kind of tagging approach as we could observe a lot of autofluorescence in the green channel, making it often hard to distinguish true positive

from false positive signal or, on the other hand, not seeing true positive signal. We are still missing the same thorough readout of the GIRK2 mCherry tag, therefore the question, whether a different fluorescence protein may facilitate analysis is still arguable also in light of what has been reporter by (Xia et al. 2017). Indeed, in our hands, the signal detection was beyond what has been reported so far, which may depend on more efficient differentiation methods or also a brighter signal in the green channel. Taken together these considerations, there is no indication that a different fluorescent protein may really improve the readout.

For the cell lines we recreated, we see a big potential in using them for FACS sorting. We have shown that the visualization of the endogenous signal is possible with a flow cytometer and would allow us to sort these cells. We are currently engaged in developing reproducible sorting protocols for DA neurons, which will require some setup work as neuronal cells are very fragile and susceptible to mechanical stress. Once this sorting procedure is in place, we will pursue this direction in order to be able to create a pure DA cell culture and thereby overcoming one of the biggest limitations of i*n vitro* differentiation approaches.

We are still missing the double knock-in line, which will be produced once we have a better understanding of the reporter system and more data on the GIRK2-mCherry tandem. This will be of further significance when we are able to sort TH positive cells on day 20 and then observe GIRK2 expression during maturation.

Once a double knock-in line will be used for FACS sorting, this novel model delivers remarkable possible applications to shed light on A9 DA neurons and their susceptibility. Not only will a functional readout be easier on purified populations of DA neurons in general, but also A9 neurons can be singled out more easily and tested under the same conditions as non-A9 DA neurons. In addition, pharmacological screenings will be rendered more significant in such a manner.

We have shown that different lines can be knocked in with these constructs and in the future, the used constructs will be used also on lines derived from patients carrying PD causing mutations. In this way, one can draw comparisons from functional or pharmacological readouts between DA neurons from healthy individuals and patients and understand even more the neurodegenerative process underlying PD.

The work of this thesis is further of significance to the ongoing evolutions in gene therapy and its potential therapeutic applications. The success of gene therapy is due to the establishment of safe transduction methods using replication deficient retroviral vectors (Lisa Li, Nakano, and Hotta 2013). Several clinical studies applying autologous transplantation of bone marrow cells treated with gene therapy vectors showed tremendous success treating diseases affecting majorly cells of the hematopoietic system

(Hacein-Bey-Abina et al. 2010; Cavazzana-Calvo et al. 2010). *In vivo* delivery of AAV vectors to liver, retina or nervous system also delivered promising clinical outcomes (Dunbar et al. 2018).

Retroviral approaches in gene therapy, however, are based on gene addition instead of correction. CRISPR/Cas9 provides a novel targeted approach to correction of the endogenous mutated gene. In fact, we have shown that not only is CRISPR/Cas9 adapt for insertion or correction of single nucleotides, but also for insertion of large fragments. Diseases that are caused by large genome deletions or translocations are possible to be corrected in this manner, as for example Wiskott-Aldrich syndrome or x-linked severe immunodeficiency (X-SCID). In the context of PD (and other neurodegenerative disorders), a potential therapeutic approach could be represented by cell replacement therapy , either for patients with genomic PD (e.g.: large deletions in the Parkin gene (PARK2),) and for idiopathic PD. Corrected healthy hiPSC cells could be differentiated into DA neurons and an autologous transplantation could be the eventual goal of a cell replacement therapy, thus dramatically reducing also the impact of potential graft versus host disease.

6 References

Abeliovich, A., and R. Hammond. 2007. 'Midbrain dopamine neuron differentiation: Factors and fates', *Dev Biol*, 304: 447-54.

Abou-Sleiman, P. M., M. M. Muqit, and N. W. Wood. 2006. 'Expanding insights of mitochondrial dysfunction in Parkinson's disease', *Nat Rev Neurosci*, 7: 207-19.

Amit, M., M. K. Carpenter, M. S. Inokuma, C. P. Chiu, C. P. Harris, M. A. Waknitz, J. Itskovitz-Eldor, and J. A. Thomson. 2000. 'Clonally derived human embryonic stem cell lines maintain pluripotency and proliferative potential for prolonged periods of culture', *Dev Biol*, 227: 271-8.

Ashkan, K., P. Rogers, H. Bergman, and I. Ughratdar. 2017. 'Insights into the mechanisms of deep brain stimulation', *Nat Rev Neurol*, 13: 548-54.

Bae, E., H. Lee, E. Rockenstein, D. Ho, E. Park, N. Yang, P. Desplats, E. Masliah, and S. Lee. 2012. 'Antibody-Aided Clearance of Extracellular α-Synuclein Prevents Cell-to-Cell Aggregate Transmission', *The Journal of Neuroscience*, 32: 13454.

Bajpai, R., J. Lesperance, M. Kim, and A. V. Terskikh. 2008. 'Efficient propagation of single cells Accutase-dissociated human embryonic stem cells', *Mol Reprod Dev*, 75: 818-27.

Barini, E., A. Miccoli, F. Tinarelli, K. Mulholland, H. Kadri, F. Khanim, L. Stojanovski, K. D. Read, K. Burness, J. J. Blow, Y. Mehellou, and M. M. K. Muqit. 2018. 'The Anthelmintic Drug Niclosamide and Its Analogues Activate the Parkinson's Disease Associated Protein Kinase PINK1', *Chembiochem*, 19: 425-29.

Barker, R. A., M. Parmar, L. Studer, and J. Takahashi. 2017. 'Human Trials of Stem Cell-Derived Dopamine Neurons for Parkinson's Disease: Dawn of a New Era', *Cell Stem Cell*, 21: 569-73.

Barrangou, R., C. Fremaux, H. Deveau, M. Richards, P. Boyaval, S. Moineau, D. A. Romero, and P. Horvath. 2007. 'CRISPR Provides Acquired Resistance Against Viruses in Prokaryotes', *Science*, 315: 1709.

Bartus, R. T., M. S. Weinberg, and R. J. Samulski. 2014. 'Parkinson's Disease Gene Therapy: Success by Design Meets Failure by Efficacy', *Molecular Therapy*, 22: 487-97.

Begum, A. N., C. Guoynes, J. Cho, J. Hao, K. Lutfy, and Y. Hong. 2015. 'Rapid generation of sub-type, region-specific neurons and neural networks from human pluripotent stem cell-derived neurospheres', *Stem cell research*, 15: 731-41.

Bernheimer, H., W. Birkmayer, O. Hornykiewicz, K. Jellinger, and F. Seitelberger. 1973. 'Brain dopamine and the syndromes of Parkinson and Huntington Clinical, morphological and neurochemical correlations', *Journal of the Neurological Sciences*, 20: 415-55.

Bjorklund, A., and S. B. Dunnett. 2007. 'Dopamine neuron systems in the brain: an update', *Trends Neurosci*, 30: 194-202.

Bolam, J. P., and Y. Smith. 1990. 'The GABA and substance P input to dopaminergic neurones in the substantia nigra of the rat', *Brain Res*, 529: 57-78.

Bolam, J. P., and E. K. Pissadaki. 2012. 'Living on the edge with too many mouths to feed: Why dopamine neurons die', *Movement Disorders*, 27: 1478-83.

Bolotin, A., B. Quinquis, A. Sorokin, and S. D. Ehrlich. 2005. 'Clustered regularly interspaced short palindrome repeats (CRISPRs) have spacers of extrachromosomal origin', *Microbiology*, 151: 2551-61.

Braak, H., K. Del Tredici, U. Rub, R. A. de Vos, E. N. Jansen Steur, and E. Braak. 2003. 'Staging of brain pathology related to sporadic Parkinson's disease', *Neurobiol Aging*, 24: 197-211.

Brinkman, E. K., T. Chen, M. Amendola, and B. van Steensel. 2014. 'Easy quantitative assessment of genome editing by sequence trace decomposition', *Nucleic Acid Research*, 42.

Byers, B., B. Cord, H.N. Nguyen, B. Schüle, L. Fenno, P. C. Lee, K. Deisseroth, J. W. Langston, R.R. Pera, and T. D. Palmer. 2011. 'SNCA Triplication Parkinson's Patient's iPSC-derived DA Neurons Accumulate α-Synuclein and Are Susceptible to Oxidative Stress', *PLoS One*, 6: e26159.

Cantuti-Castelvetri, I., C. Keller-McGandy, B. Bouzou, G. Asteris, T. W. Clark, M. P. Frosch, and D. G. Standaert. 2007. 'Effects of Gender on Nigral Gene Expression and Parkinson Disease', *Neurobiology of disease*, 26: 606-14.

Cavazzana-Calvo, M., E. Payen, O. Negre, G. Wang, K. Hehir, F. Fusil, J. Down, M. Denaro, T. Brady, K. Westerman, R. Cavallesco, B. Gillet-Legrand, L. Caccavelli, R. Sgarra, L. Maouche-Chrétien, F. Bernaudin, R. Girot, R. Dorazio, G. Mulder, A. Polack, A. Bank, J. Soulier, J. Larghero, N. Kabbara, B. Dalle, B. Gourmel, G. Socie, S. Chrétien, N. Cartier, P. Aubourg, A. Fischer, K. Cornetta, F. Galacteros, Y. Beuzard, E. Gluckman, F. Bushman, S. Hacein-Bey-Abina, and P. Leboulch. 2010. 'Transfusion independence and HMGA2 activation after gene therapy of human β-thalassaemia', *Nature*, 467: 318.

Chambers, S. M., c. A. Fasano, E. P. Papapetrou, M. Tomishima, M. Sadelain, and L. Studer. 2009. 'Highly efficient neural conversion of human ES and iPS cells by dual inhibition of SMAD signaling', *Nat Biotech*, 27: 275-80.

Chang, D., M. A. Nalls, I. B. Hallgrimsdottir, J. Hunkapiller, M. van der Brug, F. Cai, G. A. Kerchner, G. Ayalon, B. Bingol, M. Sheng, D. Hinds, T. W. Behrens, A. B. Singleton, T. R. Bhangale, and R. R. Graham. 2017. 'A meta-analysis of genome-wide association studies identifies 17 new Parkinson's disease risk loci', *Nat Genet*, 49: 1511-16.

Chen, L., K. Trujillo, W. Ramos, P. Sung, and A. E. Tomkinson. 2001. 'Promotion of Dnl4-catalyzed DNA end-joining by the Rad50/Mre11/Xrs2 and Hdf1/Hdf2 complexes', *Mol Cell*, 8: 1105-15.

Choong, C. J., and H. Mochizuki. 2017. 'Gene therapy targeting mitochondrial pathway in Parkinson's disease', *J Neural Transm (Vienna)*, 124: 193-207.

Chung, C. Y., H. Seo, K. C. Sonntag, A. Brooks, L. Lin, and O. Isacson. 2005. 'Cell type-specific gene expression of midbrain dopaminergic neurons reveals molecules involved in their vulnerability and protection', *Hum Mol Genet*, 14: 1709-25.

Cookson, M. R. 2010. 'The role of leucine-rich repeat kinase 2 (LRRK2) in Parkinson's disease', *Nat Rev Neurosci*, 11: 791-7.

Daher, J. P., H. A. Abdelmotilib, X. Hu, L. A. Volpicelli-Daley, M. S. Moehle, K. B. Fraser, E. Needle, Y. Chen, S. J. Steyn, P. Galatsis, W. D. Hirst, and A. B. West. 2015. 'Leucine-rich Repeat Kinase 2 (LRRK2) Pharmacological Inhibition Abates alpha-Synuclein Gene-induced Neurodegeneration', *J Biol Chem*, 290: 19433-44.

Dahlstroem, A., and K. Fuxe. 1964. 'EVIDENCE FOR THE EXISTENCE OF MONOAMINE-CONTAINING NEURONS IN THE CENTRAL NERVOUS SYSTEM. I. DEMONSTRATION OF MONOAMINES IN THE CELL BODIES OF BRAIN STEM NEURONS', *Acta Physiol Scand Suppl*: Suppl 232:1-55.

Dauer, W., and S. Przedborski. 2003a. 'Parkinson's disease: mechanisms and models', *Neuron*, 39: 889-909.

Dauer, W., and S. Przedborski. 2003b. 'Parkinson's Disease', *Neuron*, 39: 889-909.

Dawson, T. M., H.S. Ko, and V. L. Dawson. 2010. 'Genetic Animal Models of Parkinson's Disease', *Neuron*, 66: 646-61.

Deng, H., J. Jankovic, Y. Guo, W. Xie, and W. Le. 2005. 'Small interfering RNA targeting the PINK1 induces apoptosis in dopaminergic cells SH-SY5Y', *Biochem Biophys Res Commun*, 337: 1133-8.

Deuschl, G., S. Paschen, and K. Witt. 2013. 'Chapter 10 - Clinical outcome of deep brain stimulation for Parkinson's disease.' in Andres M. Lozano and Mark Hallett (eds.), *Handbook of Clinical Neurology* (Elsevier).

Dolmetsch, R., and D. H. Geschwind. 2011. 'The human brain in a dish: the promise of iPSC-derived neurons', *Cell*, 145: 831-4.

Dunbar, C. E., K. A. High, J. K. Joung, D. B. Kohn, K. Ozawa, and M. Sadelain. 2018. 'Gene therapy comes of age', *Science*, 359.

Dzamko, N., A. Gysbers, G. Perera, A. Bahar, A. Shankar, J. Gao, Y.Fu, and G. M. Halliday. 2017. 'Toll-like receptor 2 is increased in neurons in Parkinson's disease brain and may contribute to alpha-synuclein pathology', *Acta Neuropathologica*, 133: 303-19.

Eberling, J. L., A. P. Kells, P. Pivirotto, J. Beyer, J. Bringas, H. J. Federoff, J. Forsayeth, and K. S. Bankiewicz. 2009. 'Functional effects of AAV2-GDNF on the dopaminergic nigrostriatal pathway in parkinsonian rhesus monkeys', *Hum Gene Ther*, 20: 511-8.

Emborg, M. E., M. Carbon, J. E. Holden, M. J. During, Y. Ma, C. Tang, J. Moirano, H. Fitzsimons, B. Z. Roitberg, E. Tuccar, A. Roberts, M. G. Kaplitt, and D. Eidelberg. 2007. 'Subthalamic glutamic acid decarboxylase gene therapy: changes in motor function and cortical metabolism', *J Cereb Blood Flow Metab*, 27: 501-9.

Evans, M. J., and M. H. Kaufman. 1981. 'Establishment in culture of pluripotential cells from mouse embryos', *Nature*, 292: 154.

Falkenburger, B. H., T. Saridaki, and E. Dinter. 2016. 'Cellular models for Parkinson's disease', *J Neurochem*, 139 Suppl 1: 121-30.

Fasano, C. A., S. M. Chambers, G. Lee, M. J. Tomishima, and L. Studer. 2010. 'Efficient derivation of functional floor plate tissue from human embryonic stem cells', *Cell Stem Cell*, 6: 336-47.

Fedele, S., G. Collo, K. Behr, J. Bischofberger, S. Müller, T. Kunath, K. Christensen, A. L. Gündner, M. Graf, R. Jagasia, and V. Taylor. 2017. 'Expansion of human midbrain floor plate progenitors from induced pluripotent stem cells increases dopaminergic neuron differentiation potential', *Scientific Reports*, 7: 6036.

Ferese, R., N. Modugno, R. Campopiano, M. Santilli, S. Zampatti, E. Giardina, A. Nardone, D. Postorivo, F. Fornai, G. Novelli, E. Romoli, S. Ruggieri, and S. Gambardella. 2015. 'Four Copies of SNCA Responsible for Autosomal Dominant Parkinson's Disease in Two Italian Siblings', *Parkinson's Disease*, 2015: 546462.

Ferri, A. L., W. Lin, Y. E. Mavromatakis, J. C. Wang, H. Sasaki, J. A. Whitsett, and S. L. Ang. 2007. 'Foxa1 and Foxa2 regulate multiple phases of midbrain dopaminergic neuron development in a dosage-dependent manner', *Development*, 134: 2761-9.

Fuji, R. N., M. Flagella, M. Baca, M. A. Baptista, J. Brodbeck, B. K. Chan, B. K. Fiske, L. Honigberg, A. M. Jubb, P. Katavolos, D. W. Lee, S. C. Lewin-Koh, T. Lin, X. Liu, S. Liu, J. P. Lyssikatos, J. O'Mahony, M. Reichelt, M. Roose-Girma, Z. Sheng, T. Sherer, A. Smith, M. Solon, Z. K. Sweeney, J. Tarrant, A. Urkowitz, S. Warming, M. Yaylaoglu, S. Zhang, H. Zhu, A. A. Estrada, and R. J. Watts. 2015. 'Effect of selective LRRK2 kinase inhibition on nonhuman primate lung', *Sci Transl Med*, 7: 273ra15.

Gilbert, F., M. Feder, G. Balaban, D. Brangman, D. K. Lurie, R. Podolsky, V. Rinaldt, N. Vinikoor, and J. Weisband. 1984. 'Human Neuroblastomas and Abnormalities of Chromosomes 1 and 17', *Cancer Research*, 44: 5444.

Gong, C., P. Bongiorno, A. Martins, N. C. Stephanou, H. Zhu, S. Shuman, and M. S. Glickman. 2005. 'Mechanism of nonhomologous end-joining in mycobacteria: a low-fidelity repair system driven by Ku, ligase D and ligase C', *Nature Structural &Amp; Molecular Biology*, 12: 304.

Grealish, S., E. Diguet, A. Kirkeby, B. Mattsson, A. Heuer, Y. Bramoulle, N. Van Camp, A. L. Perrier, P. Hantraye, A. Bjorklund, and M. Parmar. 2014. 'Human ESC-derived dopamine neurons show similar preclinical efficacy and potency to fetal neurons when grafted in a rat model of Parkinson's disease', *Cell Stem Cell*, 15: 653-65.

Grealish, S., B. Mattsson, P. Draxler, and A. Bjorklund. 2010. 'Characterisation of behavioural and neurodegenerative changes induced by intranigral 6-hydroxydopamine lesions in a mouse model of Parkinson's disease', *Eur J Neurosci*, 31: 2266-78.

Greggio, E., S. Jain, A. Kingsbury, R. Bandopadhyay, P. Lewis, A. Kaganovich, M. P. van der Brug, A. Beilina, J. Blackinton, K.J. Thomas, R. Ahmad, D. W. Miller, S. Kesavapany, A. Singleton, A. Lees, R. J. Harvey, K. Harvey, and M. R. Cookson. 2006. 'Kinase activity is required for the toxic effects of mutant LRRK2/dardarin', *Neurobiology of disease*, 23: 329-41.

Hacein-Bey-Abina, S., J. Hauer, A. Lim, C. Picard, G. P. Wang, C. C. Berry, C. Martinache, F. Rieux-Laucat, S. Latour, B. H. Belohradsky, L. Leiva, R. Sorensen, M. Debré, J. L. Casanova, S. Blanche, A.Durandy, F. D. Bushman, A. Fischer, and M. Cavazzana-Calvo. 2010. 'Efficacy of Gene Therapy for X-Linked Severe Combined Immunodeficiency', *New England Journal of Medicine*, 363: 355-64.

Halliday, G., M. T. Herrero, K. Murphy, H. McCann, F. Ros-Bernal, C. Barcia, H. Mori, F. J. Blesa, and J. A. Obeso. 2009. 'No Lewy pathology in monkeys with over 10 years of severe MPTP Parkinsonism', *Mov Disord*, 24: 1519-23.

Hartfield, E. M., M. Yamasaki-Mann, H. J. Ribeiro Fernandes, J. Vowles, W. S. James, S. A. Cowley, and R. Wade-Martins. 2014. 'Physiological characterisation of human iPS-derived dopaminergic neurons', *PLoS One*, 9: e87388.

Hatano, Y., Y. Li, K. Sato, S. Asakawa, Y. Yamamura, H. Tomiyama, H. Yoshino, M. Asahina, S. Kobayashi, S. Hassin-Baer, C. S. Lu, A. R. Ng, R. L. Rosales, N. Shimizu, T. Toda, Y. Mizuno, and N. Hattori. 2004. 'Novel PINK1 mutations in early-onset parkinsonism', *Ann Neurol*, 56: 424-7.

Hertz, N.T, A. Berthet, M.L. Sos, K. S Thorn, A. L Burlingame, K. Nakamura, and K. M Shokat. 2013. 'A Neo-Substrate that Amplifies Catalytic Activity of Parkinson’s-Disease-Related Kinase PINK1', *Cell*, 154: 737-47.

Hu, Z., Z. Liu, X. Li, and X. Deng. 2017. 'Stimulation of synapse formation between stem cell-derived neurons and native brainstem auditory neurons', *Scientific Reports*, 7: 13843.

Imaizumi, Y., Y Okada, W. Akamatsu, M. Koike, N. Kuzumaki, H. Hayakawa, T. Nihira, T. Kobayashi, M. Ohyama, S. Sato, M. Takanashi, M. Funayama, A. Hirayama, T. Soga, T. Hishiki, M. Suematsu, T. Yagi, D. Ito, A. Kosakai, K. Hayashi, M. Shouji, A. Nakanishi, N. Suzuki, Y. Mizuno, N. Mizushima, M. Amagai, Y. Uchiyama, H. Mochizuki, N. Hattori, and H. Okano. 2012. 'Mitochondrial dysfunction associated with increased oxidative stress and α-synuclein accumulation in PARK2 iPSC-derived neurons and postmortem brain tissue', *Molecular Brain*, 5: 35.

Jansen, R., J. D. Embden, W. Gaastra, and L. M. Schouls. 2002. 'Identification of genes that are associated with DNA repeats in prokaryotes', *Mol Microbiol*, 43: 1565-75.

Jinek, M., K. Chylinski, I. Fonfara, M. Hauer, J. A. Doudna, and E. Charpentier. 2012. 'A Programmable Dual-RNA–Guided DNA Endonuclease in Adaptive Bacterial Immunity', *Science*.

Joksimovic, M., B. A. Yun, R. Kittappa, A. M. Anderegg, W. W. Chang, M. M. Taketo, R. D. McKay, and R. B. Awatramani. 2009. 'Wnt antagonism of Shh facilitates midbrain floor plate neurogenesis', *Nat Neurosci*, 12: 125-31.

Kalia, L. V., S. K. Kalia, and A. E. Lang. 2015. 'Disease-modifying strategies for Parkinson's disease', *Mov Disord*, 30: 1442-50.

Kalinderi, K., S. Bostantjopoulou, and L. Fidani. 2016. 'The genetic background of Parkinson's disease: current progress and future prospects', *Acta Neurol Scand*, 134: 314-26.

Kaplitt, M. G., A. Feigin, C. Tang, H. L. Fitzsimons, P. Mattis, P. A. Lawlor, R. J. Bland, D. Young, K. Strybing, D. Eidelberg, and M. J. During. 2007. 'Safety and tolerability of gene therapy with an adeno-associated virus (AAV) borne GAD gene for Parkinson's disease: an open label, phase I trial', *Lancet*, 369: 2097-105.

Kells, A. P., J. Eberling, X. Su, P. Pivirotto, J. Bringas, P. Hadaczek, W. C. Narrow, W. J. Bowers, H. J. Federoff, J. Forsayeth, and K. S. Bankiewicz. 2010. 'Regeneration of the MPTP-Lesioned Dopaminergic System after Convection-Enhanced Delivery of AAV2-GDNF', *The Journal of Neuroscience*, 30: 9567.

Kelly, B. B., E. Hedlund, C. Kim, H. Ishiguro, O. Isacson, D. M. Chikaraishi, K. S. Kim, and G. Feng. 2006. 'A tyrosine hydroxylase-yellow fluorescent protein knock-in reporter system labeling dopaminergic neurons reveals potential regulatory role for the first intron of the rodent tyrosine hydroxylase gene', *Neuroscience*, 142: 343-54.

Kempster, P. A., B. Hurwitz, and A. J. Lees. 2007. 'A new look at James Parkinson's 'Essay on the Shaking Palsy'', *Neurology*, 69: 482-85.

Khaliq, Z. M., and B. P. Bean. 2010. 'Pacemaking in dopaminergic ventral tegmental area neurons: depolarizing drive from background and voltage-dependent sodium conductances', *J Neurosci*, 30: 7401-13.

Kikuchi, T., Morizane, A., Doi, D., Magotani, H., Onoe, H., Hayashi, T., Mizuma, H., Takara, S., Takahashi, R., Inoue, H., et al. (2017). Human iPS cell-derived dopaminergic neurons function in a primate Parkinson's disease model. Nature 548, 592.

Kim, C., D. Ho, J. Suk, S. You, S. Michael, J. Kang, S. J. Lee, E. Masliah, D. Hwang, H. Lee, and S. Lee. 2013. 'Neuron-released oligomeric α-synuclein is an endogenous agonist of TLR2 for paracrine activation of microglia', *Nature Communications*, 4: 1562.

Kirik, D., E. Cederfjäll, G. Halliday, and A. Petersén. 2017. 'Gene therapy for Parkinson's disease: Disease modification by GDNF family of ligands', *Neurobiology of disease*, 97: 179-88.

Kirkeby, A., S. Grealish, D. A. Wolf, J. Nelander, J. Wood, M. Lundblad, O. Lindvall, and M. Parmar. 2012. 'Generation of regionally specified neural progenitors and functional neurons from human embryonic stem cells under defined conditions', *Cell Rep*, 1: 703-14.

Kirkeby, A., S. Nolbrant, K. Tiklova, A. Heuer, N. Kee, T. Cardoso, D. R. Ottosson, M. J. Lelos, P. Rifes, S. B. Dunnett, S. Grealish, T. Perlmann, and M. Parmar. 2017. 'Predictive Markers Guide Differentiation to Improve Graft Outcome in Clinical Translation of hESC-Based Therapy for Parkinson's Disease', *Cell Stem Cell*, 20: 135-48.

Kordower, J. H., C. W. Olanow, H. B. Dodiya, Y. Chu, T. G. Beach, C. H. Adler, G. M. Halliday, and R. T. Bartus. 2013. 'Disease duration and the integrity of the nigrostriatal system in Parkinson's disease', *Brain*, 136: 2419-31.

Koyano, F., K. Okatsu, H. Kosako, Y. Tamura, E. Go, M. Kimura, Y. Kimura, H. Tsuchiya, H. Yoshihara, T. Hirokawa, T. Endo, E. A. Fon, J. F. Trempe, Y. Saeki, K. Tanaka, and N. Matsuda. 2014. 'Ubiquitin is phosphorylated by PINK1 to activate parkin', *Nature*, 510: 162-6.

Kriks, S., J. W. Shim, J. Piao, Y. M. Ganat, D. R. Wakeman, Z. Xie, L. Carrillo-Reid, G. Auyeung, C. Antonacci, A. Buch, L. Yang, M. F. Beal, D. J. Surmeier, J. H. Kordower, V. Tabar, and L. Studer. 2011. 'Dopamine neurons derived from human ES cells efficiently engraft in animal models of Parkinson's disease', *Nature*, 480: 547-51.

Kruger, R., W. Kuhn, T. Muller, D. Woitalla, M. Graeber, S. Kosel, H. Przuntek, J. T. Epplen, L. Schols, and O. Riess. 1998. 'Ala30Pro mutation in the gene encoding alpha-synuclein in Parkinson's disease', *Nat Genet*, 18: 106-8.

Kutty, R. K., G. Santostasi, J. Horng, and G. Krishna. 1991. 'MPTP-induced ATP depletion and cell death in neuroblastoma X glioma hybrid NG 108-15 cells: protection by glucose and sensitization by tetraphenylborate', *Toxicol Appl Pharmacol*, 107: 377-88.

Kuznetsova, A. Y., M. A. Huertas, A. S. Kuznetsov, C. A. Paladini, and C. C. Canavier. 2010. 'Regulation of Firing Frequency in a Computational Model of a Midbrain Dopaminergic Neuron', *Journal of computational neuroscience*, 28: 389-403.

Lammel, S., A. Hetzel, O. Hackel, I. Jones, B. Liss, and J. Roeper. 2008. 'Unique properties of mesoprefrontal neurons within a dual mesocorticolimbic dopamine system', *Neuron*, 57: 760-73.

Langston, J. W., P. Ballard, J. W. Tetrud, and I. Irwin. 1983. 'Chronic Parkinsonism in humans due to a product of meperidine-analog synthesis', *Science*, 219: 979-80.

Lees, A. J., J. Hardy, and T. Revesz. 2009. 'Parkinson's disease', *Lancet*, 373: 2055-66.

Lehnen, D., S. Barral, T. Cardoso, S. Grealish, A. Heuer, A. Smiyakin, A. Kirkeby, J. Kollet, H. Cremer, M. Parmar, A. Bosio, and S. Knöbel. 2017. 'IAP-Based Cell Sorting Results in Homogeneous Transplantable Dopaminergic Precursor Cells Derived from Human Pluripotent Stem Cells', *Stem Cell Reports*, 9: 1207-20.

LeWitt, P. A., A. R. Rezai, M. A. Leehey, S. G. Ojemann, A. W. Flaherty, E. N. Eskandar, S. K. Kostyk, K. Thomas, A. Sarkar, M. S. Siddiqui, S. B. Tatter, J. M. Schwalb, K. L. Poston, J. M. Henderson, R. M. Kurlan, I. H. Richard, L. Van Meter, C. V. Sapan, M. J. During, M. G. Kaplitt, and A. Feigin. 2011. 'AAV2-GAD gene therapy for advanced Parkinson's disease: a double-blind, sham-surgery controlled, randomised trial', *Lancet Neurol*, 10: 309-19.

Li, J., V. N. Uversky, and A. L. Fink. 2001. 'Effect of familial Parkinson's disease point mutations A30P and A53T on the structural properties, aggregation, and fibrillation of human alpha-synuclein', *Biochemistry*, 40: 11604-13.

Li, J., E. Englund, J. L. Holton, D. Soulet, P. Hagell, A. J. Lees, T. Lashley, N. P. Quinn, S. Rehncrona, A. Björklund, H. Widner, T. Revesz, O. Lindvall, and P. Brundin. 2008. 'Lewy bodies in grafted neurons in subjects with Parkinson's disease suggest host-to-graft disease propagation', *Nature Medicine*, 14: 501.

Lin, M. K., and M. J. Farrer. 2014. 'Genetics and genomics of Parkinson's disease', *Genome Med*, 6: 48.

Lisa Li, H., T. Nakano, and A. Hotta. 2013. 'Genetic correction using engineered nucleases for gene therapy applications', *Development, Growth & Differentiation*, 56: 63-77.

Liu, J., X. Wang, Y. Lu, C. Duan, G. Gao, L. Lu, and H. Yang. 2017. 'Pink1 interacts with α-synuclein and abrogates α-synuclein-induced neurotoxicity by activating autophagy', *Cell Death &Amp; Disease*, 8: e3056.

Lo Bianco, C., B. L. Schneider, N. Bauer, A. Sajadi, A. Brice, T. Iwatsubo, and P. Aebischer. 2004. 'Lentiviral vector delivery of parkin prevents dopaminergic degeneration in an α-synuclein rat model of Parkinson's disease', *Proceedings of the National Academy of Sciences of the United States of America*, 101: 17510-15.

Lobbestael, E., L. Civiero, T. De Wit, J. M. Taymans, E. Greggio, and V. Baekelandt. 2016. 'Pharmacological LRRK2 kinase inhibition induces LRRK2 protein destabilization and proteasomal degradation', *Scientific Reports*, 6: 33897.

Lopes, F. M., R. Schroder, M. L. da Frota, Jr., A. Zanotto-Filho, C. B. Muller, A. S. Pires, R. T. Meurer, G. D. Colpo, D. P. Gelain, F. Kapczinski, J. C. Moreira, C. Fernandes Mda, and F. Klamt. 2010. 'Comparison between proliferative and neuron-like SH-SY5Y cells as an in vitro model for Parkinson disease studies', *Brain Res*, 1337: 85-94.

Luo, J., M. G. Kaplitt, H. L. Fitzsimons, D. S. Zuzga, Y. Liu, M. L. Oshinsky, and M. J. During. 2002. 'Subthalamic GAD gene therapy in a Parkinson's disease rat model', *Science*, 298: 425-9.

Maitra, A., D. E. Arking, N. Shivapurkar, M. Ikeda, V. Stastny, K. Kassauei, G. Sui, D. J. Cutler, Y. Liu, S. N. Brimble, K. Noaksson, J. Hyllner, T. C. Schulz, X. Zeng, W. J. Freed, J. Crook, S. Abraham, A. Colman, P. Sartipy, S. Matsui, M. Carpenter, A. F. Gazdar, M. Rao, and A. Chakravarti. 2005. 'Genomic alterations in cultured human embryonic stem cells', *Nat Genet*, 37: 1099-103.

Makarova, K. S., D. H. Haft, R. Barrangou, S. J. Brouns, E. Charpentier, P. Horvath, S. Moineau, F. J. Mojica, Y. I. Wolf, A. F. Yakunin, J. van der Oost, and E. V. Koonin. 2011. 'Evolution and classification of the CRISPR-Cas systems', *Nat Rev Microbiol*, 9: 467-77.

Mali, P., K. M. Esvelt, and G. M. Church. 2013. 'Cas9 as a versatile tool for engineering biology', *Nature Methods*, 10: 957.

Martin, G. R. 1981. 'Isolation of a pluripotent cell line from early mouse embryos cultured in medium conditioned by teratocarcinoma stem cells', *Proceedings of the National Academy of Sciences*, 78: 7634.

Matsuda, W., T. Furuta, K. C. Nakamura, H. Hioki, F. Fujiyama, R. Arai, and T. Kaneko. 2009. 'Single nigrostriatal dopaminergic neurons form widely spread and highly dense axonal arborizations in the neostriatum', *J Neurosci*, 29: 444-53.

Mendivil-Perez, M., C. Velez-Pardo, and M. Jimenez-Del-Rio. 2016. 'Neuroprotective Effect of the LRRK2 Kinase Inhibitor PF-06447475 in Human Nerve-Like Differentiated Cells Exposed to Oxidative Stress Stimuli: Implications for Parkinson's Disease', *Neurochem Res*, 41: 2675-92.

Miyaoka, Y., A. H. Chan, L. M. Judge, J. Yoo, M. Huang, T. D. Nguyen, P. P. Lizarraga, P. So, and B. R. Conklin. 2014. 'Isolation of single-base genome-edited human iPS cells without antibiotic selection', *Nature Methods*, 11: 291.

Mojica, F. J., C. Diez-Villasenor, J. Garcia-Martinez, and E. Soria. 2005. 'Intervening sequences of regularly spaced prokaryotic repeats derive from foreign genetic elements', *J Mol Evol*, 60: 174-82.

Munoz-Sanjuan, I., and A. H. Brivanlou. 2002. 'Neural induction, the default model and embryonic stem cells', *Nat Rev Neurosci*, 3: 271-80.

Nalls, N. A., C. Blauwendraat, C. L. Vallerga, K. Heilbron, S. Bandres-Ciga, D. Chang, M. Tan, D. A. Kia, A. J. Noyce, A. Xue, J. Bras, E. Young, R. von Coelln, J. Simon-Sanchez, C. Schulte, M. Sharma, L. Krohn, L. Pihlstrom, A. Siitonen, H. Iwaki, H. Leonard, F. Faghri, J. R. Gibbs, D. G. Hernandez, S. W. Scholz, J. A. Botia, M. Martinez, J. Corvol, S. Lesage, J. Jankovic, L. M. Shulman, M. Sutherland, P. Tienari, K. Majamaa, M. Toft, A. Brice, J. Yang, Z. Gan-Orr, T. M. Gasser, P. M. Heutink, J. M. Shulman, N. A. Wood, D. A. Hinds, J. R. Hardy, H. R. Morris, J. M. Gratten, P. M. Visscher, R. R. Graham, and A B. Singleton. 2018. 'Parkinson's disease genetics: identifying novel risk loci, providing causal insights and improving estimates of heritable risk', *bioRxiv*.

Narendra, D., J. E. Walker, and R. Youle. 2012. 'Mitochondrial quality control mediated by PINK1 and Parkin: links to parkinsonism', *Cold Spring Harb Perspect Biol*, 4.

Nguyen, H., N., B. Byers, B. Cord, A. Shcheglovitov, J. Byrne, P. Gujar, K. Kee, B. Schüle, R. E Dolmetsch, W. Langston, T. D Palmer, and R. Reijo Pera. 2011. 'LRRK2 Mutant iPSC-Derived DA Neurons Demonstrate Increased Susceptibility to Oxidative Stress', *Cell Stem Cell*, 8: 267-80.

Norrman, K., Y. Fischer, B. Bonnamy, F. Wolfhagen Sand, P. Ravassard, and H. Semb. 2010. 'Quantitative Comparison of Constitutive Promoters in Human ES cells', *PLoS One*, 5: e12413.

Nussbaum, R. L., and C. E. Ellis 2003. 'Alzheimer's Disease and Parkinson's Disease', *New England Journal of Medicine*, 348: 1356-64.

Okun, M. S., H. H. Fernandez, R. L. Rodriguez, and K. D. Foote. 2007. 'Identifying candidates for deep brain stimulation in Parkinson's disease: the role of the primary care physician', *Geriatrics*, 62: 18-24.

Olanow, C. W., and S. B. Prusiner. 2009. 'Is Parkinson's disease a prion disorder?', *Proceedings of the National Academy of Sciences*, 106: 12571.

Olgiati, S., A. Thomas, M. Quadri, G. J. Breedveld, J. Graafland, H. Eussen, H. Douben, A. de Klein, Marco Onofrj, and V. Bonifati. 2015. 'Early-onset parkinsonism caused by alpha-synuclein gene triplication: Clinical and genetic findings in a novel family', *Parkinsonism & Related Disorders*, 21: 981-86.

Oliveira, L. M. A., L. J. Falomir-Lockhart, M. G. Botelho, K. H. Lin, P. Wales, J. C. Koch, E. Gerhardt, H. Taschenberger, T. F. Outeiro, P. Lingor, B. Schüle, D. J. Arndt-Jovin, and T. M. Jovin. 2015. 'Elevated α-synuclein caused by SNCA gene triplication impairs neuronal differentiation and maturation in Parkinson's patient-derived induced pluripotent stem cells', *Cell Death & Disease*, 6: e1994.

Ono, Y., T. Nakatani, Y. Sakamoto, E. Mizuhara, Y. Minaki, M. Kumai, A. Hamaguchi, M. Nishimura, Y. Inoue, H. Hayashi, J. Takahashi, and T. Imai. 2007. 'Differences in neurogenic potential in floor plate cells along an anteroposterior location: midbrain dopaminergic neurons originate from mesencephalic floor plate cells', *Development*, 134: 3213-25.

Pahlman, S., S. Mamaeva, G. Meyerson, M. E. Mattsson, C. Bjelfman, E. Ortoft, and U. Hammerling. 1990. 'Human neuroblastoma cells in culture: a model for neuronal cell differentiation and function', *Acta Physiol Scand Suppl*, 592: 25-37.

Pallone, J. A. 2007. 'Introduction to Parkinson's disease', *Dis Mon*, 53: 195-9.

Pardo, B., B. Gómez-González, and A. Aguilera. 2009. 'DNA Repair in Mammalian Cells', *Cellular and Molecular Life Sciences*, 66: 1039-56.

Parkinson, J. 1817. *An Essay on Shaking Palsy* (Whittingham and Rowland for Sherwood, Neely and Jones: London).

Pattaro, C., F. Marroni, A. Riegler, D. Mascalzoni, I. Pichler, C. B. Volpato, U. Dal Cero, A. De Grandi, C. Egger, A. Eisendle, C. Fuchsberger, M. Gögele, S. Pedrotti, G. K. Pinggera, S. A. Stefanov, F. D. Vogl, C. J. Wiedermann, T. Meitinger, and P. P. Pramstaller. 2007. 'The genetic study of three population microisolates in South Tyrol (MICROS): study design and epidemiological perspectives', *BMC Medical Genetics*, 8: 29.

Patten, I., and M. Placzek. 2000. 'The role of Sonic hedgehog in neural tube patterning', *Cell Mol Life Sci*, 57: 1695-708.

Perez, F. A., and R. D. Palmiter. 2005. 'Parkin-deficient mice are not a robust model of parkinsonism', *Proceedings of the National Academy of Sciences of the United States of America*, 102: 2174.

Polymeropoulos, M. H., C. Lavedan, E. Leroy, S. E. Ide, A. Dehejia, A. Dutra, B. Pike, H. Root, J. Rubenstein, R. Boyer, E. S. Stenroos, S. Chandrasekharappa, A. Athanassiadou, T. Papapetropoulos, W. G. Johnson, A. M. Lazzarini, R. C. Duvoisin, G. Di Iorio, L. I. Golbe, and R. L. Nussbaum. 1997. 'Mutation in the alpha-synuclein gene identified in families with Parkinson's disease', *Science*, 276.

Presgraves, S. P., T. Ahmed, S. Borwege, and J. N. Joyce. 2004. 'Terminally differentiated SH-SY5Y cells provide a model system for studying neuroprotective effects of dopamine agonists', *Neurotox Res*, 5: 579-98.

Ramsden, N., J. Perrin, Z. Ren, B. Dae Lee, N. Zinn, V. L. Dawson, D. Tam, M. Bova, M. Lang, G. Drewes, M. Bantscheff, F. Bard, T. M. Dawson, and C. Hopf. 2011. 'Chemoproteomics-Based Design of Potent LRRK2-Selective Lead Compounds That Attenuate Parkinson's Disease-Related Toxicity in Human Neurons', *ACS Chemical Biology*, 6: 1021-28.

Ran, F. A., P. D. Hsu, J. Wright, V. Agarwala, D. A. Scott, and F. Zhang. 2013a. 'Genome engineering using the CRISPR-Cas9 system', *Nat Protoc*, 8: 2281-308.

Ran, F. A., P. D. Hsu, J. Wright, V. Agarwala, D. A. Scott, and F. Zhang. 2013b. 'Genome engineering using the CRISPR-Cas9 system', *Nature Protocols*, 8: 2281.

Rao, S. S., L. A. Hofmann, and A. Shakil. 2006. 'Parkinson's disease: diagnosis and treatment', *Am Fam Physician*, 74: 2046-54.

Reyes, S., V. Cottam, D. Kirik, K. L. Double, and G. M. Halliday. 2013. 'Variability in neuronal expression of dopamine receptors and transporters in the substantia nigra', *Mov Disord*, 28: 1351-9.

Saez-Atienzar, S., L. Bonet-Ponce, J. R. Blesa, F. J. Romero, M. P. Murphy, J. Jordan, and M. F. Galindo. 2014. 'The LRRK2 inhibitor GSK2578215A induces protective autophagy in SH-SY5Y cells: involvement of Drp-1-mediated mitochondrial fission and mitochondrial-derived ROS signaling', *Cell Death &Amp; Disease*, 5: e1368.

San Filippo, J., P. Sung, and H. Klein. 2008. 'Mechanism of Eukaryotic Homologous Recombination', *Annual Review of Biochemistry*, 77: 229-57.

Sandor, C., P. Robertson, C. Lang, A. Heger, H. Booth, J. Vowles, L. Witty, R. Bowden, M. Hu, S. A. Cowley, R. Wade-Martins, and c. Webber. 2017. 'Transcriptomic profiling of purified patient-derived dopamine neurons identifies convergent perturbations and therapeutics for Parkinson's disease', *Hum Mol Genet*, 26: 552-66.

Sardi, S. P., J. Clarke, C. Viel, M. Chan, T. J. Tamsett, C. M. Treleaven, J. Bu, L. Sweet, M. A. Passini, J. C. Dodge, W. H. Yu, R. L. Sidman, S. H. Cheng, and L. S. Shihabuddin. 2013. 'Augmenting CNS

glucocerebrosidase activity as a therapeutic strategy for parkinsonism and other Gaucher-related synucleinopathies', *Proc Natl Acad Sci U S A*, 110: 3537-42.

Schüle, B., P., R. A. Reijo, L., J. William,. 2009. 'Can cellular models revolutionize drug discovery in Parkinson's disease?', *Biochimica et Biophysica Acta (BBA) - Molecular Basis of Disease*, 1792: 1043-51.

Seniuk, N. A., W. G. Tatton, and C. E. Greenwood. 1990. 'Dose-dependent destruction of the coeruleus-cortical and nigral-striatal projections by MPTP', *Brain Res*, 527: 7-20.

Sidransky, E., M.A. Nalls, J.O. Aasly, J. Aharon-Peretz, G. Annesi, E.R. Barbosa, A. Bar-Shira, D. Berg, J. Bras, A. Brice, C.-M. Chen, L.N. Clark, C. Condroyer, E.V. De Marco, A. Dürr, M.J. Eblan, S. Fahn, M.J. Farrer, H.-C. Fung, Z. Gan-Or, T. Gasser, R. Gershoni-Baruch, N. Giladi, A. Griffith, T. Gurevich, C. Januario, P. Kropp, A.E. Lang, G.-J. Lee-Chen, S. Lesage, K. Marder, I.F. Mata, A. Mirelman, J. Mitsui, I. Mizuta, G. Nicoletti, C. Oliveira, R. Ottman, A. Orr-Urtreger, L.V. Pereira, A. Quattrone, E. Rogaeva, A. Rolfs, H. Rosenbaum, R. Rozenberg, A. Samii, T. Samaddar, C. Schulte, M. Sharma, A. Singleton, M. Spitz, E.-K. Tan, N. Tayebi, T. Toda, A.R. Troiano, S. Tsuji, M. Wittstock, T.G. Wolfsberg, Y.-R. Wu, C.P. Zabetian, Y. Zhao, and S.G. Ziegler. 2009. 'Multicenter Analysis of Glucocerebrosidase Mutations in Parkinson's Disease', *New England Journal of Medicine*, 361: 1651-61.

Smith, Wanli W., Zhong Pei, Haibing Jiang, Valina L. Dawson, Ted M. Dawson, and Christopher A. Ross. 2006. 'Kinase activity of mutant LRRK2 mediates neuronal toxicity', *Nature Neuroscience*, 9: 1231.

Soldner, F., J. Laganiere, A. W. Cheng, D. Hockemeyer, Q. Gao, R. Alagappan, V. Khurana, L. I. Golbe, R. H. Myers, S. Lindquist, L. Zhang, D. Guschin, L. K. Fong, B. J. Vu, X. Meng, F. D. Urnov, E. J. Rebar, P. D. Gregory, H. S. Zhang, and R. Jaenisch. 2011. 'Generation of isogenic pluripotent stem cells differing exclusively at two early onset Parkinson point mutations', *Cell*, 146: 318-31.

Soldner, Frank, Josée Laganière, Albert W Cheng, Dirk Hockemeyer, Qing Gao, Raaji Alagappan, Vikram Khurana, Lawrence I Golbe, Richard H Myers, Susan Lindquist, Lei Zhang, Dmitry Guschin, Lauren K Fong, B. Joseph Vu, Xiangdong Meng, Fyodor D Urnov, Edward J Rebar, Philip D Gregory, H. Steve Zhang, and Rudolf Jaenisch. 2011. 'Generation of Isogenic Pluripotent Stem Cells Differing Exclusively at Two Early Onset Parkinson Point Mutations', *Cell*, 146: 318-31.

Spemann, H., and H. Mangold. 1924. 'über Induktion von Embryonalanlagen durch Implantation artfremder Organisatoren', *Archiv für mikroskopische Anatomie und Entwicklungsmechanik*, 101: 458-58.

Steinbeck, J. A, and L. Studer. 2015. 'Moving Stem Cells to the Clinic: Potential and Limitations for Brain Repair', *Neuron*, 86: 187-206.

Stern, M. B., A. Lang, and W. Poewe. 2012. 'Toward a redefinition of Parkinson's disease', *Mov Disord*, 27: 54-60.

Stirnemann, J., N. Belmatoug, F. Camou, C. Serratrice, R. Froissart, C. Caillaud, T. Levade, L. Astudillo, J. Serratrice, A. Brassier, C. Rose, T. Billette de Villemeur, and M. G. Berger. 2017. 'A Review of Gaucher Disease Pathophysiology, Clinical Presentation and Treatments', *International Journal of Molecular Sciences*, 18: 441.

Storch, A., A. Kaftan, K. Burkhardt, and J. Schwarz. 2000. '6-Hydroxydopamine toxicity towards human SH-SY5Y dopaminergic neuroblastoma cells: independent of mitochondrial energy metabolism', *J Neural Transm (Vienna)*, 107: 281-93.

Sulzer, D. 2007. 'Multiple hit hypotheses for dopamine neuron loss in Parkinson's disease', *Trends Neurosci*, 30: 244-50.

Swistowski, A., J. Peng, Q. Liu, P. Mali, M. S. Rao, L. Cheng, and X. Zeng. 2010. 'Efficient generation of functional dopaminergic neurons from human induced pluripotent stem cells under defined conditions', *Stem Cells*, 28: 1893-904.

Tada, T., and M. Sheng. 2006. 'Molecular mechanisms of dendritic spine morphogenesis', *Current Opinion in Neurobiology*, 16: 95-101.

Tagliati, M., C. Martin, and R. Alterman. 2010. 'Lack of Motor Symptoms Progression in Parkinson's Disease Patients With Long-Term Bilateral Subthalamic Deep Brain Stimulation', *International Journal of Neuroscience*, 120: 717-23.

Takahashi, K., and S. Yamanaka. 2006. 'Induction of Pluripotent Stem Cells from Mouse Embryonic and Adult Fibroblast Cultures by Defined Factors', *Cell*, 126: 663-76.

Taymans, J. M., and E. Greggio. 2016. 'LRRK2 Kinase Inhibition as a Therapeutic Strategy for Parkinson's Disease, Where Do We Stand?', *Curr Neuropharmacol*, 14: 214-25.

Thomson, J. A., J. Itskovitz-Eldor, S. S. Shapiro, M. A. Waknitz, J. J. Swiergiel, V. S. Marshall, and J. M. Jones. 1998. 'Embryonic Stem Cell Lines Derived from Human Blastocysts', *Science*, 282: 1145.

Trinh, J., and M. Farrer. 2013. 'Advances in the genetics of Parkinson disease', *Nat Rev Neurol*, 9: 445-54.

Volta, M., A. J. Milnerwood, and M. J. Farrer. 2015. 'Insights from late-onset familial parkinsonism on the pathogenesis of idiopathic Parkinson's disease', *Lancet Neurol*, 14: 1054-64.

Wang, Y., F. Wang, R. Wang, P. Zhao, and Q. Xia. 2015. '2A self-cleaving peptide-based multi-gene expression system in the silkworm Bombyx mori', *Scientific Reports*, 5: 16273.

Warren Olanow, C., R. T. Bartus, T. L. Baumann, S. Factor, N. Boulis, M. Stacy, D. A. Turner, W. Marks, P. Larson, P. A. Starr, J. Jankovic, R. Simpson, R. Watts, B. Guthrie, K. Poston, J. M. Henderson, M. Stern, G. Baltuch, C. G. Goetz, C. Herzog, J. H. Kordower, R. Alterman, A. M. Lozano, and A. E. Lang. 2015. 'Gene delivery of neurturin to putamen and substantia nigra in Parkinson disease: A double-blind, randomized, controlled trial', *Ann Neurol*, 78: 248-57.

West, A. B., D. J. Moore, S. Biskup, A. Bugayenko, W. W. Smith, C. A. Ross, V. L. Dawson, and T. M. Dawson. 2005. 'Parkinson's disease-associated mutations in leucine-rich repeat kinase 2 augment kinase activity', *Proceedings of the National Academy of Sciences of the United States of America*, 102: 16842.

Wilson, S. I., A. Rydstrom, T. Trimborn, K. Willert, R. Nusse, T. M. Jessell, and T. Edlund. 2001. 'The status of Wnt signalling regulates neural and epidermal fates in the chick embryo', *Nature*, 411: 325-30.

Woodard, C. M., B. A. Campos, S. H. Kuo, M. J. Nirenberg, M. W. Nestor, M. Zimmer, E. V. Mosharov, D. Sulzer, H. Zhou, D. Paull, L. Clark, E. E. Schadt, S. P. Sardi, L. Rubin, K. Eggan, M. Brock, S. Lipnick, M. Rao, S. Chang, A. Li, and S. A. Noggle. 2014. 'iPSC-derived dopamine neurons reveal differences between monozygotic twins discordant for Parkinson's disease', *Cell Rep*, 9: 1173-82.

Xia, N., F. Fang, P. Zhang, J. Cui, C. Tep-Cullison, T. Hamerley, H. J. Lee, T. Palmer, B. Bothner, J. H. Lee, and R. R. Pera. 2017. 'A Knockin Reporter Allows Purification and Characterization of mDA Neurons from Heterogeneous Populations', *Cell Rep*, 18: 2533-46.

Zhang, Jian-Ping, Xiao-Lan Li, Guo-Hua Li, Wanqiu Chen, Cameron Arakaki, Gary D. Botimer, David Baylink, Lu Zhang, Wei Wen, Ya-Wen Fu, Jing Xu, Noah Chun, Weiping Yuan, Tao Cheng, and Xiao-Bing Zhang. 2017. 'Efficient precise knockin with a double cut HDR donor after CRISPR/Cas9-mediated double-stranded DNA cleavage', *Genome Biology*, 18: 35.

Zhang, P., N. Xia, and R. A. Reijo Pera. 2014. 'Directed dopaminergic neuron differentiation from human pluripotent stem cells', *J Vis Exp*: 51737.

Zimprich, A., S. Biskup, P. Leitner, P. Lichtner, M. Farrer, S. Lincoln, J. Kachergus, M. Hulihan, R. J. Uitti, D. B. Calne, A. J. Stoessl, R. F. Pfeiffer, N. Patenge, I. Carballo Carbajal, P. Vieregge, F. Asmus, B. Müller-Myhsok, D. W. Dickson, T. Meitinger, T. M. Strom, Z. K. Wszolek, and T. Gasser. 2004. 'Mutations in LRRK2 Cause Autosomal-Dominant Parkinsonism with Pleomorphic Pathology', *Neuron*, 44: 601-07.

7 Appendix

7.1 List of abbreviations

(v/v)	volume per volume
(w/v)	weight per volume
°C	degree Celsius
µg	microgram
µl	microliter
µM	micromolar
A	Adenine/ Ampere
α	Anti or alpha
AF	Alexa Fluor
BDNF	brain derived neurotrophic factor
bFGF	basic fibroblast growth factor
BMP	Bone Morphogenetic Protein
bp	base pairs
β	beta
C	Cytosine
CaCl2	Calcium chloride
cAMP	cyclic adenosine monophosphate
Cas9	Caspase 9
CRISPR	Clustered Regularly Interspaced Short Palindromic Repeats
DA	Dopamine/ dopaminergic
DMEM	Dulbecco's Modified Eagle Medium
DMSO	Dimethyl sulfoxide
DNA	Deoxyribonucleic acid
dNTPs	deoxynucleoside triphosphate
ds	double strand
DSB	double strand break
dUTP	deoxyuridine triphosphate
E. coli	Escherichia coli
EDTA	Ethylenediaminetetraacetic acid
eGFP	enhanced green fluorescent protein
EGTA	ethylene glycol tetraacetic acid
ELISA	enzyme-linked immunosorbent assay
FBS	fetal bovine serum
FGF	Fibroblast growth factor
FGF 8b	Fibroblast growth factor 8b
FGF8	Fibroblast growth factor 8

Fig	Figure
FISH	fluorescence *in situ* hybridization
fw	forward
G	Guanine
g	gram
GABA	gamma-Aminobutyric acid
GDNF	glial derived growth factor
GFP	Green fluorescent protein
GIRK2	G protein-activated inward rectifier potassium channel 2
h	hour
HDR	homology directed repair
HEPES	(4-(2-hydroxyethyl)-1-piperazineethanesulfonic acid
hESCs	human embryonic stem cells
hiPSCs	human induced pluripotent stem cells
hPSCs	human pluripotent stem cells
HRP	Horseradish peroxidase
Hz	Hertz
ICC	Immunocytochemistry
Indel	Insertion and deletion
KCl	potassium chloride
kg	kilogram
KO-DMEM	Knock-Out DMEM
KOSR	Knock out serum replacement
l	Litre
λ	Lambda
LB	Luria Broth
M	Molar
MCS	multicloning site
mDA	midbrain dopaminergic
MEM	modified Eagle's Medium
mEPSC	miniature excitatory post synaptic current
mg	milligram
Mg-ATP	Magnesium adenosine triphosphate
$MgCl_2$	Magnesium Chloride
min	Minute
ml	Millilitre
mM	millimolar
mmol	millimole
mol	Mole
Na2	disodium
NaCl	Sodium chloride

NaDoc	Sodium Deoxycholate
Na-GTP	Sodium guanosine triphosphate
NEAA	non-essential amino acids
ng	nanogram
nl	nanolitre
nM	nanomolar
nmol	nanomole
nt	nucleotide
ON	overnight
pA	Picoampere
PAM	protospacer adjacent motifs
PBS	Phosphate-Buffered Saline
PCR	Polymerase chain reaction
Pen/Strep	Penicillin/Streptomycin
PFA	Paraformaldehyde
pg	picogram
RNA	Ribonucleic acid
ROCK-Inhibitor	Rho associated protein kinase inhibitor
rv	reverse
SAG	Smoothened agonist
SD	standard deviation
SDS	Sodium dodecyl sulphate
sec	second
SEM	standard error of the mean
sgRNA	single guide ribonucleic acid
ss	single strand
SSC	Saline Sodium Citrate
T	Thymine
Tab	Table
TBS	Tris-Buffered Saline
TBS-T	Tris-Buffered Saline Tween
TE	Tris-EDTA
TGF-β3	Tumor growth factor beta 3
TH	Tyrosine Hydroxylase
Tris	tris(hydroxymethyl)aminomethane
Tris HCl	Tris hydrochloride
U	Uracile
UV	ultraviolet
w/	with
w/o	without
WT	wild type

7.2 List of reagents

Product name	cat no.	supplier
2-Mercaptoethanol	M3701	Sigma Aldrich®
2-Mercaptoethanol (50 mM)	31350010	Gibco™
AatII	R0117S	New England Biolabs®
Acetic Acid	45726-1L	Sigma Aldrich®
Acetonitrile, HPLC grade, ≥99.93%	270717	Sigma Aldrich®
Agarose Certified™ Molecular Biology	1613101	BioRad
Agarose, low gelling temperature bioreagent	A9414-25G	Sigma Aldrich®
Alexa Fluor®488 donkey anti-rat	A24876	Invitrogen™ Molecular Probes™
Alexa Fluor®488 goat anti-mouse IgG3	A24877	Invitrogen™ Molecular Probes™
Alexa Fluor®555 donkey anti-rabbit	A24869	Invitrogen™ Molecular Probes™
Alexa Fluor®555 goat anti-mouse IgM	A24871	Invitrogen™ Molecular Probes™
Alexa Fluor™ 488 Tyramide Reagent	B40953	invitrogen™
Alkaline Phosphatase Staining Kit II	00-0055	StemGent®
All-in-One™ qPCR Mix	QP004	GeneCopoeia™
Amersham CyDye Value Packs (Mono-Reactive NHS Ester) Cy3 NHS Ester	PA13101	GE Healthcare Life Sciences
Aminoallyl-dUTP sodium salt	A0410	Sigma Aldrich®
Ampicillin sodium salt	69-52-3	Sigma Aldrich®
AmpliTaq Gold™ DNA Polymerase with Buffer II and MgCl2	N8080241	Applied Biosystems
Anti-Kir3.2 (GIRK2) Antibody	APC-006	alomone labs
Anti-MAP2 antibody	ab5392	abcam
Anti-mCherry antibody	ab167453	abcam
Anti-Tyrosine Hydroxylase Antibody, clone LNC1	MAB318	Millipore
B-27™ Supplement (50X), serum free	17504001	Gibco™
BbsI	R0539S	New England Biolabs®
Betaine Solution	B0300	Sigma Aldrich®
Blotting Paper Whatman	10427804	GE Healthcare Life Sciences
Certified molecular biology Agarose	1613101	BioRad
CF-1 MEF 2M IRR, Gibco CF1 Mouse Embryonic Fibroblasts, Irradiated 2M,GSC-6201G	A34180	GlobalStem
Clarity Western ECL Substrate	1705061	BioRad
cOmplete™ Protease Inhibitor Cocktail	04693116001 Roche	Sigma Aldrich®
Corning® Matrigel® Growth Factor Reduced (GFR) Basement Membrane Matrix, *LDEV-free	354230	Corning®
Corning® Matrigel® hESC-Qualified Matrix, *LDEV-free	354277	Corning®
COT Human DNA from human placenta DNA, enriched for repetitive sequences	11581074001	Roche
CutSmart® Buffer	B7204S	New England Biolabs®

D-(+)Glucose	47829	Sigma Aldrich®
ddPCR™ Copy Number Assay: mcherry FAM	dCNS507694046	BioRad
ddPCR™ Copy Number Assay: RPP30, Human, HEX	dHsaCP2500350	BioRad
ddPCR™ Supermix for Probes (No dUTP)	1863025	BioRad
Deoxynucleoside Triphosphate Set	11969064001	Sigma Aldrich®
Deoxyribonuclease I from bovine pancreas	D4263	Sigma Aldrich®
Dibutyryl-cAMP PKA activator	BML-CN125-0100	Enzo Life Scienes©
Dimethyl sulfoxide	D2650	Sigma Aldrich®
DMEM, high glucose, GlutaMAX™	31966021	Gibco™
DMEM/F-12, GlutaMAX™ Supplement	31331028	Gibco™
DNA Polymerase I (10 U/µL)	EP0041	ThermoFisher Scientific™
DNase I recombinant	4536282001	Sigma Aldrich®
Donkey Anti-Chicken IgY, Alexa Fluor® 647 Conjugate, Species Adsorbed: H, M, R, B, Gt, Gp, Eq, Rb, Sh, Ht Antibody	AP194SA6	Millipore
Donkey anti-Mouse IgG (H+L) Highly Cross-Adsorbed Secondary Antibody, Alexa Fluor 488	A-21202	Invitrogen™
Donkey anti-Mouse IgG (H+L) Highly Cross-Adsorbed Secondary Antibody, Alexa Fluor 555	A-31570	Invitrogen™
Donkey anti-Rabbit IgG (H+L) Highly Cross-Adsorbed Secondary Antibody, Alexa Fluor 488	A-21206	Invitrogen™
Donkey anti-Rabbit IgG (H+L) Highly Cross-Adsorbed Secondary Antibody, Alexa Fluor 555	A-31572	Invitrogen™
Donkey serum 10 ml - (0.01% thimerosal)	D9663	Sigma-Aldrich
Dopamine ELISA kit	BA-E-5300	ImmuSmol
Droplet Generation Oil for Probes	1863005	BioRad
DROPLET READER OIL	1863004	BioRad
Dry Milk, Blotting-Grade Blocker	1706404	BioRad
EcoRI HF ®	R3101S	New England Biolabs®
EcoRV HF ®	R3195S	New England Biolabs®
EmbryoMax® 0.1% Gelatin in Sterile Water	ES-006-B	Millipore
Ethanol absolute, Baker analyzed	80.252.500	Avantar J.T.Baker
Fetal Bovine Serum, embryonic stem cell-qualified, US origin	16141079	Gibco™
FETAL BOVINE SERUM, USA ORIGIN, STERILE	F2442-500ML	Sigma Aldrich®
Fibroblast Growth Factor basic Protein, Human recombinant	GF003	Millipore
Fluorescence Mounting Medium (Dako Omnis)	S3023	Dako
Formamide ≥99.5% (GC), BioReagent, for molecular biology	F9037	Sigma Aldrich®
GelStar™ Nucleic Acid Gel Stain 10,000X	LO50535	Lonza
GFP Tag Polyclonal Antibody	A-11122	Invitrogen™
GlutaMAX™ Supplement I 100X	35050061	Gibco™

HEK 293T cells stably expressing Cas9		
Horse Serum, heat inactivated, New Zealand origin	26050070	Gibco™
Human BDNF, research grade	130-096-285	Miltenyi Biotec
Human FGF-8b, research grade	130-095-731	Miltenyi Biotec
Human GDNF, research grade	130-096-290	Miltenyi Biotec
Human HNF-3 beta /FoxA2 Antibody	AF2400	R&D Systems
Human TGF-β3, research grade	130-094-007	Miltenyi Biotec
illustra GenomiPhi V2 DNA Amplification Kits	25660032	GE Healthcare Life Sciences
Immun-Blot® PVDF Membrane	1620177	BioRad
KaryoMAX™ Colcemid™ Solution in HBSS	15210040	Gibco™
KnockOut™ DMEM	10829018	Gibco™
KnockOut™ Serum Replacement	10828028	Gibco™
Laminin from mouse Engelbreth-Holm-Swarm (EHS) sarcoma	11243217001	Sigma Aldrich®
L-Ascorbic acid	A7506-25G	Sigma Aldrich®
LB Agar, Miller, microbiologically tested	L3027	Fluka
Lipofectamine™ LTX Reagent with PLUS™ Reagent	15338100	ThermoFisher Scientific™
LIVE/DEAD™ Fixable Near-IR Dead Cell Stain Kit, for 633 or 635 nm excitation	L10119	invitrogen™
LMX1A Polyclonal Antibody	PA5-34470	invitrogen™
Mastercycler® pro	6321000515	Eppendorf
MAX Efficiency Stbl2 ™ Competent Cells	10268019	Invitrogen™
MEM Non-Essential Amino Acids Solution (100X)	11140035	Gibco™
Methanol Puriss. p.a., ACS Reagent, Reag. ISO, Reag. Ph. Eur., ≥99.8% (GC)	32213-4X2.5L	Honeywell Research Chemicals
MgCl2 (magnesium chloride) (25 mM)	R0971	ThermoFisher Scientific™
Microscope slides Superforst 76x76mm	100205M	ThermoFisher Scientific™
Monoclonal Anti-β-Actin antibody produced in mouse, clone AC-74, purified immunoglobulin, buffered aqueous solution	A2228	Sigma Aldrich®
Mouse Anti-Rabbit IgG Antibody, HRP conjugate, Species Adsorbed	AP188P	Millipore
mouse anti-SSEA4	A24866	Invitrogen™ Molecular Probes™
mouse anti-TRA-1-60	A24868	Invitrogen™ Molecular Probes™
N-2 Supplement (100X)	17502048	Gibco™
NEBuffer™ 2.1	B7202S	New England Biolabs®
Neurobasal® Medium	21103049	Gibco™
NotI HF ®	R3189S	New England Biolabs®
NP-40 IGEPAL® CA-630	I8896-100ML	Sigma Aldrich®
NucBlue® Fixed Cell ReadyProbes® Reagent	R37606	Invitrogen™
NucleoSpin® Plasmid	740.588.250	Macherey-Nagel
NuPAGE® LDS Sample Buffer (4x)	NP0008	Invitrogen™

NuPAGE™ Antioxidant	NP0005	Invitrogen™
NuPAGE™ Bis-Tris Welcome Pack, 4-12%, 10-well	NP032A	Invitrogen™
NuPAGE™ MOPS SDS Running Buffer (20X)	NP0001	Invitrogen™
NuPAGE™ Sample Reducing Agent (10X)	NP0004	Invitrogen™
NuPAGE™ Transfer Buffer	NP0006	Invitrogen™
One Shot™ Stbl3™ Chemically Competent *E. coli*	C737303	Invitrogen™
One Shot™ TOP10 Chemically Competent *E. coli*	C404003	Invitrogen™
Opti-MEM® I Reduced Serum Medium	31985047	Invitrogen™
Paraformaldehyde	P6148-500G	Sigma Aldrich®
PBS, pH 7.4	10010015	Gibco™
pcDNA3-EGFP (Plasmid #13031)	(Plasmid #13031)	Addgene
Penicillin-Streptomycin (10,000 U/mL)	15140122	Gibco™
PhosSTOP™	PHOSS-RO Roche	Sigma Aldrich®
Pierce™ BCA Protein Assay Kit (Thermo Scientific)	23225	ThermoFisher Scientific™
Ponceau S	P3504	Sigma Aldrich®
Potassium chloride ≥99.0%	P9541-500G	Sigma Aldrich®
Precision Plus Protein™ All Blue Prestained Protein Standards	1610373	BioRad
PrimePCR™ ddPCR™ Expression Probe Assay: KCNJ6, Human, HEX	dHsaCPE5047523	BioRad
PrimePCR™ ddPCR™ Expression Probe Assay: TH, Human, HEX	dHsaCPE5192176	BioRad
Proteinase K, from Tritirachium album	P6556-10MG	Sigma Aldrich®
PSC 4-Marker Immunocytochemistry Kit	A24881	Invitrogen™ Molecular Probes™
PSC Dopaminergic Neuron Differentiation Kit	A3147701	Gibco™
PSD95 (7E3) Mouse mAb	#36233	Cell Signalin Technology®
pX459V2.0-eSpCas9(1.1)	108292	Addgene
PureLink™ HiPure Plasmid Midiprep Kit	K210004	invitrogen™
Puromycin dihydrochloride	sc-108071A	Santa Cruz Biotechnology®
Q5® High-Fidelity 2X Master Mix	M0492S	New England Biolabs®
QIAamp ® DNA Blood Mini Kit	51104	Qiagen
QIAquick ® Gel Extraction Kit	28706	Qiagen
QIAquick ® PCR Purification Kit	28104	Qiagen
QIAquick ® PCR Purification Kit	28106	Qiagen
Quant-iT™ PicoGreen™ dsDNA Assay Kit	P11496	invitrogen™
Rabbit Anti-Mouse IgG Antibody, HRP conjugate	AP160P	Millipore
rabbit anti-OCT4	A24867	Invitrogen™ Molecular Probes™
Rabbit Ig (Whole Ab), biotinylated	RPN1004-2ML	GE Healthcare Life Sciences
rat anti-SOX2	A24759	Invitrogen™ Molecular Probes™
RNeasy® Mini Kit	74104	Qiagen
Round cover glasses, 14mm, CB00140RAC2	MENZCB00140RAC20	ThermoFisher Scientific™

S.O.C. Medium	15544034	invitrogen™
Smoothened Agonist, SAG	566660-1MG	Calbiochem®
Sodium chloride	479689	Carlo Erba
Sodium deoxycholate ≥97% (titration) 100 g (NaDoc)	D6750-100G	Sigma Aldrich®
Sodium dodecyl sulphate BioUltra, ≥99.0% (GC) 500 g	71725-500G	Sigma Aldrich®
SpeI	R0133S	New England Biolabs®
StemMACS™ iPS-Brew XF	130-104-368	Miltenyi Biotec
StemMACS™ CHIR99021	130-103-926	Miltenyi Biotec
StemMACS™ DAPT	130-110-489	Miltenyi Biotec
StemMACS™ LDN-193189	130-103-925	Miltenyi Biotec
StemMACS™ Purmorphamine	130-104-465	Miltenyi Biotec
StemMACS™ SB431542	130-105-336	Miltenyi Biotec
StemMACS™ Y27632	130-104-169	Miltenyi Biotec
StemPro® Accutase® Cell Dissociation Reagent	A1110501	Gibco™
Streptavidin-Biotinylated Horseradish Peroxidase Complex	RPN1051-2ML	GE Healthcare Life Sciences
SuperScript™ VILO™ cDNA Synthesis Kit	11754050	invitrogen™
Synapsin-1 (D12G5) XP® Rabbit mAb	#5297	Cell Signalin Technology®
T4 DNA Ligase	M0202S	New England Biolabs®
T4 DNA Ligase Reaction Buffer	B0202S	New England Biolabs®
T7 Endonuclease I	BM0302L	New England Biolabs®
TaqMan® Gene Expression Assay, eGFP, FAM	Mr04097229_mr	ThermoFisher Scientific™
Tau antibody	GTX116044	GeneTex
Tetracycline ≥98.0% (NT)	87128	Sigma Aldrich®
Tris Trizma® base	T6066	Sigma Aldrich®
Triton™ X-100	T8787	Sigma Aldrich®
TrypLE Express	12604013	ThermoFisher Scientific™
Trypsin-EDTA (0.05%), phenol red	25300054	Gibco™
UltraPure™ 0.5M EDTA, pH 8.0	15575020	invitrogen™
UltraPure™ Salmon Sperm DNA Solution	15632011	invitrogen™
VECTASHIELD Antifade Mounting Medium with DAPI	H-1200	Vector laboratories
XbaI	R0145S	New England Biolabs®
XhoI	R0146S	New England Biolabs®
Zero Blunt™ TOPO™ PCR Cloning Kit	450031	invitrogen™

7.3 List of machinery and apparatus

Product Name	Supplier
Mastercycler® pro S 230 V/50 – 60 Hz	Eppendorf
ChemiDoc™ Imaging Systems	BioRad
Neon™ Transfection System	invitrogen™
CFX96 Touch™ Real-Time PCR Detection System	BioRad
Confocal laser scanning microscope Leica TCS SP8	Leica
ZEISS Axio Vert.A1 – Inverted Microscope for Advanced Routine	Zeiss
Eppendorf Centrifuge 5418/R	Eppendorf
Nanodrop 1000 Spectrophotometer	ThermoScientific
DG8™ cartridges for QX100/QX200 Droplet Generator	BioRad
PCR Plate Heat Seal, foil, pierceable	BioRad
DG8™ Gaskets for QX200™/QX100™ Droplet Generator	BioRad
PX1™ PCR Plate Sealer	BioRad
QX200™ Droplet Generator	BioRad
QX200™ Droplet Reader	BioRad
Eppendorf™96-Well twin.tec™ PCR Plates	Fisher Scientific
Microscope slide, Menzel 76x26mm	ThermoScientific
SpectraMax 190 Microplate Reader	Molecular Devices
Victor X3	Perkin Elmer
Mini-PROTEAN® Tetra Cell	BioRad
XCell SureLock® Mini-Cell Electrophoresis Cell	invitrogen™
Eclipse-Ti microscope	Nikon
MultiClamp 700B amplifier	Molecular devices
Sutter P-1000 puller	Sutter Instruments
EnVision Multimode Plate Reader	Perkin Elmer

7.4 List of primers

Code	Name/Purpose	Sequence 5' to 3'
CU 23	hGIRK sg1 F	CACCGCCAAAGTTTAGTGCCCTAGC
CU 24	hGIRK sg1 R	AAACGCTAGGGCACTAAACTTTGGC
CU 25	hGIRK sg2 F	CACCGCCAGCTAGGGCACTAAACTT
CU 26	hGIRK sg2 R	AAACAAGTTTAGTGCCCTAGCTGGC
CU 27	hGIRK sg3 F	CACCGCAAAGTTTAGTGCCCTAGCT
CU 28	hGIRK sg3 R	AAACAGCTAGGGCACTAAACTTTGC
CU 29	hGIRK sg4 F	CACCGGAGAAGGGTTTGCCCAGCTA
CU 30	hGIRK sg4 R	AAACTAGCTGGGCAAACCCTTCTCC
CU 31	hGIRK sg5 F	CACCGAGAGAAGGGTTTGCCCAGCT
CU 32	hGIRK sg5 R	AAACAGCTGGGCAAACCCTTCTCTC
CU 33	hTH sg1 F	CACCGGCCCATGCGCTGAGTGCCAT
CU 34	hTH sg1 R	AAACATGGCACTCAGCGCATGGGCC
CU 35	hTH sg2 F	CACCGTGCGCTGAGTGCCATTGGCT
CU 36	hTH sg2 R	AAACAGCCAATGGCACTCAGCGCAC
CU 37	hTH sg3 F	CACCGAGTGCCATTGGCTAGGTGCA
CU 38	hTH sg3 R	AAACTGCACCTAGCCAATGGCACTC
CU 39	hTH sg4 F	CACCGGACGCCGTGCACCTAGCCAA
CU 40	hTH sg4 R	AAACTTGGCTAGGTGCACGGCGTCC
RF34	in U6 promoter	GGCCTATTTCCCATGATTCC
CU 41	hTH left HA F	GCAGACCTACAGGACTGGGG
CU 42	hTH right HA R	GGGGGCCACACTGAGGTTCC
CU 43	Left HA F	GCCGATATCGGCCTCTAGCTTAAAAGCAGCCTAAG
CU 44	Right HA R	CTAGCTAGCGAGACACAAACAAAGGCCATGCAC
CU 45	Right HA F GIRK	CCTGGAGAATGAATCCAAAGTTTCTAGACCCCTCGAGTGCCCTAGCTGGGCAAACCCTTCTC
CU 46	Left HA R GIRK	GAGAAGGGTTTGCCCAGCTAGGGCACTCGAGGGGTCTAGAAACTTTGGATTCATTCTCCAGG
CU 47	hTH right HA F	CCTTGCCCATGCGCTGAGTGCCATTGGCTCTAGACCCCTCGAGGTGCACGGCGTCCCTGAGGGCCCTTCC
CU 48	hTH left HA R	GGAAGGGCCCTCAGGGACGCCGTGCACCTCGAGGGGTCTAGAGCCAATGGCACTCAGCGCATGGGCAAGG
CU 59	TH Surveyor F	GGCTTAGGGATATGGTCAAGG
CU 60	TH Surveyor R	TGTTGGGTGCTCTCTCTGGA
CU 61	GIRK Surveyor F	GGCCAGGACTCTCTCATTGT
CU 62	GIRK Surveyor R	TTGCCATCTACCAGACCTCTCA
	SOX-2 fw	GGGAAATGGGAGGGGTGCAAAAGAGG
	SOX-2 rev	TTGCGTGAGTGTGGATGGGATTGGTG
	OCT3/4 fw	GACAGGGGGAGGGGAGGAGCTAGG
	OCT3/4 rev	CTTCCCTCCAACCAGTTGCCCCAAAC
	NANOG fw	TGCAAGAACTCTCCAACATCCT
	NANOG rev	ATTGCTATTCTTCGGCCAGTT
	ACTB fw	ATAGCACAGCCTGGATAGCAACGTAC
	ACTB rv	CACCTTCTACAATGAGCTGCGTGTG

	FBXO15 fw	GCCAGGAGGTCTTCGCTGTA
	FBXO 15 rv	AATGCACGGCTAGGGTCAAA
	EBNA-1 fw	ATCAGGGCCAAGACATAGAGATG
	EBNA-1 rev	GCCAATGCAACTTGGACGTT
CU 55	left FW Primer	AGGAGCTATGCCTCACGCAT
CU 60	TH Surveyor R	TGTTGGGTGCTCTCTCTGGA
CU 17	T2A Fw	AGGGCAGAGGAAGTCTTCTA
CU 58	Right RV Primer	ACCAGGGGAGGTTGGGAA
CU 71	mcherry Fw	AGGATAACATGGCCATCTCAA
CU 77	Screen 2 Bleo Fw	GAGGGCCCCTTAATATAACTTC
CU 79	Screen 3 m cherry Fw	GCATGGACGAGCTGTACAAG
CU 83	Screen 2/3 TH gen Rv	AAATCCAGCCCCCATCCTG
GIRK2 Long Probe 1	GIRK2 Long Probe 1 fw	GTGCAAATTCAGGTGGGTG
GIRK2 Long Probe 1	GIRK2 Long Probe 1 rv	CCGCATGTTAGAAGACTTCCT
GIRK2 Long Probe 1	GIRK2 Long Probe 1 FAM probe	CACTGATCTGTGGCCTCTAGCT
GIRK2 Long Probe 2	GIRK2 Long Probe 2 fw	GTGCAAATTCAGGTGGGTG
GIRK2 Long Probe 2	GIRK2 Long Probe 2 rv	CCGCATGTTAGAAGACTTCCT
GIRK2 Long Probe 2	GIRK2 Long Probe 2 FAM probe	AAGCAGCCTAAGTGTAGTTCCAT
TH Long Probe 1	TH Long Probe 1 fw	GGACACCATCCGTGAGAA
TH Long Probe 1	TH Long Probe 1 rv	CCGCATGTTAGAAGACTTCCT
TH Long Probe 1	TH Long Probe 1FAM probe	AGGGGCAGACCTACAGGAC
TH Long Probe 2	TH Long Probe 2 fw	GGACACCATCCGTGAGAA
TH Long Probe 2	TH Long Probe 2 rv	CCGCATGTTAGAAGACTTCCT
TH Long Probe 2	TH Long Probe 2 FAM probe	TCAAGGCCAGTCTTGGAGGT
CU 85	THgenom FISH Fw	CTAGACTAGTTGGCTGCCCGCAGGAAGGA
CU 86	THgenom FISH Rv	TCCACAGGACGTCCTCACAA
CU 87	GIRK FISH Fw	GGACTAGTGCTAATTTTGTAAGGTCTGTA
CU 88	GIRK FISH Rv	GATATCACAGATCAGTGTTACCCT
CU 103	FOXA2 Fw	CCGTTCTCCATCAACAACCT
CU 104	FOXA2 Rv	GGGGTAGTGCATCACCTGTT
CU 105	LMX1A Fw	CGCATCGTTTCTTCTCCTCT
CU 106	LMX1A Rv	CAGACAGACTTGGGGCTCAC

CU 149	TH Fw	GGAAGGCCGTGCTAAACCT
CU 150	TH Rv	GGATTTTGGCTTCAAACGTCTC
CU 155	GIRK2 Fw	GACCTGAAGTGGAGATTCAACC
CU 156	GIRK2 Rv	TGTATGCGATCAACCACCAGA

Acknowledgments

My deepest and sincerest gratitude goes to Corrado Corti. Without him, I would not be writing these acknowledgments now. He believed in me from the first day and kept supporting me throughout what was a very tough road to success. He kept spirits high, when I lost them and kept faith with me. He was the best teacher, mentor and colleague I could have ever wished for during this important part of my scientific education. I feel deeply indebted to him.

I was very happy to have my fellow PhD student Julia by my side for the last years. Julia, with you, working was always fun and we developed a valuable friendship. We learned together, which made it easier and I value your opinion very much.

I thank Mattia Volta and Dayne Beccano-Kelly for sharing their immense knowledge with me and helping me to grow as a scientist. The conversations with them, whether scientific or personal, have impressed me and shaped my way of reasoning.

The period spent in Oxford allowed my research to make a major step forward and helped me in my development as a scientist to become more independent, more critical and open minded. Therefore, I express my gratitude to Dr. Sally Cowley for a warm welcome into her group and teaching me.

I thank Prof. Michele Zoli for supervising my PhD and advising my work.

Ginetta Collo gave very important and useful advice on my cell culture work, for which I thank her very much.

Mein persönlichster Dank geht an meinen Partner Markus. Ich weiß, dass es für dich schwierig ist zu verstehen, was ich tue und warum überhaupt und trotzdem hast du mich immer unterstützt. Du bist der wichtigste Mensch in meinem Leben. Jeden Tag nach Hause zu kommen und dich zu sehen, hat alles viel leichter gemacht. Ich liebe dich. Danke!

Ich danke meiner Familie, vor allem meinen Eltern, die immer ein offenes Ohr für mich haben und zur Not einfach mit mir auf den Berg gehen. Das hilft immer. Danke an meine Geschwister, Katrin und Michael, weil ich weiß, dass ihr euch mit mir freut, über das, was ich geschafft habe. Man nimmt sich seine Geschwister unbewusst als Beispiel, mit euch habe ich zwei gute.

Danke auch an meine Tante Hansi, die mir immer die Daumen drückt.